Diamido- and diaminocarbene complexes of the late d-block metals

Collins, Lee

Award date:
2016

Awarding institution:
University of Bath

DIAMIDO- AND DIAMINOCARBENE COMPLEXES OF THE LATE D-BLOCK METALS

Lee Russell Collins

A thesis submitted in partial fulfilment of the requirements for the degree of

Doctor of Philosophy

University of Bath

Department of Chemistry

March 2016

Signed..... Date.....

CONTENTS

CHAPTER THREE: Synthesis and Reactivity of Copper Alkoxide Complexes

CHAPTER FOUR: Discovery of Facile Migratory Insertion Reactions with Metal-Bound Diamidocarbenes

CHAPTER FIVE: Migratory Insertion Reactions of Copper Hydrides

CHAPTER SIX: Synthesis and Stabilisation of Copper Hydrides

CHAPTER SEVEN: Experimental Procedures and Characterising Data

APPENDICES

ACKNOWLEDGEMENTS

I would like to thank Professor Mike Whittlesey for giving me the opportunity to work in his lab, and for being an excellent supervisor. I have learnt so much from my time here, and Mike has made that all possible. His enthusiasm for research is infectious, and his experience in chemistry has been invaluable in teaching me how to manage my research.

I would also like to thank Dr Mary Mahon and Dr John Lowe for their help with X-ray crystallography and NMR spectroscopy. Their expertise has solved so many problems, and I am grateful for all of the time they have spent teaching me and helping out when the work needed an expert's eye.

Collaborations have played an important part in my PhD, and I would like to give particular thanks to Professor Stuart Macgregor and Nasir Rajabi for their work on DFT calculations, and for helping me to understand them.

The lab group, past and present, have been fantastic to work and socialise with. I have really enjoyed our time together, and I hope we keep in touch. Thanks especially to our brilliant post-doc Dr Ian Riddlestone for his advice, Friday afternoon ideas and never ending patience when solving my crystal structures.

Finally, I would like to thank Alina, and my family and friends, for their love and support throughout my time here in Bath.

ABSTRACT

This Thesis is concerned with the synthesis and reactivity of N-heterocyclic carbene (NHC) complexes of copper and the implications of NHC electrophilicity for late d-block metal catalysed reductive processes. Comparison of two NHCs with different electronic, but similar steric properties (the diamidocarbene 6-MesDAC and its diaminocarbene analogue 6-Mes) reveals contrasting reactivity, with implications for the use of electrophilic NHCs in reductive catalytic processes.

The first diamidocarbene complexes of copper are synthesised, beginning with the isolation of a series of monomeric to tetrameric copper chloride complexes (6-MesDAC)CuCl (**3**) and (6-MesDAC)$_2$(CuCl)$_n$ (**1**: n = 2; **2**: n =3; **4**: n = 4). Complexes **1** and **2**, as well as the homoleptic complex [(6-MesDAC)$_2$Cu][BF$_4$] (**6**), are found to be less successful CuAAC catalysts than related diaminocarbene complexes [(NHC)$_2$Cu][BF$_4$] (**7**: NHC = 6-Mes; **8**: NHC = 7-Mes; **9**: NHC = 7-*o*-Tol). New methodology is developed for the synthesis of the NHC copper alkoxide complexes (6-MesDAC)CuO^{t}Bu (**11**) and (6-Mes)CuO^{t}Bu (**20**) by the protonolysis of the copper aryl complexes (6-MesDAC)CuMes (**12**) and (6-Mes)CuMes (**19**). Complex **11** undergoes a range of thermal and hydrolytic decomposition reactions by ring opening of 6-MesDAC.

The diaminocarbene complexes (6-Mes)ZnMe$_2$ (**25**) and (7-Mes)ZnMe$_2$ (**26**) are found to be active catalysts for the ROP of *rac*-lactide. In contrast, (6-MesDAC)MR$_2$ (**27**: ZnEt$_2$; **29**: ZnMe$_2$; **31**: CdMe$_2$) complexes undergo a facile migratory insertion process. This migratory insertion process also applies to copper hydride complexes, with both 6-MesDAC and 6-Mes found to be susceptible to copper hydride migratory insertion. Only the less electrophilic 6-Mes is able to support reductive catalysis (for example, alkyne semi-reduction and ketone hydrosilylation), and the hydride complex [(6-Mes)CuH]$_2$ (**38**) is characterised at low temperature. The products of migratory insertion (6-MesDAC·H)Cu(P(*p*-Tol)$_3$) (**34**) and (6-Mes·H)Cu(6-Mes) (**35**) are isolated and the mechanisms of their formation investigated through DFT calculations. Lewis acids are found to stabilise copper hydrides with respect to migratory insertion. The first mononuclear, Lewis acid stabilised, copper hydride complexes (6-Mes)CuHBEt$_3$ (**39**) and (6-Mes)CuHB(C$_6$F$_5$)$_3$ (**42**) are isolated and investigated by a QTAIM analysis.

ABBREVIATIONS

Chemical

$[6\text{-Mes}\cdot H]^+$	1,3-bis(2,4,6-trimethylphenyl)-4,5,6-trihydropyrimidinium
$[IAd\cdot H]^+$	1,3-bis(1-adamantyl)imidazolium
$[ICy\cdot H]^+$	1,3-dicyclohexylimidazolium
$[IPh\cdot H]^+$	1,3-diphenylimidazolium
$[NHC\cdot H]^+$	imidazolium
$[OAc]^-$	acetate
$[OTf]^-$	trifluoromethanesulfonate
$[X]^-$	halide
12-crown-4	1,4,7,10-tetraoxacyclododecane
18-crown-6	1,4,7,10,13,16-hexaoxacyclooctadecane
5-MesDAC	1,3-bis(2,4,6-trimethylphenyl)-4,5-diketoimidazol-2-ylidene
6-Dipp	1,3-bis(2,6-di-*iso*-propylphenyl)-4,5,6-trihydropyrimidin-2-ylidene
6-DippDAC	1,3-bis(2,6-di-*iso*-propylphenyl)-4,6-diketo-5,5-dimethylpyrimidin-2-ylidene
6-Me	1,3-dimethyl-4,5,6-trihydropyrimidin-2-ylidene
6-Me·H	1,3-dimethyl-2,4,5,6-tetrahydropyrimidin-2-yl
6-MeDAC	1,3,5,5-tetramethyl-4,6-diketo-pyrimidin-2-ylidene
6-MeDAC=CH_2	1,3,5,5-tetramethyl-2-methylene-4,6-diketo-pyrimidine
6-MeDAC·H	1,3,5,5-tetramethyl-2-hydro-4,6-diketopyrimid-2-yl
6-MeDAC·Me	1,2,3,5,5-pentamethyl-4,6-diketopyrimid-2-yl
6-Mes	1,3-bis(2,4,6-trimethylphenyl)-4,5,6-trihydropyrimidin-2-ylidene
6-Mes·H	1,3-bis(2,4,6-trimethylphenyl)-2,4,5,6-tetrahydropyrimid-2-yl
6-MesDAC	1,3-bis(2,4,6-trimethylphenyl)-4,6-diketo-5,5-dimethylpyrimidin-2-ylidene
6-MesDAC=CH_2	1,3-bis(2,4,6-trimethylphenyl)-2-methylene-4,6-diketo-5,5-dimethylpyrimidine

6-MesDAC=O	1,3-bis(2,4,6-trimethylphenyl)-4,6-diketo-5,5-dimethylpyrimidin-2-one
6-MesDAC·Et	1,3-bis(2,4,6-trimethylphenyl)-2-ethyl-4,6-diketo-5,5-dimethylpyrimid-2-yl
6-MesDAC·H	1,3-bis(2,4,6-trimethylphenyl)-2-hydro-4,6-diketo-5,5-dimethylpyrimid-2-yl
6-MesDAC·HCl	1,3-bis(2,4,6-trimethylphenyl)-2-chloro-4,6-diketo-5,5-dimethylpyrimidine
6-MesDAC·HOH	1,3-bis(2,4,6-trimethylphenyl)-2-hydroxy-4,6-diketo-5,5-dimethylpyrimidine
6-MesDAC·Me	1,3-bis(2,4,6-trimethylphenyl)-2,5,5-trimethyl-4,6-diketo-pyrimid-2-yl
6-MesDAC·^{t}Bu	1,3-bis(2,4,6-trimethylphenyl)-2-*tert*-butyl-4,6-diketo-5,5-dimethylpyrimid-2-yl
7-Dipp	1,3-bis(2,6-di-*iso*-propylphenyl)-4,5,6,7-tetrahydro[1,3]diazepin-2-ylidene
7-Mes	1,3-bis(2,4,6-trimethylphenyl)-4,5,6,7-tetrahydro[1,3]diazepin-2-ylidene
7-MesDAC	1,3-bis(2,4,6-trimethylphenyl)-4,7-diketobenzo[e][1,3]diazepin-2-ylidene
7-*o*-Tol	1,3-bis(2-methylphenyl)-4,5,6,7-tetrahydro[1,3]diazepin-2-ylidene
9-BBN	9-borabicyclo[3.3.1]nonane
Ad	1-adamantyl
Ar	aryl
BINAP	2,2’-bis(diphenylphosphino)-1,1’-binapthyl
Bn	benzyl
C_6D_6	deuterated benzene
C_7D_8	deuterated toluene
CAAC	cyclic alkyl amino carbene
CD_2Cl_2	deuterated dichloromethane
Cl_2IPr	1,3-bis(2,6-di-*iso*-propylphenyl)-4,5-dichloroimidazol-2-ylidene

cod	cyclooctadiene
Cp*	pentamethylcyclopentadienyl
CuAAC	copper catalysed [2+3] cycloaddition of terminal alkynes and azides
Cy	cyclohexyl
DAC	diamidocarbene
Dipp	2,6-di-*iso*-propylphenyl
dippe	1,3-bis(di-*iso*-propylphosphino)ethane
dme	dimethoxyethane
dmpe	dimethylphosphinoethane
DMSO	dimethyl sulfoxide
dppe	bis(diphenylphospino)ethane
Et	ethyl
Hex	hexyl
HMDS	hexamethyldisilylamide
HOMO	highest occupied molecular orbital
hpp	hexahydropyrimidopyrimidine
IAd	1,3-bis(1-adamantyl)imidazol-2-ylidene
ICy	1,3-dicyclohexylimidazol-2-ylidene
IMe_4	1,3,4,5-tetramethylimidazol-2-ylidene
IMes	1,3-bis(2,4,6-trimethylphenyl)imidazol-2-ylidene
IPh	1,3-diphenylimidazol-2-ylidene
^{i}Pr	*iso*-propyl
IPr	1,3-bis(2,6-di-*iso*-propylphenyl)imidazol-2-ylidene
$I^{t}Bu$	1,3-di-*tert*-butylimidazol-2-ylidene
L	ligand
LUMO	lowest occupied molecular orbital
M	metal
Me	methyl
$^{Me_2}I^{i}Pr$	1,3-di-*iso*-propyl-4,5-dimethylimidazol-2-ylidene
Mes	2,4,6-trimethylphenyl
MO	molecular orbital
Nacnac	N,N-bis(2,6-di-*iso*-propylphenyl)-β-diketiminate

NHC	N-heterocyclic carbene
N-SHC	thioaminocarbene
Ph	phenyl
Ph_2Ppypz	2-diphenylphosphino-6-pyrazol-1-ylpyridine
Phen	1,10-phenanthroline
Pin	2,3-dimethyl-2,3-butanediolate
PLA	poly lactic acid
Py	pyridine
QTAIM	quantum theory of atoms in molecules
R	alkyl or aryl substituent
rac-	racemic-
RENHC	ring expanded N-heterocyclic carbene
ROP	ring opening polymerisation
SIMe	1,3-dimethylimidazolin-2-ylidene
SIMes	1,3-bis(2,4,6-trimethylphenyl)imidazolin-2-ylidene
SIPr	1,3-bis(2,6-di-*iso*-propylphenyl)imidazolin-2-ylidene
SI^tBu	1,3-di-*tert*-butylimidazolin-2-ylidene
^tBu	*tert*-butyl
THF	tetrahydrofuran
THF-d_8	deuterated tetrahydrofuran
tmeda	tetramethylethylenediamine
TMS	trimethylsilyl
TMS_3Cp	1,2,4-tris(trimethylsilyl)cyclopentadienyl
^{TMS}Cp	trimethylsilylcyclopentadienyl
tmta	1,3,5-trimethyl-1,3,5-triazinane
Tol	tolyl
$Tp^{tBu,Me}$	hydrotris(3-*tert*-butyl-5-methylpyrazol-1-yl)borate)

Units and Spectroscopy

%	percentage
%V_{Bur}	percentage buried volume
{^{1}H}	proton decoupled
{^{11}B}	boron decoupled
°	degrees
Å	Ångström
br	broad
cm^{-1}	wavenumbers
COSY	correlation spectroscopy
d	doublet
DOSY	diffusion-ordered NMR spectroscopy
eq	equivalents
GPC	gel permeation chromatography
HMBC	heteronuclear multiple bond correlation
HSQC	heteronuclear single quantum coherence
Hz	hertz
i-	*ipso*-
IR	infra red
J	scalar coupling constant
K	Kelvin
kcal	kilocalorie
m	multiplet
m-	*meta*-
mbar	millibar
mg	milligrams
MHz	megahertz
mL	millilitre
M_n	polymer molecular weight
mol	mole
mol %	mole percent
mol^{-1}	per mole
n-	*neo*-

NMR	nuclear magnetic resonance
NOE	nuclear Overhauser effect
NOESY	nuclear Overhauser effect spectroscopy
o-	*ortho*-
p	pentet
p-	*para*-
PDI	polydispersity index
P_m	probability of meso diads
ppm	parts per million
PXRD	powder X-ray diffraction
q	quartet
r_H	hydrodynamic radius
s	singlet
t	triplet
TEP	Tolman electronic parameter
δ	chemical shift
η	viscosity

CHAPTER ONE

CHAPTER ONE: Introduction

1.1 N-Heterocyclic Carbenes

Carbenes are neutral, divalent carbon compounds possessing a triplet or singlet ground state. First proposed to exist over one hundred years ago,[1] carbenes gained relevance in organic and organometallic chemistry through pioneering work by Doering in the 1950s and by Fischer in the 1960s respectively.[2,3] Since the 1990s, carbene chemistry has received a large amount of attention thanks to the isolation of a variety of persistent triplet and singlet carbenes.[4] An N-heterocyclic carbene (NHC) is a heterocycle of four or more atoms containing a singlet carbene. In their most common form, this carbene is located α to two nitrogen atoms in an imidazole based heterocycle (Figure 1.1).

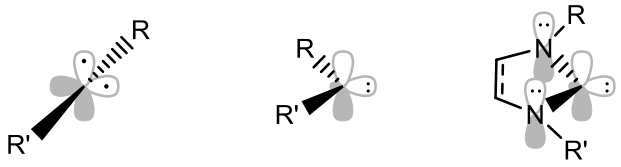

Figure 1.1: Diagrams of an sp hybridised triplet carbene (left), an sp^2 hybridised singlet carbene (centre) and an N-heterocyclic carbene (right). R and R' represent most commonly either alkyl or aryl groups.

1.2 History of NHCs

The first direct syntheses of transition metal NHC complexes were reported in 1968.[5,6] Öfele synthesised a series of $(NHC)Cr(CO)_5$ complexes by the reaction of $Na_2Cr(CO)_5$ with $NHC{\cdot}Cl_2$ precursors.[5] Wanzlick and co-workers demonstrated that reaction of two equivalents of the imidazolium salt $[IPh{\cdot}H][ClO_4]$ with $Hg(OAc)_2$ resulted in the in-situ deprotonation of $[IPh{\cdot}H][ClO_4]$ and subsequent formation of $[(IPh)_2Hg][ClO_4]_2$ (Scheme 1.1), which was later structurally characterised.[7]

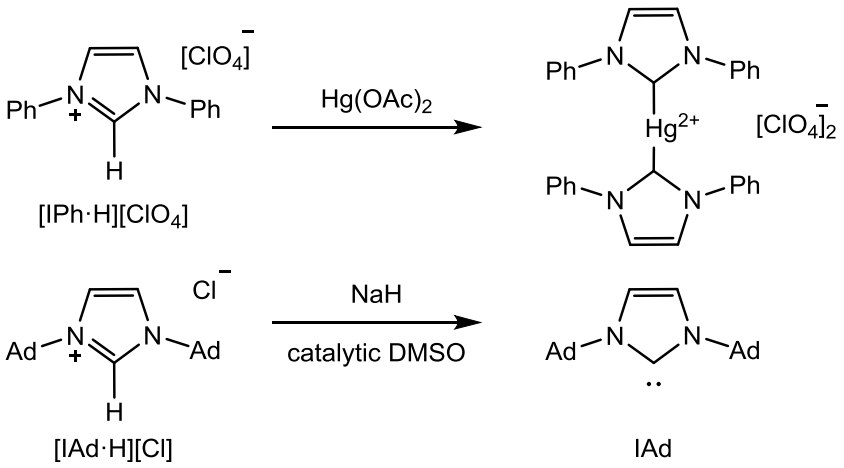

Scheme 1.1: Landmark NHC compounds. Reaction of $[IPh{\cdot}H][ClO_4]$ with $Hg(OAc)_2$, resulting in the formation of $[(IPh)_2Hg][ClO_4]_2$ (top).[6] Reaction of [IAd·H][Cl] with NaH and DMSO, resulting in the formation of the free NHC IAd (bottom).[8]

In 1991, Arduengo and co-workers reported the first isolable and structurally characterised NHC (IAd, Scheme 1.1).[8] The remarkable stability of IAd, which did not decompose upon melting at 513 K, was attributed to the steric protection of its bulky adamantyl groups preventing dimerisation.[9] However, the isolation of four further NHCs in 1992, including the methyl substituted IMe_4 (Figure 1.3, far left),[10] demonstrated that sterics are not the sole factor in determining the stability of an NHC.

1.3 Electronic Structure and Stability of NHCs

The electronic structure of NHCs is fundamental to their thermodynamic stability. The electronegative α-amino substituents serve to lower the energy of the carbene's sp^2 lone pair through inductive withdrawal of electron density, whilst at the same time raising the energy of the vacant p orbital through mesomeric donation (Figure 1.2).[11]

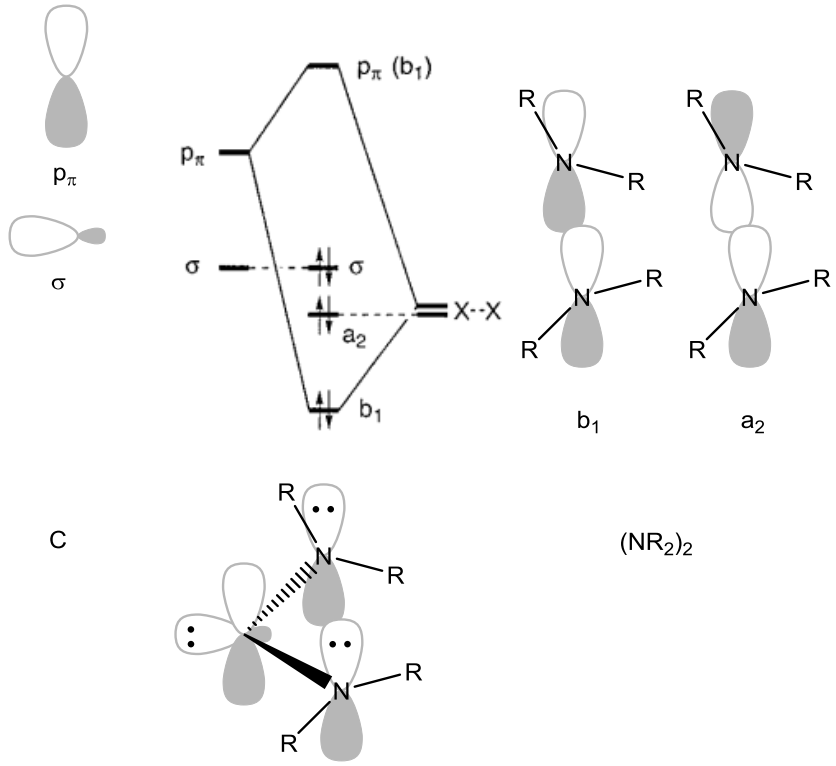

Figure 1.2: Molecular orbital diagram of a diaminocarbene.[4]

The MO diagram in Figure 1.2 shows the two non-bonding frontier orbitals of an sp^2 hybridised carbene (σ and p_π) interacting with linear combinations of the p orbitals of two amine substituents (labelled b_1 and a_2). Interaction of the in-phase b_1 combination with the carbenic p_π orbital results in MOs (labelled b_1 and $p_\pi(b_1)$) which can interact with metal fragments to form weak $b_1 \rightarrow d$ and $d \rightarrow p_\pi(b_1)$ bonding interactions.[12] The highest occupied molecular orbital (HOMO) consists of a σ orbital which is not perturbed by mesomeric effects. Nonetheless, inductive withdrawal of electron density by the electronegative nitrogen atoms does lower the energy of the HOMO. The resultant HOMO/LUMO gap is sufficient (greater than 46 kcal mol^{-1})[13,14] to stabilise a singlet ground state. Furthermore, the carbon-centered, non-bonding HOMO accounts for the C2 nucleophilicity of NHCs whilst the high energy of the LUMO explains why NHCs are generally poor π-acceptors.

A further factor contributing to the stability of NHCs is the aromaticity (calculated to account for 15 kcal mol^{-1})[14] of imidazol-2-ylidenes (Figure 1.3, left). Whilst many NHCs with a saturated backbone (imidazolin-2-ylidenes, Figure 1.3, right) are isolable, they often require kinetic stabilisation by bulky N-substituents to compensate for their reduced thermodynamic stability. For example, the mesityl

substituted imidazolin-2-ylidene SIMes is isolable, but its methyl substituted analogue SIMe is unstable with respect to dimerisation (Figure 1.3).[15,16]

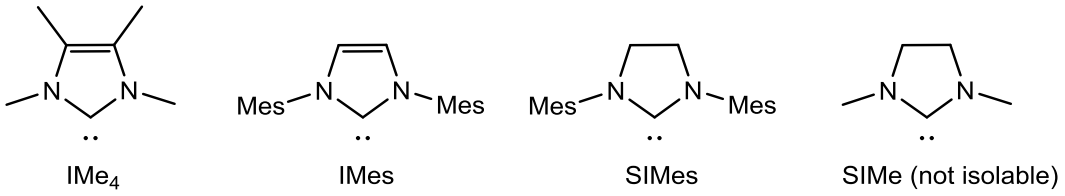

Figure 1.3: Examples of the effects of aromaticity and steric bulk in stabilising NHCs. Both of the imidazol-2-ylidenes IMe_4 and IMes (far left and centre left, respectively) are isolable.[10] However, of the non-aromatic imidazolin-2-ylidenes SIMes and SIMe (centre right and far right, respectively), only the bulky SIMes is isolable.[15,16]

1.4 Tunability of NHCs

As neutral, two-electron σ-donor ligands, NHCs are often compared to phosphines. NHCs are stronger nucleophiles than phosphines, as evidenced by their lower pKa values and lower Tolman electronic parameters.[i] This increased nucleophilicity results in the formation of stronger metal-ligand bonds. Consequently, NHCs are less prone to dissociation and have more potential to stabilise well defined co-ordination spheres, ideal for tuning the geometry of a metal centre. A further advantage over phosphines is the ease with which the steric demands of an NHC can be modified through the synthesis of imidazolium and 4,5-dihydroimidazolium salts (Scheme 1.2).

[i] The Tolman electronic parameter (TEP) of a ligand (L) is defined as the frequency of the A_1 CO stretching mode of $(L)Ni(CO)_3$ in CH_2Cl_2 and is a useful measure of ligand donor strength, particularly when applied to phosphines.[17] Crabtree showed that the average CO stretching frequency of $(L)Ir(CO)_2Cl$ is another convenient measure for comparing the σ-donor properties of both phosphines and NHCs, with this data showing a very good correlation to TEP data.[18] Nolan used this method to show that NHCs are stronger σ-donors than phosphines, with only small variations between NHCs with different N-substituents.[19]

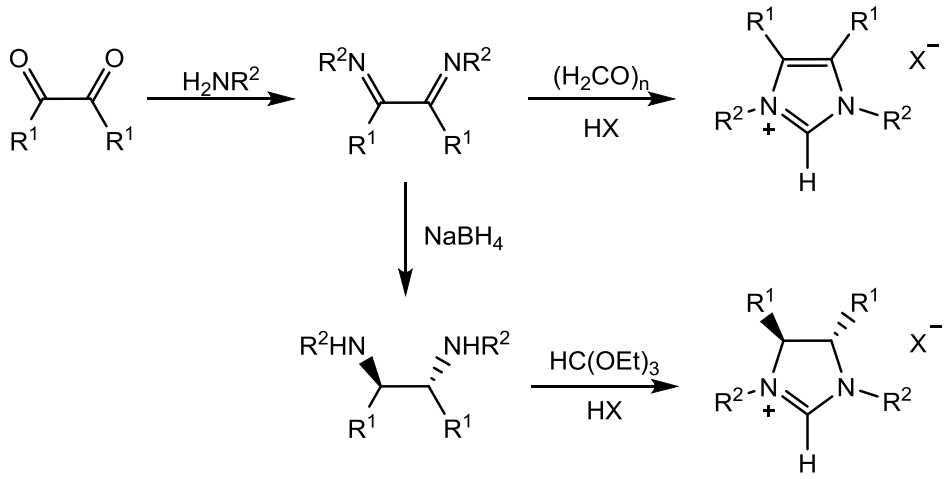

Scheme 1.2: Synthesis of substituted imidazolium (top) and 4,5-dihydroimidazolium (bottom) salts.

Reaction of substituted glyoxals with a range of primary amines allows access to a diverse range of diimines, which upon condensation with paraformaldehyde yield their respective imidazolium salts. Alternatively, reduction of these diimines followed by condensation with triethylorthoformate allows access to saturated 4,5-dihydroimidazolium salts. Deprotonation of these salts (sometimes preceded by salt metathesis to a non co-ordinating anion) produces NHCs which may either be isolated or used in-situ.

With four functionalisable ring positions, five-membered NHCs offer a highly tunable platform. The steric protection afforded to a metal centre is particularly sensitive to the nature of the NHC N-substituents, since these are oriented in such a way that they flank the C-M bond. The steric bulk of an NHC as part of an organometallic complex may be quantified by the percentage buried volume ($\%V_{Bur}$),[i] with typical values ranging from 26.1 % for IMe_4 to 47.0 % for SIPr (both measured for their respective (NHC)AuCl complexes).[20,21]

Whilst the N-substituents have a significant effect on the steric bulk of an NHC, they often have very little effect on the electronic structure (as evidenced by very similar TEPs).[19] However, functionalisation of the heterocycle itself can significantly alter

[i] The Tolman cone angle fails to accurately represent the steric properties of NHCs due to their planar structure and approximate C_s symmetry. The $\%V_{Bur}$ quantifies the proportion of a sphere surrounding a metal which is occupied by a ligand, and is calculated from crystallographic data using the SambVca program.[20] This measure is sensitive to both the nature of the complex and the ligand, and allows for comparisons between different NHCs and phosphines.[21]

the electronic properties of an NHC by modifying its HOMO and LUMO energies. Figure 1.4 shows some examples of heterocycle-functionalised NHCs, along with average CO stretching frequencies for their corresponding $(NHC)Rh(CO)_2Cl$ complexes.[22] Electron donating substituents, for example an anionic alkoxide, strongly enhance σ-donation. Electron withdrawing substituents on the other hand, for example nitriles, make the NHC a weaker σ-donor.

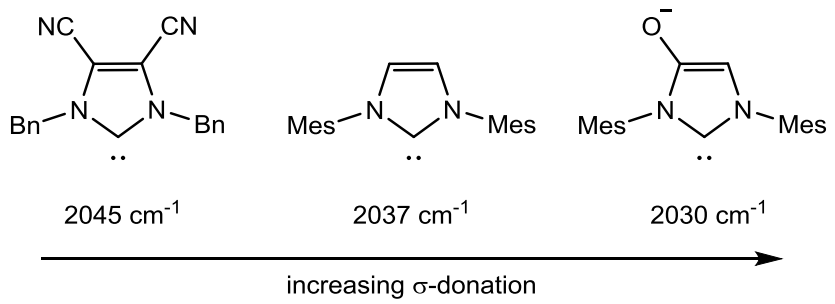

Figure 1.4: Examples of heterocycle-functionalised NHCs alongside their corresponding $(NHC)Rh(CO)_2Cl$ complexes' average CO stretching frequencies as a measure of σ-donating strength.[22]

Due to their highly tunable electronic and steric properties, NHCs have become ubiquitous in organocatalytic and organometallic chemistry; their diverse electronic and steric properties benefitting countless catalytic processes.[23] Perhaps the most celebrated use of NHCs in catalysis is the development of the second generation Grubbs alkene metathesis catalyst in 1999 (Scheme 1.3).[24,25] The substitution of PCy_3 for SIMes resulted in a complex with higher catalytic activity for ring closing metathesis and greatly expanded the substrate scope of the reaction.

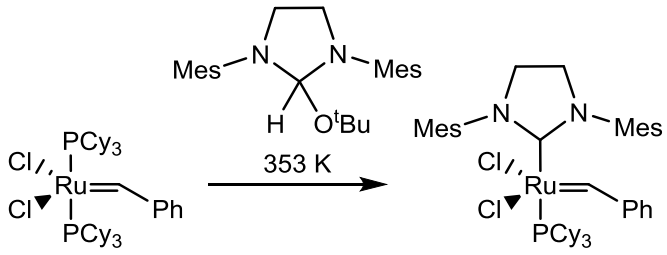

Scheme 1.3: Synthesis of Grubbs' second generation alkene metathesis catalyst by reaction of Grubbs' first generation alkene metathesis catalyst with SIMes (formed by thermolytic deprotection).[24]

1.5 Ring Expanded NHCs

Even greater scope for NHC design can be achieved by expanding the NHC ring size from five-membered to six, seven or higher.[26] The salt precursors to such ring expanded NHCs (RENHCs) can be isolated in a similar manner to imidazolium salts,[27] with condensation of a diamine with triethylorthoformate to yield the corresponding heterocycle salt. A more convenient synthetic procedure is to reflux an acetonitrile solution of dihaloalkane and formamidine in the presence of K_2CO_3 (Scheme 1.4); subsequent anion exchange and deprotonation of the resultant salts generates a wide range of RENHCs.[28]

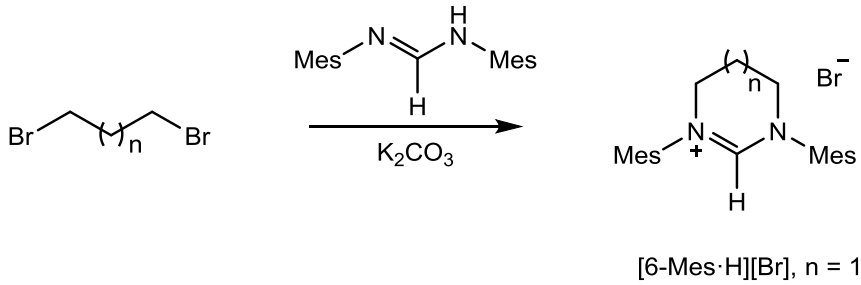

Scheme 1.4: Synthesis of [6-Mes·H][Br] by reaction of dimesitylformamidine with dibromopropane.[28]

The geometric constraints of a larger heterocycle result in greater proximity of the N-substituents to the carbenic carbon than in imidazol-2-ylidenes, thus providing greater steric protection to a metal centre and assisting in the kinetic stabilisation of low co-ordinate complexes.[26,28,29] Furthermore, the wider N-C-N angle results in a decrease of the s-character of the carbon centred HOMO, thereby increasing its energy and resulting in greater nucleophilicity as well as a smaller HOMO/LUMO gap.[28]

1.6 Cyclic Alkyl Amino Carbenes

Another strategy for increasing the nucleophilicity of a carbene is the replacement of an inductively withdrawing amine with an inductively donating tertiary alkyl group. In 2004, Bertrand and co-workers isolated the first such alkyl amino carbene (Figure 1.5, left).[30] The acyclic t*ert*-butyl-di-*iso*-propylamino carbene was shown to be amongst the most nucleophilic of (di-)amino carbenes. However, as well as raising the energy of the HOMO, the removal of one of the π-donating amines also lowered

the energy of the LUMO, resulting in enhanced electrophilicity. Indeed, this alkyl amino carbene demonstrated electrophilic reactivity, such as undergoing cyclopropanation with methyl acrylate.[30] Further experimentation was limited by the decomposition of this carbene in solution at room temperature over 72 hours.

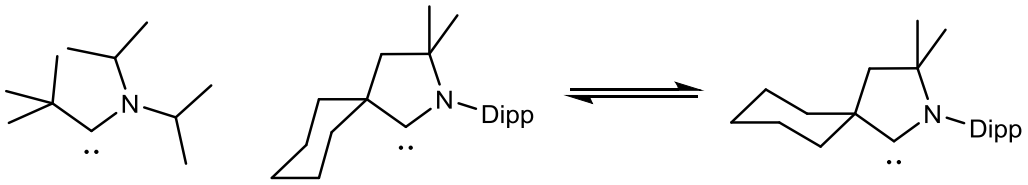

Figure 1.5: Examples of alkyl amino carbenes. The first isolated alkyl amino carbene (left). Cyclohexyl substituted CAACs allow for flexibility in the steric demands of the carbene (right).

The following year, Bertrand and co-workers reported a series of cyclic alkyl amino carbenes (CAACs) which were indefinitely stable in solution.[31] CAACs were found to be the strongest σ-donors of all reported (di-)amino carbenes. In addition, the location of a quaternary carbon α to the carbene allowed for enhanced, and even flexible, steric protection of the carbenic carbon (Figure 1.5, right). Unlike diaminocarbenes, alkyl amino carbenes proved capable of activating dihydrogen and ammonia.[32] A mechanism was proposed in which the nucleophilicity of these carbenes sufficed to polarise and partially deprotonate dihydrogen and ammonia, resulting in either a pseudo-hydride or pseudo-amide which attacked the carbene's p_π orbital.

Through a combination of their steric demands and strong σ-donating as well as π-accepting properties, CAACs have been found to benefit a range of applications in Pd,[31] Au,[33] and Ru catalysed processes.[34] They are also capable of stabilising some remarkable organometallic complexes including a series of $(CAAC)_2M$ complexes (M = Au, Cu, Co, Fe, Ni, Mn, Zn), with each metal formally in a zero oxidation state.[35]

1.7 Diamidocarbenes

A diamidocarbene (DAC) is a functionalised NHC with carbonyls α to each nitrogen, resulting in significantly enhanced electrophilicity. In the case of diaminocarbenes, the lone pair of each amine donates to the vacant p_π orbital of the carbenic carbon. In DACs, the amine lone pairs not only donate to the p_π orbital of the carbene, but also to the anti-bonding π* orbitals of the carbonyl substituents. This reduced occupancy of the carbenic p_π orbital results in a lowering of the energy of the LUMO and consequently greater electrophilicity (Figure 1.6).

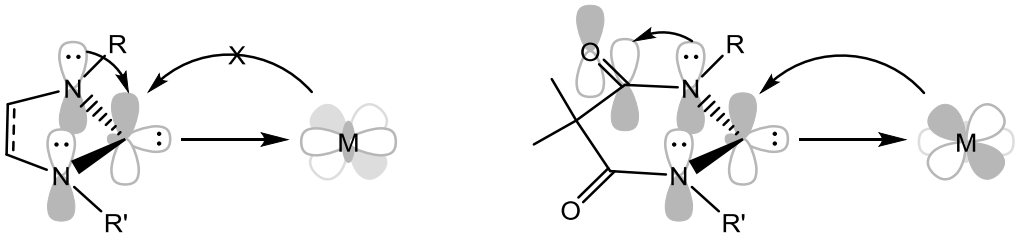

Figure 1.6: Orbital representation of the enhanced electron accepting properties of diamidocarbenes (right) compared to diaminocarbenes (left) due to the mesomeric withdrawal of electron density by carbonyl substituents.

In 2009, Bielawski and co-workers reported the synthesis of the first diamidocarbene, 6-DippDAC (Scheme 1.5).[36] They demonstrated its electrophilic character by reaction with CO to form a heterocumulene product. Remarkably, CO could be removed under vacuum, making 6-DippDAC the first organic compound to reversibly bind CO (Scheme 1.5).[36] Further study of 6-DippDAC was complicated by an intramolecular C-H activation process at room temperature, which also prevented its isolation.

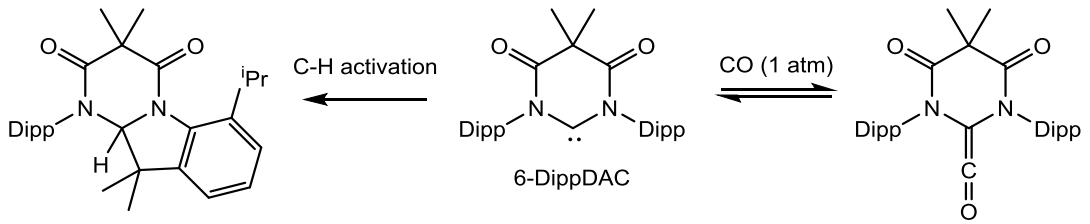

Scheme 1.5: Reactivity of the diamidocarbene 6-DippDAC.

1.7.1 6-MesDAC

One year later, the mesityl substituted diamidocarbene 6-MesDAC was synthesised through deprotonation of 6-MesDAC·HCl (Scheme 1.6).[37] In contrast to all diamino [NHC·H][X] salt precursors, 6-MesDAC·HCl is a covalent molecule and soluble in non-polar solvents due to the hypothetical $[6\text{-MesDAC}\cdot H]^+$ cation being so electrophilic at the C2 position that the chloride counterion binds covalently. However, its C-Cl bond is weak (C-Cl = 1.888(2) Å; cf: average sp^3 C-Cl distance = 1.76 Å)[38] and 6-MesDAC·HCl is very sensitive to nucleophilic displacement of chloride, requiring its synthesis to be conducted under strictly anhydrous conditions.[37]

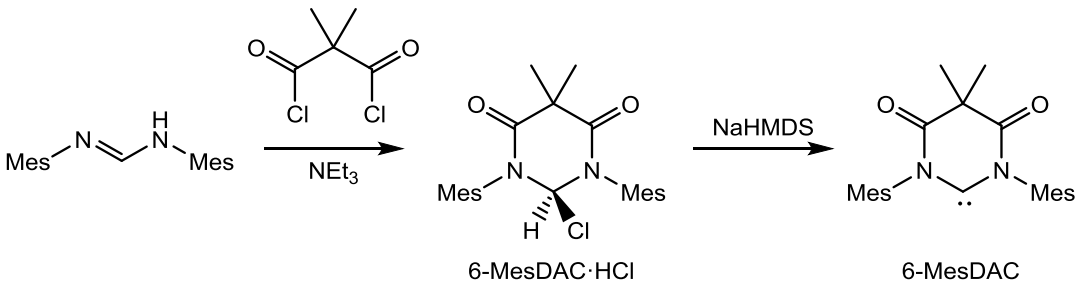

Scheme 1.6: Synthesis of 6-MesDAC·HCl and its deprotonation to yield the diamidocarbene 6-MesDAC.[37]

6-MesDAC only undergoes intramolecular C-H activation at 373 K,[39] and this greater stability allowed for its isolation and structural characterisation.[37] X-ray diffraction analysis of 6-MesDAC showed the average $C_{(carbene)}$-N bond length (1.371(3) Å) to be significantly longer than that of the analogous diaminocarbene 6-Mes (1.3464(12) Å).[28] This reduction in double bond character demonstrates the reduced mesomeric donation of 6-MesDAC's nitrogen lone pairs to the carbenic carbon due to their partial donation to the carbonyl π^* orbitals (Figure 1.5). This extended conjugated system is further evidenced by the average C-O bond length of 6-MesDAC (1.212(3) Å) being intermediate between that of a ketone and that of an amide. $^{13}C\{^1H\}$ NMR spectroscopy also demonstrates the electron deficiency of 6-MesDAC; the carbenic carbon resonating at 277.7 ppm, significantly downfield of the diamino analogue 6-Mes (244.9 ppm).

6-MesDAC displays electrophilic properties and its reactivity with a range of organic and inorganic substrates has been explored, including numerous examples of E-H (E = B,[40] C,[39] N,[41] Si,[42] P)[43] bond activation and [2+1] cycloaddition (Scheme 1.7).[44,45]

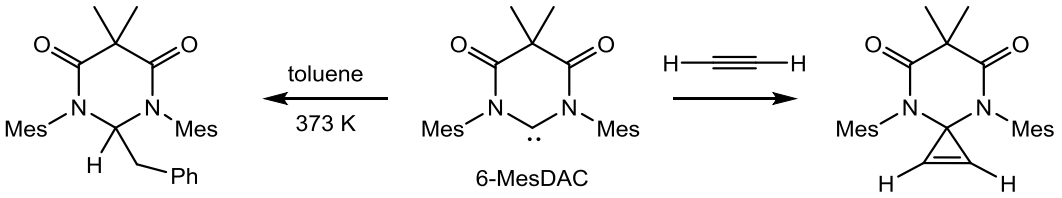

Scheme 1.7: C-H activation of toluene by 6-MesDAC at 373 K (left).[39] [2+1] cycloaddition of 6-MesDAC with HC≡CH to form a diamidocyclopropene (right).[44]

The organometallic chemistry of 6-MesDAC has received only limited attention in the literature,[i] but the known examples exemplify the π-accepting character of 6-MesDAC. For example, (6-MesDAC)Ni(PPh_3)Br was found to have a significantly shorter Ni-C bond length (1.8702(18) Å) than its diaminocarbene analogue (6-Mes)Ni(PPh_3)Br (1.942(2) Å) due to the greater π-accepting properties of 6-MesDAC (Figure 1.7).[49] Similarly, (6-MesDAC)Rh(cod)Cl was found to have the shortest Rh-$C_{(NHC)}$ bond (2.010(2) Å) of any (NHC)Rh(cod)Cl complex (ranging from 2.036(2) Å to 2.090(3) Å),[50] in part due to increased π back-bonding from rhodium. (6-MesDAC)Rh(cod)Cl also exhibits the highest frequency $^{13}C\{^1H\}$ chemical shift (δ = 245.2 ppm) of any NHC-Rh complex (δ = 175-225 ppm),[51] further demonstrating the electron deficiency of 6-MesDAC.

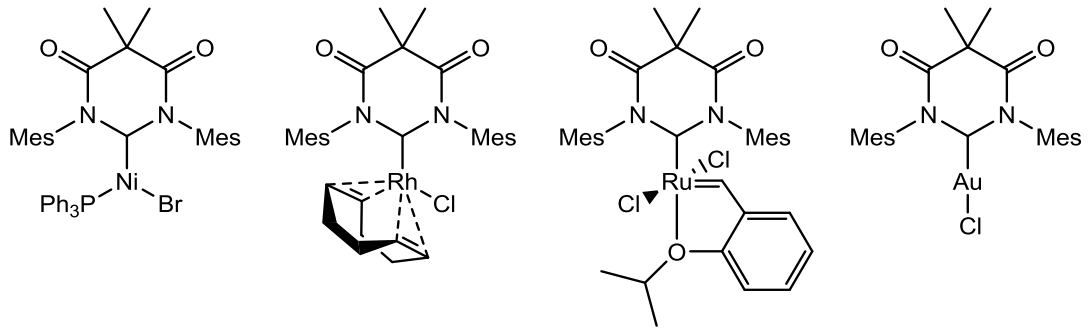

Figure 1.7: Examples of 6-MesDAC complexes: (6-MesDAC)Ni(PPh_3)Br (far left),[49] (6-MesDAC)Rh(cod)Cl (centre left),[50] (6-MesDAC)Ru(=C(H)PhO^{i}Pr)Cl_2 (centre right),[52] (6-MesDAC)AuCl (far right).[46]

[i] The organometallic chemistry of other diamidocarbenes (6-DippDAC,[36,46] 5-MesDAC,[47] 7-MesDAC)[48] has similarly received little attention in the literature.

A Hoveyda-Grubbs alkene metathesis catalyst (Figure 1.7, centre right) was synthesised with 6-MesDAC in place of PCy_3 and found to be a successful catalyst for ring closing metathesis, particularly for the more sterically demanding substrate diethyl diallylmalonate.[52] In contrast, (6-MesDAC)AuCl was found to be a poor pre-catalyst for gold(I) catalysed 1,6-enyne cyclisation.[46]

1.8 NHC Copper Chemistry

In 1993, Arduengo and co-workers synthesised and structurally characterised $[(IMes)_2Cu][OTf]$, the first NHC complex of copper, by reaction of two equivalents of IMes with CuOTf.[53] The first use of an NHC in copper catalysis was reported in 2001 by Woodward and co-workers, who demonstrated that use of SIMes resulted in a dramatic rate enhancement of the copper catalysed conjugate addition reaction of $ZnEt_2$ to α,β-unsaturated carbonyls.[54] In the fifteen to twenty years since these initial reports, NHCs have become widely studied ligands in copper chemistry, and are implicated in a wide range of catalytic processes.[55–57] Successful catalysts are often formed in-situ by the combination of air stable precursors ([NHC·H][X] salt, MO^tBu base and copper(I) precursor – Cu(II) salts may also be used in combination with a reducing agent). This procedural simplicity is convenient from a synthetic perspective, but often leaves ambiguity over the exact nature of the catalytically active species and the mechanism of reactivity.

1.8.1 NHC Copper Catalysed Hydrosilylation

Amongst the diverse applications of copper in catalysis,[57] hydrosilylation is an example of chemistry for which copper is increasingly employed as a replacement for more precious metal catalysts. In 2003, Sadighi and Buchwald showed that (IPr)CuCl was a successful precatalyst for the conjugate reduction of α,β-unsaturated ketones and esters, using a hydrosilane as the reductant.[58] One year later, Nolan and co-workers found that a range of NHCs were effective ligands for the copper catalysed hydrosilylation of ketones.[59] These initial studies proposed that the active catalyst could be an (NHC)CuH complex, formed through a sequence of reactions as shown in Scheme 1.8.

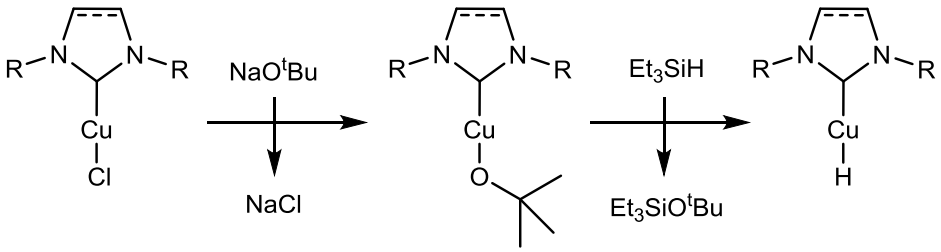

Scheme 1.8: Mechanism of in-situ formation of a catalytically relevant (NHC)CuH complex.

In this process, (NHC)CuCl (itself often formed in situ from a mixture of [NHC·H][X], NaO^{t}Bu and CuCl) undergoes salt metathesis with NaO^{t}Bu, resulting in the formation of (NHC)CuO^{t}Bu and NaCl. This alkoxide complex reacts with a hydrosilane, resulting in the formation of (NHC)CuH and a silylether by-product.

A commonly proposed mechanism for (NHC)CuH catalysed ketone hydrosilylation involves initial insertion of ketone into the Cu-H bond, leading to the formation of a copper alkoxide complex which subsequently undergoes σ-bond metathesis with hydrosilane to close the catalytic cycle (Scheme 1.9).

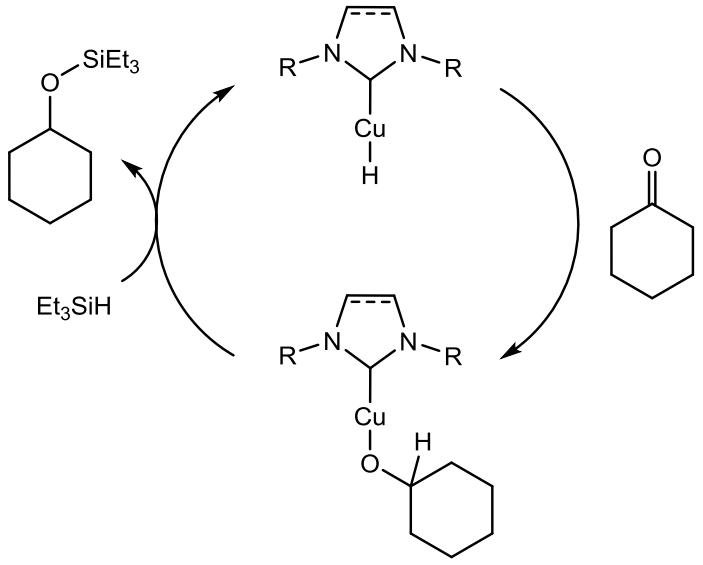

Scheme 1.9: Proposed catalytic cycle for the (NHC)CuH catalysed hydrosilylation of cyclohexanone.

This catalytic cycle is a viable suggestion, but there is very little direct supporting evidence due to the highly reactive nature of (NHC)CuH complexes and the in-situ methods often employed in catalysis. Nolan observed that excess base accelerated

such in-situ catalytic reactions, and proposed that the formation of hypervalent silicon species could be assisting σ-bond metathesis in a more complicated process.[60]

Studies of isolable (phosphine)CuH complexes have shown them to be inert towards ketones in the absence of hydrosilane, despite themselves being very active hydrosilylation catalysts in the presence of silane.[61] Indeed, a first order rate dependence on the concentration of hydrosilane has been observed with chiral (BINAP)CuH catalysts.[62] Further insights were gained by Nikonov and co-workers, who were able to show that a deuterium labelled hydrosilane reduced benzaldehyde to a deuterated benzyl alcohol without incorporating deuterium into the $[(PPh_3)CuH]_6$ catalyst, thereby proving that the Cu-H bond had not participated in the reduction reaction.[63] Following these observations, several different mechanisms have been proposed based on the formation of highly reactive Cu(III) or hypervalent silicon intermediates (Scheme 1.10, top),[62] or with copper acting as a Lewis acid catalyst (Scheme 1.10, bottom).[63]

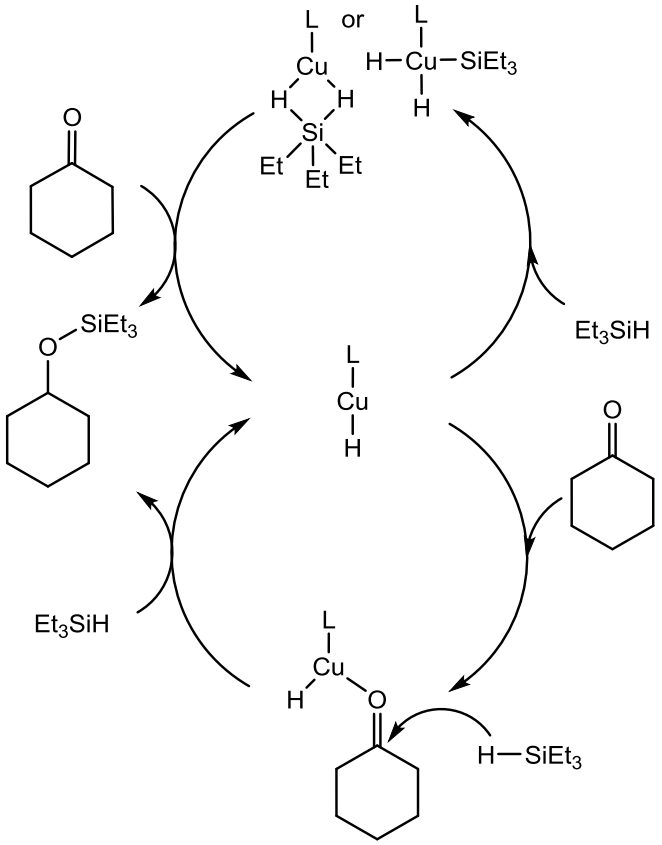

Scheme 1.10: Proposed catalytic cycles for the copper catalysed hydrosilylation of ketones.

Understanding the mechanism of a reaction is vital for knowing which properties are desirable in the design of improved ligand systems. Such properties could include increased hydride nucleophilicity, increased copper Lewis acidity or increased stability of Cu(III) or hypervalent silicon intermediates, for instance. However, advancing mechanistic understanding is held back by the paucity of isolated (NHC)CuOR,[64–66] and (NHC)CuH complexes in the literature.[64,67,68] This Thesis will discuss the synthesis, stability and reactivity of a range of NHC copper complexes with relevance to homogeneous catalysis, focusing on the effects of NHC electrophilicity.

1.9 Thesis Aims

This Thesis will explore the late d-block metal chemistry of the diamidocarbene 6-MesDAC and its diamino analogue 6-Mes. The σ-donating strength of an NHC is often cited as the dominant factor in its electronic contribution towards the reactivity of an organometallic complex, and has consequently been the focus of much research. This Thesis will focus on the often overlooked property of NHC π-acceptance through the study of two NHCs with significantly different electrophilicities, with 6-MesDAC having much greater electrophilic character than 6-Mes. Through their comparison, this Thesis will analyse the consequences of NHC electrophilicity for the stability and reactivity of late d-block metal species, with particular attention paid to complexes of relevance to copper catalysed reductive processes.

The steric bulk of these six-membered NHCs may be crucial for the kinetic stabilisation of highly reactive species. Furthermore, by virtue of providing very similar steric protection to a metal centre, the differences between the stability and reactivity of the metal complexes of 6-MesDAC and 6-Mes can be attributed with greater confidence to their electronic differences.

This Thesis will be structured around the attempted synthesis of an (NHC)CuH complex (Scheme 1.8), exploring in turn the synthesis, stability and reactivity of copper chloride (Chapter Two), alkoxide (Chapter Three) and hydride (Chapters Five and Six) complexes of 6-MesDAC and 6-Mes.

1.10 References for Chapter One

(1) Arduengo III, A. J.; Krafczyk, R. *Chem. Unserer Zeit* **1998**, *32*, 6–14.

(2) Doering, W. von E.; Hoffmann, A. K. *J. Am. Chem. Soc.* **1954**, *76*, 6162–6165.

(3) Fischer, E. O.; Maasböl, A. *Angew. Chem. Int. Ed.* **1964**, *3*, 580–581.

(4) Bourissou, D.; Guerret, O.; Gabbaï, F. P.; Bertrand, G. *Chem. Rev.* **1999**, *100*, 39–92.

(5) Öfele, K. *Angew. Chem. Int. Ed.* **1968**, *7*, 950–950.

(6) Wanzlick, H. W.; Schönherr, H. J. *Angew. Chem. Int. Ed.* **1968**, *7*, 141–142.

(7) Luger, P.; Ruban, G. *Acta Crystallogr., Sect. B Struct. Sci.* **1971**, *27*, 2276–2279.

(8) Arduengo III, A. J.; Harlow, R. L.; Kline, M. *J. Am. Chem. Soc.* **1991**, *113*, 361–363.

(9) Wanzlick, H. W. *Angew. Chem. Int. Ed.* **1962**, *1*, 75–80.

(10) Arduengo III, A. J.; Dias, H. V. R.; Harlow, R. L.; Kline, M. *J. Am. Chem. Soc.* **1992**, *114*, 5530–5534.

(11) Boehme, C.; Frenking, G. *J. Am. Chem. Soc.* **1996**, *118*, 2039–2046.

(12) Scott, N. M.; Dorta, R.; Stevens, E. D.; Correa, A.; Cavallo, L.; Nolan, S. P. *J. Am. Chem. Soc.* **2005**, *127*, 3516–3526.

(13) Hoffmann, R. *J. Am. Chem. Soc.* **1968**, *90*, 1475–1485.

(14) Heinemann, C.; Müller, T.; Apeloig, Y.; Schwarz, H. *J. Am. Chem. Soc.* **1996**, *118*, 2023–2038.

(15) Arduengo III, A. J.; Goerlich, J. R.; Marshall, W. J. *J. Am. Chem. Soc.* **1995**, *117*, 11027–11028.

(16) Denk, M. K.; Thadani, A.; Hatano, K.; Lough, A. J. *Angew. Chem. Int. Ed.* **1997**, *36*, 2607–2609.

(17) Tolman, C. A. *Chem. Rev.* **1977**, *77*, 313–348.

(18) Chianese, A. R.; Li, X.; Janzen, M. C.; Faller, J. W.; Crabtree, R. H. *Organometallics* **2003**, *22*, 1663–1667.

(19) Kelly III, R. A.; Clavier, H.; Giudice, S.; Scott, N. M.; Stevens, E. D.; Bordner, J.; Samardjiev, I.; Hoff, C. D.; Cavallo, L.; Nolan, S. P. *Organometallics* **2008**, *27*, 202–210.

(20) Poater, A.; Cosenza, B.; Correa, A.; Giudice, S.; Ragone, F.; Scarano, V.;

Cavallo, L. *Eur. J. Inorg. Chem.* **2009**, *2009*, 1759–1766.

(21) Clavier, H.; Nolan, S. P. *Chem. Commun.* **2010**, *46*, 841–861.

(22) Benhamou, L.; Vujkovic, N.; César, V.; Gornitzka, H.; Lugan, N.; Lavigne, G. *Organometallics* **2010**, *29*, 2616–2630.

(23) Díez-González, S.; Marion, N.; Nolan, S. P. *Chem. Rev.* **2009**, *109*, 3612–3676.

(24) Scholl, M.; Ding, S.; Lee, C. W.; Grubbs, R. H. *Org. Lett.* **1999**, *1*, 953–956.

(25) Huang, J.; Stevens, E. D.; Nolan, S. P.; Petersen, J. L. *J. Am. Chem. Soc.* **1999**, *121*, 2674–2678.

(26) Li, J.; Shen, W.; Li, X. *Curr. Org. Chem.* **2012**, *16*, 2879–2891.

(27) Alder, R. W.; Blake, M. E.; Bortolotti, C.; Bufali, S.; Butts, C. P.; Linehan, E.; Oliva, J. M.; Guy Orpen, A.; Quayle, M. J. *Chem. Commun.* **1999**, 241–242.

(28) Iglesias, M.; Beetstra, D. J.; Knight, J. C.; Ooi, L.; Stasch, A.; Coles, S.; Male, L.; Hursthouse, M. B.; Cavell, K. J.; Dervisi, A.; Fallis, I. A. *Organometallics* **2008**, *27*, 3279–3289.

(29) Page, M. J.; Lu, W. Y.; Poulten, R. C.; Carter, E.; Algarra, A. G.; Kariuki, B. M.; Macgregor, S. A.; Mahon, M. F.; Cavell, K. J.; Murphy, D. M.; Whittlesey, M. K. *Chem. Eur. J.* **2013**, *19*, 2158–2167.

(30) Lavallo, V.; Mafhouz, J.; Canac, Y.; Donnadieu, B.; Schoeller, W. W.; Bertrand, G. *J. Am. Chem. Soc.* **2004**, *126*, 8670–8671.

(31) Lavallo, V.; Canac, Y.; Präsang, C.; Donnadieu, B.; Bertrand, G. *Angew. Chem. Int. Ed.* **2005**, *44*, 5705–5709.

(32) Frey, G. D.; Lavallo, V.; Donnadieu, B.; Schoeller, W. W.; Bertrand, G. *Science* **2007**, *316*, 439–441.

(33) Lavallo, V.; Frey, G. D.; Donnadieu, B.; Soleilhavoup, M.; Bertrand, G. *Angew. Chem. Int. Ed.* **2008**, *47*, 5224–5228.

(34) Anderson, D. R.; Lavallo, V.; O'Leary, D. J.; Bertrand, G.; Grubbs, R. H. *Angew. Chem. Int. Ed.* **2007**, *46*, 7262–7265.

(35) Soleilhavoup, M.; Bertrand, G. *Acc. Chem. Res.* **2015**, *48*, 256–266.

(36) Hudnall, T. W.; Bielawski, C. W. *J. Am. Chem. Soc.* **2009**, *131*, 16039–16041.

(37) Hudnall, T. W.; Moerdyk, J. P.; Bielawski, C. W. *Chem. Commun.* **2010**, *46*, 4288–4290.

(38) Cordero, B.; Gómez, V.; Platero-Prats, A. E.; Revés, M.; Echeverría, J.; Cremades, E.; Barragán, F.; Alvarez, S. *Dalton Trans.* **2008**, 2832–2838.

(39) Moerdyk, J. P.; Bielawski, C. W. *Chem. Eur. J.* **2013**, *19*, 14773–14776.

(40) Lastovickova, D. N.; Bielawski, C. W. *Organometallics* **2016**, *35*, 706–712.

(41) Moerdyk, J. P.; Blake, G. A.; Chase, D. T.; Bielawski, C. W. *J. Am. Chem. Soc.* **2013**, *135*, 18798–18801.

(42) Lastovickova, D. N.; Moerdyk, J. P.; Kelley, A. R.; Bielawski, C. W. *J. Phys. Org. Chem.* **2015**, *28*, 75–78.

(43) Chase, D. T.; Moerdyk, J. P.; Bielawski, C. W. *Org. Lett.* **2014**, *16*, 812–815.

(44) Moerdyk, J. P.; Bielawski, C. W. *J. Am. Chem. Soc.* **2012**, *134*, 6116–6119.

(45) Moerdyk, J. P.; Bielawski, C. W. *Nat. Chem.* **2012**, *4*, 275–280.

(46) Arumugam, K.; Varghese, B.; Brantley, J. N.; Konda, S. S. M.; Lynch, V. M.; Bielawski, C. W. *Eur. J. Org. Chem.* **2014**, *2014*, 493–497.

(47) Braun, M.; Frank, W.; Reiss, G. J.; Ganter, C. *Organometallics* **2010**, *29*, 4418–4420.

(48) Hudnall, T. W.; Tennyson, A. G.; Bielawski, C. W. *Organometallics* **2010**, *29*, 4569–4578.

(49) Poulten, R. C.; López, I.; Llobet, A.; Mahon, M. F.; Whittlesey, M. K. *Inorg. Chem.* **2014**, *53*, 7160–7169.

(50) César, V.; Lugan, N.; Lavigne, G. *Eur. J. Inorg. Chem.* **2010**, *2010*, 361–365.

(51) Tapu, D.; Dixon, D. A.; Roe, C. *Chem. Rev.* **2009**, *109*, 3385–3407.

(52) Moerdyk, J. P.; Bielawski, C. W. *Organometallics* **2011**, *30*, 2278–2284.

(53) Arduengo III, A. J.; Rasika Dias, H. V.; Calabrese, J. C.; Davidson, F. *Organometallics* **1993**, *12*, 3405–3409.

(54) Fraser, P. K.; Woodward, S. *Tetrahedron Lett.* **2001**, *42*, 2747–2749.

(55) Lin, J. C. Y.; Huang, R. T. W.; Lee, C. S.; Bhattacharyya, A.; Hwang, W. S.; Lin, I. J. B. *Chem. Rev.* **2009**, *109*, 3561–3598.

(56) Nolan, S. P.; Marion, N.; Díez-González, S. *Chem. Rev.* **2009**, *109*, 3612–3676.

(57) Lazreg, F.; Nahra, F.; Cazin, C. S. J. *Coord. Chem. Rev.* **2015**, *293-294*, 48–79.

(58) Jurkauskas, V.; Sadighi, J. P.; Buchwald, S. L. *Org. Lett.* **2003**, *5*, 2417–2420.

(59) Kaur, H.; Zinn, F. K.; Stevens, E. D.; Nolan, S. P. *Organometallics* **2004**, *23*, 1157–1160.

(60) Díez-González, S.; Kaur, H.; Zinn, F. K.; Stevens, E. D.; Nolan, S. P. *J. Org. Chem.* **2005**, *70*, 4784–4796.

(61) Lipshutz, B. H.; Noson, K.; Chrisman, W.; Lower, A. *J. Am. Chem. Soc.* **2003**, *125*, 8779–8789.

(62) Issenhuth, J. T.; Dagorne, S.; Bellemin-Laponnaz, S. *Adv. Synth. Catal.* **2006**, *348*, 1991–1994.

(63) Shirobokov, O. G.; Kuzmina, L. G.; Nikonov, G. I. *J. Am. Chem. Soc.* **2011**, *133*, 6487–6489.

(64) Mankad, N. P.; Laitar, D. S.; Sadighi, J. P. *Organometallics* **2004**, *23*, 3369–3371.

(65) Goj, L. A.; Blue, E. D.; Munro-Leighton, C.; Gunnoe, T. B.; Petersen, J. L. *Inorg. Chem.* **2005**, *44*, 8647–8649.

(66) Goj, L. A.; Blue, E. D.; Delp, S. A.; Gunnoe, T. B.; Cundari, T. R.; Pierpont, A. W.; Petersen, J. L.; Boyle, P. D. *Inorg. Chem.* **2006**, *45*, 9032–9045.

(67) Frey, G. D.; Donnadieu, B.; Soleilhavoup, M.; Bertrand, G. *Chem. Asian J.* **2011**, *6*, 402–405.

(68) Jordan, A. J.; Wyss, C. M.; Bacsa, J.; Sadighi, J. P. *Organometallics* **2016**, *35*, 613–616.

CHAPTER TWO

CHAPTER TWO: Neutral and Cationic Diamidocarbene Complexes of Copper

Some of the work in this Chapter has been published in:[1,2]

Copper Diamidocarbene Complexes: Characterization of Monomeric to Tetrameric Species: Collins, L. R.; Lowe, J. P.; Mahon, M. F.; Poulten, R. C.; Whittlesey, M. K. *Inorg. Chem.* **2014**, *53*, 2699 − 2707

Use of Ring-Expanded Diamino- and Diamidocarbene Ligands in Copper Catalyzed Azide−Alkyne "Click" Reactions: Collins, L. R.; Rookes, T. M.; Mahon, M. F.; Riddlestone, I. M.; Whittlesey, M. K. *Organometallics* **2014**, *33*, 5882 − 5887

2.1 Isolation of $(6\text{-MesDAC})_2(CuCl)_n$ Complexes

With the aim of synthesising (6-MesDAC)CuCl, preliminary experiments were conducted between CuCl and 6-MesDAC, produced in-situ from 6-MesDAC·HCl (Scheme 2.1).

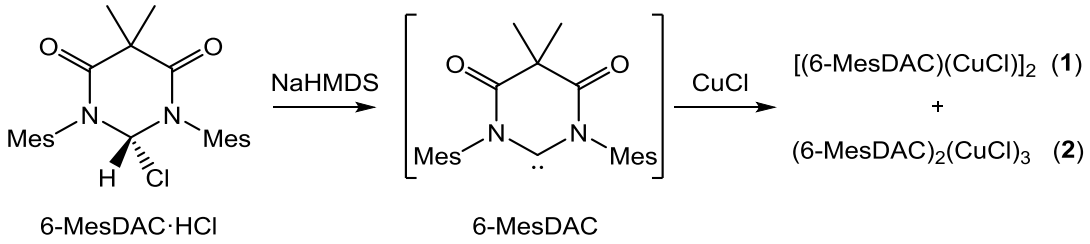

Scheme 2.1: Reaction scheme for the addition of CuCl to in-situ generated 6-MesDAC.

The reaction shown in Scheme 2.1 was first monitored by ^{1}H NMR spectroscopy. This revealed that the reaction between 6-MesDAC and CuCl in THF is complete within seconds at room temperature and that the resultant product is stable in solution. The ^{1}H NMR data were consistent with a product in possession of a single carbene environment. However, the chemical shifts of this set of resonances proved irreproducible between experiments, with peak positions varying over a range of up to 0.07 ppm. Such results suggest that each experiment led to different mixtures of products being formed, and that these products were in a fast exchange regime on the NMR timescale. Upon scaling up this reaction and crystallising the resultant powder, two distinctive types of crystal were evident. Both types were analysed by single crystal X-ray diffraction. The dark red, needle shaped crystals were shown to

be the dimeric complex [(6-MesDAC)(CuCl)]$_2$ (**1**, Figure 2.1). The bright orange, block shaped crystals were found to be (6-MesDAC)$_2$(CuCl)$_3$ (**2**, Figure 2.2). Both complexes were characterised by X-ray crystallography as well as ^{1}H and ^{13}C{^{1}H} NMR and IR spectroscopy. Each displays a single set of NMR resonances (**1** = 6.81; **2** = 6.77 (4 H, s, *m*-ArH) ppm; **1** = 2.22; **2** = 2.15 (6 H, s, *p*-ArCH_3) ppm; **1** = 2.05; **2** = 2.11 (12 H, s, *o*-ArCH_3) ppm; **1** = 1.34; **2** = 1.38 (6 H, s, C(CH_3)$_2$) ppm), consistent with a single 6-MesDAC environment. The N^{13}CN chemical shifts (**1** = 212.7 ppm; **2** = 214.9 ppm) are consistent with other late d-block metal complexes with diamidocarbene ligands.[3–7] Complexes **1** and **2** display identical IR bands for symmetric and asymmetric stretching of 6-MesDAC's two carbonyls. The stretching frequencies of 1740 cm^{-1} and 1717 cm^{-1} are consistent with other metal-bound diamidocarbenes with six-membered rings.[3,4,6] These stretching frequencies are significantly higher than for an amide carbonyl, and more closely resemble data recorded for the diketone 2,2-dimethyl-1,3-cyclohexanedione (1732 cm^{-1} and 1702 cm^{-1}).[8]

2.1.1 Molecular Structures of [(6-MesDAC)(CuCl)]$_2$ (1) and (6-MesDAC)$_2$(CuCl)$_3$ (2)

Concentrated toluene solutions of compounds **1** and **2** layered with hexanes yielded crystals suitable for X-ray diffraction studies. The molecular structure of **1** is shown in Figure 2.1 and the molecular structure of **2** is shown in Figure 2.2. A table of selected bond lengths and angles for both compounds is presented in Table 2.1.

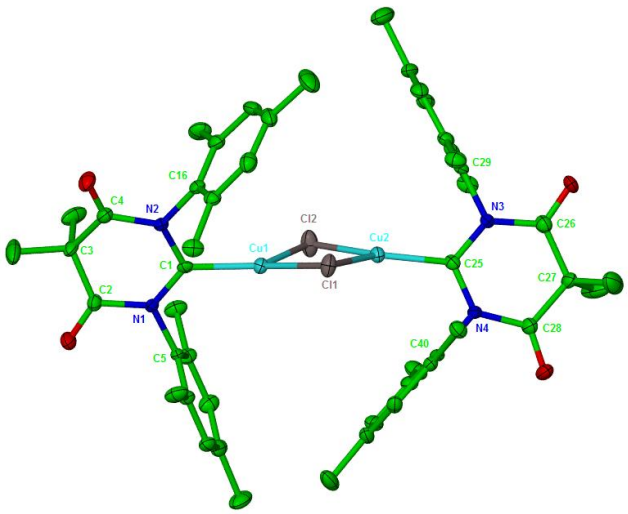

Figure 2.1: Displacement ellipsoid plot (30 % probability) of [(6-MesDAC)(CuCl)]$_2$ (**1**). H atoms omitted for clarity. Selected bond lengths (Å) and angles (°): Cu(1)-C(1) 1.871(5), Cu(1)-Cl(1) 2.2650(17), Cu(1)-Cl(2) 2.3001(17), Cu(2)-C(25) 1.867(5), Cu(2)-Cl(2) 2.2548(17), Cu(2)-Cl(1) 2.2936(16), N(1)-C(1)-N(2) 116.7(4), C(1)-Cu(1)-Cl(1) 132.65(17), C(1)-Cu(1)-Cl(2) 126.72(16), Cl(1)-Cu(1)-Cl(2) 99.31(6), N(3)-C(25)-N(4) 116.3(4), C(25)-Cu(2)-Cl(1) 124.70(17), C(25)-Cu(2)-Cl(2) 135.16(17), Cl(1)-Cu(2)-Cl(2) 99.80(6).

Complex **1** consists of an approximately planar (CuCl)$_2$ core in which the two carbenes are canted relative to each other with a dihedral angle between the NCN planes of 40.7°. Both Cu(1) and Cu(2) are trigonal planar in geometry. Of the four Cu-Cl bonds, one pair (Cu(1)-Cl(2) and Cu(2)-Cl(1) = average length of 2.296 Å) is approximately 0.04 Å longer than the other (Cu(1)-Cl(1) and Cu(2)-Cl(2) = average length of 2.260 Å), resulting in a rectangular structure. The Cu-C bond lengths (1.867(5) Å and 1.871(5) Å) are shorter than related dimeric [(NHC)CuCl]$_2$ complexes in the literature.[9,10] They are even on the short side of reported monomeric, two-coordinate (NHC)CuCl complexes (the shortest being (IPr)CuCl with a Cu-C bond length of 1.881(7) Å).[11–13]

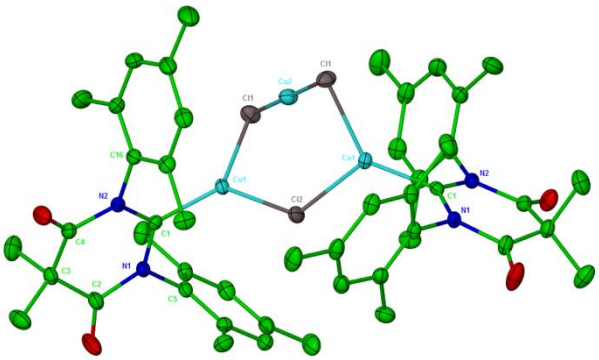

Figure 2.2: Displacement ellipsoid plot (30 % probability) of $(6\text{-MesDAC})_2(CuCl)_3$ (**2**). H atoms omitted for clarity. Selected bond lengths (Å) and angles (°): Cu(1)-C(1) 1.8860(18), Cu(1)-Cl(1) 2.2729(6), Cu(1)-Cl(2) 2.2948(4), Cu(1)-Cu(2) 2.8136(3), Cu(2)-Cl(1) 2.1372(5), N(1)-C(1)-N(2) 117.16(16), C(1)-Cu(1)-Cl(1) 134.40(5), C(1)-Cu(1)-Cl(2) 119.64(6), Cl(1)-Cu(1)-Cl(2) 105.93(2), Cl(1)-Cu(2)-Cl(1') 179.75(3). Symmetry transformations used to generate equivalent atoms: (-x+1, y, -z+3/2).

Complex **2** consists of a $(CuCl)_3$ core of unprecedented geometry.[14] Cu(2) and Cl(2) lie on a twofold rotational axis. Of the two equivalent Cl(1)s, one is situated above and one below the plane of Cu(1), Cu(2) and Cl(2), each on the opposite side of the plane to their proximal carbene. This structure contains two distinct copper environments. Cu(1) is trigonal planar, bound by a carbene and two chlorides, as in complex **1**. Indeed, as shown in Table 2.1, the bonds common to the two structures show no significant difference in length. Cu(2), however, is not ligated by a carbene but instead lies solely between two chlorides in a trans-linear geometry (Cl(1)-Cu(2)-Cl(1') = 179.75(3)°). The Cu(2)-Cl bonds are significantly shorter (by approximately 0.15 Å) than the Cu(1)-Cl bonds, consistent with other linear, unligated $CuCl_2$ moieties found in copper chloride clusters.[14] Furthermore, a weak metal-metal bonding interaction appears to exist based on the Cu(1)-Cu(2) distance of 2.8136(3) Å being less than double the covalent radius of copper (1.32(4) Å).[15]

Parameter	1	2
Cu(1)-C(1)	1.871(5)	1.8860(18)
Cu(1)-Cl(1)	2.2650(17)	2.2729(6)
Cu(1)-Cl(2)	2.3001(17)	2.2948(4)
Cu(2)-Cl(1)	---	2.1372(5)
Cl(1)-Cu(1)-Cl(2)	99.31(6)	105.93(2)

Table 2.1: Selected bond lengths (Å) and angles (°) for compounds **1** and **2**.

Neither complex is the expected monomeric (6-MesDAC)CuCl. This is surprising, given the examples of NHCs with much smaller steric bulk supporting monomeric copper halide complexes in the literature, such as the five-membered NHC complex (IMes)CuCl.[13] A possible explanation for the dimeric nature of **1** could be the enhanced electrophilicity of a diamidocarbene compared to a diaminocarbene. In a hypothetical monomeric (6-MesDAC)CuCl, the electron accepting (6-MesDAC-Cu)$^{\delta+}$ fragment would readily accept the electron density of a (Cl)$^{\delta-}$ from a neighbouring monomeric unit in a Lewis acid - Lewis base interaction. A dimeric $(CuCl)_2$ unit would thus be formed. One could even attribute the rectangular geometry of **1** to this inequality in bonding character.

2.2 Solution Phase Studies

NMR analysis of crystalline samples of both complexes gave reproducible ^{1}H NMR spectra (Figure 2.3). Complexes **1** and **2** clearly exist as independent complexes with unique chemical environments and do not simply dissociate to monomeric [(6-MesDAC)(CuCl)] in solution. However, mixtures of the two complexes produce ^{1}H NMR spectra with chemical shifts intermediate between the two clean crystalline samples (Figure 2.3, middle spectrum). Addition of CuCl to **1** generates **2**, and addition of 6-MesDAC to **2** generates **1**. To probe a potential dynamic exchange process, variable temperature NMR studies were conducted. A 1:1 mixture of **1** and **2** was dissolved in C_7D_8 and cooled at regular intervals. However, even at 180 K, no change was observed in the ^{1}H NMR spectrum.

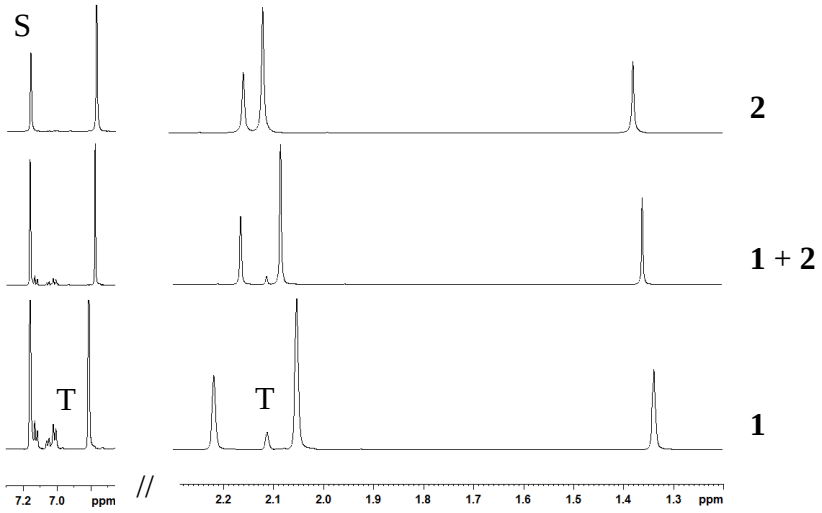

Figure 2.3: ^{1}H NMR spectra (500 MHz, C_6D_6, 298 K) of complex **2** (top), an equimolar mixture of complexes **1** and **2** (middle), and complex **1** (bottom). All samples were prepared from crystalline samples of **1** and **2**. S denotes residual C_6D_5H. T denotes toluene liberated from the crystalline samples of **1**.

To understand more about the complexes' nuclearity in solution, DOSY NMR experiments were conducted and the resultant hydrodynamic radii (r_H) compared to their solid state radii ($r_{X\text{-}ray}$). These results are presented in Table 2.2.

Complex	$\mathbf{r_H}$	$\mathbf{r_{X\text{-}ray}}$
1	5.3	5.9
2	6.1	6.0

Table 2.2: Hydrodynamic and solid state radii (Å) for compounds **1** and **2**. Hydrodynamic radii calculated from ^{1}H NMR DOSY experiments in C_7D_8. See Appendix for details. Values of $r_{X\text{-}ray}$ calculated from molar volumes derived using the CPK model approximation in Spartan 14.[16]

For complex **2**, r_H and $r_{X\text{-}ray}$ (6.1 Å and 6.0 Å, respectively) are in very good agreement, which indicates that the trimeric structure of **2** is maintained in solution. For complex **1**, r_H (5.3 Å) is markedly lower than for complex **2**, despite very similar solid state radii. Whilst many approximations are made in obtaining values of r_H, this does provide some evidence to suggest that **1** is more prone to dissociation

in solution.[i] Further evidence for this behaviour was obtained by recrystallising complex **1** from Et_2O at 238 K. The resultant red crystals were analysed by X-ray crystallography and found to consist of a 1 : 1 mixture of complex **1** and the monomer [(6-MesDAC)(CuCl)] (**3**, Figure 2.4). Whilst this is clear evidence for the viability of a monomeric species in the solid state, crystalline samples of **1**·**3** became indistinguishable from crystalline samples of complex **1** upon dissolution in benzene or toluene, as evidenced by identical ^{1}H NMR chemical shifts and DOSY diffusion coefficients.

2.2.1 Molecular Structure of [(6-MesDAC)(CuCl)]$_2$·[(6-MesDAC)(CuCl)] (1·3)

A concentrated Et_2O solution of compound **1** was slowly evaporated at 238 K, yielding crystals suitable for X-ray diffraction studies. The molecular structure of **1**·**3** is shown in Figure 2.4.

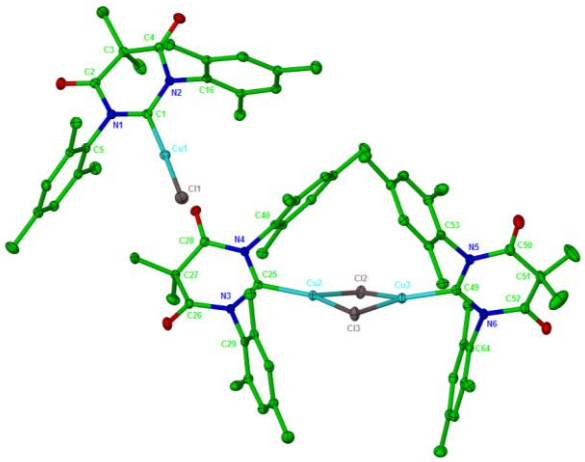

Figure 2.4: Displacement ellipsoid plot (30 % probability) of [(6-MesDAC)(CuCl)]$_2$·[(6-MesDAC)(CuCl)] (**1**·**3**). H atoms omitted for clarity. Selected bond lengths (Å) and angles (°): Cu(1)−C(1) 1.886(2), Cu(1)−Cl(1) 2.1150(7), Cu(2)−C(25) 1.885(2), Cu(2)−Cl(2) 2.3139(7), Cu(2)−Cl(3) 2.2974(7), Cu(3)−C(49) 1.875(2), Cu(3)−Cl(2) 2.2745(7), Cu(3)−Cl(3) 2.2906(7), N(1)-C(1)-

[i] Hydrodynamic radii (r_H) were calculated using the Stokes-Einstein equation ($D = (K_BT)/(6\pi\eta r_H)$) which assumes the diffusion of spherical, non-interacting particles in a homogeneous solvent which is itself not subject to bulk diffusion. Attempts were made to ensure homogeneity by careful choice of solute concentrations. A double stimulated echo pulse sequence was employed to correct for thermal convection within the NMR tube. However, complexes **1** and **2** inevitably experience intermolecular forces in solution, and as shown by their solid state structures, are not spherical.

N(2) 116.9(2), C(1)−Cu(1)−Cl(1) 173.46(8), N(3)-C(25)-N(4) 116.3(2), C(25)-Cu(2)-Cl(2) 130.41(7), C(25)-Cu(2)-Cl(3) 133.77(7), Cl(2)−Cu(2)−Cl(3) 95.79(2), N(5)-C(49)-N(6) 117.0(2), C(49)-Cu(3)-Cl(2) 133.15(8), C(49)-Cu(3)-Cl(3) 129.64(8), Cl(2)-Cu(3)-Cl(3) 97.08(2).

The structure in Figure 2.4 comprises one monomeric [(6-MesDAC)(CuCl)] and one dimeric $[(6\text{-MesDAC})(CuCl)]_2$. The metrics of the carbenes in the dimeric unit are similar to those of **1** in Figure 2.1 with no significant differences in N-C-N angles or C-Cu bond lengths. The $(CuCl)_2$ core is slightly distorted from the rectangular geometry of **1**, with more acute Cl-Cu-Cl angles (**1**·**3** = 95.79(2)° and 97.08(2)°; **1** = 99.31(6)° and 99.80(6)°) and on average, longer Cu-Cl bond lengths (**1**·**3** = average of 2.2941(7) Å; **1** = average of 2.2784(17) Å). The monomeric unit shows no difference in its Cu-C bond length to either **1** or **2**, but has a much shorter Cu-Cl bond length (2.1150(7) Å; similar to that in the sterically demanding (IAd)CuCl = 2.1114(6) Å),[13] reflecting the stability of trans-linear geometry (173.46(8)°) about d^{10} copper, as well as the non-bridging nature of the chloride.

2.3 Isolation of $(6\text{-MesDAC})_2(CuCl)_4$ (4)

Analysis of the structures of **1** and **2** led to the design of selective syntheses for these complexes. Firstly, 6-MesDAC was isolated in multigram quantities,[17] and then reacted in controlled stoichiometries with CuCl (Scheme 2.2). In a 1 : 1 stoichiometry, a red solution was immediately formed, and upon crystallisation of the resultant powder, solely red, needle shaped crystals of **1** were isolated in 69 % yield. With a 2 : 3 stoichiometry, an orange solution was formed and crystallisation of the resultant product yielded orange, block shaped crystals of **2** in 84 % yield. These complexes could be quantitatively interconverted by addition of either CuCl to **1** or 6-MesDAC to **2**.

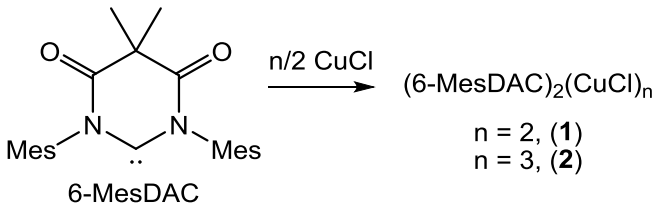

Scheme 2.2: Reaction scheme for the controlled syntheses of complexes **1** and **2**.

Remarkably, when the reaction shown in Scheme 2.2 was conducted with an excess of CuCl, a further product could be isolated. With a 5 : 1 excess of CuCl to 6-MesDAC, an orange solution formed immediately. Crystallisation of the resultant product gave a mixture of crystals. Orange, block shaped crystals of **2** were the predominant product, but a small number of brown crystals were also isolated (3 % yield). Analysis by single crystal X-ray diffraction revealed this minor product to be $(6\text{-MesDAC})_2(CuCl)_4$ (**4**, Figure 2.5). Complex **4** proved to be unstable in benzene solution, precipitating a pale powder (presumably CuCl) and leaving a mixture of **1** and **2** in solution (as evidenced by NMR spectra as described in Section 2.2), precluding its solution phase characterisation. IR spectra (KBr disc) revealed similar carbonyl stretching frequencies (1743 cm^{-1} and 1719 cm^{-1}) to those of **1** and **2**.

2.3.1 Molecular Structure of $(6\text{-MesDAC})_2(CuCl)_4$ (4)

A concentrated toluene solution of **2** in the presence of excess CuCl, layered with hexanes, precipitated crystals of **4** suitable for X-ray diffraction studies. The molecular structure of **4** is shown in Figure 2.5. Table 2.3 gives selected bond lengths and angles for compound **4**.

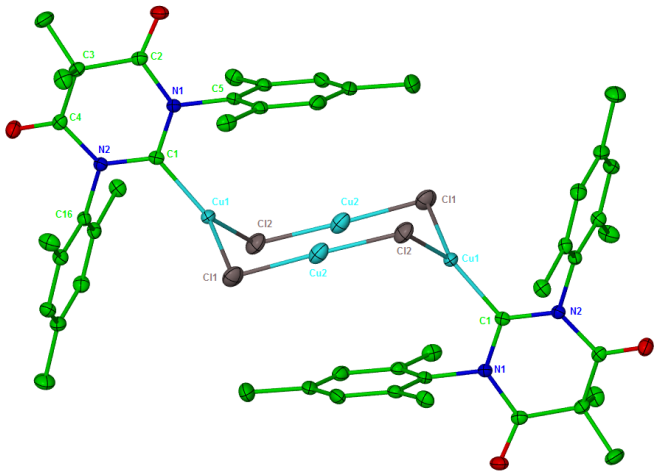

Figure 2.5: Displacement ellipsoid plot (30 % probability) of (6-MesDAC)$_2$(CuCl)$_4$ (**4**). H atoms omitted for clarity. Selected bond lengths (Å) and angles (°): Cu(1)-C(1) 1.886(2), Cu(1)-Cl(1) 2.2735(7), Cu(1)-Cl(2) 2.2911(7), Cu(2)-Cl(1) 2.1187(8), Cu(2)-Cl(2) 2.1145(8), N(1)-C(1)-N(2) 116.79(17), C(1)-Cu(1)-Cl(1) 125.33(6), C(1)-Cu(1)-Cl(2') 127.49(6), Cl(1)-Cu(1)-Cl(2') 107.15(3), Cl(1)-Cu(2)-Cl(2) 171.38(3). Symmetry transformations used to generate equivalent atoms: (-x+1, -y, -z+2).

Complex **4** consists of a (CuCl)$_4$ core in a pseudo-chair conformation. This complex is the first example of such a structure supported by two monodentate ligands, although derivatives stabilised by bipyridyl,[18] (1H-pyrazol-1-yl)pyridine,[19] and N-SHC ligands are known.[14,20] Two copper environments are present in this centrosymmetric structure. Cu(1) is bound by one carbene and two chlorides in a trigonal planar geometry, with no significant difference in bond lengths to complexes **1** or **2** (Table 2.3). Cu(2) is not ligated by a carbene, but by two chlorides in a trans-linear geometry (Cl(1)-Cu(2)-Cl(2) = 171.38(3)°). Similarly to complex **2**, the Cu(2)-Cl bonds are significantly shorter than either of the Cu(1)-Cl bonds.

Parameter	2	4
Cu(1)-C(1)	1.886(2)	1.886(2)
Cu(1)-Cl(1)	2.2729(6)	2.2735(7)
Cu(1)-Cl(2)	2.2948(4)	2.2911(7)
Cu(2)-Cl(1)	2.1372(5)	2.1187(8)
Cl(1)-Cu(1)-Cl(2)	105.93(2)	107.15(3)

Table 2.3: Selected bond lengths (Å) and angles (°) for compound **4**. Data for compound **2** is included for comparison.

2.4 Isolation of $[(6\text{-MesDAC})_2Cu][PF_6]$ (5)

Mixtures of **1** and **2** are also obtained as the major products when in-situ generated 6-MesDAC is reacted with $[Cu(MeCN)_4][PF_6]$ in the same reaction vessel. If 6-MesDAC is generated in-situ in THF, and then filtered into a new vessel containing $[Cu(MeCN)_4][PF_6]$, only small amounts of **1** and **2** are formed. Once these have been extracted into toluene and removed by filtration, a large amount of pale green precipitate remains, which may be extracted into CH_2Cl_2 and isolated by filtration. Analysis by X-ray crystallography showed this new product to be the cationic, homoleptic bis-carbene complex $[(6\text{-MesDAC})_2Cu][PF_6]$ (**5**, Figure 2.6). In-situ generation of NHCs has been shown to result in mixtures of neutral (NHC)CuX and cationic $[(NHC)_2Cu][X]$ species in previous studies.[13] As expected, **5** may also be prepared as the only copper containing product by reaction of isolated 6-MesDAC with $[Cu(MeCN)_4][PF_6]$ under conditions free of chloride (Scheme 2.3). Complex **5** was fully characterised in CD_2Cl_2 solution (owing to its exclusive solubility in highly polar solvents) and the solid state. Its carbenic carbon resonance was located by $^{13}C\{^1H\}$ NMR spectroscopy at 213.0 ppm at an almost identical chemical shift to those of complexes **1** and **2**. In the IR spectrum, the carbonyl bands of **5** appear at 1768 cm^{-1} and 1738 cm^{-1}, approximately 25 cm^{-1} higher in frequency than for the copper chloride complexes.

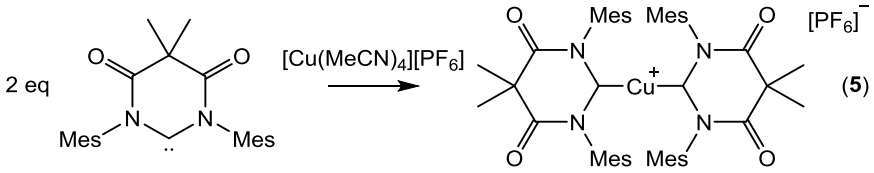

Scheme 2.3: Reaction scheme for the selective formation of $[(6\text{-MesDAC})_2Cu][PF_6]$ (**5**).

2.4.1 Molecular Structure of $[(6\text{-MesDAC})_2Cu][PF_6]$ (5)

A concentrated dichloromethane solution of compound **5** layered with hexanes yielded crystals suitable for X-ray diffraction studies. The molecular structure of the cation in **5** is shown in Figure 2.6.

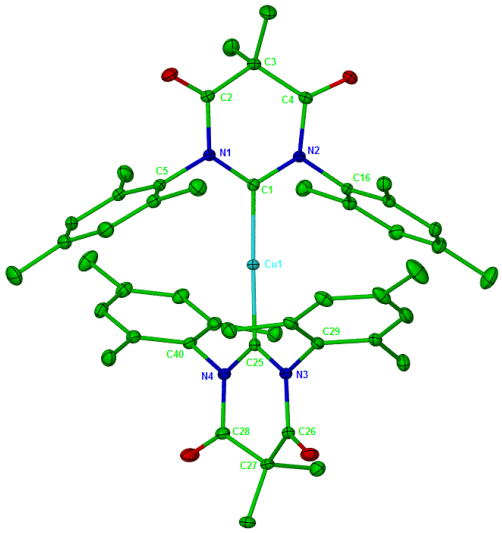

Figure 2.6: Displacement ellipsoid plot (30 % probability) of $[(6\text{-MesDAC})_2Cu][PF_6]$ (**5**). H atoms and counterion omitted for clarity. Selected bond lengths (Å) and angles (°): Cu(1)-C(1) 1.927(2), Cu(1)-C(25) 1.926(2), N(1)-C(1)-N(2) 117.59(18), C(1)-Cu(1)-C(25) 178.39(9), N(3)-C(25)-N(4) 117.41(18).

Complex **5** consists of two carbenes in a trans-linear geometry about Cu(1) (C(1)-Cu(1)-C(25) = 178.39(9)°). The Cu-C bond lengths of **5** (1.927(2) Å) are significantly longer (by approximately 0.04 Å) than those found in the copper chloride complexes **1**, **2**, **3** and **4**. This is perhaps in part due to steric repulsion of the bulky mesityl substituents, despite the ligands' almost orthogonal relationship (dihedral angle between the NCN planes = 71°). The less sterically demanding

$[(IMes)_2Cu][PF_6]$ has an inter-ligand torsion angle of 67.05° and shorter Cu-C bond lengths of 1.871(3) Å.[21]

2.5 Catalytic Potential of Diamidocarbenes: A Comparison with Diaminocarbenes for the Copper Catalysed Cycloaddition of Azides and Terminal Alkynes

The copper catalysed [2+3] cycloaddition of terminal alkynes and azides (CuAAC) represents the best known and most commonly utilised example of 'Click' chemistry.[22] 'Click' reactions are operationally simple, useful in the modular construction of a broad range of products, conducted neat or in environmentally benign solvents and with no need for reagents or products to be purified by chromatography. CuAAC represents a significant advantage over thermal Huisgen cycloaddition by selectively forming the 1,4-substituted isomer and operating at room temperature (Scheme 2.4).[23]

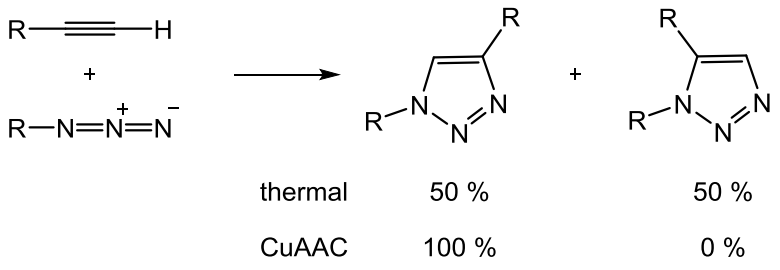

Scheme 2.4: Reaction scheme for the cycloaddition of azides and terminal alkynes showing typical product distributions under thermal and copper catalysed conditions.

Very simple copper salts are successful precatalysts for CuAAC under 'Click' conditions, for example, $CuSO_4 \cdot 5H_2O$ in the presence of ascorbic acid generates a successful copper(I) catalyst.[24] Amongst the ligands used to control and enhance CuAAC reactivity, NHCs have been some of the most successful.[25] (NHC)Cu(halide) and $[(NHC)_2Cu]^+$ complexes were first shown to be successful catalysts by Nolan and co-workers.[26] Despite a vast range of NHCs being explored in the literature,[13,27] no RENHCs or DACs have been used for CuAAC. A range of RENHC complexes were thus synthesised and, together with the 6-MesDAC complexes described above, investigated as precatalysts for CuAAC under 'Click' conditions.

2.6 Isolation of $[(6\text{-MesDAC})_2Cu][BF_4]$ (6), $[(6\text{-Mes})_2Cu][BF_4]$ (7), $[(7\text{-Mes})_2Cu][BF_4]$ (8) and $[(7\text{-}o\text{-Tol})_2Cu][BF_4]$ (9)

Three cationic, homoleptic RENHC copper complexes ($[(6\text{-Mes})_2Cu][BF_4]$ (**7**), $[(7\text{-Mes})_2Cu][BF_4]$ (**8**) and $[(7\text{-}o\text{-Tol})_2Cu][BF_4]$ (**9**)) were synthesised in an analogous manner to **5** by combination of $[Cu(MeCN)_4][BF_4]$ with the respective free carbenes. The $[(6\text{-Mes})_2Cu]^+$ cation (although with a mixed occupancy $[Cu(halide)_2]^-$ counterion) was reported by Buchmeiser in 2005, synthesised from in-situ generated 6-Mes.[28] 7-*o*-Tol was generated in-situ in the presence of $[Cu(MeCN)_4][BF_4]$ to circumvent known difficulties in carbene isolation.[29] $[(6\text{-MesDAC})_2Cu][BF_4]$ (**6**) was also synthesised for direct comparison to the other systems with a tetrafluoroborate anion. The $[BF_4]^-$ anion was chosen due to its apparent better performance in catalysis compared to $[PF_6]^-$.[27] All reactions proceeded at room temperature in THF with precipitation of the desired products as colourless solids. Reaction yields decreased with increasing steric bulk of the NHCs (**7** (6-Mes) = 79 %; **9** (7-*o*-Tol) = 48 %; **8** (7-Mes) = 17 %) although the yield could be increased by raising the reaction temperature (yield of **8** increased from 17 % at 298 K to 25 % at 323 K). These cationic complexes all proved to be very similar to **5** in being air and water stable, soluble in CH_2Cl_2 and chloroform, and readily crystallised from CH_2Cl_2/hexane. The carbenic $^{13}C\{^1H\}$ NMR signals shift downfield as ring size increases (**7** (6-Mes) = 199.3 ppm; **8** (7-Mes) = 208.6 ppm) but in all cases, resonate upfield of the diamidocarbene complexes (**5** and **6** (6-MesDAC) = 213.0 ppm).[30,31] Measurement of the carbenic carbon signal for complex **9** was complicated by the presence of what may be different rotameric isomers of **9**, resulting from different orientations of the tolyl methyl groups (Figure 2.7).

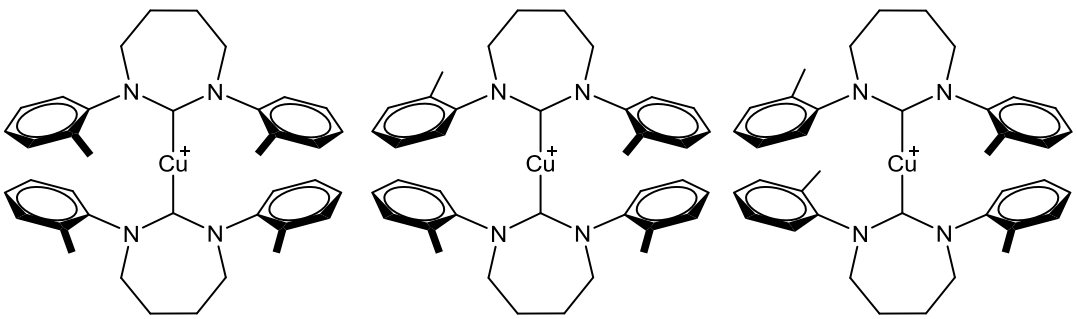

Figure 2.7: Possible rotameric forms of $[(7\text{-}o\text{-Tol})_2Cu][BF_4]$ (**9**): Syn-syn (left), syn-anti (centre), anti-anti (right).

Variable temperature NMR studies were conducted but, even at 204 K, no distinction could be made between the species in solution (Figure 2.8). A $^{13}C\{^{1}H\}$ NMR spectrum could be recorded at 224 K, with the observation of two carbenic carbon resonances at 207.2 (major) and 206.6 (minor) ppm, each consistent with a copper co-ordinated seven-membered RENHC.

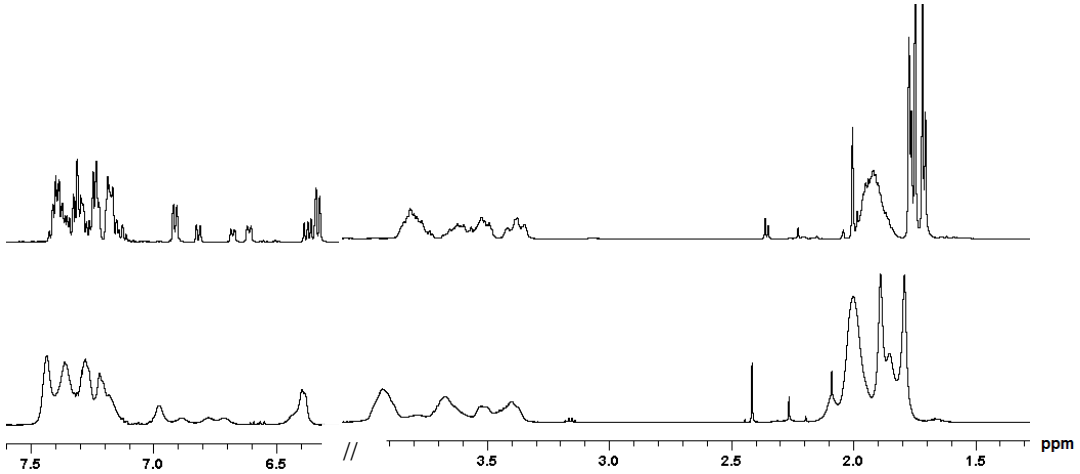

Figure 2.8: ^{1}H NMR spectra (500 MHz, CD_2Cl_2) of complex **9** recorded at 204 K (top) and 298 K (bottom).

2.6.1 Molecular Structures of [(6-Mes)$_2$Cu][BF$_4$] (7), [(7-Mes)$_2$Cu][BF$_4$] (8) and [(7-*o*-Tol)$_2$Cu][BF$_4$] (9)

Concentrated dichloromethane solutions of **7**, **8** and **9** layered with hexanes precipitated crystals suitable for X-ray diffraction studies and the molecular structures of the cations are shown in Figure 2.9. The SambVca program was used to determine $\%V_{Bur}$ values for each of these complexes,[32] and these are presented with selected bond lengths and angles in Table 2.4, alongside values for complex **5** for comparison.

Parameter	5	7	8	9
Cu-C	1.927(2); 1.926(2)	1.927(2)	1.954(2); 1.944(2)	1.910(5); 1.905(5)
N-C-N	117.5(3); 117.4(2)	117.3(2)	118.5(2); 118.5(2)	118.3(4); 117.7(5)
C-Cu-C	178.4(1)	178.9(1)	179.1(1)	173.3(2)
N-C-Cu-C-N	71	72	88	84
$\%V_{Bur}$	41.8; 41.6	41.2; 41.2	41.9; 42.4	40.8; 41.4

Table 2.4: Selected bond lengths (Å), angles (°) and $\%V_{Bur}$ for compounds **5**, **7**, **8** and **9**.[i]

Complexes **7**, **8** and **9** each consist of two carbenes in a trans-linear geometry about a central copper atom. Analysis of the bond lengths and angles (Table 2.4) reveals several trends when comparing complexes **5**, **7**, **8** and **9**. The diamino- and diamidocarbenes 6-Mes and 6-MesDAC have very similar steric demands, as evidenced by the identical metrics of complexes **5** and **7**. The slightly larger $\%V_{Bur}$ values for 6-MesDAC are due to the greater steric bulk of its functionalised backbone compared to the saturated backbone of 6-Mes, but this has no significant influence on the steric environment around the carbenic carbon. 7-Mes, with its wider NCN angle (118.5(2)°; cf: complex **7** (6-Mes) = 117.3(2)°), exerts a greater steric effect than the six-membered ring carbenes. This can be observed in its longer Cu-C bond lengths (1.954(2) Å and 1.944(2) Å; cf: complex **7** (6-Mes) = 1.927(2) Å), despite the greater σ-donor strength of 7-Mes compared to 6-Mes.[30] Furthermore, the two NHCs in complex **8** orient themselves such that their NCN planes are almost perpendicular to relieve some of this steric repulsion. Even though 7-*o*-Tol consists of a seven-membered ring with a wide NCN angle (118.3(4)° and 117.7(5)°), the smaller N-aryl substituents make this the smallest of the four NHCs, with the shortest Cu-C bonds and adopting the least trans-linear geometry of all the complexes.

[i] $\%V_{Bur}$ values were calculated using the Samb*V*ca program with a sphere radius of 3.5 Å and a Cu-C bond length of 1.9 Å.[32]

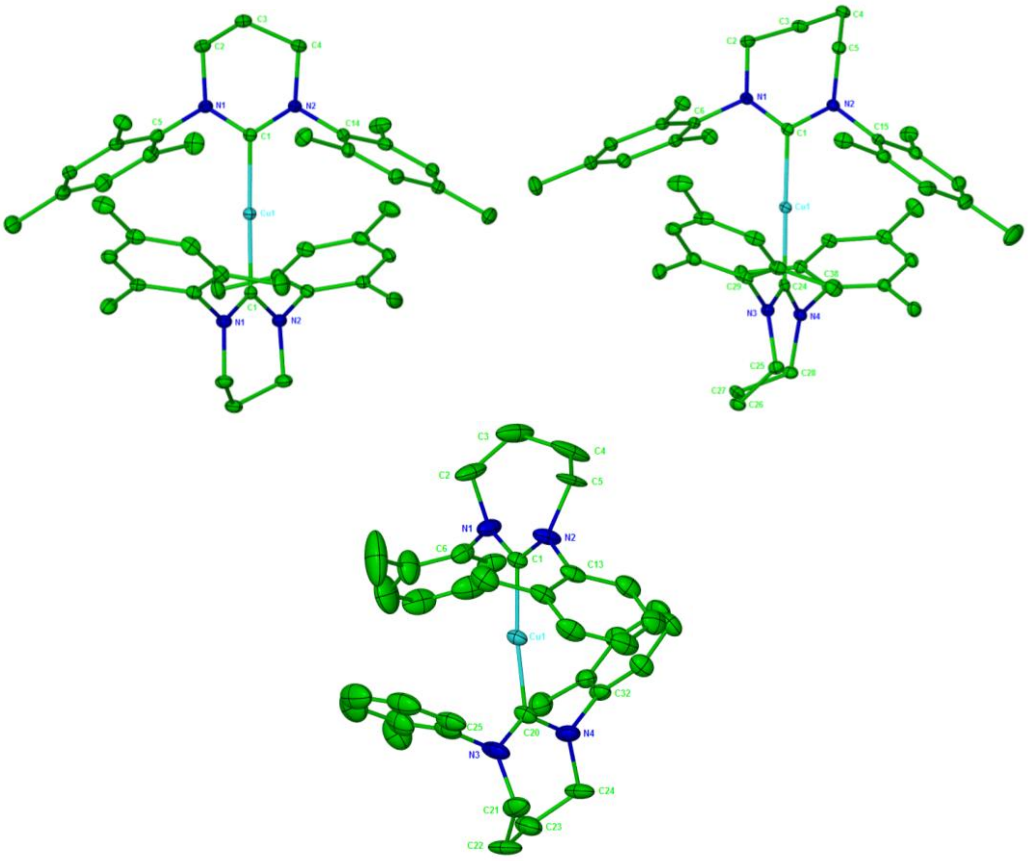

Figure 2.9: Displacement ellipsoid plots (30 % probability) of [(6-Mes)$_2$Cu][BF$_4$] (**7**), [(7-Mes)$_2$Cu][BF$_4$] (**8**) and [(7-*o*-Tol)$_2$Cu][BF$_4$] (**9**, syn-syn conformer). H atoms and counterions omitted for clarity. Selected bond lengths (Å) and angles (°):

Complex **7**: Cu(1)-C(1) 1.9266(19), N(1)-C(1)-N(2) 117.29(17), C(1)-Cu(1)-C(1') 178.93(12). Symmetry transformations used to generate equivalent atoms: (-x+1, y, -z+3/2).

Complex **8**: Cu(1)-C(1) 1.9540(19), Cu(1)-C(24) 1.9436(19), N(1)-C(1)-N(2) 118.48(17), C(1)-Cu(1)-C(24) 179.12(9), N(3)-C(24)-N(4) 118.47(17).

Complex **9**: Cu(1)-C(1) 1.910(5), Cu(1)-C(20) 1.905(5), N(1)-C(1)-N(2) 118.3(4), C(1)-Cu(1)-C(20) 173.3(2), N(3)-C(20)-N(4) 117.7(5).

2.7 Catalyst Screening for CuAAC Under 'Click' Conditions

A preliminary catalytic study was conducted to assess whether the enhanced steric bulk and basicity of RENHCs or the greater electrophilicity of DACs have any benefits in promoting cuprous catalytic activity compared to five-membered NHCs. Complexes **1**, **2** and **5** - **9** were evaluated under neat conditions using the model

system of benzylazide and phenylacetylene (Scheme 2.5). The results are summarised in Table 2.5.

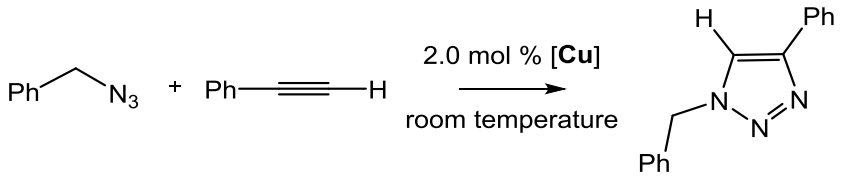

Scheme 2.5: Model system used for catalyst screening. Reactions were conducted without solvent, or 'on water'.

Disappointingly, very low conversions were observed for all 6-MesDAC complexes. The RENHC complexes were more effective catalysts, with the seven membered ring carbenes performing better than 6-Mes. Lowering the catalyst loading for these successful catalysts revealed that complex **9** (7-*o*-Tol) is the most active system. This activity compares favourably to the two most active five-membered NHC systems: $[(ICy)_2Cu][PF_6]$ (99 % conversion in 1.5 hours, on water) and $[(IAd)_2Cu][BF_4]$ (100 % conversion in 3 hours, on water).[27]

Complex	Conversion (%)	
	Neat	On-Water
1	2	100 (13)
2	5	100 (30)
5	<1	91
6	<1	95 (8)
7	98 (18)	56
8	>99 (59)	>99
9	100 (98)	76

Table 2.5: Results of catalyst screening. Conditions: azide (0.50 mmol), alkyne (0.51 mmol), H_2O (0 or 0.5 mL), Cu precursor (2 mol %), 180 minutes. Conditions for results in parentheses: azide (0.50 mmol), alkyne (0.51 mmol), Cu precursor (0.5 mol %), 45 minutes. Conversions were determined by ^1H NMR spectroscopy as an average of three runs.

When the conditions of catalysis were changed to be performed 'on-water', both of the seven-membered NHC systems were again more active than the 6-Mes system, with **8** (7-Mes) now the most successful catalyst. Remarkably, the 6-MesDAC systems showed a dramatic rate enhancement when used 'on-water', with complexes **1** and **2** achieving 100 % conversion within 3 hours. We are unaware of any other Cu-NHC catalyst where the effect of water is so apparent. Reducing the diamidocarbene catalyst loadings to 0.5 mol % showed that complex **2** was the most successful catalyst. However for this model system, complex **9** under neat conditions is still a better catalyst than **2** under 'on-water' conditions.

2.7.1 Substrate Scope

Having found two successful catalysts, one containing a diamidocarbene (**2**) and one with a ring expanded diaminocarbene (**9**), the substrate scope of these systems was expanded to a range of alkynes with either benzyl- or hexylazide (Figure 2.10). No attempts were made to optimise the reaction conditions, with all reactions conducted under identical conditions to allow discrimination between activities. In general, conversions were poor, although the high activities of complex **2** towards Me_2NCH_2CCH and of complex **9** in reactions of PhCCH with either azide stand out.

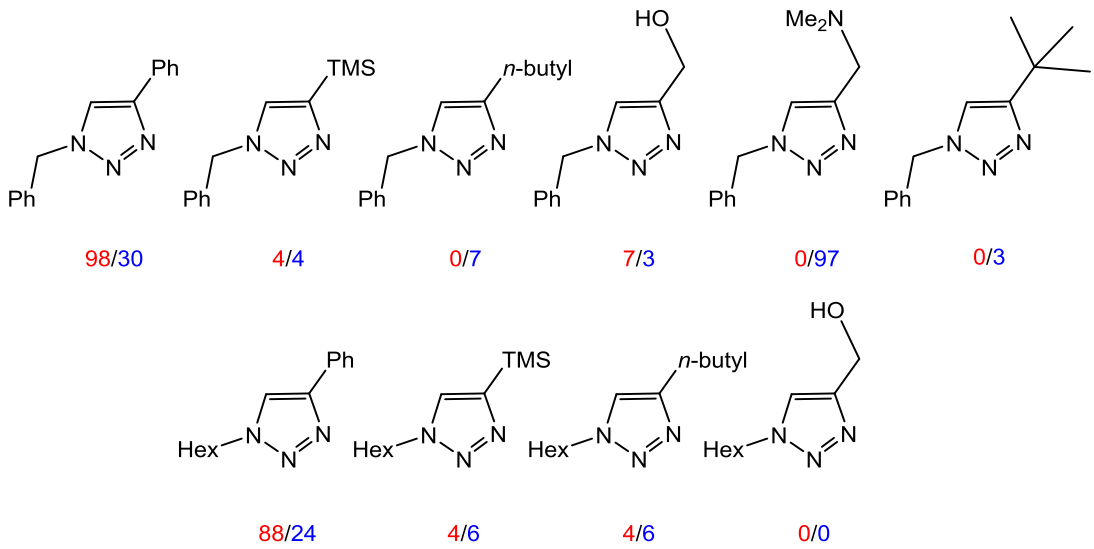

Figure 2.10: Substrate screening (0.50 mmol azide, 0.51 mmol alkyne, 0.5 mol % of Cu precursor, 45 minutes) with complex **9** under neat conditions (percentage conversions in red) and with complex **2** on 0.5 mL of water (percentage conversions in blue).

2.7.2 Comparison of Catalytic Activity

This catalytic study was conducted to determine whether RENHCs or DACs have any advantage over five-membered ring NHCs for CuAAC. The RENHC complexes **7**-**9** show good activity for CuAAC under neat conditions, comparable to their five-membered counterparts. Complex **9** is the most active towards the model system of phenyl acetylene and benzyl azide, with its activity (98 % conversion, 0.5 mol %, 45 minutes) comparable to the state-of-the-art in the literature ($[(ICy)_2Cu][PF_6]$ (Figure 2.11) = 99 % conversion, 0.5 mol%, 5 minutes).[27] However the RENHC complex **9** shows a very limited substrate scope, in contrast to the broadly successful five-membered ring systems.

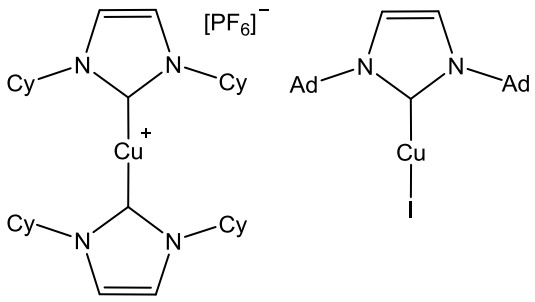

Figure 2.11: Literature examples of successful catalysts for CuAAC: $[(ICy)_2Cu][PF_6]$ (left), (IAd)CuI (right).

The DAC complexes **1**, **2**, **5** and **6** show almost no activity under neat conditions. However, when conducted 'on-water', the complexes are all successful catalysts. To our knowledge, this is the only example of such a water-induced rate enhancement in CuAAC chemistry. The most active DAC system is the trimeric copper chloride complex **2**. Whilst active ('on-water' conditions, 30 % conversion, 0.5 mol %, 45 minutes), this complex is less active than the RENHC complexes, and compares poorly to the most active copper halide complexes in the literature ((IAd)CuI (Figure 2.11): neat conditions, 99 % conversion, 0.8 mol %, 10 mins).[13]

2.7.3 Mechanism of CuAAC

This study was conducted as a preliminary assessment of the utility of RENHCs and DACs in CuAAC catalysis. However, the results also raise some important mechanistic questions. In 2008, Nolan proposed a catalytic pathway (Scheme 2.6) in which carbene dissociates from $[(NHC)_2Cu]^+$ and deprotonates a terminal alkyne, forming $[(NHC{\cdot}H)]^+$ and an (NHC)Cu(alkynyl) complex. This complex then undergoes a formal [2+3] cycloaddition with azide to form an (NHC)Cu(triazolide) complex which can deprotonate the imidazolium salt to form the triazole product and reform the $[(NHC)_2Cu]^+$ complex.[27]

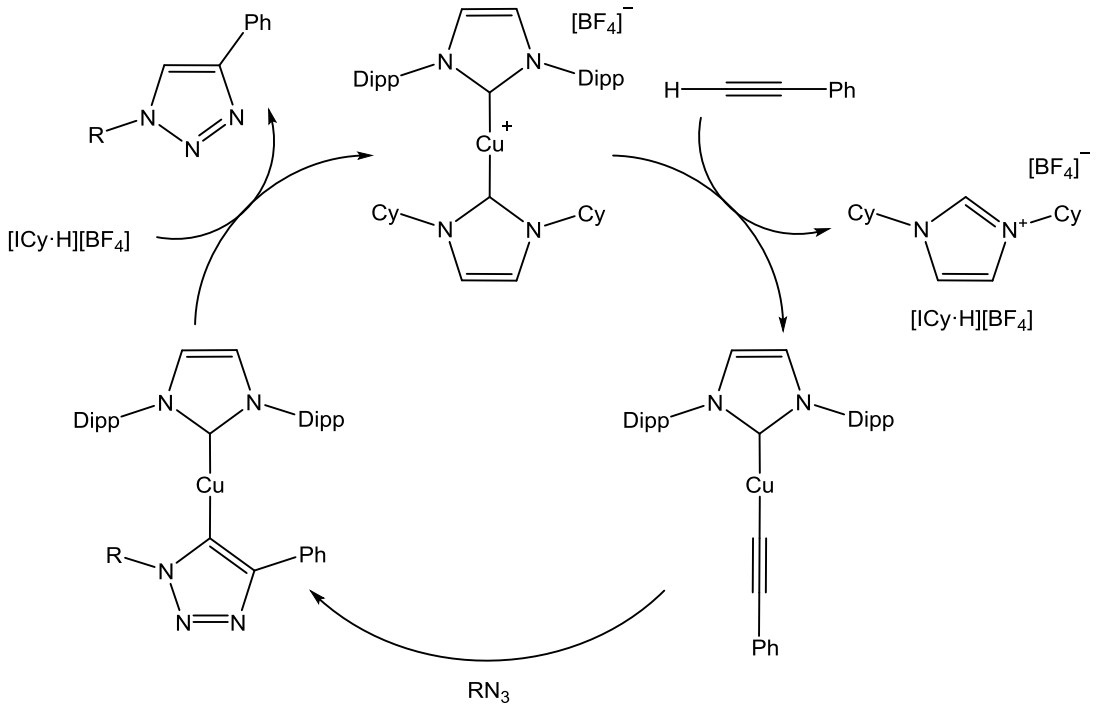

Scheme 2.6: Mononuclear catalytic cycle proposed by Nolan.[27,33]

This mononuclear mechanism is supported by the observation of [NHC·H][X] formation under catalytic conditions,[33] as well as the recent isolation of (NHC)Cu(alkynyl) and (NHC)Cu(triazolide) complexes (Figure 2.12).[34]

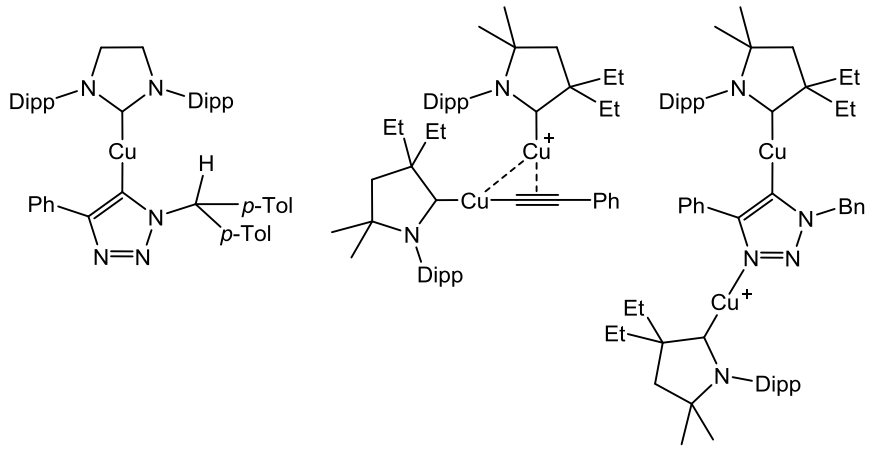

Figure 2.12: Structurally characterised complexes which are potential intermediates in CuAAC: (SIPr)Cu(triazolide) (left), $[(CAAC)Cu(\mu\text{-alkynyl})Cu(CAAC)]^+$ (centre), $[(CAAC)Cu(\mu\text{-triazolide})Cu(CAAC)]^+$ (right).

More complicated mechanisms have since been proposed, invoking dinuclear intermediates (Scheme 2.7).[35] Dinuclear copper complexes have been shown to exhibit exceptional activity,[36] and have even been isolated (Figure 2.12), structurally characterised and interconverted to reproduce the proposed catalytic steps.[37]

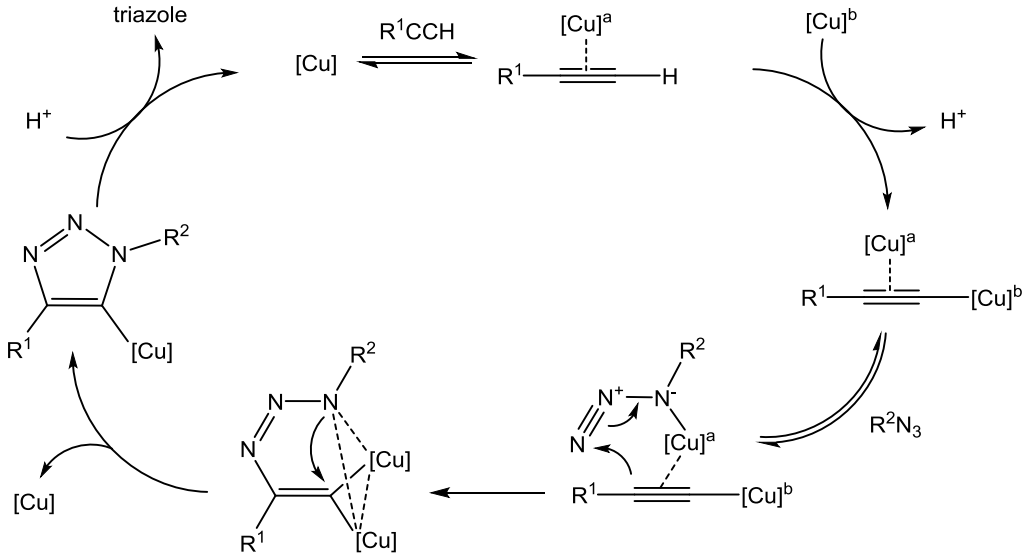

Scheme 2.7: Dinuclear catalytic cycle proposed by Fokin.[35]

Our results have revealed that more basic seven-membered NHCs have greater activity than six-membered ring systems. This could support the proposal that carbene dissociation from $[(RENHC)_2Cu]^+$ is necessary, with the carbene acting as a base towards alkyne. The rate enhancement observed for the 6-MesDAC systems

'on-water', however, contradicts this. Carbene dissociation and subsequent alkyne deprotonation would afford covalent 6-MesDAC·HX species, owing to the highly electrophilic character of [6-MesDAC·H]$^{+}$.[5] Furthermore, these 6-MesDAC·HX species have been reported to react instantaneously with water to form 6-MesDAC·HOH, which could presumably not re-enter the catalytic cycle.[17] NMR analysis of completed catalytic reactions involving complex **6** revealed no 6-MesDAC·HOH, with the parent complex as the only 6-MesDAC containing species. The nature of the active species therefore remains undetermined, and merits further investigation. Furthermore, the di- and trimeric copper halide complexes **1** and **2** provide a good opportunity to investigate the viability of multi-metallic co-operative effects in CuAAC chemistry.

2.8 Conclusion

This Chapter has described the first diamidocarbene complexes of copper and shown that in-situ generation of 6-MesDAC is not suitable for the selective preparation of DAC copper complexes. Reaction of the free carbene with CuCl resulted in an unexpected series of monomeric to tetrameric complexes, depending on the conditions employed. Reaction of $[Cu(MeCN)_4][X]$ with 6-MesDAC and a range of RENHCs produced a series of cationic, homoleptic complexes. The activity of all of these complexes was investigated for CuAAC under 'Click' conditions. The ring expanded diaminocarbene systems were successful catalysts under neat conditions, with $[(7\text{-}o\text{-Tol})_2Cu][BF_4]$ (**9**) achieving activities comparable to the best five-membered ring NHC systems, albeit with a much narrower substrate scope. The diamidocarbene systems were inactive under neat conditions, but showed a dramatic rate enhancement in the presence of water. The trinuclear $(6\text{-MesDAC})_2(CuCl)_3$ (**2**) showed the greatest activity under these conditions. The potential implications of these findings for the mechanism of CuAAC warrant further study.

2.9 References for Chapter Two

(1) Collins, L. R.; Lowe, J. P.; Mahon, M. F.; Poulten, R. C.; Whittlesey, M. K. *Inorg. Chem.* **2014**, *53*, 2699–2707.

(2) Collins, L. R.; Rookes, T. M.; Mahon, M. F.; Riddlestone, I. M.; Whittlesey, M. K. *Organometallics* **2014**, *33*, 5882–5887.

(3) Moerdyk, J. P.; Bielawski, C. W. *Organometallics* **2011**, *30*, 2278–2284.

(4) Arumugam, K.; Varghese, B.; Brantley, J. N.; Konda, S. S. M.; Lynch, V. M.; Bielawski, C. W. *Eur. J. Org. Chem.* **2014**, *2014*, 493–497.

(5) César, V.; Lugan, N.; Lavigne, G. *Eur. J. Inorg. Chem.* **2010**, *2010*, 361–365.

(6) Hudnall, T. W.; Bielawski, C. W. *J. Am. Chem. Soc.* **2009**, *131*, 16039–16041.

(7) Hudnall, T. W.; Tennyson, A. G.; Bielawski, C. W. *Organometallics* **2010**, *29*, 4569–4578.

(8) Törmäkangas, O. P.; Toivola, R. J.; Karvinen, E. K.; Koskinen, A. M. . *Tetrahedron* **2002**, *58*, 2175–2181.

(9) Gimeno, M. C.; Laguna, A.; Visbal, R. *Organometallics* **2012**, *31*, 7146–7157.

(10) Humenny, W. J.; Mitzinger, S.; Khadka, C. B.; Najafabadi, B. K.; Vieira, I.; Corrigan, J. F. *Dalton Trans.* **2012**, *41*, 4413–4422.

(11) Mankad, N. P.; Gray, T. G.; Laitar, D. S.; Sadighi, J. P. *Organometallics* **2004**, *23*, 1191–1193.

(12) César, V.; Barthes, C.; Farré, Y. C.; Cuisiat, S. V; Vacher, B. Y.; Brousses, R.; Lugan, N.; Lavigne, G. *Dalton Trans.* **2013**, *42*, 7373–7385.

(13) Díez-González, S.; Escudero-Adán, E. C.; Benet-Buchholz, J.; Stevens, E. D.; Slawin, A. M. Z.; Nolan, S. P. *Dalton Trans.* **2010**, *39*, 7595–7606.

(14) Peng, R.; Li, M.; Li, D. *Coord. Chem. Rev.* **2010**, *254*, 1–18.

(15) Cordero, B.; Gómez, V.; Platero-Prats, A. E.; Revés, M.; Echeverría, J.; Cremades, E.; Barragán, F.; Alvarez, S. *Dalton Trans.* **2008**, 2832–2838.

(16) Pregosin, P. S.; Kumar, P. G. A.; Fernández, I. *Chem. Rev.* **2005**, *105*, 2977–2998.

(17) Hudnall, T. W.; Moerdyk, J. P.; Bielawski, C. W. *Chem. Commun.* **2010**, *46*, 4288–4290.

(18) Moreno, Y.; Spodine, E.; Vega, A.; Saillard, J.-Y. *Inorg. Chim. Acta.* **2003**, *350*, 651–655.

(19) Liu, H. Y.; Yu, Z. T.; Yuan, Y. J.; Yu, T.; Zou, Z. G. *Tetrahedron* **2010**, *66*, 9141–9144.

(20) Han, X.; Weng, Z.; Young, D. J.; Jin, G. X.; Hor, T. S. A. *Dalton Trans.* **2014**, *43*, 1305–1312.

(21) Díez-González, S.; Stevens, E. D.; Scott, N. M.; Petersen, J. L.; Nolan, S. P. *Chem. Eur. J.* **2008**, *14*, 158–168.

(22) Kolb, H. C.; Finn, M. G.; Sharpless, K. B. *Angew. Chem. Int. Ed.* **2001**, *40*, 2004–2021.

(23) Huisgen, R. *Angew. Chem. Int. Ed.* **1963**, *2*, 565–598.

(24) Rostovtsev, V. V; Green, L. G.; Fokin, V. V; Sharpless, K. B. *Angew. Chem. Int. Ed.* **2002**, *41*, 2596–2599.

(25) Lazreg, F.; Nahra, F.; Cazin, C. S. J. *Coord. Chem. Rev.* **2015**, *293-294*, 48–79.

(26) Díez-González, S.; Correa, A.; Cavallo, L.; Nolan, S. P. *Chem. Eur. J.* **2006**, *12*, 7558–7564.

(27) Díez-González, S.; Nolan, S. P. *Angew. Chem. Int. Ed.* **2008**, *47*, 8881–8884.

(28) Bantu, B.; Wang, D.; Wurst, K.; Buchmeiser, M. R. *Tetrahedron Lett.* **2005**, *61*, 12145–12152.

(29) Iglesias, M.; Beetstra, D. J.; Kariuki, B.; Cavell, K. J.; Dervisi, A.; Fallis, I. A. *Eur. J. Inorg. Chem.* **2009**, *2009*, 1913–1919.

(30) Iglesias, M.; Beetstra, D. J.; Knight, J. C.; Ooi, L.; Stasch, A.; Coles, S.; Male, L.; Hursthouse, M. B.; Cavell, K. J.; Dervisi, A.; Fallis, I. A. *Organometallics* **2008**, *27*, 3279–3289.

(31) Tapu, D.; Dixon, D. A.; Roe, C. *Chem. Rev.* **2009**, *109*, 3385–3407.

(32) Poater, A.; Cosenza, B.; Correa, A.; Giudice, S.; Ragone, F.; Scarano, V.; Cavallo, L. *Eur. J. Inorg. Chem.* **2009**, *2009*, 1759–1766.

(33) Lazreg, F.; Slawin, A. M. Z.; Cazin, C. S. J. *Organometallics* **2012**, *31*, 7969–7975.

(34) Nolte, C.; Mayer, P.; Straub, B. F. *Angew. Chem. Int. Ed.* **2007**, *46*, 2101–2103.

(35) Worrell, B. T.; Malik, J. a; Fokin, V. V *Science* **2013**, *340*, 457–460.

(36) Berg, R.; Straub, J.; Schreiner, E.; Mader, S.; Rominger, F.; Straub, B. F. *Adv. Synth. Catal.* **2012**, *354*, 3445–3450.

(37) Jin, L.; Tolentino, D. R.; Melaimi, M.; Bertrand, G. *Sci. Adv.* **2015**, *1*, e1500304.

CHAPTER THREE

CHAPTER THREE: Synthesis and Reactivity of Copper Alkoxide Complexes

Some of the work in this Chapter has been published in:[1,2]

Copper Diamidocarbene Complexes: Characterization of Monomeric to Tetrameric Species: Collins, L. R.; Lowe, J. P.; Mahon, M. F.; Poulten, R. C.; Whittlesey, M. K. *Inorg. Chem.* **2014**, *53*, 2699 − 2707

A Comparison of the Stability and Reactivity of Diamido- and Diaminocarbene Copper Alkoxide and Hydride Complexes: Collins, L. R.; Riddlestone, I. M.; Mahon, M. F.; Whittlesey, M. K. *Chem. Eur. J.* **2015**, *21*, 14075 – 14084

3.1 Partial Salt Metathesis of $[(6\text{-MesDAC})(CuCl)]_2$ (1) with MO^tBu

The salt metathesis of (NHC)CuCl complexes is a common procedure in the literature to generate (NHC)CuOR (R = alkyl, aryl) complexes.[3] Such alkoxide complexes, whether used in-situ or isolated,[4,5] are important precursors for a wide range of catalytically relevant species, for example $[(NHC)CuH]_n$ or $(NHC)CuBR_2$.[6–8] To assess whether (DAC)CuOR complexes can be synthesised by salt metathesis, preliminary reactions were conducted and monitored by ^1H NMR spectroscopy.

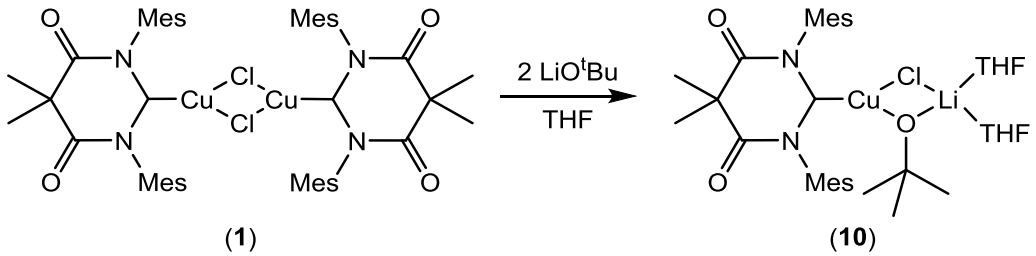

(**1**) (**10**)

Scheme 3.1: Reaction scheme for the partial salt metathesis of **1** with LiO^tBu.

Samples of $[(6\text{-MesDAC})(CuCl)]_2$ (**1**) were dissolved in THF-d_8 and then mixed with two equivalents of MO^tBu (M = Li, Na, K) (Scheme 3.1). Each reaction proceeded at room temperature, with complete consumption of complex **1** within seconds. In reactions with KO^tBu and NaO^tBu, orange solutions were formed but no products could be identified from their complicated ^1H NMR spectra. In contrast, reaction with LiO^tBu proceeded cleanly, producing a dark red-purple solution with

^{1}H and ^{7}Li NMR spectra consistent with the formation of complex **10**, the product of partial salt metathesis (Scheme 3.1).

3.1.1 Characterisation of (6-MesDAC)Cu(μ-Cl)(μ-O^{t}Bu)Li(THF)$_2$ (10)

Deep purple THF solutions of complex **10** were found to be stable for days, as confirmed by ^{1}H and ^{7}Li NMR spectroscopy. Unexpectedly, upon removal of the volatiles from this purple solution, a green solid was isolated. Re-dissolution of the green solid in THF-d_8 yielded a red solution with identical NMR resonances to the original purple solution of **10** (alongside some minor decomposition products). To further investigate this behaviour, the reaction was again conducted according to Scheme 3.1, but in non-deuterated THF. After 40 minutes, the volatiles were removed and the green solid was thoroughly dried in vacuo. This residue was then dissolved in THF-d_8, and the ^{1}H NMR spectrum shown in Figure 3.1 was recorded.

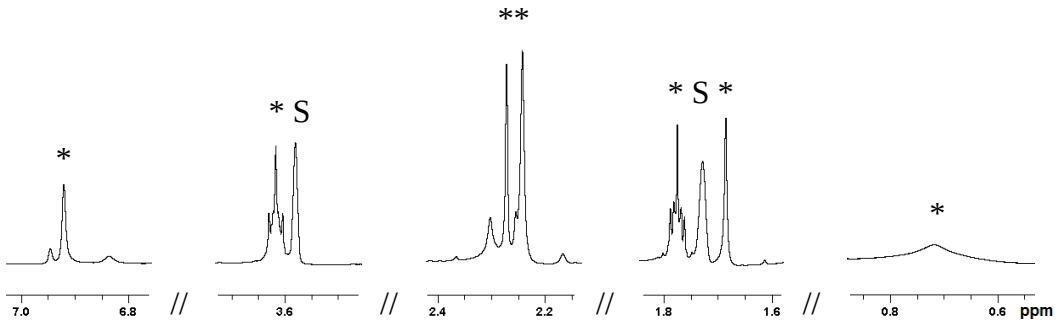

Figure 3.1: ^{1}H NMR spectrum (THF-d_8, 500 MHz, 298 K). S denotes residual protio solvent. * denotes resonances attributed to complex **10**.

This spectrum is consistent with **10** containing a single 6-MesDAC environment (as shown by the appearance of a set of resonances between 6.91-1.67 ppm in a ratio of 4 : 6 : 12 : 6) and also displays a low frequency signal (0.64 ppm)[i] characteristic of a bridging *tert*-butoxide group. The ^{7}Li NMR spectrum displays a singlet at -0.74 ppm and DOSY NMR experiments show the ^{7}Li diffusion coefficient (7.5×10^{-10} m^2 s^{-1}) to be very similar to that of the carbene (7.3×10^{-10} m^2 s^{-1}), consistent with them being in the same molecule. Furthermore, integration of the spectrum in Figure 3.1 reveals that two equivalents of THF per carbene were retained, despite exposing the

[i] Chemical exchange of O^{t}Bu with residual LiO^{t}Bu (1.10 ppm), as confirmed by EXSY NMR experiments, resulted in a broad resonance. This chemical exchange process could be suppressed at low temperatures and, at 200 K, a sharp resonance at 0.64 ppm was observed.

sample to a vacuum of <0.04 mbar for 1 hour before dissolution in THF-d_8. The chemical shifts of the THF (3.62 and 1.77 ppm) match those of freely solvated THF;[9] the absence of downfield shifting due to metal co-ordination can be explained by rapid exchange with the deuterated solvent. Instability in the absence of THF precluded further characterisation of **10**. Numerous attempts to crystallise **10** by slow evaporation of reaction mixtures were unsuccessful and exchange of solvent resulted only in crystals of **1** (from toluene/hexane) or **1·3** (from Et_2O/hexane). Attempts to extract lithium by addition of 12-crown-4 were also unsuccessful.

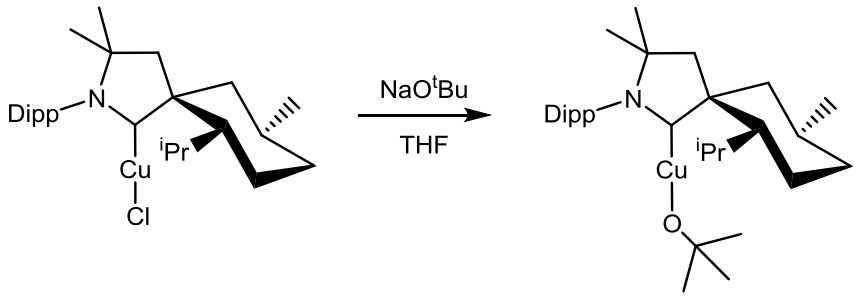

Scheme 3.2: Successful salt metathesis with a (CAAC)CuCl complex, resulting in the formation of (CAAC)CuO^{t}Bu.[10]

The formation of such an 'ate' complex by partial salt metathesis of an (NHC)CuCl complex is unprecedented. In almost all other instances, the expected (NHC)CuOR complex is formed, for instance (IPr)CuO^{t}Bu.[5] The reason for the different reactivity of this diamidocarbene system is unclear. The high electrophilicity of 6-MesDAC could be a factor, however, a similarly electrophilic CAAC system reported by Bertrand undergoes salt metathesis with NaO^{t}Bu to yield (CAAC)CuO^{t}Bu in 92% yield (Scheme 3.2).[10]

3.2 New Methodology for the Synthesis of Copper Alkoxide Complexes

In 1972, Saegusa and co-workers reported the synthesis of $[CuO^tBu]_4$ and used it for the cupration of PhC≡CH and cyclopentadiene. PEt_3 was found to help control this reactivity, and the phosphine stabilised copper alkoxide $[(PEt_3)CuO^tBu]_2$ was isolated.[11] Since this initial report, only a handful of $[(L)CuO^tBu]_n$ complexes have been synthesised from $[CuO^tBu]_4$ (L = PR_3,[11–13] CO,[14,15] RNC,[14,16] RC≡CR)[17] and none where L = NHC.

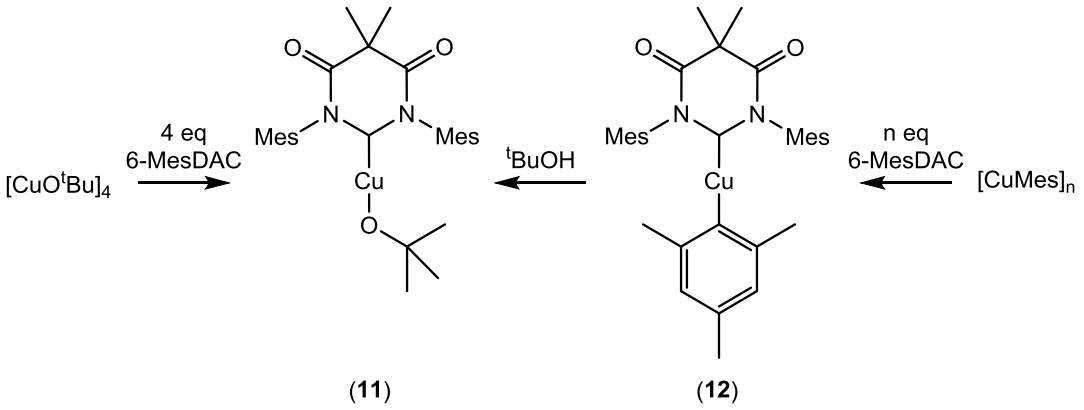

Scheme 3.3: New synthetic routes to (6-MesDAC)CuO^{t}Bu (**11**).

Reaction of four equivalents of 6-MesDAC with [CuO^{t}Bu]$_4$ in benzene immediately yielded a red solution (Scheme 3.3), from which (6-MesDAC)CuO^{t}Bu (**11**) was isolated as an orange powder in 72 % yield. A diagnostic high frequency $^{13}C\{^1H\}$ carbenic resonance was located at 213.5 ppm, and the O^{t}Bu resonances were located at 1.21 ppm and 68.7/36.8 ppm in the ^1H and $^{13}C\{^1H\}$ NMR spectra respectively. Complex **11** proved to be highly air and moisture sensitive and also degraded over time in solution (Section 3.4). As a result, analytically pure material could not be obtained from this synthetic procedure due to continued decomposition during any procedure designed to remove existing impurities. A more convenient synthetic approach was the reaction of (6-MesDAC)CuMes (**12**, vide infra) with a small excess of ^{t}BuOH (resulting in protonolysis of mesitylene), whereby the only workup required was to evaporate the volatiles from the reaction mixture (Scheme 3.3). Furthermore, if not stirred, **11** could be isolated from the reaction mixture as crystalline material (65 % yield), owing to its much lower solubility than the mesityl derivative **12**. Analytically pure material could thus be isolated and the monomeric nature of complex **11** was confirmed by X-ray crystallography (Figure 3.2).

3.2.1 Molecular Structure of (6-MesDAC)CuO^{t}Bu (11)

Single crystals of **11** precipitated from concentrated solutions of **12** and ^{t}BuOH. However, these crystals were found to be irreconcilably twinned. Overnight re-crystallisation from a concentrated THF solution layered with hexane yielded crystals which were suitable for an X-ray structure determination (although still twinned about the *a* axis).

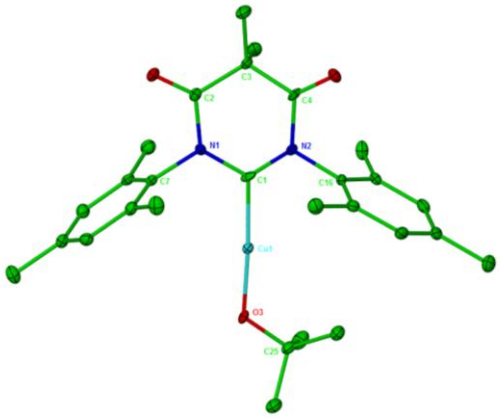

Figure 3.2: Displacement ellipsoid plot (30 % probability) of (6-MesDAC)CuO^{t}Bu (**11**). H atoms omitted for clarity. Selected bond lengths (Å) and angles (°): Cu(1)-C(1) 1.864(7), Cu(1)-O(3) 1.805(5), O(3)-C(25) 1.419(9), N(1)-C(1)-N(2) 118.0(6), C(1)-Cu(1)-O(3) 176.3(3), Cu(1)-O(3)-C(25) 122.7(5).

Complex **11** is two co-ordinate with the ligands arranged in a trans-linear (C-Cu-O = 176.3(3)°) geometry. The Cu-C (1.864(7) Å) and Cu-O (1.805(5) Å) distances show no difference to those reported for the five-membered carbene analogues (IPr)CuO^{t}Bu (Cu-C = 1.8641(18) Å; Cu-O = 1.8104(13) Å),[5] (IPr)CuOEt (Cu-C = 1.863(5) Å; Cu-O = 1.799(3) Å)[18] and (SIPr)CuOEt (Cu-C = 1.861(8) Å; Cu-O = 1.793(7) Å).[19]

3.3 Synthesis of (6-MesDAC)CuMes (12)

$[CuMes]_n$[i] has received far more attention in the literature than $[CuO^tBu]_4$, as a versatile synthon for the incorporation of copper into homo- and heterometallic clusters as well as a precursor for copper mediated stoichiometric and catalytic functional group transformations.[20–23] However, the characterisation of discrete (L)CuMes complexes remains rare (L = NHC,[24] [Ti](C≡CR)$_2$)[25] (Figure 3.3).

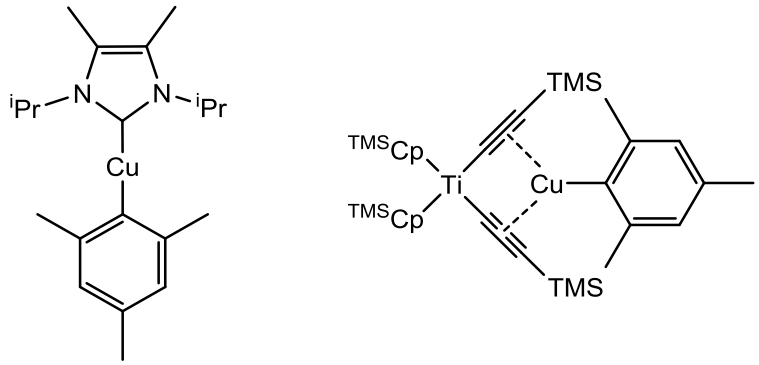

Figure 3.3: Examples of (L)CuMes complexes: ($^{Me_2}I^iPr$)CuMes (left),[24] ($^{TMS}Cp)_2Ti(C≡CTMS)_2CuMes$ (right).[25]

(6-MesDAC)CuMes (**12**) was synthesised by addition of 6-MesDAC to 1/n equivalents of $[CuMes]_n$ in benzene (Scheme 3.3), forming a red solution immediately. Upon removal of the volatiles, crystallisation from benzene and hexane yielded red crystals of the complex in 87 % yield. $^{13}C\{^1H\}$ NMR spectroscopy revealed characteristic high frequency signals for both the copper bound carbenic carbon and *ipso*-mesityl carbon at 217.1 ppm and 161.1 ppm respectively.

[i] $[CuMes]_n$, first reported in 1981,[20] is known to adopt multiple aggregation states in the solid state (n = 4 or 5),[21,22] as well as in solution.[21,23]

3.3.1 Molecular Structure of (6-MesDAC)CuMes (12)

Slow evaporation of a concentrated benzene/hexane solution (1 : 2, v : v) of **12** provided X-ray quality crystals that afforded the structure shown in Figure 3.4.

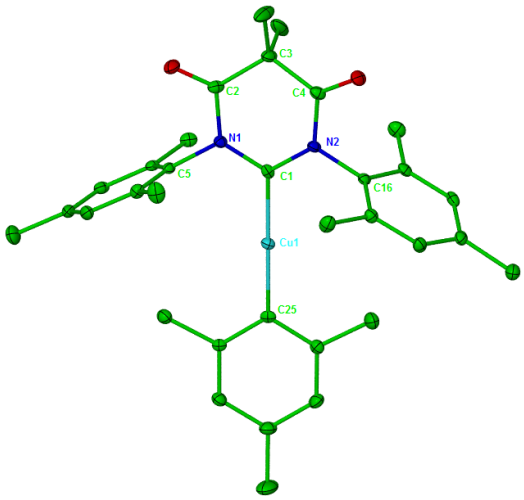

Figure 3.4: Displacement ellipsoid plot (30 % probability) of (6-MesDAC)CuMes (**12**). H atoms omitted for clarity. Selected bond lengths (Å) and angles (°): Cu(1)-C(1) 1.905(3), Cu(1)-C(25) 1.927(3), N(1)-C(1)-N(2) 116.3(2), C(1)-Cu(1)-C(25) 179.71(12).

Complex **12** adopts a trans-linear geometry (C-Cu-C = 179.71(12)°) with similar Cu-C bond lengths (Cu-C_{NHC} = 1.905(3) Å; Cu-C_{Mes} = 1.927(3) Å) to those of ($^{Me_2}I^{i}Pr$)CuMes (Cu-C_{NHC} = 1.911(4) Å; Cu-C_{Mes} = 1.922(4) Å, Figure 3.3).[24] The very different relative orientations of the ligands in these two complexes (dihedral angle of **12** = 4°; ($^{Me_2}I^{i}Pr$)CuMes = 84°) may be due in part to the different steric demands of the ^{i}Pr and mesityl N-substituents, but also to the presence of a stabilising interaction between the *o*-mesityl C-H bonds and N-mesityl aryl rings of **12**.[i]

[i] A similar interaction was identified in the related complex ($^{Me_2}I^{i}Pr$)Cu(2,6-dimesitylphenyl).[24]

3.4 Decomposition Reactions of (6-MesDAC)CuO^{t}Bu (11)

The extreme air and moisture sensitivity of complexes **11** and **12** required all manipulations to be conducted inside a glovebox, employing solvents stored over potassium mirrors. Exposure to incompletely dried solvents resulted in the formation of red oils which could not be purified. Whilst complex **12** was found to be stable in solution under rigorously dry and anaerobic conditions, crystalline samples of complex **11** slowly decomposed over 5 weeks at room temperature in C_6D_6 (heating to 323 K accelerated this process to occur within one week) or 2 weeks in C_7D_8 or THF-d_8. The ^{1}H NMR spectra of the decay products were reproducible between experiments (evaporation of the volatiles and redissolution in C_6D_6 also confirmed the same species were present in all three solvents), although broad, overlapping and uninformative in nature.

Before discovering that analytically pure **11** could be isolated from the reaction of **12** with ^{t}BuOH, numerous attempts were made at crystallising samples of **11** isolated from the $[CuO^tBu]_4$ synthetic procedure. On the most part, these efforts proved irreproducible. However, on two separate occasions, red crystals of the dimeric complex **13** were isolated in up to 17 % yield (Scheme 3.4). Complex **13** contains two different copper environments, ligated by intact, as well as ring-opened 6-MesDAC ligands. We refer to this product of carbene activation as the "ring exploded carbene complex", owing to the extrusion of a carbenic carbon to form a mesitylisonitrile ligand, leaving behind a dianionic carboxyamidate chelating ligand, through the formal insertion of 'Cu-O' into the heterocyclic ring. Complex **13** was fully characterised (vide infra), however its ^{1}H NMR resonances were broad and uninformative (Figure 3.5) and thus could not be unequivocally matched with the species observed in ^{1}H NMR spectra recorded when crystalline samples of **11** were left to decompose in solution. ^{1}H NMR spectra recorded at low temperature showed significant differences to those recorded at room temperature, but did not aid in the assignment of any resonances (Figure 3.5). It is likely that multiple species and aggregates are present in solution during the decay of **11**, and that **13** is one of the more crystalline arrangements of these fragments.

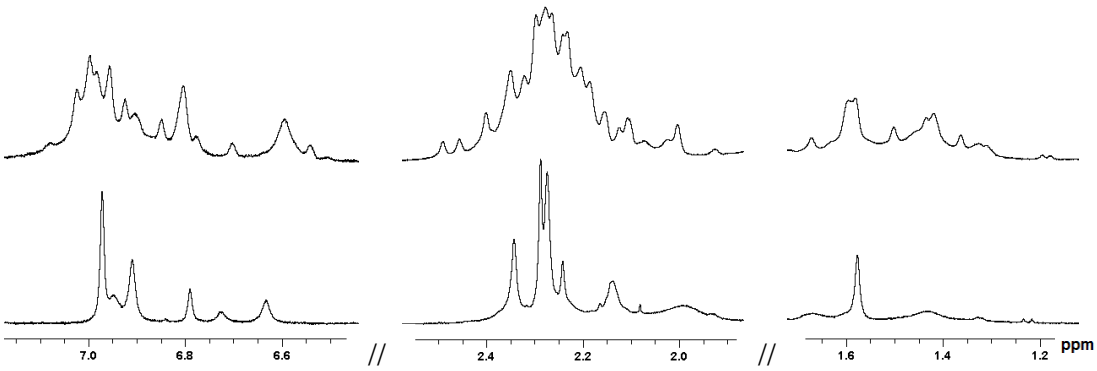

Figure 3.5: ^{1}H NMR spectra (500 MHz, THF-d_8) of complex **13** recorded at 223 K (top) and 298 K (bottom).

3.4.1 Hydrolysis of (6-MesDAC)CuO^{t}Bu (11)

To further investigate the decay of **11**, we first sought to rule out 'adventitious moisture' or traces of air. Identical samples were prepared by dissolving crystalline samples of **11** in C_6D_6 in J. Young's capped NMR tubes, inside the glove box, and then systematically exposed to air or moisture on a Schlenk line. In the case of exposure to air, five tubes were prepared and exposed to air for 1, 5, 10 or 30 seconds and then resealed, with the fifth remaining under argon as a control. The four tubes which were exposed to air followed a different decomposition pathway to the control. ^{1}H NMR analysis showed that all four samples exposed to air converted to the known urea 6-MesDAC=O,[26] alongside unidentified organometallic species, at a rate that increased with increasing exposure time (Scheme 3.4). In all of the anaerobic decomposition reactions, no signals of the urea were identified, thus ruling out air leakage as the cause of this decomposition.

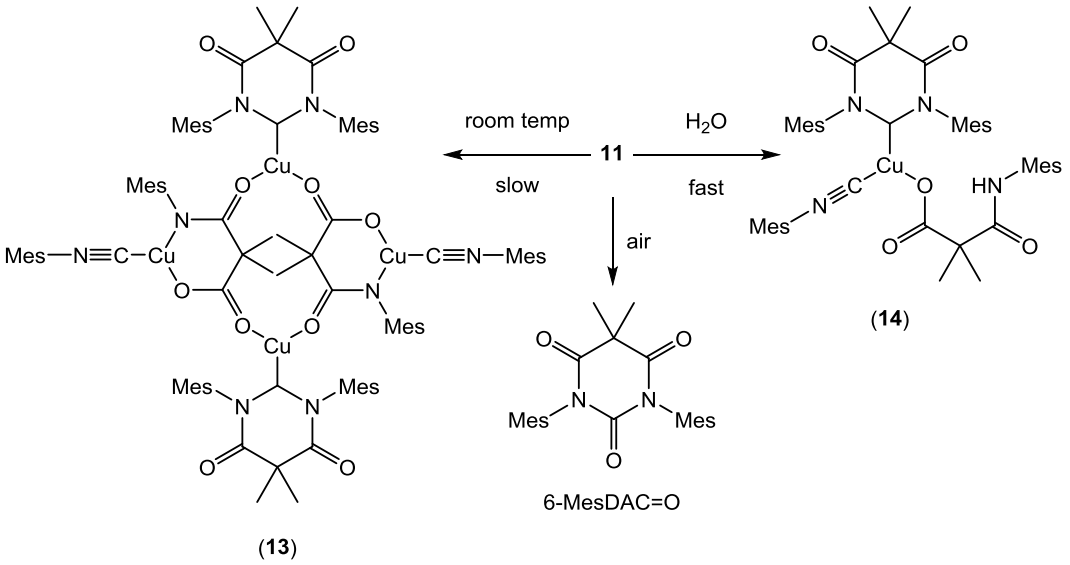

Scheme 3.4: Decomposition reactions of complex **11**.

Addition of stoichiometric amounts (4.5 equivalents) of water to a THF solution of **11** resulted in the immediate formation of a deep red solution, which faded rapidly to a yellow solution containing a yellow precipitate. The precipitate was isolated and characterised by PXRD as Cu_2O (see Appendix for details). ^{1}H and $^{13}C\{^{1}H\}$ NMR spectroscopy of the yellow solution revealed a very clean reaction had taken place to generate $^{t}BuOH$ (1.05 ppm)[9] and (6-MesDAC)Cu(CNMes)(OC(O)C(Me)$_2$C(O)N(H)Mes) (**14**), which was isolated in 54 % yield. Scheme 3.4 shows that **14** contains the same organic fragments as **13**, but now bonded to a single copper atom, and with the carboxyamidate ligand only monoanionic (NH located at 10.66 ppm by ^{1}H NMR spectroscopy). ^{1}H NMR spectra of **14** reveal four resonances for a C_s symmetric 6-MesDAC ligand (4 : 12 : 6 : 6 ratio), alongside seven (2 : 2 : 6 : 3 : 6 : 6 : 3 ratio) further resonances which are attributed to the de-symmetrised products of 6-MesDAC activation. An intense absorption band in the IR spectrum at 2154 cm^{-1} is characteristic of an isonitrile and the presence of five distinct bands between 1741 cm^{-1} and 1608 cm^{-1} are consistent with the five different carbonyls in complex **14**.

3.4.2 Molecular Structures of 13 and (6-MesDAC)Cu(CNMes)(OC(O)C(Me)$_2$C(O)N(H)Mes) (14)

Crystals of **13** suitable for X-ray diffraction studies were isolated from toluene solutions of **11** layered with hexane. Single crystals of **14** were grown by diffusion of hexane into a saturated toluene solution. Their molecular structures are shown in Figure 3.6, with selected bond lengths and angles presented in Table 3.1.

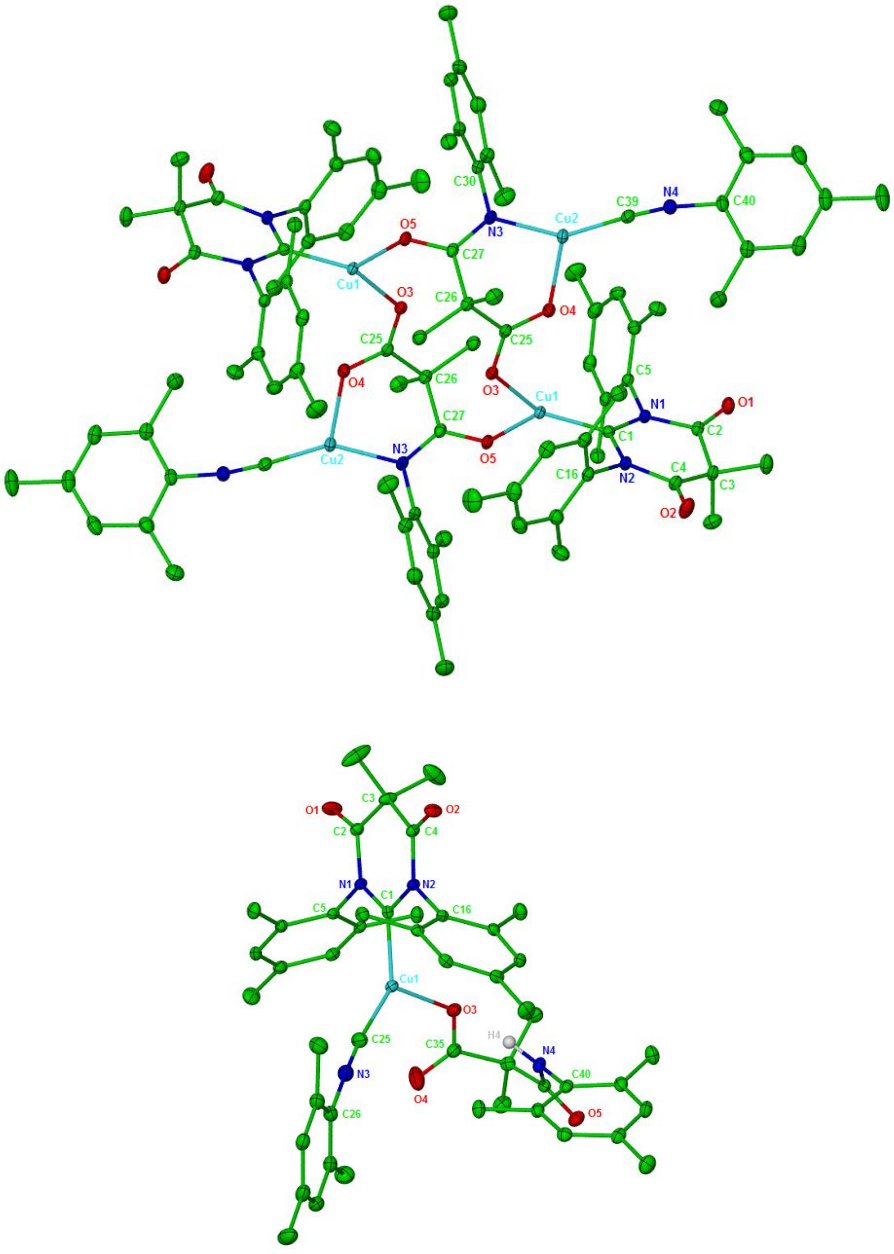

Figure 3.6: Displacement ellipsoid plots (30 % probability) of **13** and (6-MesDAC)Cu(CNMes)(OC(O)C(Me)$_2$C(O)N(H)Mes) (**14**). H atoms omitted for clarity. Selected bond lengths and angles are presented in Table 3.1.

Complex **13** crystallises as a centrosymmetric dimer, with each half containing two different copper environments. Cu(1) is three co-ordinate, ligated by 6-MesDAC and also by one carboxylate (κ^1-O), and one amidate (κ^1-O), each from separate halves of the dimeric structure. Cu(2) is also three co-ordinate, bound to mesitylisonitrile and chelated by one carboxyamidate (κ^2-O,N). Complex **14** contains the same ligands as **13**, all bound to a single, three co-ordinate copper atom.

Parameter	**13**	**14**
$Cu\text{-}C_{6\text{-}MesDAC}$	1.846(2)	1.904(3)
Cu-CNMes	1.815(2)	1.886(4)
C≡NMes	1.157(3)	1.171(5)
$Cu\text{-}O_2C$	1.9664(14) 2.0255(16)	1.973(2)
O-C(O)R	1.250(3) 1.268(3)	1.216(5) 1.275(4)
Cu-OC(R)N(R)	1.969(1)	---
O-C(R)N(R)	1.266(2)	1.214(4)
Cu-N(R)C(O)R	1.9411(17)	---
N-C(O)R	1.316(3)	1.360(4)
$N\text{-}C_{(NHC)}\text{-}N$	115.85(17)	116.3(3)

Table 3.1: Selected bond lengths (Å) and angles (°) of complexes **13** and **14**.

The $Cu\text{-}C_{6\text{-}MesDAC}$ and Cu-CNMes bonds of **14** are each significantly longer than those of **13**, perhaps as a consequence of both 6-MesDAC and CNMes being co-ordinated to the same metal centre. However, the metrics of 6-MesDAC and CNMes themselves show no difference between the two structures. The carboxylate ligand is anionic in both complexes; in complex **14**, this is bonded in a κ^1-O fashion with the copper bound C-O bond (1.275(4) Å) significantly longer than the terminal C=O bond (1.216(5) Å). In complex **13**, the carboxylate is bridging between two copper centres (μ^2, κ^1-O, κ^1-O), and the C-O bonds are accordingly similar to eachother in length (1.250(3) Å and 1.268(3) Å), reflecting the delocalisation of anionic charge across the carboxylate. The amide of **14** is protonated at nitrogen with C-N and C-O bond lengths typical of aryl amides (**14**: C-N = 1.360(4) Å; C-O = 1.214(4) Å, 2-chloro-N-phenylacetamide: C-N = 1.350(6) Å; C-O = 1.226(6) Å)[27] and the amide proton forms a hydrogen bond with the copper bound oxygen atom of the carboxylate (N-H··O = 135.42°). In complex **13**, the amide is anionic and bridging

(μ^2, κ^1-O, κ^1-N) two copper centres. The C-O bond (1.266(2) Å) is longer than the corresponding bond in **14** (1.214(4) Å), and the C-N bond shorter (**13** = 1.316(3) Å; **14** = 1.360(4) Å), reflecting a significant degree of delocalisation across the anionic amidate of **13**.

3.4.3 Attempted Synthesis of (6-MesDAC)CuOH

Addition of water to **12** also generated **14**, although less cleanly and with mesitylene as the byproduct in place of ^{t}BuOH. That the same product can be formed from both complexes **11** and **12** suggests the intermediacy of a common species, namely (6-MesDAC)CuOH. A proposed mechanism is shown in Scheme 3.5. Protonolysis of **11** or **12** with water generates ^{t}BuOH or mesitylene respectively, alongside (6-MesDAC)CuOH. Nucleophilic attack at an amide of 6-MesDAC by hydroxide, and transfer of electron density through the conjugated π-system of the heterocycle to an electrophilic $[(6\text{-MesDAC})Cu]^+$ fragment, yields half an equivalent each of species **A** and **B**. This process could be concerted or stepwise, and could involve discrete ions as the nucleophile and electrophile, or else these may remain ion-paired as (6-MesDAC)CuOH complexes. Subsequent loss of mesitylisonitrile from **A** would result in the formation of thermodynamically unstable CuOH, which then effectively disproportionates to give one quarter of an equivalent of Cu_2O (7.0 mg (0.10 equivalents) of Cu_2O was isolated as an orange precipitate and characterised by PXRD (see Appendix for details) from a reaction starting from 251 mg of **11**) along with one quarter of an equivalent of water. Addition of mesitylisonitrile to **B**, proton transfer from the carboxylic acid to the more basic amidate and subsequent rearrangement yields complex **14**.

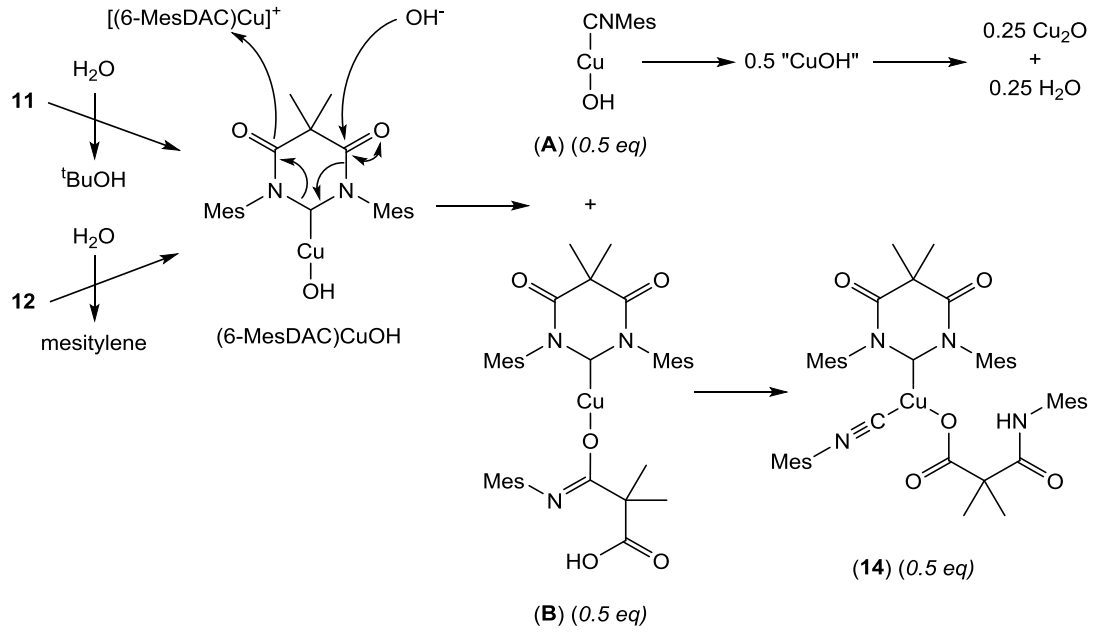

Scheme 3.5: Proposed mechanism for the decomposition of (6-MesDAC)CuOH.

Several attempts were made to synthesise (6-MesDAC)CuOH under anhydrous conditions to establish its role in the formation of **14**. Salt metathesis from complex **1** with KOH in THF was unsuccessful and showed no consumption of starting material by ^{1}H NMR spectroscopy. Stirring **1** and KOH together in THF overnight, followed by extraction into toluene and crystallisation of the residue did yield single crystals, although these were assessed by X-ray diffraction to have a unit cell identical to that of **1**. Treatment of **1** with KOH in H_2O did result in decomposition (despite the aqueous stability of **1**), but nothing could be isolated from the resultant mixtures.

Attempts at salt metathesis from complex **11** also failed to yield the desired hydroxide complex, but addition of one equivalent of KOH to **11** in THF did result in complete consumption of the starting material. A simple ^{1}H NMR spectrum (6.42 (2 H, s, *m*-ArH), 2.32 (6 H, s, *o*-ArCH_3), 2.21 (9 H, s, O^{t}Bu), 1.91 (3 H, s, *p*-ArCH_3) ppm) was produced which was attributed to ^{t}BuOCuCNMes (Scheme 3.6), alongside a large amount of an insoluble salt. Addition of a THF solution of 18-crown-6 to this precipitate immediately solubilised it, and subsequent work up identified the product as (18-crown-6)K(OC(O)C(Me)$_2$C(O)N(H)Mes) (**15**), whose structure is shown in Figure 3.7. Complex **15** consists of the same carboxyamidate fragment as found in complexes **13** and **14** and its isolation lends further weight to

the proposed nucleophilic attack mechanism (Scheme 3.5) for the formation of **14**. A similar reaction mechanism for the formation of **15** is proposed in Scheme 3.6.

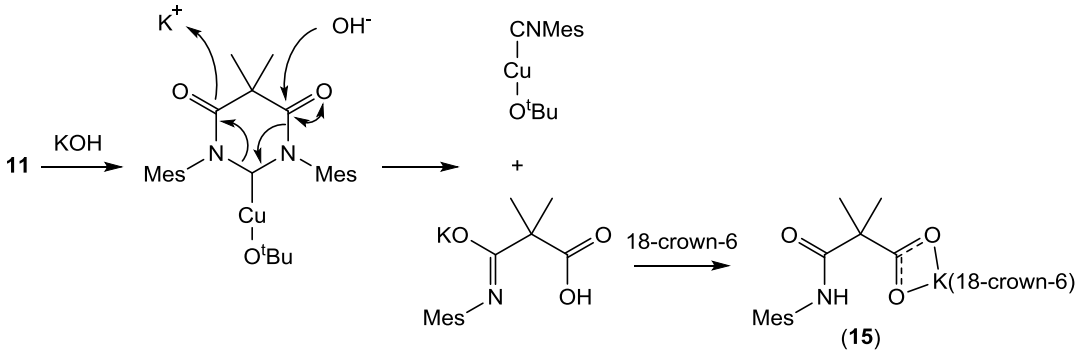

Scheme 3.6: Proposed mechanism for the formation of complex **15**.

3.4.4 Molecular Structure of (18-crown-6)K(OC(O)C(Me)$_2$C(O)N(H)Mes) (15)

Crystals of complex **15** were grown from a saturated THF solution layered with hexanes.

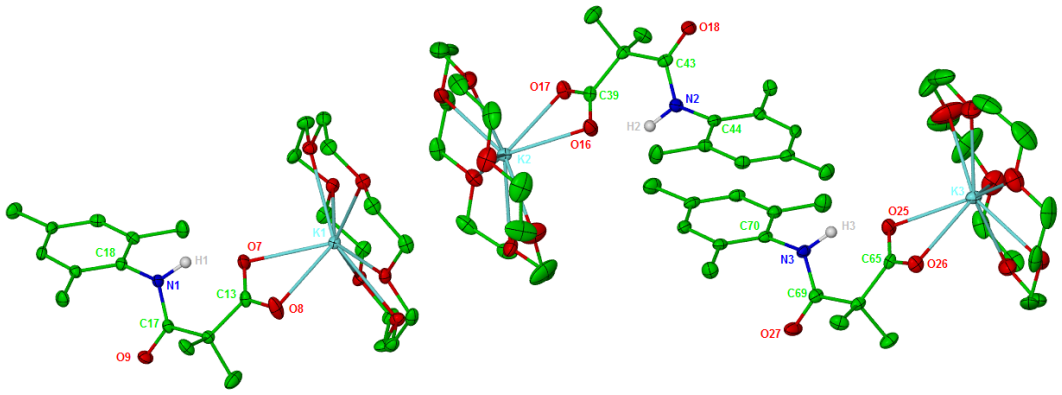

Figure 3.7: Displacement ellipsoid plot (30 % probability) of (18-crown-6)K(O_2CC(Me)$_2$C(O)N(H)Mes) (**15**). H atoms omitted for clarity (except for H(1), H(2) and H(3)). Selected bond lengths (Å) and angles (°): K(1)-$O_{(crown\ ether)}$ between 2.819(3) and 2.945(3), K(1)-O(7) 2.759(3), K(1)-O(8) 2.685(4), C(13)-O(7) 1.260(6), C(13)-O(8) 1.240(6), C(17)-O(9) 1.225(5), C(17)-N(1) 1.353(6), H(1)-O(7) 1.762, O(7)-C(13)-O(8) 124.1(5), N(1)-H(1)-O(7) 146.28.

As shown in Figure 3.7, the asymmetric unit of **15** consists of three independent molecules with a π-π stacking interaction (inter-ring distance = 3.34 Å) evident

between the mesityls of adjacent molecules as well as a staggered, face-to-face arrangement of the 18-crown-6 ligands. The metrics of the three molecules are very similar, and only those of the first molecule will be discussed. The potassium centre is κ^6 co-ordinated to the macrocyclic crown ether, and also chelated by one carboxylate which shows significant charge delocalisation, evidenced by its equivalent C-O distances (1.260(6) Å and 1.240(6) Å), which are similar to those in complex **13** (1.250(3) Å and 1.268(3) Å). The bond lengths of the amide (C-O = 1.225(5) Å; C-N = 1.353(6) Å) are identical to those of the amide in complex **14** (C-O = 1.214(4) Å; C-N = 1.360(4) Å) and a hydrogen bond is also evident between the amide proton and one carboxylate oxygen (N-H··O = 146.28°).

3.4.5 Common Decay Processes of 6-MesDAC Copper Complexes

Complexes **13**, **14** and **15** all reveal a common theme to the decomposition of **11**. Schemes 3.5 and 3.6 show proposed nucleophilic attack mechanisms for the formation of **14** and **15**. In these reactions, the nucleophiles are most likely hydroxide, with the counterpart electrophile being $[(6\text{-MesDAC})Cu]^+$ or K^+ respectively. In the formation of the "ring exploded carbene complex" **13**, the mechanism is less clear. The role of air or moisture in this reaction has been discounted and a thermal decay process is supported by: (i) faster decomposition in more polar solvents (**11** decomposes more rapidly in THF and toluene compared to in benzene) which perhaps help to stabilise the transition state polarisation inherent in nucleophilic attack; (ii) the marked increase in rate upon heating, with **11** decomposing in all cases to the same mixture of products. Although carbene activation reactions are known (Figure 3.8),[28–30] NHCs are commonly thought of as robust heterocyclic supporting ligands. These results represent a rare study into the decomposition of metal bound NHCs and suggest that metal bound diamidocarbenes may be unsuitable for applications involving strong nucleophiles, due to the potential for amide activation, and subsequent isonitrile elimination.

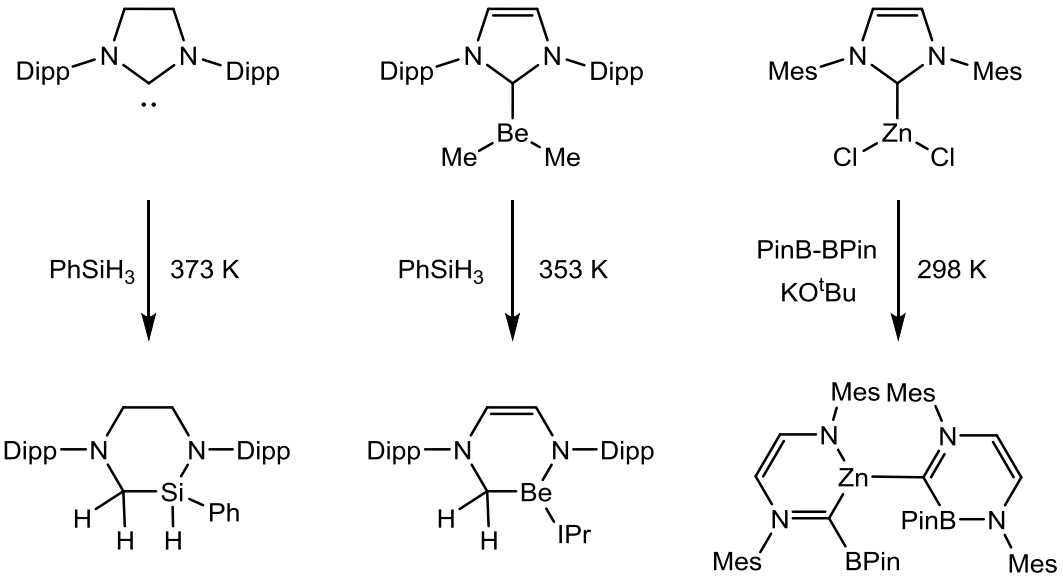

Figure 3.8: Examples of NHC C-N activation by hydrosilane (left),[28] beryllium hydride (centre),[29] and zinc boryl species (right).[30]

3.5 Mesityl and Alkoxide Complexes as Versatile Synthons

Complexes **11** and **12** can be isolated as crystalline material in good yields (65 % and 87 % respectively) and their onward reactivity investigated with efforts taken to minimise the effects of the decomposition reactions described above (strictly anaerobic conditions, with solvents stored over potassium mirrors, and minimising the time spent with complex **11** in solution). Due to the unavailability of in-situ methods or salt metathesis as discussed in Chapter 2, complexes **11** and **12** are vital entry points to a range of organometallic copper complexes supported by diamidocarbene ligands. Protonolysis of **12** (or **11**) with protic reagents, alongside the σ-bond metathesis of **11** with silyl or boryl reagents, allows diamidocarbene supported copper chemistry to be explored. This methodology is also synthetically useful for other NHCs, as will be discussed later in this Chapter. Scheme 3.7 shows some of the diamidocarbene complexes which may be accessed by protonolysis of complexes **11** or **12**.

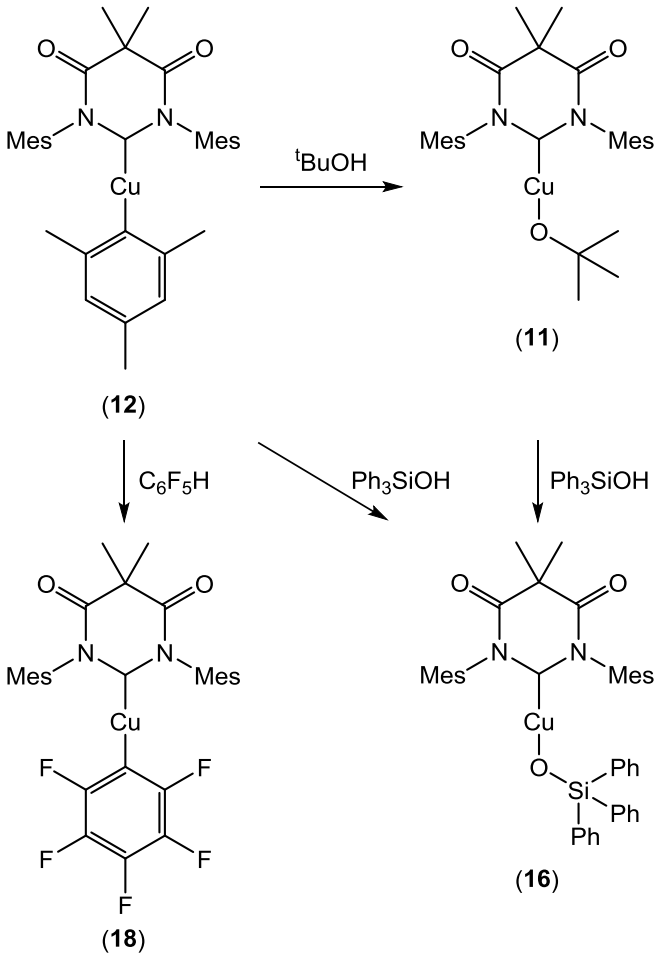

Scheme 3.7: Examples of protonolysis of complexes **11** and **12**.

3.6 Isolation of (6-MesDAC)CuOSiPh$_3$ (16)

Ph_3SiOH was reacted with **12** in benzene solution to bring about the immediate formation of a bright yellow solution. ^1H NMR spectroscopy revealed the elimination of mesitylene (6.73 and 2.17 ppm) and formation of the silanoxide complex (6-MesDAC)CuOSiPh$_3$ (**16**). The carbenic $^{13}C\{^1H\}$ NMR resonance was located at 202.5 ppm, significantly downfield of the signals in the related five-membered NHC complexes (IPr)CuOSiMe$_3$ (182.4 ppm)[31] and (IPr)CuOSiMe$_2$Ph (183.2 ppm),[32] consistent with a six-membered ring carbene.[33]

Addition of 6-MesDAC to $[CuOSiPh_3]_4$ also generated complex **16**.[34] Furthermore, protonolysis of **11** with Ph_3SiOH also allowed for the isolation of **16** (86 % yield), on account of the greater acidity of silanols over alcohols (pKa of Ph_3SiOH = 10.8 in THF;[35] pKa of ^{t}BuOH = 16.5 in water).[36] Its molecular structure is shown in Figure 3.9.

3.6.1 Molecular Structure of (6-MesDAC)CuOSiPh$_3$ (16)

Single crystals of **16** were grown from a toluene solution layered with hexane.

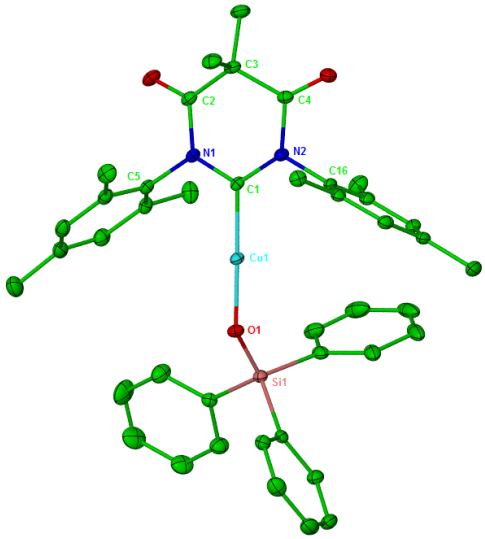

Figure 3.9: Displacement ellipsoid plot (30 % probability) of (6-MesDAC)CuOSiPh$_3$ (**16**). H atoms omitted for clarity. Selected bond lengths (Å) and angles (°): Cu(1)-C(1) 1.858(2), Cu(1)-O(1) 1.7947(14), O(1)-Si(1) 1.5969(15), N(1)-C(1)-N(2) 117.27(18), C(1)-Cu(1)-O(1) 178.79(8), Cu(1)-O(1)-Si(1) 133.59(10).

Complex **16** is monomeric and trans-linear about copper (C-Cu-O = 178.79(8)°), with identical Cu-C (1.858(2) Å) and Cu-O (1.7947(14) Å) bond lengths to those in the structurally characterised five-membered ring NHC complex (IPr)CuOSiMe$_2$Ph (1.854(2) Å and 1.797(2) Å respectively).[32] These two complexes also exhibit very similar O-Si bond lengths (**16** = 1.5969(15) Å; (IPr)CuOSiMe$_2$Ph = 1.602(2) Å) and Cu-O-Si bond angles (**16** = 133.59(10)°; (IPr)CuOSiMe$_2$Ph = 134.62(9)°).

3.6.2 Synthesis of [(6-MesDAC)CuN$_3$]$_2$ (17)

Complex **16** is stable towards air and moisture, in stark contrast to the highly sensitive alkoxide complex **11**. This translated into an extremely limited reactivity of **16**. No reaction occurred with an excess of Et$_3$SiH, even at 333 K, perhaps due to the bulky nature of triphenylsilanoxide in combination with a six-membered NHC. The sterically undemanding TMSN$_3$ reacted with **16**, undergoing a σ-bond metathesis reaction to form Me$_3$SiOSiPh$_3$ (identified by a characteristic singlet in

the ^{1}H NMR spectrum at 0.20 ppm)[37] and the dinuclear copper azide complex [(6-MesDAC)CuN$_3$]$_2$ (**17**). The ^{1}H NMR spectrum of **17** shows a single 6-MesDAC environment, with the carbenic resonance located at 209.7 ppm in the ^{13}C{^{1}H} NMR spectrum. As well as the characteristic IR bands for the 6-MesDAC carbonyls (1740 cm^{-1} and 1717 cm^{-1}), an intense band is found at 2059 cm^{-1} for the N=N=N asymmetric stretching mode. This frequency is significantly lower than those of organic azides (2170-2080 cm^{-1})[38] and consistent with other dinuclear copper complexes with bridging azide ligands (for example, [(Ph$_2$Ppypz)$_2$Cu$_2$(N$_3$)]$^{+}$ = 2037 cm^{-1}).[39]

3.6.3 Molecular Structure of [(6-MesDAC)CuN$_3$]$_2$ (17)

Single crystals of **17** were grown from a toluene solution layered with hexane.

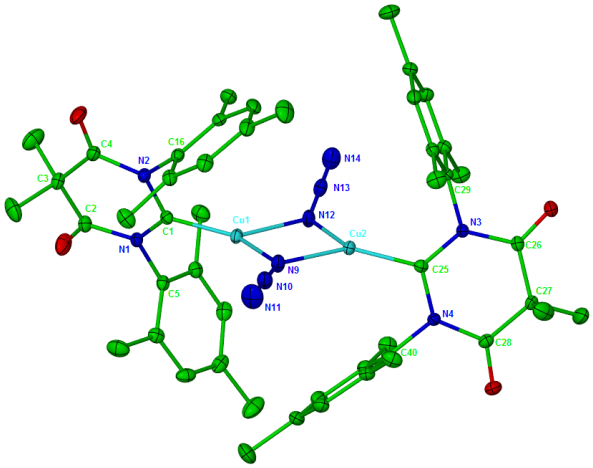

Figure 3.10: Displacement ellipsoid plot (30 % probability) of [(6-MesDAC)CuN$_3$]$_2$ (**17**). H atoms omitted for clarity. Selected bond lengths (Å) and angles (°): Cu(1)-C(1) 1.858(2), Cu(1)-N(9) 1.979(2), Cu(1)-N(12) 2.022(2), Cu(2)-C(25) 1.860(2), Cu(2)-N(9) 1.981(2), Cu(2)-N(12) 2.009(2), N(9)-N(10) 1.204(3), N(10)-N(11) 1.150(3), N(12)-N(13) 1.202(3), N(13)-N(14) 1.153(3), N(1)-C(1)-N(2) 116.71(19), C(1)-Cu(1)-N(9) 139.93(9), C(1)-Cu(1)-N(12) 132.88(9), N(9)-Cu(1)-N(12) 85.76(8), Cu(1)-N(9)-Cu(2) 95.17(9), Cu(1)-N(12)-Cu(2) 92.97(9), N(9)-Cu(2)-N(12) 86.08(8), N(9)-Cu(2)-C(25) 139.77(10), N(12)-Cu(2)-C(25) 132.19(9), N(3)-C(25)-N(4) 116.97(19).

Structurally characterised examples of copper(I) azides are rare, and no complex has previously been reported with N-heterocyclic carbene ligands. The range of known co-ordination modes is shown in Figure 3.11.

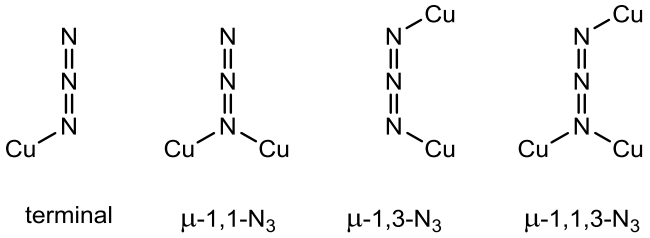

Figure 3.11: The co-ordination modes of azides: terminal (left, for example (dppe)Cu(N_3)(μ-dppe)Cu(N_3)(dppe)),[40] μ-1,1-N_3 (centre left, for example [(Ph_2Ppypz)$_2$Cu$_2$(N_3)]$^+$),[39] μ-1,3-N_3 (centre right, for example [(Ph_3P)$_2$Cu(N_3)]$_2$),[41] μ-1,1,3-N_3 (right, for example [(pyrazinecarboxamide)Cu(N_3)]$_\infty$).[42]

Complex **17** is dimeric, with two μ-1,1-N_3 azides, thus forming an unprecedented Cu_2N_2 structural motif amongst copper(I) azides. Complex **17** closely resembles the dimeric copper chloride complex **1**, perhaps reflecting the pseudohalide character of a μ-1,1-N_3 ligand. However, rather than adopting the rectangular geometry of **1**, the Cu_2N_2 core of **17** is distorted by having one azide closer to the centre of the core (Cu-N = 1.979(2) Å and 1.981(2) Å) than the other (Cu-N = 2.022(2) Å and 2.009(2) Å). The Cu-C bond lengths (1.858(2) Å and 1.860(2) Å) show no difference to those in complex **1** (1.871(5) Å and 1.867(5) Å). Each azide has a long proximal N-N bond (1.204(3) Å and 1.202(3) Å) and a short terminal N-N bond (1.150(3) Å and 1.153(3) Å), reflecting a reduction in bond order due to π back donation upon co-ordination to copper.

3.7 Synthesis of (6-MesDAC)CuC_6F_5 (18)

The introduction of fluorine-containing functional groups into organic molecules is of significant interest due to the applications of fluoro-organic compounds in materials, medical imaging and pharmaceuticals.[43] Copper containing fluorinating agents are increasingly employed in stoichiometric as well as catalytic applications. For example, (Phen)CuC_6F_5 (Figure 3.12) has been used to introduce the pentafluorophenyl group to aryl iodides,[44] hydroxylamines,[45] or propargyl phosphates.[46] Recently, a co-operative bimetallic system was used to catalyse the pentafluorophenylation of challenging aryl chlorides via a transmetallation mechanism, with (IPr)CuC_6F_5 (Figure 3.12) a crucial component.[47]

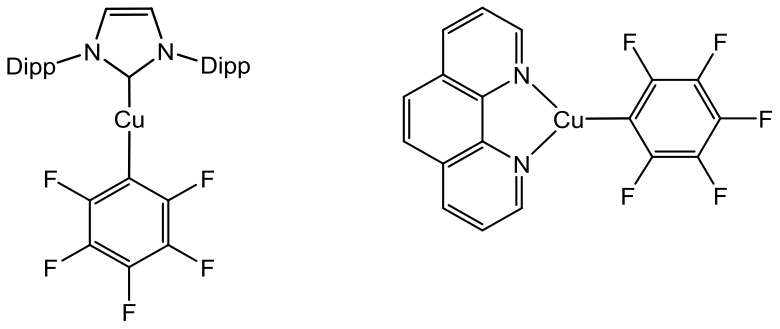

Figure 3.12: Examples of (L)CuC_6F_5 complexes employed in pentafluorophenylation reactions: (IPr)CuC_6F_5 (left),[47] (Phen)CuC_6F_5 (right).[44]

Addition of C_6F_5H to a benzene solution of **12** resulted in no reaction at room temperature, however heating the mixture to 333 K overnight formed mesitylene and (6-MesDAC)CuC_6F_5 (**18**) in quantitative yield. The lower reactivity of C_6F_5H compared to Ph_3SiOH is presumably a consequence of the lower acidity of C_6F_5H (pKa = 25.8).[48] **18** displays characteristic ^{19}F NMR signals, at very similar frequencies to those reported for (IPr)CuC_6F_5 (**18** = -112.5, -159.4, -163.0 ppm; (IPr)CuC_6F_5 = -115.9, -161.5, -164.2 ppm). Initial studies into pentafluorophenylation reactions with **18** will be discussed alongside those for (6-Mes)CuC_6F_5 (**22**, vide infra) in Section 3.9.

3.7.1 Molecular Structure of (6-MesDAC)CuC$_6$F$_5$ (18)

Single crystals of **18** were grown by slow evaporation of a benzene/hexane (1 : 4, v : v) solution.

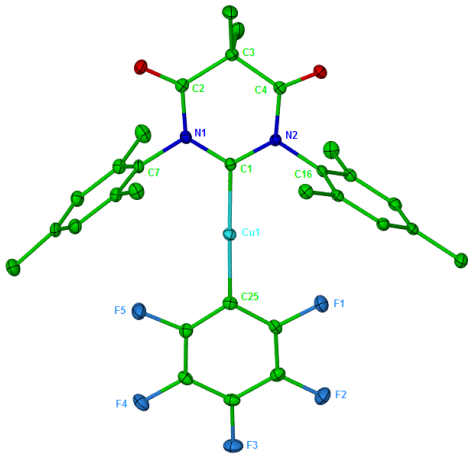

Figure 3.13: Displacement ellipsoid plot (30 % probability) of (6-MesDAC)CuC$_6$F$_5$ (**18**). H atoms omitted for clarity. Selected bond lengths (Å) and angles (°): Cu(1)-C(1) 1.902(3), Cu(1)-C(25) 1.922(3), N(1)-C(1)-N(2) 118.5(2), C(1)-Cu(1)-C(25) 175.41(11).

Complex **18** is the first structurally characterised (NHC)CuC$_6$F$_5$ complex and, as expected, is trans-linear (C-Cu-C = 175.41(11)°) about copper. The Cu-C$_6$F$_5$ bond length (1.922(3) Å) is slightly longer than reported for a range of substituted pyridine and bipyridine (Py)CuC$_6$F$_5$ complexes (1.8873(19) Å - 1.907(2) Å).[49] **18** adopts a co-planar arrangement of the carbene heterocycle and pentafluorophenyl ring (dihedral angle of 9°), whereby the *ortho*-fluorine substituents are oriented towards the N-mesityl substituents of 6-MesDAC. This coplanarity was also observed for complex **12** and, whilst the steric arguments presented there are still true for **18**, it raises the question of possible electronic communication between the π-accepting DAC and the mesityl or pentafluorophenyl π-systems.

3.8 Synthesis of Diaminocarbene Complexes

The methodology described above for diamidocarbenes was borne out by necessity due to the unavailability of the literature standard reaction of salt metathesis as an entry route to (6-MesDAC)CuOR chemistry. The mesityl complex **12** provided

alternative access to this chemistry, as well as proving a versatile synthon for the synthesis of a range of other complexes. This methodology is synthetically useful and, as shown in Scheme 3.8, applicable to NHCs other than 6-MesDAC.

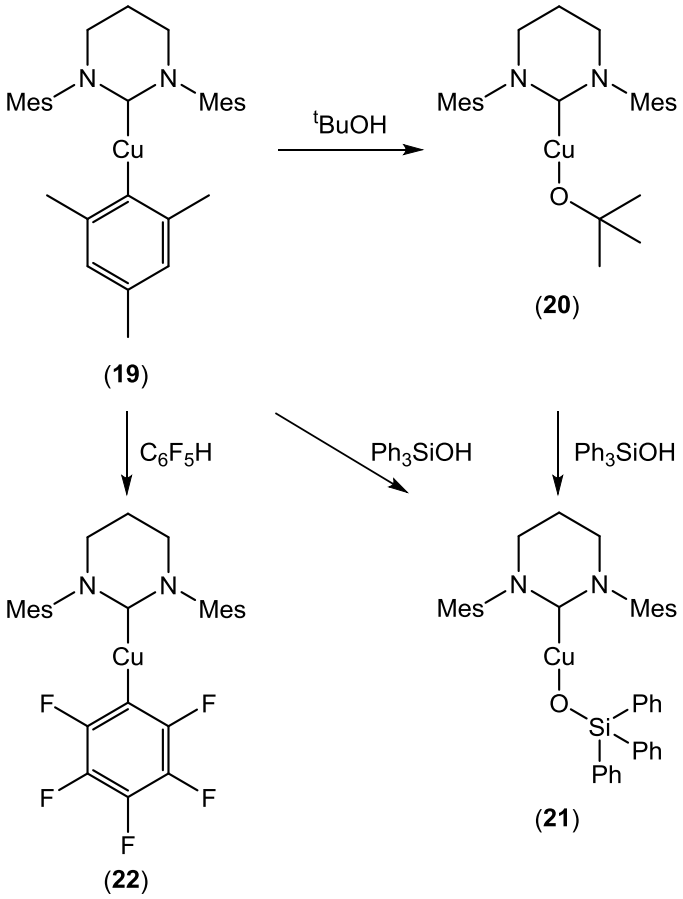

Scheme 3.8: (6-Mes)CuMes (**19**) as a precursor to a range of complexes via protonolysis.

3.8.1 Synthesis of (6-Mes)CuMes (19)

(6-Mes)CuMes (**19**) was synthesised by addition of a benzene solution of 6-Mes to $[CuMes]_n$, and isolated in 95 % yield as a white powder. Complex **19** is significantly less soluble in aromatic solvents than its 6-MesDAC analogue **12**. The carbenic carbon of **19** (205.1 ppm) resonated upfield of that of **12** (217.1 ppm). This relative deshielding of 6-MesDAC compared to 6-Mes was also observed in a series of Ru based alkene metathesis catalysts containing RENHCs and DACs.[50]

3.8.2 Synthesis of (6-Mes)CuO^{t}Bu (20)

Stirring a benzene solution of **19** with ^{t}BuOH overnight and subsequent removal of volatiles afforded (6-Mes)CuO^{t}Bu (**20**) as a white powder in 90 % yield. Analysis by ^{1}H and ^{13}C{^{1}H} NMR spectroscopy revealed resonances for the O^{t}Bu moiety at 1.20 ppm and 68.7/36.8 ppm respectively, while the carbenic resonance was located at 203.5 ppm, approximately 10 ppm upfield of that in the 6-MesDAC analogue **11** (213.5 ppm). In contrast to the 6-MesDAC complex **11**, **20** displayed poor solubility in benzene and toluene, but proved to be far more robust, with solutions being stable under anhydrous conditions for several weeks. Addition of water to a C_6D_6 solution of **20** resulted in the formation of an unidentified pale precipitate, alongside a colourless solution which was analysed by ^{1}H NMR spectroscopy and found to consist of ^{t}BuOH (1.05 ppm)[9] and an unidentified 6-Mes derivative.[i]

3.8.3 Synthesis of (6-Mes)CuOSiPh$_3$ (21)

(6-Mes)CuOSiPh$_3$ (**21**) was synthesised by addition of Ph$_3$SiOH to either **19** or **20** in benzene, or alternatively by addition of 6-Mes to [CuOSiPh$_3$]$_4$ in toluene. In all cases, **21** was isolated as a white powder in good yields. Its poor solubility required its characterisation in CD_2Cl_2, where the carbenic carbon was located at 202.0 ppm in the ^{13}C{^{1}H} NMR spectrum.

3.8.4 Synthesis of (6-Mes)CuC$_6$F$_5$ (22)

Addition of C_6F_5H to complex **19** generated (6-Mes)CuC_6F_5 (**22**), which was isolated in 73 % yield. Whereas the reaction of C_6F_5H with the 6-MesDAC analogue **12** required extended reaction times and heating to 333 K, the reaction with **19** reached completion after just 3 hours at room temperature. Complex **22** displays a very similar ^{19}F NMR spectrum to **18** (**22** = -112.3, -161.3, -163.6 ppm; **18** = -112.5, -159.4, -163.0 ppm). The ^{13}C signals for the pentafluorophenyl ring were not observed, but the carbenic carbon resonance was located at 203.1 ppm (14 ppm upfield of that in complex **18**) in the ^{13}C{^{1}H} NMR spectrum.

[i] Addition of water to (SIPr)Cu(OAc)$_2$ and SI^{t}Bu resulted in ring opening to give the corresponding amine formamides H(Dipp)N(CH$_2$)$_2$N(Dipp)C(O)H,[51] and H(^{t}Bu)N(CH$_2$)$_2$N(^{t}Bu)C(O)H respectively.[52] The formation of H(Mes)N(CH$_2$)$_3$N(Mes)C(O)H by hydrolysis of **20** was ruled out by comparison of the ^{1}H NMR spectrum with published values (6.91 (4 H, s, *m*-ArH), 3.33 (4 H, t, $^3J_{HH}$ = 5.9 Hz, NCH$_2$), 2.29-2.24 (20 H, m, overlapping) ppm) for that compound.[53]

3.8.5 Molecular Structures of (6-Mes)CuMes (19), (6-Mes)CuO^{t}Bu (20), (6-Mes)CuOSiPh$_3$ (21) and (6-Mes)CuC$_6$F$_5$ (22)

Single crystals of **19** and **21** were grown from saturated benzene (**19**) or CH_2Cl_2 (**21**) solutions layered with hexane. Complexes **20** and **22** precipitated from concentrated reactions of **19** with ^{t}BuOH or C_6F_5H, respectively, in benzene.

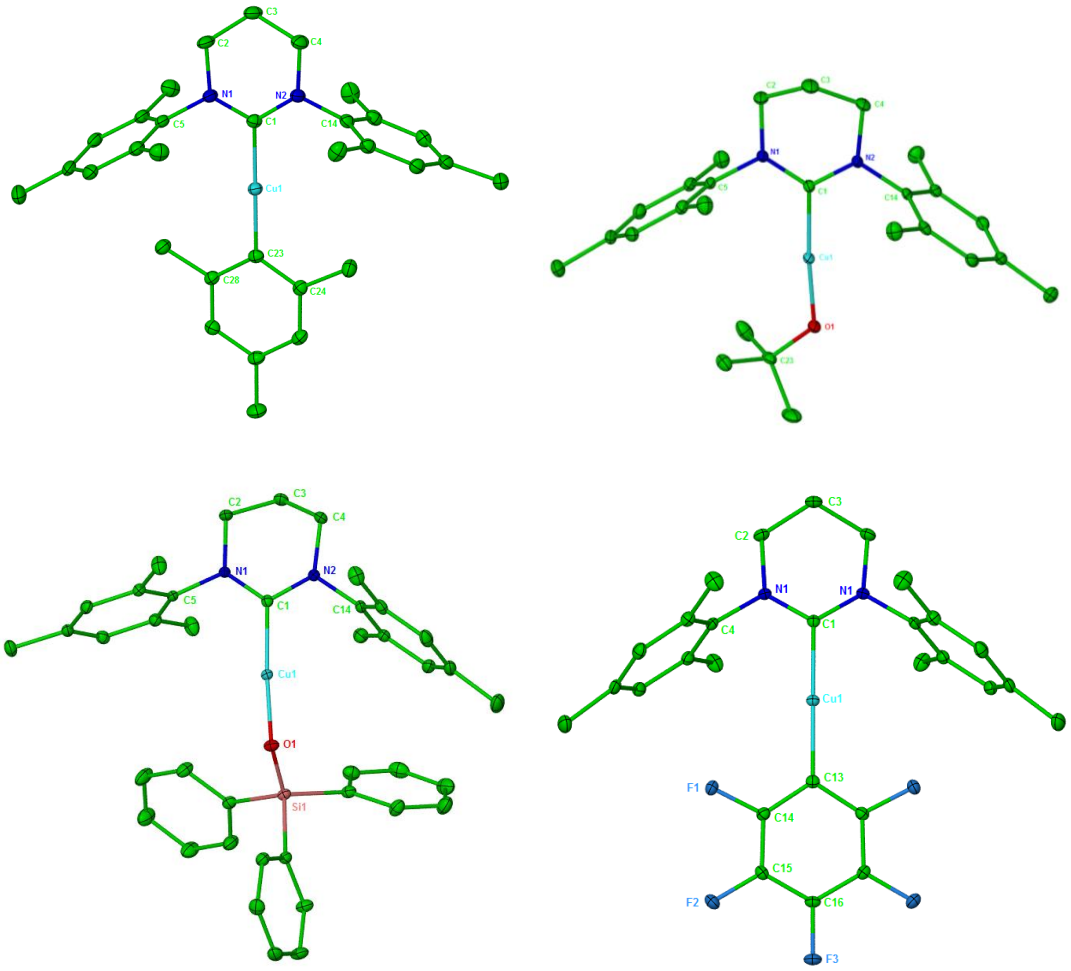

Figure 3.14: Displacement ellipsoid plots (30 % probability) of (6-Mes)CuMes (**19**, top left), (6-Mes)CuO^{t}Bu (**20**, top right), (6-Mes)CuOSiPh$_3$ (**21**, bottom left) and (6-Mes)CuC$_6$F$_5$ (**22**, bottom right). H atoms omitted for clarity. Selected bond lengths (Å) and angles (°):

Complex **19**: Cu(1)-C(1) 1.928(3), Cu(1)-C(23) 1.926(2), N(1)-C(1)-N(2) 116.43(18), C(1)-Cu(1)-C(23) 179.37(9).

Complex **20**: Cu(1)-C(1) 1.874(2), Cu(1)-O(1) 1.8016(15), O(1)-C(23) 1.407(3), N(1)-C(1)-N(2) 117.65(18), C(1)-Cu(1)-O(1) 175.31(8), Cu(1)-O(1)-C(23) 124.75(13).

Complex **21**: Cu(1)-C(1) 1.8783(15), Cu(1)-O(1) 1.8089(10), O(1)-Si(1) 1.5960(11), N(1)-C(1)-N(2) 117.00(13), C(1)-Cu(1)-O(1) 176.22(6), Cu(1)-O(1)-Si(1) 132.06(7).
Complex **22**: Cu(1)-C(1) 1.921(3), Cu(1)-C(13) 1.916(3), N(1)-C(1)-N(1') 118.8(2), C(1)-Cu(1)-C(13) 173.28(10). Symmetry transformations used to generate equivalent atoms: (x, y, -z+1/2).

All four complexes have very similar metrics to their 6-MesDAC analogues (**12**, **11**, **16** and **18** respectively) due to the identical steric demands of 6-MesDAC and 6-Mes, exemplified by their equal N-C-N angles (for example, **12** = 116.3(2)°; **19** = 116.43(18)°). However, the different electronic properties of 6-Mes and 6-MesDAC do result in some structural differences. The Cu-C_{NHC} bond lengths of the 6-Mes copper aryl complexes **19** (1.928(3) Å) and **22** (1.921(3) Å) are longer than those of their 6-MesDAC counterparts **12** (1.905(3) Å) and **18** (1.902(3) Å). With the coplanar arrangement of the aryl and carbene ligands in complexes **12**, **18**, **19** and **22**, a significant (C_{aryl}-p_π)-(Cu-d_π)-(C_{NHC}-p_π) interaction may be expected. The enhanced π-accepting character of 6-MesDAC may thus explain the stronger Cu-C_{NHC} bonds formed in complexes **12** and **18**. The 6-Mes silanoxide complex **21** also exhibits a longer Cu-C_{NHC} bond (1.8783(15) Å) than its 6-MesDAC analogue **16** (1.858(2) Å). Furthermore, the Cu-O bond of **21** (1.8089(10) Å) is longer than that of **16** (1.7947(14) Å). These structural differences between **21** and **16** suggest that the π-accepting nature of 6-MesDAC enhances the (O-p_π)-(Cu-d_π) bonding with silanoxide, strengthening both the Cu-O and Cu-C_{NHC} bonds of **16**. Alkoxides are weak π-donor ligands, and accordingly the Cu-C_{NHC} bond lengths of **20** (1.874(2) Å) and **11** (1.864(7) Å) are identical.

3.9 (6-MesDAC)CuC$_6$F$_5$ (18) and (6-Mes)CuC$_6$F$_5$ (22) as Cross Coupling Reagents

Whilst a full investigation of pentafluorophenylation with complexes **18** and **22** was beyond the scope of this work, preliminary reactions were conducted to establish an initial comparison of activity. Addition of two equivalents of the electron poor 3,5-bis(trifluoromethyl)iodobenzene to a C_6D_6 solution of **18** or **22** resulted in the formation of new ^{1}H (7.66 and 7.44 ppm) and ^{19}F (-62.8, -143.6, -153.4 and -161.3 ppm) NMR resonances indicative of the formation of 2,3,4,5,6-pentafluoro-3',5'-bis(trifluoromethyl)-1,1'-biphenyl (Scheme 3.9).[54] Both reactions required heating, and unexpectedly, the more electron rich 6-Mes complex **22** was significantly slower at transferring the pentafluorophenyl group than the 6-MesDAC complex **18** (**18**, 323 K, 20 hours = 24 % conversion; **22**, 323 K, 24 hours = 0 % conversion; **22**, 343 K, 72 hours = 26 % conversion).

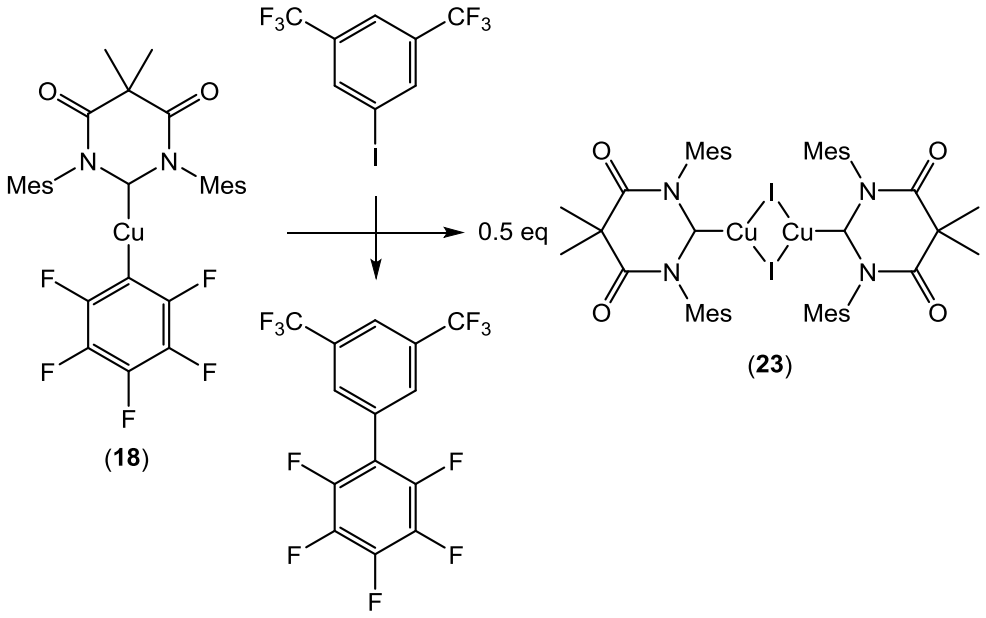

Scheme 3.9: Reaction of **18** with an aryl iodide.

The organometallic product of the reaction with **18** was identified as [(6-MesDAC)CuI]$_2$ (**23**) on the basis of its independent synthesis involving addition of 6-MesDAC to CuI in THF. Dark red/purple crystals of **23** were grown from a toluene solution layered with hexane, but were only of sufficient quality to confirm connectivity; the dimeric structure (analogous to **1**) of **23** is shown in Figure 3.15.

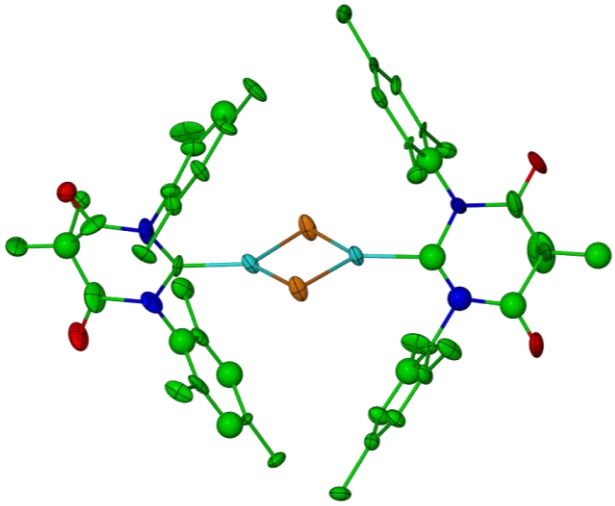

Figure 3.15: Picture confirming the connectivity of $[(6\text{-MesDAC})CuI]_2$ (**23**). H atoms omitted for clarity.

The ^{1}H NMR spectra of the organometallic product of the reaction with **22** seemed more complex than one would expect for (6-Mes)CuI, with two distinct carbene environments in a 1:8 ratio, suggesting that multiple organometallic products are being formed. To further investigate this behaviour, 6-Mes was reacted with CuI in THF. A single product was formed, and characterised by X-ray crystallography as $[(6\text{-Mes})_2Cu][CuI_2]$ (**24**, Figure 3.19). The ^{1}H NMR signals of **24** match the minor component from the reaction of **22** with aryl iodide. The major component of the reaction is likely to be the heteroleptic (6-Mes)CuI. If two organometallic complexes are each being formed in this reaction, this would raise questions about the mechanism of such a transformation. More likely is the possibility that (6-Mes)CuI is the initial product of the reaction, followed by its partial rearrangement by ligand dissociation to $[(6\text{-Mes})_2Cu][CuI_2]$ (**24**), thus explaining the observed mixture of products. The propensity of 6-Mes to form complexes containing the homoleptic $[(6\text{-Mes})_2Cu]^+$ cation will be discussed in later chapters with further examples.

3.9.1 Molecular Structure of $[(6\text{-Mes})_2Cu][CuI_2]$ (24)

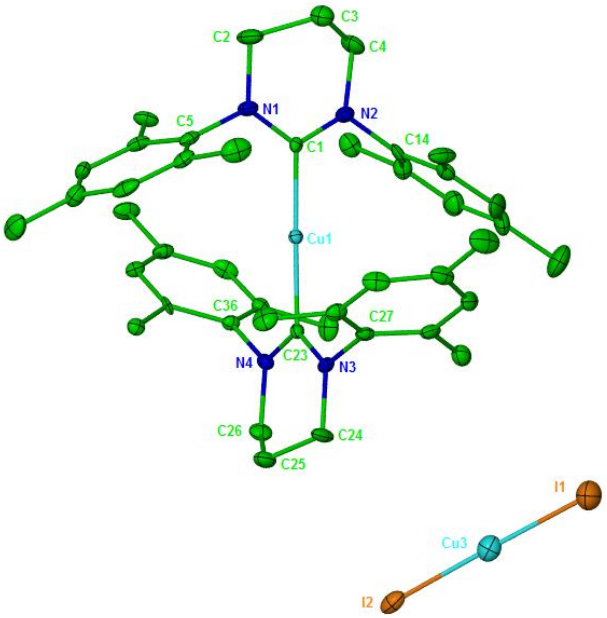

Figure 3.16: Displacement ellipsoid plot (30 % probability) of $[(6\text{-Mes})_2Cu][CuI_2]$ (**24**). H atoms omitted for clarity. Selected bond lengths (Å) and angles (°): Cu(1)-C(1) 1.920(10), Cu(1)-C(23) 1.967(10), Cu(3)-I(1) 2.397(3), Cu(3)-I(2) 2.351(2), N(1)-C(1)-N(2) 116.7(9), N(3)-C(23)-N(4) 118.6(9), C(1)-Cu(1)-C(23) 178.8(5), I(1)-Cu(3)-I(2) 178.80(10).

Complex **24** consists of two homoleptic ions. Each is approximately trans-linear (C-Cu-C = 178.8(5)°; I-Cu-I = 178.80(10)°), with the metrics of the cation matching those of the previously described $[(6\text{-Mes})_2Cu]$ $[BF_4]$ (**7**). The two Cu-I bond lengths are inequivalent (2.351(2) Å and 2.397(3) Å); lying either side of the Cu-I bond length reported for the heteroleptic (IPr)CuI complex (Cu-I = 2.3803(10) Å),[55] and the longer of the two being similar to that reported for a homoleptic mesoionic-NHC (MIC) complex ($[(MIC)_2Cu][CuI_2]$: Cu-I = 2.403(1) Å).[56]

3.9.2 Potential for Copper Catalysed Perfluoroarylation

These lead results with **18** and **22** merit further study in the future, particularly with regard to optimisation of conditions, extension to other Ar-X substrates and the synthesis of additional Cu-Ar_{Fn} derivatives. The related complexes (6-MesDAC)Cu(*p*-perfluoropyridyl) and (6-MesDAC)Cu(*p*-perfluorotolyl) were synthesised by addition of *p*-HC_5F_4N or *p*-$HC_6F_4CF_3$ respectively to complex **12** (quantitative conversion at room temperature = two days; 323 K = two hours) and spectroscopically identified from their ^{1}H and ^{19}F NMR spectra ((6-MesDAC)Cu(*p*-perfluoropyridyl) = -98.5 (2 F, br), -119.0 (2 F, br) ppm; (6-MesDAC)Cu(*p*-perfluorotolyl) = -143.3 (2 F, m), -112.2 (2 F, m), -56.0 (3 F, m) ppm).

The versatility of **12** and **19** as synthons to copper-perfluoroarenes could provide a great opportunity to gain insight into which properties of perfluoroarenes make them more or less suitable for cross-coupling reactions. Furthermore, the greater activity of 6-MesDAC over 6-Mes as a supporting ligand for this reaction suggests that the π-accepting character of NHCs warrant attention when designing systems for perfluoroarylation. Of greatest interest, would be the potential for catalytic perfluoroarylation, although preliminary attempts to reform **18** from **23** were unsuccessful. Addition of TMS-C_6F_5 to **23** resulted in no reaction, even at elevated temperatures. With salt-metathesis not a viable reaction for diamidocarbenes, and with the propensity for 6-Mes to form homoleptic copper halide complexes, the perfluoroarylation of aryl-halides may constitute a dead-end for catalysis. Exploration of different organic substrates, such as α,β-unsaturated ketones, may produce organometallic products, such as copper alkoxide complexes, which may be more easily recycled than copper halide complexes.

3.10 Conclusion

This Chapter began by demonstrating that salt metathesis of $[(6\text{-MesDAC})(CuCl)]_2$ (**1**) results in the bi-metallic ate complex $(6\text{-MesDAC})Cu(\mu\text{-Cl})(\mu\text{-O}^t\text{Bu})Li(THF)_2$ (**10**). A new methodology was developed to afford $(6\text{-MesDAC})CuO^t\text{Bu}$ (**11**) in high yields and purity by protonolysis of (6-MesDAC)CuMes (**12**) with ^{t}BuOH. A susceptibility to amide activation and subsequent isonitrile extrusion was found to be a common decomposition pathway for diamidocarbene complexes under basic conditions. Reaction of **12** with other protic reagents gave access to a range of complexes, with the evaporation of volatiles the only work up required. This simple synthetic procedure was also employed to generate a series of complexes with the ring expanded diaminocarbene 6-Mes. Despite the different electronic properties of 6-Mes and 6-MesDAC, these two series of complexes display very similar solid state structures. However, their physical properties are noticeably different: the 6-MesDAC complexes are intensely coloured and highly soluble in aromatic and polar solvents, whereas the 6-Mes complexes are all colourless and poorly soluble. The pentafluorophenyl complexes **18** and **22** were synthesised by protonolysis of the respective mesityl complexes **12** and **19** with C_6F_5H and were employed for stoichiometric cross coupling with 3,5-bis(trifluoromethyl)iodobenzene. The availability of a range of perfluorinated aromatic complexes, and the greater reactivity of **18** over **22**, warrant further study into $(NHC)Cu(Ar_{Fn})$ mediated perfluoroarylation reactions.

3.11 References for Chapter Three

(1) Collins, L. R.; Lowe, J. P.; Mahon, M. F.; Poulten, R. C.; Whittlesey, M. K. *Inorg. Chem.* **2014**, *53*, 2699–2707.

(2) Collins, L. R.; Riddlestone, I. M.; Mahon, M. F.; Whittlesey, M. K. *Chem. Eur. J.* **2015**, *21*, 14075–14084.

(3) Lazreg, F.; Nahra, F.; Cazin, C. S. J. *Coord. Chem. Rev.* **2015**, *293-294*, 48–79.

(4) Fujihara, T.; Xu, T.; Semba, K.; Terao, J.; Tsuji, Y. *Angew. Chem. Int. Ed.* **2011**, *50*, 523–527.

(5) Mankad, N. P.; Laitar, D. S.; Sadighi, J. P. *Organometallics* **2004**, *23*, 3369–3371.

(6) Nolan, S. P.; Marion, N.; Díez-González, S. *Chem. Rev.* **2009**, *109*, 3612–3676.

(7) Egbert, J. D.; Cazin, C. S. J.; Nolan, S. P. *Catal. Sci. Technol.* **2013**, *3*, 912–926.

(8) Cox, N.; Dang, H.; Whittaker, A. M.; Lalic, G. *Tetrahedron* **2014**, *70*, 4219–4231.

(9) Fulmer, G. R.; Miller, A. J. M.; Sherden, N. H.; Gottlieb, H. E.; Nudelman, A.; Stoltz, B. M.; Bercaw, J. E.; Goldberg, K. I. *Organometallics* **2010**, *29*, 2176–2179.

(10) Frey, G. D.; Donnadieu, B.; Soleilhavoup, M.; Bertrand, G. *Chem. Asian J.* **2011**, *6*, 402–405.

(11) Tsuda, T.; Hashimoto, T.; Saegusa, T. *J. Am. Chem. Soc.* **1972**, *94*, 658–659.

(12) Lemmen, T. H.; Goeden, G. V.; Huffman, J. C.; Geerts, R. L.; Caulton, K. G. *Inorg. Chem.* **1990**, *29*, 3680–3685.

(13) Van der Sluys, L. S.; Miller, M. M.; Kubas, G. J.; Caulton, K. G. *J. Am. Chem. Soc.* **1991**, *113*, 2513–2520.

(14) Tsuda, T.; Habu, H.; Horiguchi, S.; Saegusa, T. *J. Am. Chem. Soc.* **1974**, *96*, 5930–5931.

(15) Geerts, R. L.; Huffman, J. C.; Folting, K.; Lemmen, T. H.; Caulton, K. G. *J. Am. Chem. Soc.* **1983**, *105*, 3503–3506.

(16) Oguadinma, P. O.; Schaper, F. *Organometallics* **2009**, *28*, 4089–4097.

(17) Brussaard, Y.; Olbrich, F.; Behrens, U. *J. Organomet. Chem.* **1996**, *519*, 115–123.

(18) Goj, L. A.; Blue, E. D.; Munro-Leighton, C.; Gunnoe, T. B.; Petersen, J. L. *Inorg. Chem.* **2005**, *44*, 8647–8649.

(19) Goj, L. A.; Blue, E. D.; Delp, S. A.; Gunnoe, T. B.; Cundari, T. R.; Pierpont, A. W.; Petersen, J. L.; Boyle, P. D. *Inorg. Chem.* **2006**, *45*, 9032–9045.

(20) Tsuda, T.; Yazawa, T.; Watanabe, K.; Fujii, T.; Saegusa, T. *J. Org. Chem.* **1981**, *46*, 192–194.

(21) Eriksson, H.; Håkansson, M. *Organometallics* **1997**, *16*, 4243–4244.

(22) Gambarotta, S.; Floriani, C.; Chiesi-Villa, A.; Guastini, C. *J. Chem. Soc., Chem. Commun.* **1983**, 1156–1158.

(23) Stollenz, M.; Meyer, F. *Organometallics* **2012**, *31*, 7708–7727.

(24) Niemeyer, M. *Z. Anorg. Allg. Chem.* **2003**, *629*, 1535–1540.

(25) Janssen, M. D.; Köhler, K.; Herres, M.; Dedieu, A.; Smeets, W. J. J.; Spek, A. L.; Grove, D. M.; Lang, H.; van Koten, G. *J. Am. Chem. Soc.* **1996**, *118*, 4817–4829.

(26) Poulten, R. C.; López, I.; Llobet, A.; Mahon, M. F.; Whittlesey, M. K. *Inorg. Chem.* **2014**, *53*, 7160–7169.

(27) Gowda, B. T.; Kožíšek, J.; Tokarčík, M.; Fuess, H. *Acta Crystallogr. Sect. E Struct. Rep. Online* **2008**, *64*, o987.

(28) Schmidt, D.; Berthel, J. H. J.; Pietsch, S.; Radius, U. *Angew. Chem. Int. Ed.* **2012**, *51*, 8881–8815.

(29) Arrowsmith, M.; Hill, M. S.; Kociok-Köhn, G.; MacDougall, D. J.; Mahon, M. F. *Angew. Chem. Int. Ed.* **2012**, *51*, 2098–2100.

(30) Bose, S. K.; Fucke, K.; Liu, L.; Steel, P. G.; Marder, T. B. *Angew. Chem. Int. Ed. Engl.* **2014**, *53*, 1799–803.

(31) Wyss, C. M.; Tate, B. K.; Bacsa, J.; Gray, T. G.; Sadighi, J. P. *Angew. Chem. Int. Ed.* **2013**, *52*, 12920–12923.

(32) Kleeberg, C.; Cheung, M. S.; Lin, Z.; Marder, T. B. *J. Am. Chem. Soc.* **2011**, *133*, 19060–19063.

(33) Tapu, D.; Dixon, D. A.; Roe, C. *Chem. Rev.* **2009**, *109*, 3385–3407.

(34) McGeary, M. J.; Wedlich, R. C.; Coan, P. S.; Folting, K.; Caulton, K. G. *Polyhedron* **1992**, *11*, 2459–2473.

(35) Duchateau, R.; Cremer, U.; Harmsen, R. J.; Mohamud, S. I.; Abbenhuis, H. C. L.; van Santen, R. A.; Meetsma, A.; Thiele, S. K.-H.; van Tol, M. F. H.; Kranenburg, M. *Organometallics* **1999**, *18*, 5447–5459.

(36) Reeve, W.; Erikson, C. M.; Aluotto, P. F. *Can. J. Chem.* **1979**, *57*, 2747–2754.

(37) Arias-Ugarte, R.; Sharma, H. K.; Morris, A. L. C.; Pannell, K. H. *J. Am. Chem. Soc.* **2012**, *134*, 848–851.

(38) Lieber, E.; Rao, C. N. R.; Chao, T. S.; Hoffman, C. W. W. *Anal. Chem.* **1957**, *29*, 916–918.

(39) Kuang, S.-M.; Zhang, Z.-Z.; Wang, Q.-G.; Mak, T. C. W. *J. Chem. Soc., Dalton Trans.* **1997**, 4477–4478.

(40) Gaughan, A. P.; Ziolo, R. F.; Dori, Z. *Inorg. Chem.* **1971**, *10*, 2776–2781.

(41) Dori, Z.; Ziolo, R. F.; Gaughan, A. P.; Pierpont, C. G.; Eisenberg, R. *Inorg. Chem.* **1971**, *10*, 1289–1296.

(42) Goher, M. A. S.; Mautner, F. A. *J. Chem. Soc., Dalton Trans.* **1999**, 1535–1536.

(43) Liang, T.; Neumann, C. N.; Ritter, T. *Angew. Chem. Int. Ed.* **2013**, *52*, 8214–8264.

(44) Do, H.-Q.; Khan, R. M. K.; Daugulis, O. *J. Am. Chem. Soc.* **2008**, *130*, 15185–15192.

(45) Matsuda, N.; Hirano, K.; Satoh, T.; Miura, M. *Synthesis* **2012**, *44*, 1792–1797.

(46) Nakatani, A.; Hirano, K.; Satoh, T.; Miura, M. *Org. Lett.* **2012**, *14*, 2586–2589.

(47) Lesieur, M.; Lazreg, F.; Cazin, C. S. J. *Chem. Commun.* **2014**, *50*, 8927–8929.

(48) *Progress in Inorganic Chemistry, Volume 57, Page 262*; Karlin, K. D., Ed.; John Wiley & Sons, Inc.: Hoboken, NJ, USA, 2011.

(49) Doshi, A.; Sundararaman, A.; Venkatasubbaiah, K.; Zakharov, L. N.; Rheingold, A. L.; Myahkostupov, M.; Piotrowiak, P.; Jäkle, F. *Organometallics* **2012**, *31*, 1546–1558.

(50) Moerdyk, J. P.; Bielawski, C. W. *Organometallics* **2011**, *30*, 2278–2284.

(51) Kolychev, E. L.; Shuntikov, V. V; Khrustalev, V. N.; Bush, A. A.; Nechaev, M. S. *Dalton Trans.* **2011**, *40*, 3074–6.

(52) Denk, M. K.; Rodezno, J. M.; Gupta, S.; Lough, A. J. *J. Organomet. Chem.* **2001**, *617-618*, 242–253.

(53) Zhang, J.; Fu, J.; Su, X.; Wang, X.; Song, S.; Shi, M. *Chem. Asian J.* **2013**, *8*, 552–555.

(54) Chang, J. W. W.; Chia, E. Y.; Chai, C. L. L.; Seayad, J. *Org. Biomol. Chem.* **2012**, *10*, 2289–2299.

(55) Díez-González, S.; Escudero-Adán, E. C.; Benet-Buchholz, J.; Stevens, E. D.; Slawin, A. M. Z.; Nolan, S. P. *Dalton Trans.* **2010**, *39*, 7595–7606.

(56) Hohloch, S.; Duecker, F. L.; van der Meer, M.; Sarkar, B. *Molecules* **2015**, *20*, 7379–7395.

CHAPTER FOUR

CHAPTER FOUR: Discovery of Facile Migratory Insertion Reactions with Metal-Bound Diamidocarbenes

Some of the work in this Chapter has been published in:[1,2]

Lactide Polymerisation by Ring-expanded NHC Complexes of Zinc: Collins, L. R.; Moffat, L. A.; Mahon, M. F.; Jones, M. D.; Whittlesey, M. K. *Polyhedron* **2016**, *103*, 121 – 125

Unexpected Migratory Insertion Reactions of $M(alkyl)_2$ (M = Zn, Cd) and Diamidocarbenes: Collins, L. R.; Hierlmeier, G.; Mahon, M. F.; Riddlestone, I. M.; Whittlesey, M. K. *Chem. Eur. J.* **2015**, *21*, 3215 – 3218

4.1 Preface

In Chapter Five, the σ-bond metathesis reactions of Et_3SiH with (6-MesDAC)CuO^tBu (**11**) and (6-Mes)CuO^tBu (**20**) will be discussed. However, to better understand those findings, and to stay true to the actual chronology of the research, this Chapter will describe the chemistry of 6-Mes, 7-Mes and 6-MesDAC complexes of zinc and cadmium dialkyls. Simple co-ordination complexes were sought, and indeed formed in the case of the ring expanded diaminocarbenes 6-Mes and 7-Mes. However, reactions with 6-MesDAC instead led to the discovery of an extremely facile migratory insertion process for metal-bound diamidocarbenes. This migratory insertion process has far-reaching implications for copper hydride chemistry, and these will be discussed in Chapter Five.

4.2 Synthesis of (6-Mes)$ZnMe_2$ (25) and (7-Mes)$ZnMe_2$ (26)

Addition of a toluene solution of $ZnMe_2$ to a benzene solution of either 6-Mes or 7-Mes resulted in the formation of the three co-ordinate species (6-Mes)$ZnMe_2$ (**25**) and (7-Mes)$ZnMe_2$ (**26**), which were isolated as white powders in 44 % and 58 % yield respectively. These complexes were found to be highly soluble in both aromatic and polar solvents and very sensitive to air and moisture. Complex **26** was characterised by the presence of a carbenic resonance in the $^{13}C\{^1H\}$ NMR spectrum at 225.8 ppm, significantly downfield of that for **25** (214.7 ppm), consistent with the increased basicity of a seven-membered over a six-membered ring NHC.[3] The zinc methyl ^1H (**25** = -0.67 ppm; **26** = -0.75 ppm) and $^{13}C\{^1H\}$ (**25** = -8.8 ppm; **26** = -8.6

ppm) resonances are similar to those of the known five-membered ring NHC complexes (IPr)$ZnMe_2$ (-1.65 ppm; -9.5 ppm), (IMes)$ZnMe_2$ (-1.38 ppm; -7.7 ppm) and (I^tBu)$ZnMe_2$ (0.01 ppm; -7.2 ppm).[4]

4.2.1 Molecular Structures of (6-Mes)$ZnMe_2$ (25) and (7-Mes)$ZnMe_2$ (26)

Single crystals of **25** and **26** were grown from concentrated toluene solutions layered with hexane.

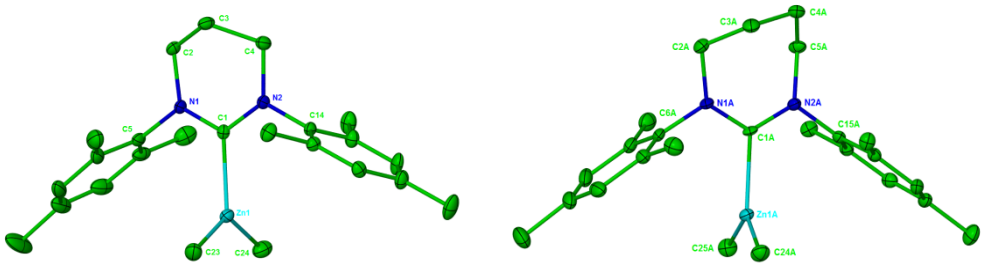

Figure 4.1: Displacement ellipsoid plots (30 % probability) of (6-Mes)$ZnMe_2$ (**25**) and (7-Mes)$ZnMe_2$ (**26**). H atoms omitted for clarity. Selected bond lengths (Å) and angles (°):

Complex **25**: Zn(1)-C(1) 2.099(3), Zn(1)-C(23) 2.005(4), Zn(1)-C(24) 2.001(4), N(1)-C(1)-N(2) 117.7(3), C(1)-Zn(1)-C(23) 115.51(14), C(1)-Zn(1)-C(24) 115.98(14), C(23)-Zn(1)-C(24) 128.51(16).

Complex **26**: Zn(1A)-C(1A) 2.100(5), Zn(1A)-C(24A) 2.014(7), Zn(1A)-C(25A) 1.995(7), N(1A)-C(1A)-N(2A) 119.6(5), C(1A)-Zn(1A)-C(24A) 117.1(3), C(1A)-Zn(1A)-C(25A) 115.7(3), C(24A)-Zn(1A)-C(25A) 127.1(3).

Analysis of the structural parameters of (NHC)$ZnMe_2$ complexes reveal that the bond lengths about zinc are insensitive to the nature of the NHC. Accordingly, the Zn-C_{Me} bond lengths of **25** (2.005(4) Å and 2.001(4) Å) are the same as those of **26** (2.014(7) Å and 1.995(7) Å) and (IPr)$ZnMe_2$ (1.990(3) Å and 1.994(3) Å) but, in all cases, longer than in crystalline $ZnMe_2$ (1.927(6) Å (α-phase); 1.911(14) Å and 1.920(13) Å (β-phase)).[5] Furthermore, no difference is seen in the Zn-C_{NHC} bond lengths of the two structures in Figure 4.1 (**25** = 2.099(3) Å; **26** = 2.100(5) Å) and these are also identical to those in (IPr)$ZnMe_2$ (2.112(2) Å),[4] (IPr)$ZnEt_2$ (2.1000(18) Å)[6] and (IAd)$ZnEt_2$ (2.096(3) Å).[7] There is, however, a strong correlation between NHC steric bulk (demonstrated by the N-C-N angle:

(IPr)$ZnMe_2$ = 103.3(2)°; **25** = 117.7(3)°; **26** = 119.6(5)°) and an increasingly orthogonal relationship between the planes of $ZnMe_2$ and the NHC ((IPr)$ZnMe_2$ = 81.1°; **25** = 84.2°; **26** = 85.8°), accompanied by a compression of the C_{Me}-Zn-C_{Me} angles ((IPr)$ZnMe_2$ = 133.4(1)°; **25** = 128.51(16)°; **26** = 127.1(3)°).[4] The manifestation of only subtle structural changes for complexes of five-, six- and seven-membered ring NHCs may be due to the competing influences of enhanced nucleophilicity and increased steric bulk of RENHCs over their five-membered ring analogues.

4.3 Ring Opening Polymerisation of *Rac*-Lactide with Complexes 25 and 26

Zinc alkyl complexes have received much interest in the literature as initiators for the ring opening polymerisation (ROP) of *rac*-lactide (Scheme 4.1). Amongst the numerous ligands used to support these complexes (for example, 8-hydroxyquinolines,[8] phosphinophenols,[9] and aminophenols),[10] NHCs offer an especially tuneable platform. However, the exact nature of the catalytic species is often unclear, with the NHC ligand seemingly prone to dissociation,[11] whereby it too can initiate organocatalysis.[12] One approach to inhibit the dissociation of NHC from zinc is to use an anionic (for example, amide or alkoxide) chelating tether,[13] although dissociation has still been observed in some cases.[6] We sought to investigate whether highly basic RENHCs are less prone to dissociation under the conditions of catalysis. Complexes **25** and **26** were thus tested for their activity in the ring opening polymerisation of *rac*-lactide, alongside the free RENHCs 6-Mes and 7-Mes, according to the conditions shown in Scheme 4.1.

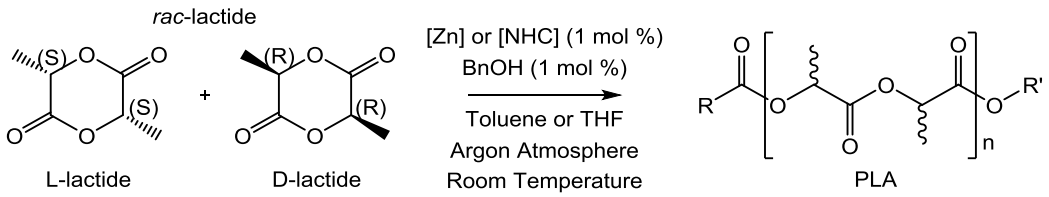

Scheme 4.1: Conditions employed for the ring opening polymerisation of *rac*-lactide to produce PLA.

4.3.1 Characterisation of Poly-*Rac*-Lactide

The success of a precatalyst for the ROP of *rac*-lactide is quantified in several ways. Most simply, the percentage conversion of the monomer into polymer within a given time frame quantifies the activity of a catalytic system. The reaction shown in Scheme 4.1 was quenched after 2 hours by opening to air and extracting the residue into CH_2Cl_2. Conversion was assessed by integration of the ^1H NMR methine resonances for *rac*-lactide (5.03 – 5.08 ppm) and PLA (5.13 – 5.30 ppm). As well as high activity, a well controlled polymerisation process is also desired, since this allows for the consistent production of PLA samples with specific physical properties. A high molecular weight (M_n) is essential for polymers with high melting points and tensile strength. The polydispersity index (PDI) represents the standard deviation of polymer molecular weights about the average (M_n). A PDI of 1.00 represents a uniform sample of polymer, with higher PDI values representing poorer control of molecular weight. PLA molecular weights were determined by GPC analysis. A further measure of polymerisation control is the stereochemistry, or tacticity, of the polymer produced. If two adjacent lactide units in a polymer chain have the same relative stereochemistry, then this is termed a meso diad (Figure 4.2). The probability of meso diads (P_m) within the polymer chain quantifies the enrichment of tacticity.

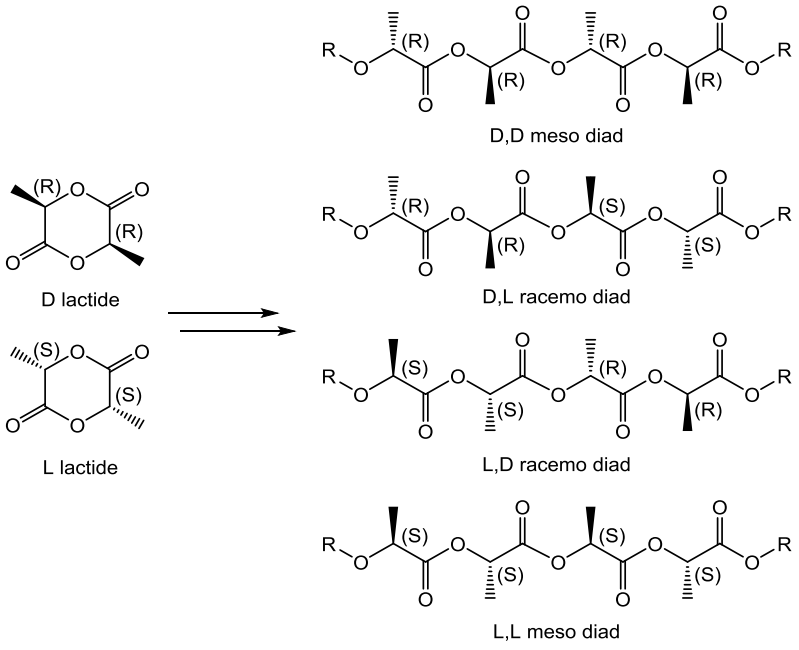

Figure 4.2: Meso and racemo diads of D- and L-lactide.

For example, random addition of D- or L-lactide to a polymer chain results in an atactic polymer with a P_m value of 0.50. Polymerisation of enantiomerically pure L-lactide would result in poly-L-lactide with a P_m value of 1.00, corresponding to 100 % meso linkages and therefore an isotactic polymer. P_m values were assessed by integration of diastereomeric tetrad methine resonances in selectively decoupled $^1H\{^1H\}$ NMR spectra.[14] The results of *rac*-lactide ROP by complexes **25**, **26** and the free RENHCs 6-Mes and 7-Mes are presented in Table 4.1.

4.3.2 Results of Catalytic ROP of *Rac*-Lactide

Catalyst	[LA]:[Cat]:[BnOH]	Conversion[a]	Solvent	M_n[b]	PDI[b]	P_m[c]
25	100:1:1	98	Toluene	21300	1.51	0.65
25[d]	100:1:1	99	Toluene	23200	1.18	0.70
25	100:1:2	99	Toluene	11100	1.30	0.60
25	100:1:1	44	THF	5700	1.11	n/d
6-Mes	100:1:1	98	Toluene	19100	1.21	0.65
6-Mes	100:1:1	77	THF	7750	1.15	0.65
26	100:1:1	98	Toluene	17550	1.10	0.65
26	100:1:1	33	THF	5800	1.11	0.50
7-Mes	100:1:1	99	Toluene	13250	1.46	0.60
7-Mes	100:1:1	60	THF	6450	1.18	0.60

Table 4.1: Results of ring opening polymerisation of *rac*-lactide. [a] Percentage conversions determined from ^1H NMR spectra. [b] Molecular weight (Daltons) distributions determined from GPC analysis. [c] Isotactic enrichments determined from $^1H\{^1H\}$ NMR spectra. [d] Conducted at 273 K.

In toluene, all four systems were highly active for the ROP of *rac*-lactide, with near quantitative conversions to PLA within 2 hours at room temperature. Reducing the temperature to 273 K still afforded near quantitative conversion, demonstrating the high activity of **25**. At this temperature, the polymerisation was also better controlled, producing PLA with a higher molecular weight (M_n at room temperature

= 21300; at 273 K = 23200), a much lower PDI (room temperature = 1.51; 273 K = 1.18) and a slightly higher P_m (room temperature = 0.65; 273 K = 0.70). Increasing the equivalents of BnOH from 1 to 2 approximately halved the molecular weight of the polymers produced at room temperature (1 equivalent = 21300; 2 equivalents = 11100), consistent with a living polymerisation.[15]

Comparing the activity of **25** with the corresponding free RENHC 6-Mes reveals that they are both active pre-catalysts for the ROP of *rac*-lactide, with both systems affording 98 % conversion to PLA within 2 hours at room temperature in toluene. However, the samples of PLA produced had different physical properties, with 6-Mes yielding PLA with a lower average molecular weight (**25** = 21300; 6-Mes = 19100) and a narrower molecular weight distribution (**25** = 1.51; 6-Mes = 1.21) than **25**. These differences suggest that a different reaction profile is in operation for each of the two systems and that the catalysis with **25** is not solely due to dissociation of free 6-Mes. The moderate isotactic enrichment of the PLA remains consistent between the two systems (P_m = 0.65), suggesting that the steric environment of the active site is similar (likely dominated by the flanking N-mesityl groups) for both 6-Mes and **25**.

Complex **26** and its corresponding free RENHC, the more sterically demanding 7-Mes, are also highly active precatlysts for the ROP of *rac*-lactide in toluene, affording near quantitative conversions in 2 hours at room temperature. The physical properties of the PLA produced again differ between the zinc complex and free NHC (M_n: **26** = 17550; 7-Mes = 13250, PDI: **26** = 1.10; 7-Mes = 1.46), in both cases leading to lower molecular weight polymers than from the analogous 6-Mes systems. The molecular weight distribution of the PLA produced by **26** had the narrowest distribution (PDI = 1.10) of the systems tested, although only moderate isotactic enrichment (P_m = 0.65) was observed.

Changing the solvent from toluene to THF significantly reduced the activity of all systems. The biggest reduction was evident for the zinc complexes, where the donor properties of THF may lead to competitive binding of solvent and substrate. In all cases, the polymers produced in THF were of low molecular weight (M_n ranging from 5700 to 7750), albeit with narrow molecular weight distributions (PDI ranging from 1.11 to 1.18). In the cases of complex **26** and 7-Mes, the moderate isotactic

enrichment previously observed in toluene was eroded to produce more atactic polymers with P_m values of 0.50 and 0.60 respectively.

4.3.3 Discussion

The results show a strong solvent effect on catalysis. In toluene, all four systems display excellent activity, although the more sterically demanding 7-Mes systems produce lower molecular weight polymers than those based on 6-Mes. In THF, the free carbenes display moderate activity, whereas the zinc complexes have very poor activity. As well as bulk activity, the discrepancy between polymerisation control with each free RENHC and its respective zinc complex also depends on solvent. In toluene, the polymers produced by the free carbenes differ significantly in their physical characteristics to those produced by the corresponding zinc complexes. In THF, the physical properties of the PLA produced by the free carbenes more closely resemble those of the PLA produced by their zinc complexes.

A possible explanation for this solvent effect could be that THF strongly inhibits the activity of metal-based catalysis due to competitive binding at the metal centre. Small amounts of carbene dissociation in THF would allow for organocatalysis to operate, and indeed dominate over the solvent-quenched organometallic reactivity (Figure 4.3). This behaviour would account for the similar physical properties of PLA produced in THF with both RENHCs and their respective zinc complexes as precatalysts. Furthermore, the lower activity of the zinc systems is accounted for by the partial dissociation leading to a lower concentration of RENHC than when isolated RENHC is used as the precatalyst. Similar levels of carbene dissociation in toluene could also lead to organocatalysis. However, the high activity of the zinc complexes in this solvent would compete with any organocatalysis and the physical properties of the polymers produced would predominantly be determined by the organometallic catalysis.

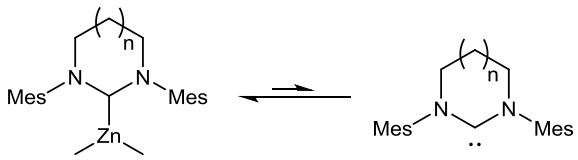

Toluene	Very high activity	Very high activity
THF	Very low activity	Moderate activity

Figure 4.3: Possible explanation of how carbene dissociation may have different effects on catalysis in toluene and THF.

More detailed mechanistic studies are required to identify the nature of the catalytically active species under these conditions, and to prove whether carbene dissociation is a contributory factor to ROP with complexes **25** and **26** as precatalysts. These preliminary results show that both the complexes and their free RENHCs are viable catalysts under the conditions employed and even for such strongly donating ligands as RENHCs, carbene dissociation still appears to take place.

4.4 Synthesis of (6-MesDAC)$ZnEt_2$ (27)

In contrast to the simple three co-ordinate adducts of $ZnMe_2$ formed with 6-Mes and 7-Mes, reaction of the diamidocarbene 6-MesDAC with dialkyl zinc precursors yielded far more complex chemistry. Addition of a heptane solution of $ZnEt_2$ to a benzene solution of 6-MesDAC at room temperature resulted in the immediate formation of a bright red solution. However, this only appeared as a flash of colour since, within seconds, this was replaced by a colourless solution and a large amount of white precipitate. When the reaction was conducted in THF-d_8, cooled in an acetone slurry (178 K), the red solution was stabilised and could be transferred to a pre-cooled NMR spectrometer, allowing for the low temperature spectroscopic characterisation of (6-MesDAC)$ZnEt_2$ (**27**). The ^{1}H NMR spectrum showed a mutually coupled triplet (0.70 ppm) and quartet (-0.48 ppm) in a 6 : 4 ratio for the two zinc ethyl groups, alongside a set of four ^{1}H resonances in a 4 : 6 : 12 : 6 ratio, consistent with a C_s symmetric, metal bound 6-MesDAC. The carbenic carbon was located in the $^{13}C\{^1H\}$ NMR spectrum at 236.9 ppm, downfield of the RENHC signals in **25** (6-Mes = 213.7 ppm) and **26** (7-Mes = 225.8 ppm).

4.5 Synthesis of [(6-MesDAC·Et)ZnEt]$_n$ (28)

Upon warming a THF-d_8 solution of **27** to just 210 K, all product resonances disappeared from the NMR spectrum with concomitant formation of a colourless solution and precipitation of a white solid. Crystallisation of this precipitate from CH_2Cl_2 layered with hexane, and analysis by X-ray diffraction, revealed the precipitate to be [(6-MesDAC·Et)ZnEt]$_n$ (**28**, Figure 4.4), the product of migratory insertion of an ethyl group from zinc onto the C2 position of 6-MesDAC (Scheme 4.2). Addition of a heptane solution of $ZnEt_2$ to a hexane suspension of 6-MesDAC at room temperature allowed the isolation of **28** in 91 % yield.

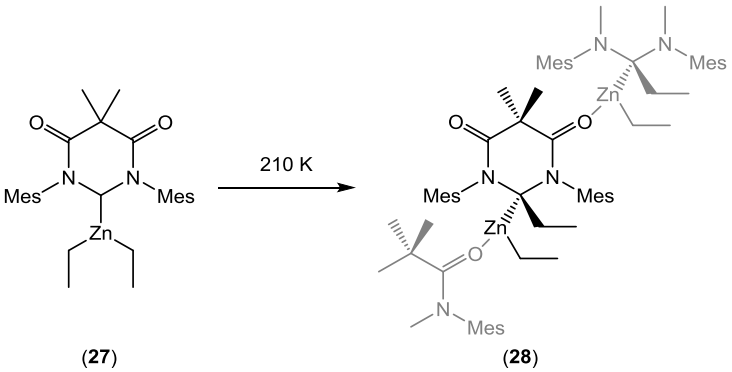

Scheme 4.2: Migratory insertion reaction of **27** to yield the polymeric complex **28**.

The newly formed 6-MesDAC·Et group is no longer a diamidocarbene, but instead a diamidoalkyl ligand. The appearance of a new resonance in the $^{13}C\{^1H\}$ NMR spectrum at 88.0 ppm is diagnostic for the quaternary carbon at the C2 position. In ^1H-^{13}C HMBC NMR spectra, this signal shows distinctive two- and three-bond couplings to ^1H resonances for the migrated ethyl group (methylene = 2.27 ppm; methyl = 0.73 ppm), which shows a significantly downfield shifted methylene ^1H NMR resonance compared to the non-migrated zinc ethyl (methylene = 0.00 ppm; methyl = 0.84 ppm). The migratory insertion to form 6-MesDAC·Et results in the C2 position becoming four co-ordinate, and therefore the loss of the plane of symmetry (perpendicular to the NCN plane) possessed by 6-MesDAC. This is evident in ^1H NMR spectra, where the two 6-MesDAC·Et backbone methyl groups are inequivalent (1.73 ppm and 1.51 ppm). Furthermore, the appearance of five ^1H NMR signals between 7.03 ppm and 2.22 ppm in a 2 : 2 : 6 : 6 : 6 ratio shows that the N-mesityl substituents are not freely rotating due to increased steric congestion.

The IR spectrum of **28** shows two carbonyl bands of equal intensity, with the higher frequency amide CO stretch (1651 cm^{-1}) similar to that of the of the ring opened hydrolysis product **14** (1684 cm^{-1}), confirming that 6-MesDAC·Et consists of two non-conjugated amides, separated by an sp^3 hybridised C2 carbon. The lower frequency (1576 cm^{-1}) of the second CO stretch is evidence of isocarbonyl bridging to zinc, as confirmed by X-ray crystallography (Figure 4.4). This results in the formation of one dimensional polymers of **28** in the solid state. DOSY ^{1}H NMR experiments suggest that **28** exists as a monomer in CD_2Cl_2 solutions, on the basis of the hydrodynamic radius (r_H = 4.7 Å) being in good agreement with the monomeric radius calculated from the solid state structure ($r_{X\text{-}ray}$ = 5.3 Å)[i]. Complex **28** was tested as a precatalyst for the ROP of *rac*-lactide under the conditions shown in Scheme 4.1, but no activity was observed.

4.5.1 Molecular Structure of [(6-MesDAC·Et)ZnEt]$_n$ (28)

Single crystals suitable for X-ray diffraction studies were grown from a saturated CH_2Cl_2 solution of **28** layered with hexane.

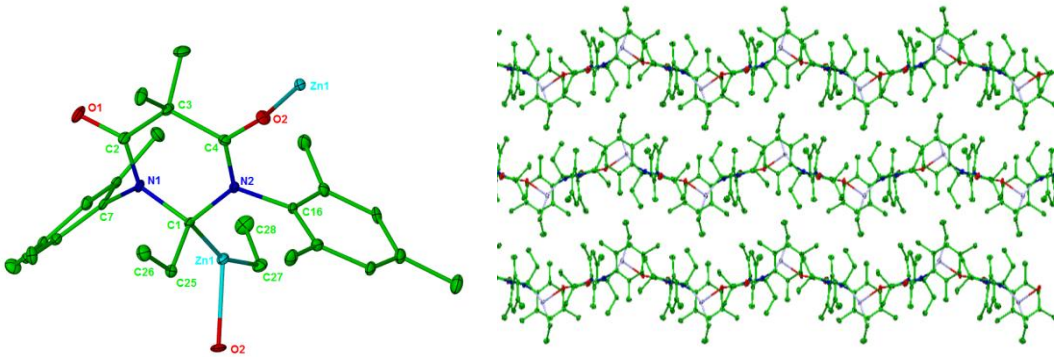

Figure 4.4: Displacement ellipsoid plot (30 % probability) of the asymmetric unit of [(6-MesDAC·Et)ZnEt]$_n$ (**28**) (left). H atoms omitted for clarity. Selected bond lengths (Å) and angles (°): Zn(1)-C(1) 2.059(4), Zn(1)-C(27) 1.998(4), Zn(1)-O(2) 2.166(3), C(2)-O(1) 1.230(5), C(4)-O(2) 1.238(5), N(1)-C(1)-N(2) 109.6(3), C(1)-Zn(1)-C(27) 159.90(17), C(1)-Zn(1)-O(2) 99.50(14), C(27)-Zn(1)-O(2) 100.44(16), C(4)-O(2)-Zn(1) 153.1(3). Displacement ellipsoid plot (30 % probability) showing three adjacent polymeric chains of [(6-MesDAC·Et)ZnEt]$_n$ (**28**) (right). H atoms omitted for clarity.

[i] $r_{X\text{-}ray}$ was calculated from $U=(4\pi(r_{X\text{-}ray})^3)/3$ in which U = volume of the unit cell/number of monomers in the unit cell.

Complex **28** is polymeric by virtue of a weak Zn-O interaction (2.166(3) Å; cf: sum of covalent radii = 1.88(6) Å).[16] The zinc centre is thus three co-ordinate in a distorted T-shape geometry ($C_{DAC\cdot Et}$-Zn-C_{Et} = 159.90(17)°; $C_{DAC\cdot Et}$-Zn-O = 99.50(14)°; C_{Et}-Zn-O = 100.44(16)°), bound to one ethyl ligand (Zn-C_{Et} = 1.998(4) Å; cf: $ZnEt_2$ = 1.948(5) Å)[5] as well as the sp^3 hybridised (N-C-N = 109.6(3)°) 6-MesDAC·Et ligand (Zn-$C_{DAC\cdot Et}$ = 2.059(4) Å).

4.6 Synthesis of (6-MesDAC)$ZnMe_2$ (29) and [(6-MesDAC·Me)ZnMe]$_n$ (30)

Addition of a toluene solution of $ZnMe_2$ to a THF-d_8 solution of 6-MesDAC at 178 K resulted in the immediate formation of a yellow solution of (6-MesDAC)$ZnMe_2$ (**29**). This complex could be fully characterised by NMR spectroscopy, and exhibited low frequency ^1H and $^{13}C\{^1H\}$ resonances (-1.40 ppm and -9.1 ppm respectively) for the two zinc methyl groups, shifted upfield of those of the RENHC complexes **25** (-0.67 ppm and -8.8 ppm) and **26** (-0.75 ppm and -8.6 ppm). The carbenic carbon was located in the $^{13}C\{^1H\}$ NMR spectrum at 237.6 ppm, at a similar frequency to that of **27** (236.9 ppm). Consistent with the thermal instability of **27**, warming a sample of **29** to 245 K resulted in the formation of a white precipitate of [(6-MesDAC·Me)ZnMe]$_n$ (**30**). ^1H NMR analysis of **30** confirmed the formation of an asymmetric 6-MesDAC·Me ligand with resonances in a 2 : 2 : 6 : 6 : 6 : 3 : 3 ratio with similar chemical shifts to those of **28**. The ^1H NMR signal for the migrated methyl was located at 1.64 ppm, significantly downfield of the zinc-bound methyl at -0.87 ppm. The poor solubility of **30**, even in CD_2Cl_2 at 318 K (under which conditions, significant decomposition became apparent over a period of hours), precluded both its characterisation by $^{13}C\{^1H\}$ NMR spectroscopy, as well as the growth of crystals for X-ray diffraction studies. However, two equal intensity CO stretching bands in the IR spectrum of **30** (1654 cm^{-1} and 1575 cm^{-1}) provide evidence for the polymeric nature of **30** in the solid state by analogy to complex **28** (1651 cm^{-1} and 1576 cm^{-1})

4.7 Synthesis of (6-MesDAC)$CdMe_2$ (31)

The high thermal sensitivity of **27** and **29** prompted us to investigate whether migratory insertion would occur at a higher or lower temperature for complexes of the 4d metal cadmium. NHC complexes of cadmium are rare,[17] with all known examples shown in Figure 4.5.[18]

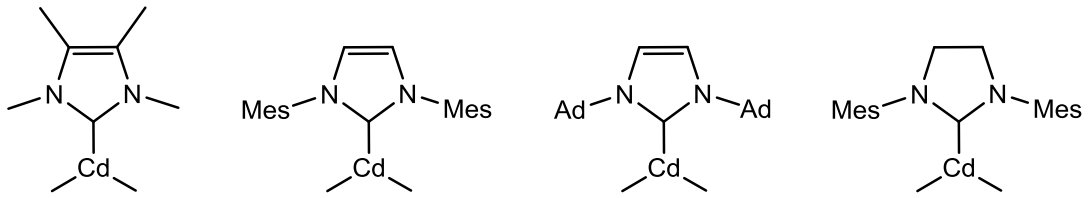

Figure 4.5: NHC complexes of cadmium: (IMe_4)$CdMe_2$ (far left), (IMes)$CdMe_2$ (centre left), (IAd)$CdMe_2$ (centre right) and (SIMes)$CdMe_2$ (far right).[18]

Addition of a hexane solution of $CdMe_2$ to a THF-d_8 solution of 6-MesDAC at 178 K resulted in the immediate formation of a yellow solution of (6-MesDAC)$CdMe_2$ (**31**), which was characterised at low temperature. The NMR spectra of **31** closely resembled those of **29**, with a single, symmetrical 6-MesDAC environment and low frequency methyl resonances (^{1}H = -1.12 ppm; ^{13}C{^{1}H} = -7.9 ppm). NMR active isotopes of cadmium (^{111}Cd: I = ½, abundance = 12.80 %; ^{113}Cd: I = ½, abundance = 12.22 %) resulted in the appearance of cadmium satellites around the methyl resonances. In the ^{13}C{^{1}H} NMR spectrum, there are two doublet satellites ($^1J_{111Cd\text{-}C}$ = 294 Hz; $^1J_{113Cd\text{-}C}$ = 309 Hz), whereas in the ^{1}H NMR spectrum, only a single, broad doublet satellite is observed ($^2J_{CdH}$ = 24.7 Hz). The carbenic carbon was located at 252.9 ppm in the ^{13}C{^{1}H} NMR spectrum, downfield of the corresponding signal in **27** (236.9 ppm). The ^{113}Cd{^{1}H} NMR spectrum shows a singlet at -263.5 ppm, significantly upfield of the five-membered ring NHC complexes (IMe_4)$CdMe_2$ (-106.2 ppm), (IMes)$CdMe_2$ (-152.6 ppm), (IAd)$CdMe_2$ (-102.6 ppm) and (SIMes)$CdMe_2$ (-142.0 ppm).[18]

4.8 Synthesis of [(6-MesDAC·Me)CdMe]$_n$ (32)

Warming a solution of **31** to 255 K resulted in the precipitation of [(6-MesDAC·Me)CdMe]$_n$ (**32**) as a white powder. Alternatively, addition of a THF solution of 6-MesDAC to a hexane solution of $CdMe_2$ at room temperature immediately led to the formation of an orange solution which, over the course of several minutes, faded with the precipitation of **32**, which was isolated in 83 % yield. This complex proved to be more soluble in CD_2Cl_2 than **30**, allowing for its purification and full characterisation in solution. The ^{1}H NMR spectrum showed resonances consistent with an asymmetric (2 : 2 : 12 : 6 : 3 : 3 ratio) 6-MesDAC·Me ligand, with the migrated methyl group exhibiting a similar ^{1}H chemical shift (1.72 ppm) to that in complex **30** (1.64 ppm). The pyramidalised C2 carbon of 6-MesDAC·Me was located in the ^{13}C{^{1}H} NMR spectrum at a similar frequency (89.5 ppm) to that for 6-MesDAC·Et in complex **28** (88.0 ppm). DOSY ^{1}H NMR studies suggest that **32** exists as a monomer in solution (r_H = 4.9 Å; $r_{X\text{-}ray}$ = 5.5 Å). IR spectroscopy of **32** in the solid state reveals two CO stretching bands (1665 cm^{-1} and 1591 cm^{-1}), consistent with an isocarbonyl bridged structure. The bridging CO stretching frequency of complex **32** is significantly higher than that of complex **28** (**32** = 1591 cm^{-1}; **28** = 1576 cm^{-1}), indicative of a weaker interaction with cadmium than with zinc.

4.8.1 Molecular Structure of [(6-MesDAC·Me)CdMe]$_n$ (32)

Crystallisation from CH_2Cl_2 and hexane confirmed the molecular structure of **32**, and its polymeric nature in the solid state (Figure 4.6).

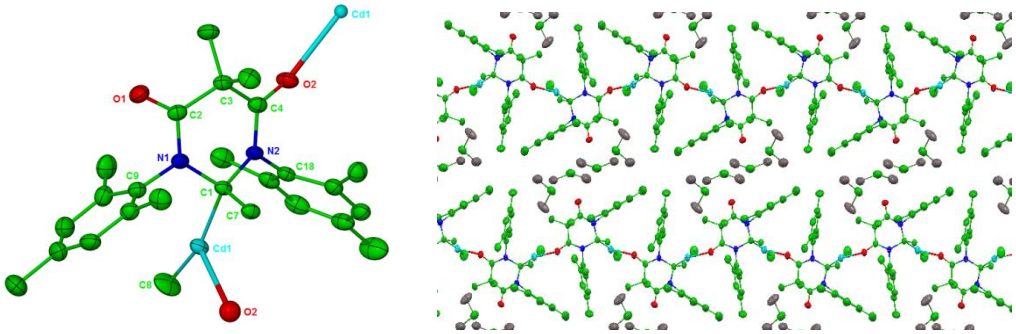

Figure 4.6: Displacement ellipsoid plot (30 % probability) of [(6-MesDAC·Me)CdMe]$_n$ (**32**) (left). H atoms omitted for clarity. Selected bond lengths (Å) and angles (°): Cd(1)-C(1) 2.197(6), Cd(1)-C(8) 2.107(8), Cd(1)-O(2)

2.416(5), C(2)-O(1) 1.226(8), C(4)-O(2) 1.227(8), N(1)-C(1)-N(2) 108.0(4), C(1)-Cd(1)-C(8) 162.1(3), C(1)-Cd(1)-O(2) 95.50(19), C(8)-Cd(1)-O(2) 102.4(3), C(4)-O(2)-Cd(1) 148.1(5). Displacement ellipsoid plot (30 % probability) showing the channels of CH_2Cl_2 between two adjacent polymeric chains of [(6-MesDAC·Me)CdMe]$_n$ (**32**) (right). H atoms omitted for clarity.

The C2 carbon of 6-MesDAC·Me is sp^3 hybridised (N-C-N = 108.0(4)°) and bonded to a three co-ordinate, distorted T-shaped cadmium centre ($C_{DAC·Me}$-Cd-C_{Me} = 162.1(3)°; $C_{DAC·Me}$-Cd-O = 95.50(19)°; C_{Me}-Cd-O = 102.4(3)°). The cadmium methyl bond is significantly shorter than those in (IMes)$CdMe_2$ (**32** = 2.107(8) Å; (IMes)$CdMe_2$ = 2.185(8) Å and 2.184(8) Å).[18] The 6-MesDAC·Me ligand also exhibits a shorter bond length to cadmium (2.197(6) Å) than the NHC in (IMes)$CdMe_2$ (2.371(7) Å). Complex **32** forms linear, one dimensional polymeric chains in the solid state by virtue of the weak O-Cd interaction (2.416(5) Å; sum of covalent radii = 2.10(11) Å).[16] The polymeric chains of **32** pack together less tightly than in complex **28**, allowing for the inclusion of two equivalents of CH_2Cl_2 per cadmium in channels perpendicular to the direction of the polymeric chains.

4.8.2 Decomposition of [(6-MesDAC·Me)CdMe]$_n$ (32)

Complex **32** was stable for weeks in dilute and homogeneous CD_2Cl_2 solutions. However, saturated solutions of **32** decomposed overnight, depositing metallic cadmium which was characterised by PXRD (see Appendix for details). ^{1}H NMR spectra of the resultant solution revealed quantitative formation of the exocyclic alkene 6-MesDAC=CH_2, identified by its vinylic ^{1}H NMR signal at 3.25 ppm,[19] alongside small quantities of methane (0.21 ppm)[20] (Scheme 4.3). Upon attempting to crystallise **32** from concentrated CH_2Cl_2 solutions layered with hexane, single crystals of the complex formed, but often appearing to nucleate from a grain of cadmium metal. Upon standing, these crystals became coated in cadmium metal. Cooling saturated CH_2Cl_2 solutions from 312 K to 293 K within two hours gave single crystals of **32** with minimal decomposition to cadmium metal.

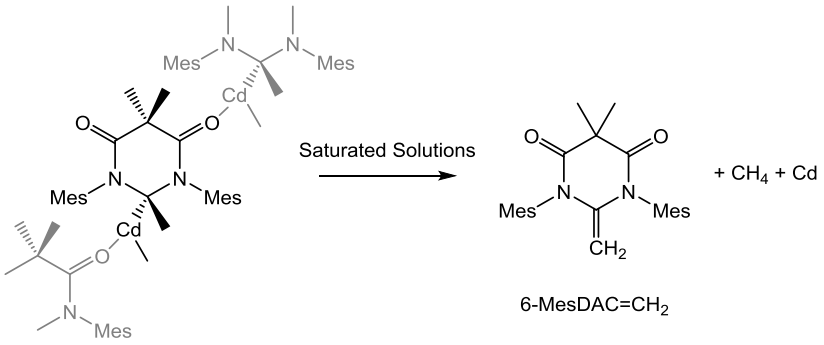

(**32**)

Scheme 4.3: Scheme showing the decomposition of **32** to metallic cadmium, methane and 6-MesDAC=CH_2.

4.8.3 DFT Studies

The mechanism of this transformation is unclear, due to its apparent heterogeneous nature. To further probe this, DFT calculations were conducted in collaboration with Macgregor and co-workers at Heriot-Watt University using a small model system in which the mesityl N-substituents are replaced by methyl groups. The first process to be modelled (black data, Figure 4.7) involved a β-hydride elimination process from the 6-MeDAC·Me ligand. This reaction results in an unstable cadmium methyl hydride species which eliminates methane and cadmium metal by reductive elimination. The overall process is exergonic (-17.4 kcal mol^{-1}), however, the transition states for both β-hydride elimination and reductive elimination are extremely high (52.0 kcal mol^{-1} and 68.3 kcal mol^{-1} respectively) and inconsistent with the room temperature reactivity that was observed. An alternative mechanism (red data, Figure 4.7) involving H atom transfer from the 6-MeDAC·Me ligand directly to cadmium methyl affords a much lower activation energy of 37.9 kcal mol^{-1}. Although lower, this barrier is still prohibitively large for the observed room temperature reactivity.

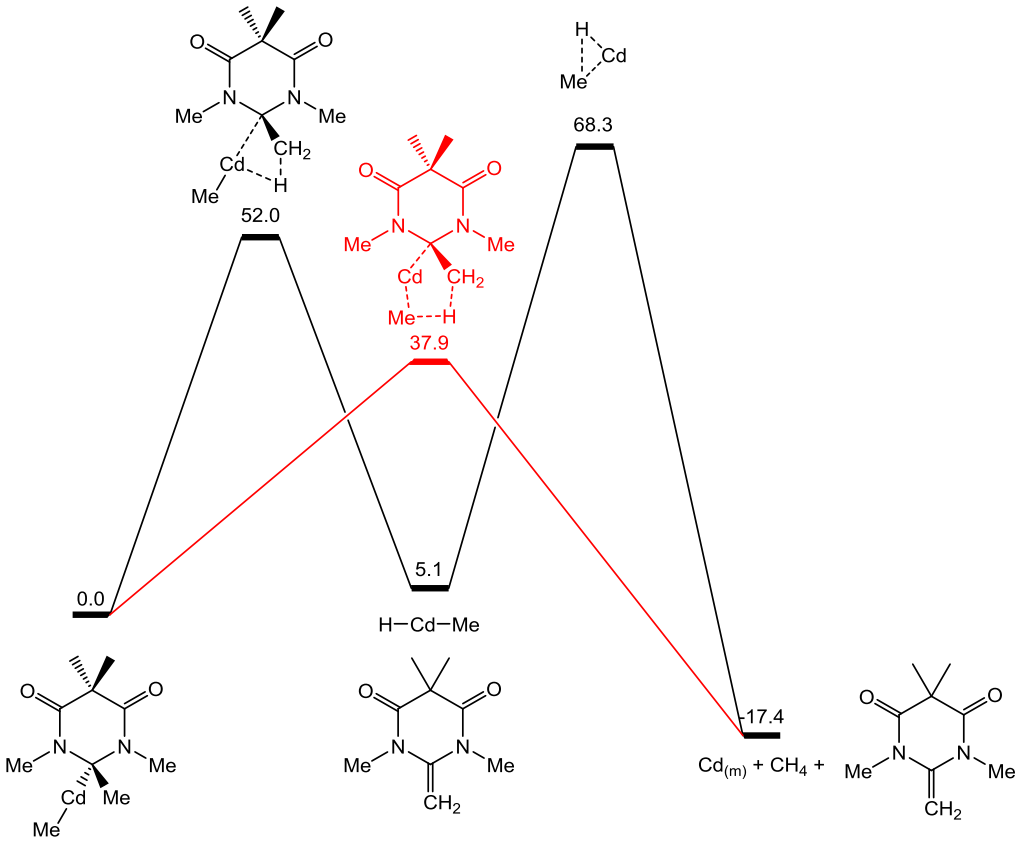

Figure 4.7: DFT calculated reaction profiles showing potential mechanisms for the decomposition of complex **32**, using the model complex (6-MeDAC·Me)CdMe. Black data: β-hydride elimination followed by reductive elimination. Red data: concerted H atom transfer. All energies are quoted in kcal mol^{-1}.

When a second molecule of 6-MeDAC·Me was introduced to the model system, an energetic minimum was found for the co-ordination of one carbonyl to cadmium, forming a dinuclear analogue of polymeric **32** (black data, Figure 4.8). This three co-ordinate cadmium species was found to undergo H atom transfer with an activation energy of 35.6 kcal mol^{-1}, a reduction of 2.3 kcal mol^{-1} compared to the mononuclear, two co-ordinate complex. This result demonstrates that aggregation serves to lower the energy barrier to the decomposition reaction, and lends support to the observation that this transformation occurs at the interface of homo- and heterogeneous conditions.

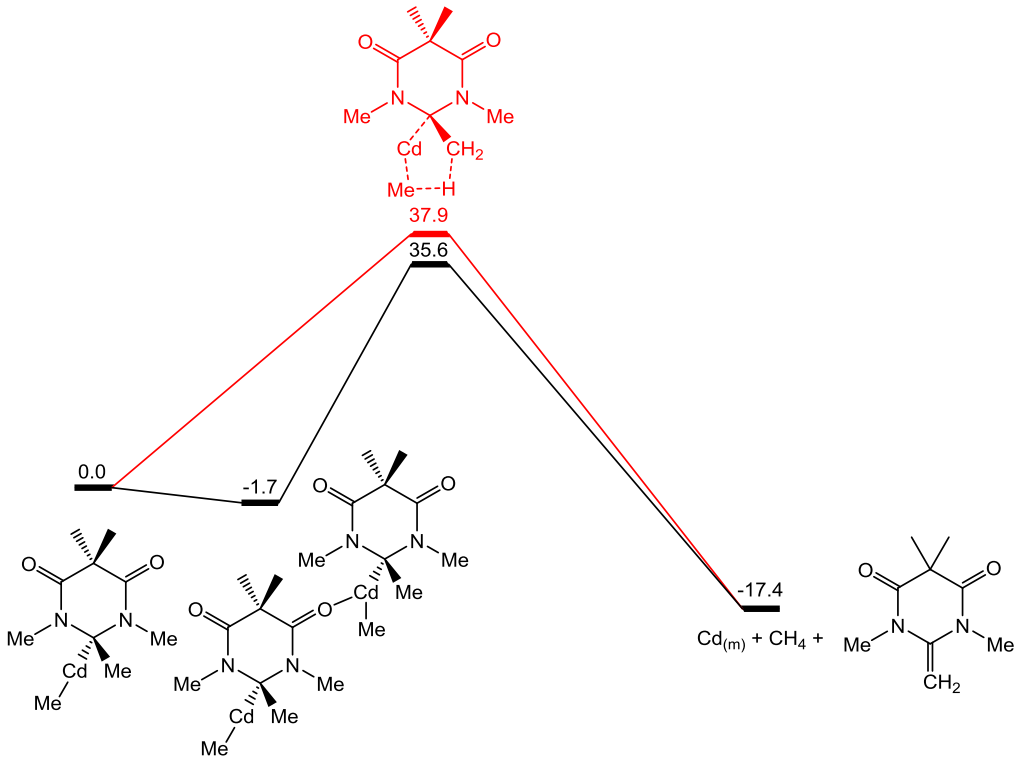

Figure 4.8: DFT calculations showing potential mechanisms for the decomposition of complex **32**, using the model complex (6-MeDAC·Me)CdMe. Black data: concerted H atom transfer of a dinuclear, three co-ordinate cadmium complex. Red data: concerted H atom transfer of a mononuclear, two co-ordinate cadmium complex. All energies are quoted in kcal mol^{-1}.

Expansion of the computational model from 6-MeDAC·Me to the full 6-MesDAC·Me system revealed that the activation barrier reduced by a further 1.6 kcal mol^{-1} (to 35.7 kcal mol^{-1}), with the overall transformation also becoming more exergonic by 4.0 kcal mol^{-1}.

Initial DFT calculations also corroborate that the decomposition reaction is exclusive to the cadmium complex **32** and does not occur for zinc complexes **28** or **30**. When the same calculations were repeated (on a model 6-MeDAC·Me system) with zinc in place of cadmium, the equivalent transformation to 6-MeDAC=CH_2, CH_4 and zinc metal was found to be less exergonic by 10.3 kcal mol^{-1} (-7.1 kcal mol^{-1}), and the activation barrier for H atom transfer higher by 8.2 kcal mol^{-1} (46.1 kcal mol^{-1}).

4.9 Preliminary Reactivity Studies of 6-Mes and 6-MesDAC with Zn^tBu_2

In collaboration with Lewinski and co-workers in Warsaw, the reactivity of 6-Mes and 6-MesDAC with Zn^tBu_2 has been investigated. Reaction of 6-Mes with Zn^tBu_2 at 195 K, followed by subsequent warming to room temperature resulted in the formation of the three co-ordinate complex (6-Mes)Zn^tBu_2. A molecular structure (Figure 4.9) was determined, although the quality of the X-ray diffraction data was sufficient only to confirm connectivity.

Upon low temperature (195 K) addition of 6-MesDAC to Zn^tBu_2, a deep blue solution was formed, presumably due to the presence of (6-MesDAC)Zn^tBu_2. Warming the sample to 263 K resulted in the formation of a yellow solution of (6-MesDAC·^{t}Bu)Zn^tBu. In contrast to the products of migratory insertion with methyl or ethyl substituents (**28**, **30** and **32**), (6-MesDAC·^{t}Bu)Zn^tBu is monomeric in the solid state (Figure 4.7). The bulky nature of *tert*-butyl presumably prevents polymerisation through isocarbonyl bridging, leading to a mononuclear zinc species in the solid state, as well as in solution. The metal centre in (6-MesDAC·^{t}Bu)Zn^tBu is two co-ordinate and approaching a linear geometry (C-Zn-C = 169.5(2)°), in contrast to the distorted T-shaped zinc centre of complex **28** (C-Zn-C = 159.90(17)°). Both of the Zn-C distances in (6-MesDAC·^{t}Bu)Zn^tBu (Zn-$C_{DAC\cdot tBu}$ = 2.018(5) Å; Zn-C_{tBu} = 1.972(6) Å) are shorter than those in **28** (Zn-$C_{DAC\cdot Et}$ = 2.059(4) Å; Zn-C_{Et} = 1.998(4) Å). The migration of the bulky *tert*-butyl group at low temperature demonstrates the extreme susceptibility of 6-MesDAC to migratory insertion processes, and gives a further example of contrasting reactivity between 6-Mes and 6-MesDAC.

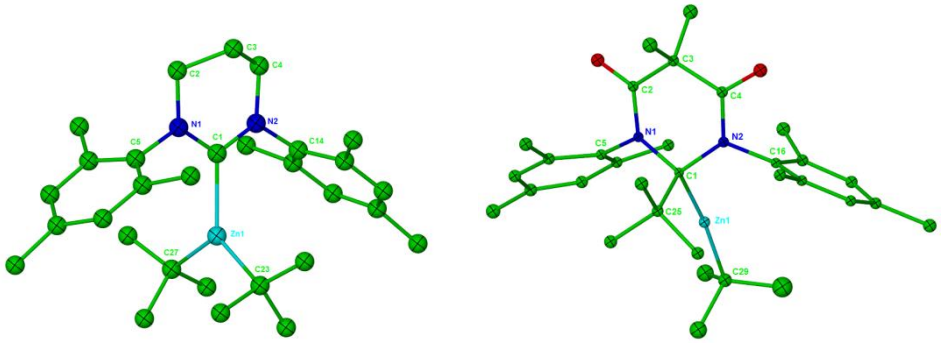

Figure 4.9: Picture showing the connectivity of (6-Mes)Zn^{t}Bu$_2$ (left). Displacement ellipsoid plot (30 % probability) of (6-MesDAC·^{t}Bu)Zn^{t}Bu (right). H atoms omitted for clarity. Selected bond lengths (Å) and angles (°): Zn(1)-C(1) 2.018(5), Zn(1)-C(29) 1.972(6), N(1)-C(1)-N(2) 109.8(4), C(1)-Zn(1)-C(29) 169.5(2).

4.10 Summary

This Chapter has described the reactivity of group 12 metal dialkyl precursors with a range of NHCs. For the RENHCs 6-Mes and 7-Mes, stable three co-ordinate complexes were formed and their applications in the ROP of *rac*-lactide investigated. This reactivity is starkly contrasted with that of the diamidocarbene 6-MesDAC. In this case, the initially formed three co-ordinate (6-MesDAC)MR$_2$ complexes are only stable at very low temperatures and, in all cases, undergo a facile migratory insertion reaction. Migratory insertion processes at metal bound NHCs are rare, and their literature precedent is discussed below.

4.11 Literature Precedent for Migratory Insertion Reactions

NHCs are typically viewed as innocent ancillary ligands. However, examples of reactivity at metal-bound NHCs are known and the study of such C-N activation processes,[21–24] normal to abnormal rearrangements,[25] or migratory insertion reactions provide valuable insight into the decomposition pathways of an ever-increasingly utilised ligand class for catalysis.[26] The literature precedent for migratory insertion reactions of NHCs is presented in Schemes 4.4, 4.5 and 4.6.

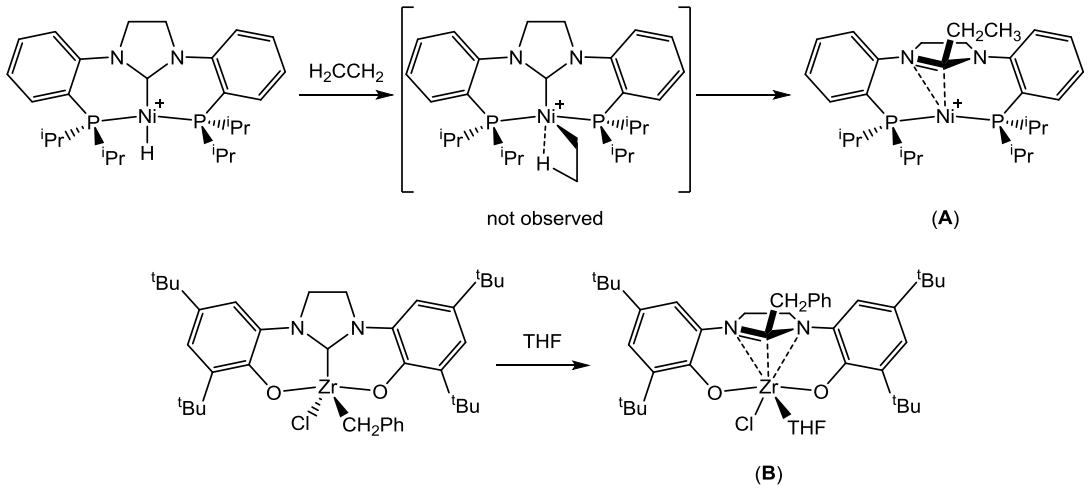

Scheme 4.4: Migratory insertion reactions of X-NHC-X pincer ligands.

The PCP and OCO pincer complexes shown in Scheme 4.4 undergo migratory insertion reactions to form η^2 and η^3 bound imidazoline products respectively. Square planar $[(PCP)NiH]^+$ reacts with ethene to afford complex **A**, the product of ethyl migratory insertion. The Ni-ethyl intermediate was not observed and DFT calculations showed that the bulky *iso*-propyl substituted ligand destabilises the expected square planar geometry of this $[(PCP)NiCH_2CH_3]^+$ intermediate, which instead adopts an agostic, pseudo square based pyramidal structure (Scheme 4.4, top). Deuterium labelling of either hydride or ethene resulted in scrambling of the labels, suggesting that the formation of this intermediate is reversible. An activation barrier of 11.1 kcal mol^{-1} was calculated for the migratory insertion reaction, consistent with the formation of **A** at room temperature.[27]

The five co-ordinate bis-phenoxide NHC pincer complex (OCO)Zr(Bn)Cl (Scheme 4.4, bottom) is stable in non-donor solvents. However, in the presence of as little as 10 equivalents of THF in toluene solution, a Lewis base assisted migratory insertion process occurs to form complex **B**. DFT calculations have shed light on the pathway, suggesting that THF co-ordination leads to a distorted octahedral intermediate, facilitating benzyl migration by the proximity of the benzyl group and NHC. DFT calculations revealed an activation barrier of 25.2 kcal mol^{-1} for a model system with unsubstituted phenoxide groups.[28]

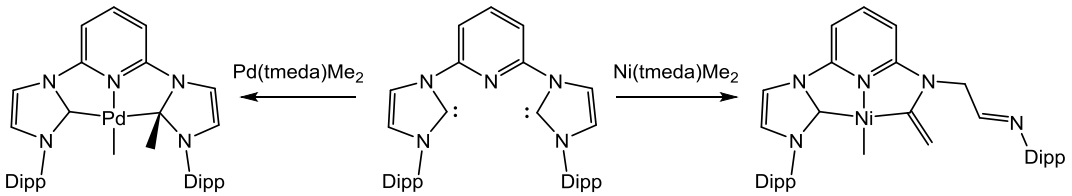

Scheme 4.5: Migratory insertion reactions of a CNC pincer ligand.

Danopoulos and co-workers reported that the bis-NHC pincer ligand shown in Scheme 4.5 undergoes migratory insertion when reacted with group 10 metal dialkyl complexes. Reaction with Pd(tmeda)Me_2 resulted in the migratory insertion of a methyl group and the isolation of an NHC-N-alkyl pincer complex (Scheme 4.5, left). DFT studies suggest that a five co-ordinate (CNC)$PdMe_2$ complex is initially formed (although this could not be experimentally observed) by ligand substitution. This disfavoured geometry for a d^8 metal raises the energy of (CNC)$PdMe_2$, resulting in a small activation barrier (7.8 kcal mol^{-1}) to migratory insertion.[29]

Analogous reactivity was proposed for the reaction with Ni(tmeda)Me_2, however, neither the five co-ordinate intermediate nor the direct product of migratory insertion was isolated. Instead, the authors propose that tmeda facilitates the base-catalysed ring opening of the migratory insertion product, affording an isolable alkenyl species (Scheme 4.5, right).[30]

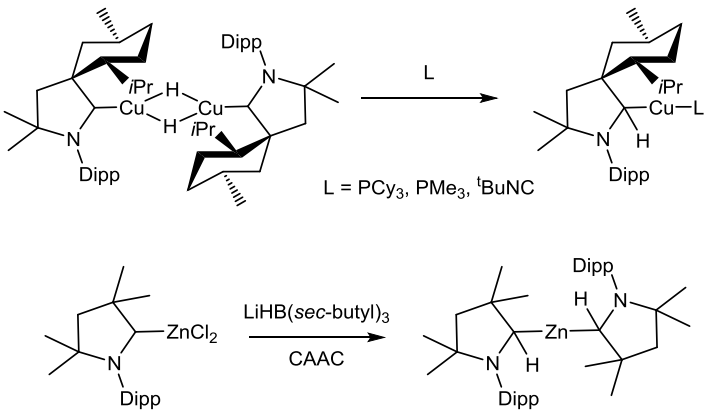

Scheme 4.6: Migratory insertion reactions of CAACs.

Addition of a range of Lewis bases to the dimeric copper hydride complex [(CAAC)CuH]$_2$ at room temperature resulted in the isolation of two co-ordinate (CAAC·H)CuL complexes (Scheme 4.6, top).[31] [(CAAC)CuH]$_2$ is a rare example

of a room temperature stable NHC copper hydride complex, and will be discussed in more detail in Chapters Five and Six in conjunction with our studies on 6-Mes and 6-MesDAC copper hydrides.

The final example of migratory insertion involves the reduction of (CAAC)$ZnCl_2$ with LiHB(*sec*-butyl)$_3$ in the presence of additional CAAC, resulting in the formation of (CAAC·H)$_2$Zn.[32] Although this reactivity is not discussed by the authors, initial formation of a zinc hydride species and subsequent migratory insertion seems a viable mechanism for the formation of this product. The inclusion of additional CAAC in the reaction mixture indicates that a Lewis base assisted migratory insertion is possible.

4.12 Discussion

From the examples described above, three interrelating factors can be identified as important in promoting migratory insertion of hydride or alkyl ligands at metal-bound NHCs. Firstly, steric pressure: the bulky, rigid pincer ligands shown in Schemes 4.4 and 4.5 enforce energetically disfavoured geometries (for example, the five co-ordinate d^8 metal complexes $[(PCP)NiEt]^+$, $(CNC)NiMe_2$ and $(CNC)PdMe_2$) which are able to adopt more stable configurations upon migratory insertion. Secondly, electrophilicity of the NHC: cyclic alkyl amino carbenes (CAACs) are amongst the most electrophilic of NHCs, and may therefore stabilise the build up of negative charge on the carbenic p_π orbital at the transition state for migratory insertion. Finally, the participation of Lewis bases: both (OCO)Zr(Cl)(Bn) and $[(CAAC)CuH]_2$ are stable complexes in the absence of a Lewis base. Co-ordination of a Lewis base to (OCO)Zr(Cl)(Bn) results in a crowded, high energy octahedral complex which undergoes migratory insertion. The role of Lewis bases in promoting migratory insertion of copper hydrides will be discussed in Chapter Five.

4.13 DFT Studies

The characterisation of the (6-MesDAC)MR_2 complexes **27**, **29** and **31** and their subsequent migratory insertion products **28**, **30** and **32**, respectively, represents a unique study into NHC migratory insertion. The experimentally determined thermal barriers to migratory insertion were seen to vary with both the nature of the metal and the alkyl group. The direct comparison of **29** with its isostructural

diaminocarbene analogue **25**, whose 6-Mes ligand does not undergo migratory insertion, shows that steric factors are not responsible for the facile migratory insertion reactions of 6-MesDAC.

Macgregor and co-workers have performed preliminary DFT calculations to further investigate this reactivity. Figure 4.10 shows a general reaction profile for the co-ordination of the small model ligand 6-MeDAC to a range of MR_2 species to form (6-MeDAC)MR_2 adducts. Migratory insertion is then modelled via a transition state with a three-membered ring formed by the carbenic carbon, the migrating group and the metal. The product of migratory insertion is modelled as a two co-ordinate, monomeric complex.[i]

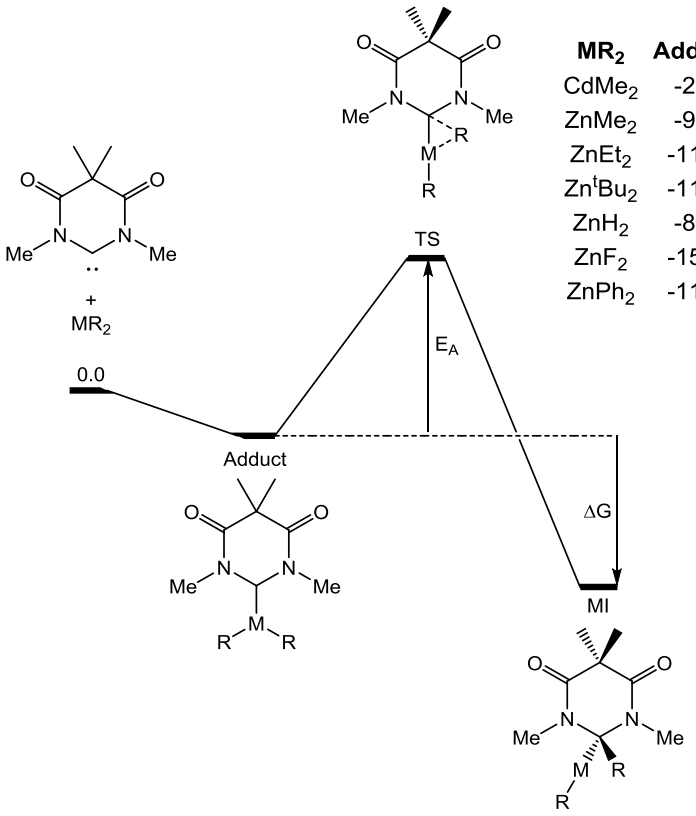

MR_2	Adduct	TS	E_A	MI	ΔG
$CdMe_2$	-2.2	8.6	10.8	-29.3	-27.1
$ZnMe_2$	-9.6	1.8	11.4	-30.0	-20.4
$ZnEt_2$	-11.4	-2.9	8.5	-32.9	-21.5
Zn^tBu_2	-11.3	-2.4	8.9	-31.0	-19.7
ZnH_2	-8.3	-3.4	4.9	-35.1	-26.8
ZnF_2	-15.6	-8.6	7.0	-12.6	3.0
$ZnPh_2$	-11.2	-3.6	7.6	-34.3	-23.1

Figure 4.10: DFT calculations on the co-ordination and migratory insertion chemistry of 6-MeDAC with MR_2 species. All energies are quoted in kcal mol^{-1}.

The experimental results are in good agreement with the DFT calculations (R = alkyl). In all four cases, adduct formation is calculated to be exergonic, consistent

[i] Higher nuclearity complexes may be expected to participate in this reactivity due to the polymeric nature of **28**, **30** and **32**. Aggregation through isocarbonyl bridging was previously found to result in the stabilisation of monomeric complexes (Figure 4.8).

with the immediate reaction of 6-MesDAC and MR_2 complexes at 178 K. Alkyl migratory insertion is calculated to be more exergonic than adduct formation (ΔG between -19.7 kcal mol^{-1} and -27.1 kcal mol^{-1}) and the calculated activation energies (E_A ranging from 8.5 kcal mol^{-1} to 11.4 kcal mol^{-1}) are consistent with the observed low temperature reactivity. However, the experimentally determined temperatures at which migratory insertion occurs (lowest to highest: $ZnEt_2$ = 211 K; $ZnMe_2$ = 245 K; $CdMe_2$ = 255 K; Zn^tBu_2 = 263 K) do not reflect the calculated activation energies (lowest to highest: $ZnEt_2$, Zn^tBu_2, $CdMe_2$, $ZnMe_2$). This discrepancy may result from the use of a simplified 6-MeDAC model system. Expansion of the model calculations to include the mesityl substituents in the case of MR_2 = $CdMe_2$ resulted in a stabilisation of all species, with the formation of (6-MesDAC)$CdMe_2$ more exergonic by 5.0 kcal mol^{-1} (6-MesDAC = -7.2 kcal mol^{-1}; 6-MeDAC = -2.2 kcal mol^{-1}). The migratory insertion process for 6-MesDAC was found to be less exergonic by 4.4 kcal mol^{-1} (6-MesDAC = -22.7 kcal mol^{-1}; 6-MeDAC = -27.1 kcal mol^{-1}) and to have a 4.0 kcal mol^{-1} higher activation energy (6-MesDAC = 14.8 kcal mol^{-1}; 6-MeDAC = 10.8 kcal mol^{-1}). These calculations show that whilst steric pressure is not solely responsible for the occurrence of migratory insertion to 6-MesDAC, steric factors do contribute to the energies of the transition states and complexes involved.

Calculations were also performed for ZnR_2 where R = H, F and Ph to predict the chemistry that may be observed. The activation energies for migratory insertion are, in all cases, smaller than for the metal dialkyls, with zinc dihydride having the smallest activation energy of just 4.9 kcal mol^{-1}. Zinc difluoride has the lowest energy transition state of any system (-8.6 kcal mol^{-1}), however, the product of fluoride migratory insertion is high in energy and migratory insertion is calculated to be endergonic (ΔG = 3.0 kcal mol^{-1}). Migratory insertion of both hydride and phenyl are calculated to be exergonic (ΔG = -26.8 kcal mol^{-1} and -23.1 kcal mol^{-1}, respectively). The results of these calculations are in agreement with the expected migratory aptitude of these ligands, but further experimental work is required to confirm or refute these predictions.

4.14 Conclusion

This Chapter began by demonstrating that the stable three co-ordinate RENHC zinc dialkyl complexes (6-Mes)$ZnMe_2$ (**25**) and (7-Mes)$ZnMe_2$ (**26**) were successful precatalysts for the ROP of *rac*-lactide to form PLA. Furthermore, the RENHCs themselves were found to be successful catalysts for this reaction and carbene dissociation from **25** and **26** could not be ruled out as a contributory factor in catalysis. In contrast, the analogous diamidocarbene complexes (6-MesDAC)$ZnEt_2$ (**27**), (6-MesDAC)$ZnMe_2$ (**29**) and (6-MesDAC)$CdMe_2$ (**31**) were only stable at very low temperatures. An extremely facile migratory insertion process was discovered for 6-MesDAC, in which an alkyl ligand migrates to the carbenic carbon, resulting in the precipitation of the polymeric complexes $[(6\text{-MesDAC}\cdot Et)ZnEt]_n$ (**28**), $[(6\text{-MesDAC}\cdot Me)ZnMe]_n$ (**30**) and $[(6\text{-MesDAC}\cdot Me)CdMe]_n$ (**32**). Migratory insertion was found to occur at temperatures as low as 211 K and even bulky alkyl groups are prone to migration, with (6-MesDAC)Zn^tBu_2 only stable at temperatures below 263 K. This co-ordination and migratory insertion chemistry of 6-MesDAC with group 12 metal dialkyl species was investigated with the help of DFT calculations. These calculations corroborate the experimental results, and also predict facile migratory insertion of hydride and phenyl groups. Further investigation is needed to evaluate the extent to which migratory insertion may preclude the isolation and synthetic utility of (6-MesDAC)MR_2 species. These findings raise important questions regarding the stability of diamidocarbene complexes under catalytic conditions, especially in cases in which alkyl or hydride ligands are also present.

4.15 References for Chapter Four

(1) Collins, L. R.; Moffat, L. A.; Mahon, M. F.; Jones, M. D.; Whittlesey, M. K. *Polyhedron* **2016**, *103*, 121–125.

(2) Collins, L. R.; Hierlmeier, G.; Mahon, M. F.; Riddlestone, I. M.; Whittlesey, M. K. *Chem. Eur. J.* **2015**, *21*, 3215–3218.

(3) Iglesias, M.; Beetstra, D. J.; Knight, J. C.; Ooi, L.; Stasch, A.; Coles, S.; Male, L.; Hursthouse, M. B.; Cavell, K. J.; Dervisi, A.; Fallis, I. A. *Organometallics* **2008**, *27*, 3279–3289.

(4) Schnee, G.; Fliedel, C.; Avilés, T.; Dagorne, S. *Eur. J. Inorg. Chem.* **2013**, *2013*, 3699–3709.

(5) Bacsa, J.; Hanke, F.; Hindley, S.; Odedra, R.; Darling, G. R.; Jones, A. C.; Steiner, A. *Angew. Chem. Int. Ed.* **2011**, *123*, 11889–11891.

(6) Jensen, T. R.; Schaller, C. P.; Hillmyer, M. A.; Tolman, W. B. *J. Organomet. Chem.* **2005**, *690*, 5881–5891.

(7) Arduengo III, A. J.; Dias, H. V. R.; Davidson, F.; Harlow, R. L. *J. Organomet. Chem.* **1993**, *462*, 13–18.

(8) Bakewell, C.; Fateh-Iravani, G.; Beh, D. W.; Myers, D.; Tabthong, S.; Hormnirun, P.; White, A. J. P.; Long, N.; Williams, C. K. *Dalton Trans.* **2015**, *44*, 12326–12337.

(9) Fliedel, C.; Rosa, V.; Alves, F. M.; Martins, A. M.; Avilés, T.; Dagorne, S. *Dalton Trans.* **2015**, *44*, 12376–12387.

(10) Williams, C. K.; Breyfogle, L. E.; Choi, S. K.; Nam, W.; Young, V. G.; Hillmyer, M. A.; Tolman, W. B. *J. Am. Chem. Soc.* **2003**, *125*, 11350–11359.

(11) Jensen, T. R.; Breyfogle, L. E.; Hillmyer, M. A.; Tolman, W. B. *Chem. Commun.* **2004**, 2504–2505.

(12) Fèvre, M.; Pinaud, J.; Gnanou, Y.; Vignolle, J.; Taton, D. *Chem. Soc. Rev.* **2013**, *42*, 2142–2172.

(13) Arnold, P. L.; Casely, I. J.; Turner, Z. R.; Bellabarba, R.; Tooze, R. B. *Dalton Trans.* **2009**, 7236–7247.

(14) Thakur, K. A. M.; Kean, R. T.; Hall, E. S.; Kolstad, J. J.; Lindgren, T. A.; Doscotch, M. A.; Siepmann, J. I.; Munson, E. J. *Macromolecules* **1997**, *30*, 2422–2428.

(15) Webster, O. W. *Science* **1991**, *251*, 887–893.

(16) Cordero, B.; Gómez, V.; Platero-Prats, A. E.; Revés, M.; Echeverría, J.; Cremades, E.; Barragán, F.; Alvarez, S. *Dalton Trans.* **2008**, 2832–2838.

(17) Budagumpi, S.; Endud, S. *Organometallics* **2013**, *32*, 1537–1562.

(18) Arduengo III, A. J.; Goerlich, J. R.; Davidson, F.; Marshall, W. J. *Z. Naturforsch.* **1999**, 1350–1356.

(19) Chase, D. T.; Moerdyk, J. P.; Bielawski, C. W. *Org. Lett.* **2014**, *16*, 812–815.

(20) Fulmer, G. R.; Miller, A. J. M.; Sherden, N. H.; Gottlieb, H. E.; Nudelman, A.; Stoltz, B. M.; Bercaw, J. E.; Goldberg, K. I. *Organometallics* **2010**, *29*, 2176–2179.

(21) Burling, S.; Mahon, M. F.; Powell, R. E.; Whittlesey, M. K.; Williams, J. M. J. *J. Am. Chem. Soc.* **2006**, *128*, 13702–13703.

(22) Caddick, S.; Cloke, F. G. N.; Hitchcock, P. B.; de K Lewis, A. K. *Angew. Chem. Int. Ed.* **2004**, *43*, 5824–5827.

(23) Kaiho, A.; Suzuki, H. *Angew. Chem. Int. Ed.* **2012**, *51*, 1408–1411.

(24) Arrowsmith, M.; Hill, M. S.; Kociok-Köhn, G.; MacDougall, D. J.; Mahon, M. F. *Angew. Chem. Int. Ed.* **2012**, *51*, 2098–2100.

(25) Day, B. M.; Pugh, T.; Hendriks, D.; Guerra, C. F.; Evans, D. J.; Bickelhaupt, F. M.; Layfield, R. A. *J. Am. Chem. Soc.* **2013**, *135*, 13338–13341.

(26) Lazreg, F.; Nahra, F.; Cazin, C. S. J. *Coord. Chem. Rev.* **2015**, *293-294*, 48–79.

(27) Steinke, T.; Shaw, B. K.; Jong, H.; Patrick, B. O.; Fryzuk, M. D.; Green, J. C. *J. Am. Chem. Soc.* **2009**, *131*, 10461–10466.

(28) Romain, C.; Miqueu, K.; Sotiropoulos, J.-M.; Bellemin-Laponnaz, S.; Dagorne, S. *Angew. Chem. Int. Ed.* **2010**, *49*, 2198–2201.

(29) Danopoulos, A. A.; Tsoureas, N.; Green, J. C.; Hursthouse, M. B. *Chem. Commun.* **2003**, 756–757.

(30) Pugh, D.; Boyle, A.; Danopoulos, A. A. *Dalton Trans.* **2008**, 1087–1094.

(31) Frey, G. D.; Donnadieu, B.; Soleilhavoup, M.; Bertrand, G. *Chem. Asian J.* **2011**, *6*, 402–405.

(32) Singh, A. P.; Samuel, P. P.; Roesky, H. W.; Schwarzer, M. C.; Frenking, G.; Sidhu, N. S.; Dittrich, B. *J. Am. Chem. Soc.* **2013**, *135*, 7324–7329.

CHAPTER FIVE

CHAPTER FIVE: Migratory Insertion Reactions of Copper Hydrides

Some of the work in this Chapter has been published in:[1]

A Comparison of the Stability and Reactivity of Diamido- and Diaminocarbene Copper Alkoxide and Hydride Complexes: Collins, L. R.; Riddlestone, I. M.; Mahon, M. F.; Whittlesey, M. K. *Chem. Eur. J.* **2015**, *21*, 14075 – 14084

5.1 NHC Copper Hydride Complexes

N-heterocyclic carbene supported copper hydrides are implicated in numerous reductive processes.[2–6] Due to the highly reactive nature of such species, and for procedural ease, these species are often formed in-situ from more stable precursors.[7,8] Most commonly, the $[(NHC)CuH]_n$ complex is synthesised by reaction of a $[(NHC)CuOR]_n$ precursor (often itself formed in-situ) with a hydrosilane (Scheme 5.1).[9]

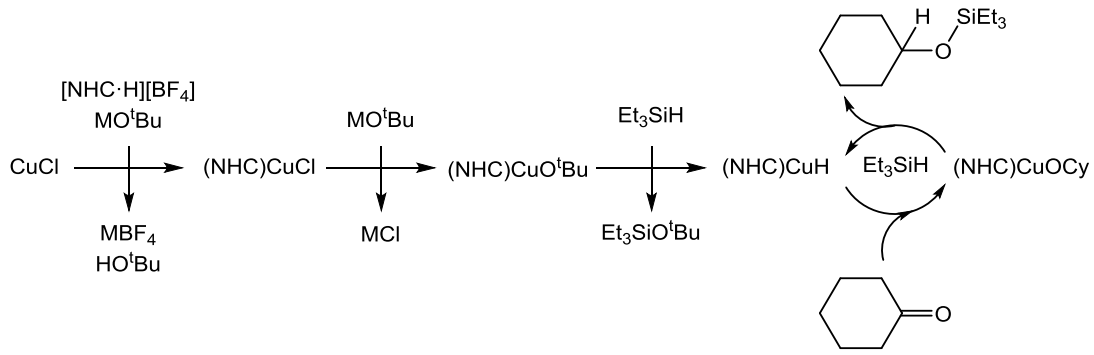

Scheme 5.1: General reaction scheme for, in-situ generated, $[(NHC)CuH]_n$ catalysed hydrosilylation of cyclohexanone.[7]

In 2004, Sadighi and co-workers reported the formation of $[(IPr)CuH]_2$ by reaction of $(IPr)CuO^tBu$ with $(EtO)_3SiH$ (Scheme 5.2).[9] An intense yellow solution of the product was formed within seconds both at room temperature in benzene and also at 228 K in pentane. However, the complex was found to be unstable and decomposed to IPr, copper metal and other unidentified products within minutes at room temperature or hours at 228 K. ^1H NMR spectroscopy showed that the copper hydride resonates at 2.67 ppm in benzene solution, in agreement with reported chemical shifts for phosphine supported copper hydrides and deuterides ($[(P(p\text{-}Tol)_3)CuH]_n$ = 3.50 ppm;[10] $[(P(NMe_2)_3)CuD]_6$ = 2.57 ppm;[11]

$[(MeC(CH_2PPh_2)_3)CuD]_2$ = 1.83 ppm).[12] Yellow crystals of $[(IPr)CuH]_2$ were isolated at low temperature, although the quality of the diffraction data served only to confirm the dimeric nature of the complex and no metrics for the Cu-H distances could be obtained. The viability of $[(IPr)CuH]_2$ as a reducing agent was confirmed by the formation of (IPr)Cu(3-hexenyl) in the reaction of (IPr)CuO^{t}Bu and $(EtO)_3SiH$ in the presence of 3-hexyne.

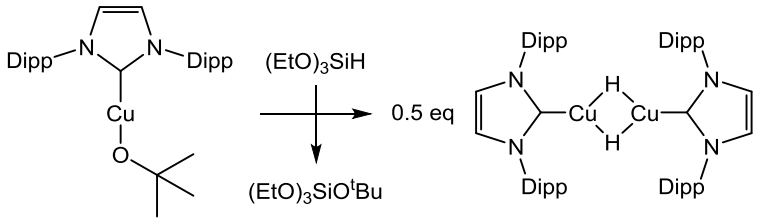

Scheme 5.2: Formation of dimeric $[(IPr)CuH]_2$ by reaction of (IPr)CuO^{t}Bu with $(EtO)_3SiH$.[9]

Despite the regularity with which $[(NHC)CuH]_n$ species are implicated in catalytic reduction processes, there is a paucity of detailed studies into the factors influencing the stability and reactivity of such complexes. The remaining chapters of this Thesis will focus on the synthesis, stability and reactivity of copper hydrides supported by 6-MesDAC and 6-Mes. This Chapter will discuss the reactivity of the hydrosilane Et_3SiH with the (NHC)CuO^{t}Bu complexes **11** (NHC = 6-MesDAC) and **20** (NHC = 6-Mes). Alternative approaches to the synthesis of copper hydrides will be discussed in Chapter Six.

5.2 Reactivity of (6-MesDAC)CuO^{t}Bu (11) with Et_3SiH

Addition of one equivalent of Et_3SiH to a benzene solution of **11** at room temperature resulted in an immediate colour change from pale orange to dark purple. Analysis by ^{1}H NMR spectroscopy revealed resonances attributable to Et_3SiO^tBu (1.20, 1.04 and 0.62 ppm), consistent with the concomitant formation of a copper hydride species. However, the presence of ^{1}H NMR resonances for one C_s symmetrical (resonances in a 4 : 6 : 12 : 6 ratio) and one desymmetrised (resonances in a 2 : 2 : 6 : 6 : 6 : 3 : 3 ratio) 6-MesDAC ligand ruled out the formation of a simple $[(6\text{-MesDAC})CuH]_n$ product. The presence of a high-frequency $^{13}C\{^1H\}$ NMR resonance (215.2 ppm) was consistent with the C_s

symmetrical ligand being a copper-bound 6-MesDAC. The desymmetrised ligand was identified as 6-MesDAC·H (Figure 5.1) with a characteristic 1H integral singlet ^{1}H NMR resonance at 5.59 ppm with HSQC ($^{1}J_{HC}$) and HMBC ($^{3}J_{HC}$) interactions to ^{13}C NMR resonances at 67.7 and 173.3 ppm respectively. The chemical shift of the C2 carbon of 6-MesDAC·H (67.7 ppm) closely resembles those of the related products of alkyl migration 6-MesDAC·Et (88.0 ppm, complex **28**) and 6-MesDAC·Me (89.5 ppm, complex **32**). In contrast to the approximately planar heterocycles of 6-MesDAC·Et (**28**) and 6-MesDAC·Me (**32**), 6-MesDAC·H adopts a boat conformer, on the basis of an NOE interaction between the migrated H and one of the two backbone methyl resonances (Figure 5.1). IR spectroscopy gave further evidence for the presence of a 1 : 1 mixture of 6-MesDAC·H and 6-MesDAC ligands by the presence of CO stretching bands at 1669 and 1635 cm^{-1} (6-MesDAC·H) and at 1733 and 1698 cm^{-1} (6-MesDAC).

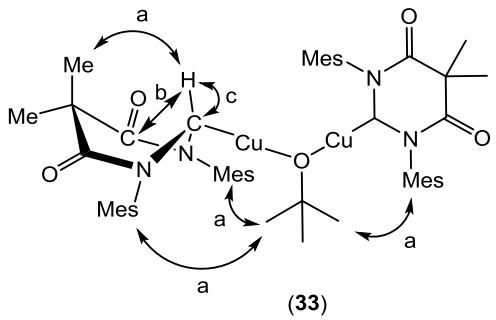

(**33**)

Figure 5.1: Diagram showing the NMR evidence for the proposed connectivity of complex **33**. [a] NOE interaction. [b] HMBC interaction. [c] HSQC interaction.

NOE interactions between a bridging *tert*-butoxide (0.33 ppm) and the *ortho*-mesityl methyl groups of both ligands confirmed that both 6-MesDAC·H and 6-MesDAC were part of the same, dinuclear complex (Figure 5.1). The formation of a dinuclear product is also consistent with the observation that only half an equivalent of Et_3SiH is consumed in the reaction. Scheme 5.3 shows a proposal for the mechanism of formation of (6-MesDAC·H)Cu(μ-O^{t}Bu)Cu(6-MesDAC) (**33**).

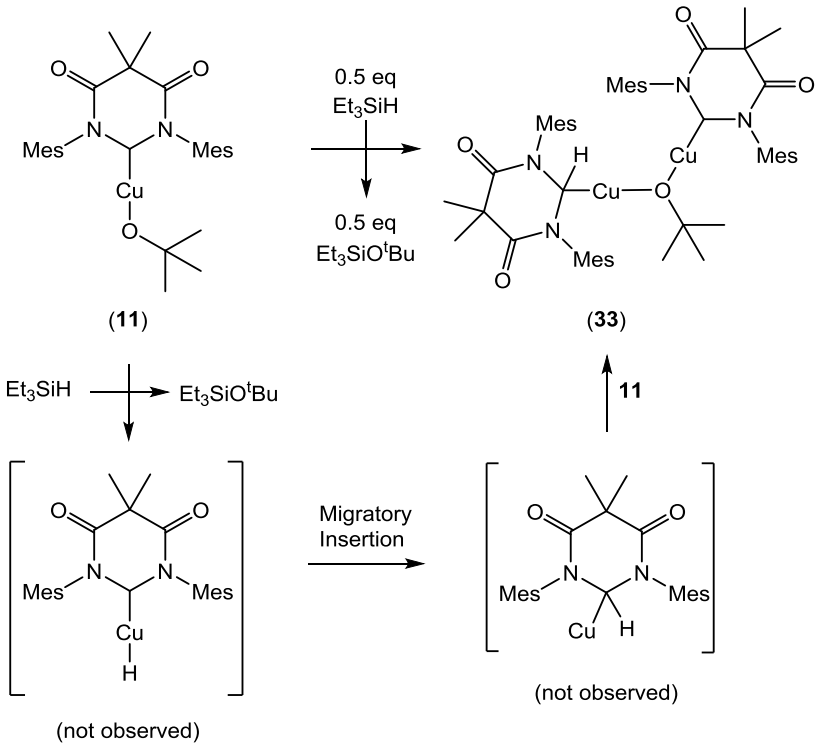

Scheme 5.3: Proposed pathway for the reaction of complex **11** with Et_3SiH, leading to the formation of complex **33**.

Initial reaction of (6-MesDAC)CuO^{t}Bu (**11**) with Et_3SiH leads to the formation of a transient (6-MesDAC)CuH species.[i] Rapid migratory insertion of the hydride on to the C2 position of 6-MesDAC results in the formation of a 6-MesDAC·H ligand, as part of an electrophilic [(6-MesDAC·H)Cu] fragment. This combines with a further equivalent of **11**, consistent with the 1 : 2 stoichiometry of the reaction, resulting in the formation of complex **33**.

[i] The description of (6-MesDAC)CuH as a mononuclear species is used here to describe the observed chemistry, and does not imply the viability of such a mononuclear species. The formation of hydride bridged dimers and related dinuclear species will be discussed alongside computational results in Section 5.4.

5.2.1 Attempted Observation of [(6-MesDAC)CuH]$_n$

All attempts at purification of **33** by washing, reprecipitation or crystallisation resulted in significant decomposition. Low temperature NMR studies were conducted in an attempt to observe the intermediate copper hydride species. Et_3SiH was added to a C_7D_8 solution of **11** at 178 K and the sample warmed inside an NMR spectrometer, however, no reaction occurred until the sample reached 235 K, at which temperature **33** was formed directly without any intermediate being observed. This result shows that copper hydride migratory insertion takes place with a lower activation energy than copper hydride formation.

Trapping experiments were conducted to try to intercept the copper hydride species before migratory insertion could occur. Addition of Et_3SiH (one equivalent) to a mixture of **11** and of PhC≡CMe or cyclohexanone (ten equivalents) at room temperature resulted in total decomposition of **11**, with no evidence of reduction. This instability under reductive conditions, and failure to trap an intermediate copper hydride species, further serves to demonstrate the limitations of 6-MesDAC as a ligand for reductive processes.

5.3 Synthesis of (6-MesDAC·H)CuP(*p*-Tol)$_3$ (34)

Trapping experiments were conducted with P(*p*-Tol)$_3$ to intercept the proposed electrophilic fragment [(6-MesDAC·H)Cu] (Scheme 5.4).

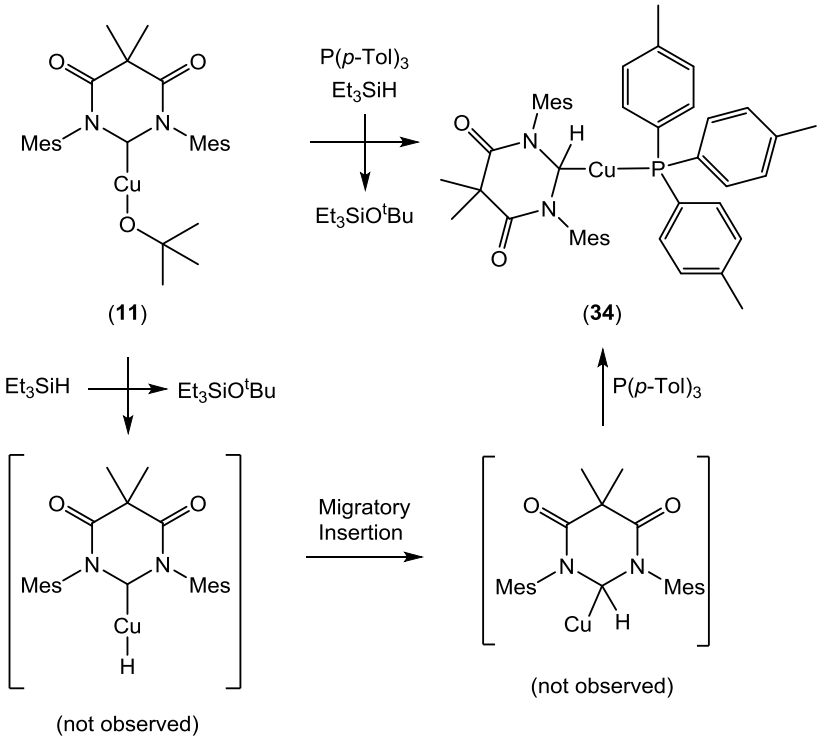

Scheme 5.4: Proposed pathway for the reaction of complex **11** with Et_3SiH in the presence of P(*p*-Tol)$_3$, leading to the formation of complex **34**.

Addition of one equivalent of Et_3SiH to a 1 : 1 mixture of **11** and P(*p*-Tol)$_3$ in benzene resulted in the immediate formation of a pale red solution of (6-MesDAC·H)CuP(*p*-Tol)$_3$ (**34**). ^{1}H NMR spectroscopy revealed that one equivalent of Et_3SiH had been consumed, forming one equivalent of Et_3SiO^tBu, in contrast to the half an equivalent of Et_3SiO^tBu formed in the absence of P(*p*-Tol)$_3$. The 6-MesDAC·H ligand displayed a similar ^{1}H NMR signal (5.96 ppm) for the migrated hydride to that of complex **33** (5.59 ppm). The $^{13}C\{^1H\}$ NMR resonances of the C2 position for these two complexes are also similar (**34** = 68.7 ppm; **33** = 67.7 ppm) but, in the case of **34**, the resonance appears as a doublet ($^2J_{CP}$ = 61.8 Hz) due to coupling with phosphine ($^{31}P\{^1H\}$ resonance located at 3.17 ppm). IR spectroscopy showed two equal intensity CO stretching bands at 1662 cm^{-1} and 1632 cm^{-1}, at similar frequencies to those of the 6-MesDAC·H ligand of **33** (1669 cm^{-1} and 1635 cm^{-1}). Addition of P(*p*-Tol)$_3$ to **33** resulted in the formation of **34**, but only alongside

other unidentified products. Complex **34** proved much more stable than complex **33**, and could be purified by reprecipitation and isolated as a red microcrystalline solid in 61 % yield.

5.3.1 Molecular Structure of (6-MesDAC·H)CuP(*p*-Tol)$_3$ (34)

Single crystals of **34** suitable for X-ray diffraction studies were grown from a saturated benzene solution layered with hexane.

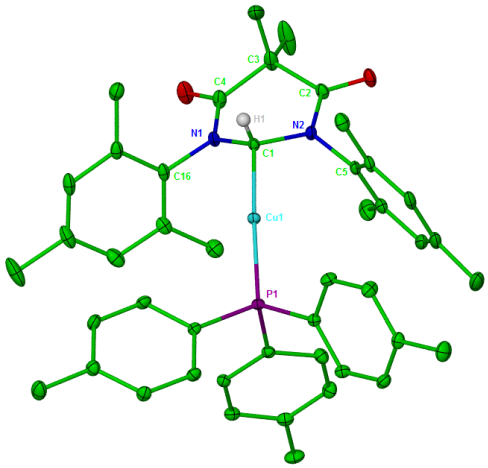

Figure 5.2: Displacement ellipsoid plot (30 % probability) of (6-MesDAC·H)CuP(*p*-Tol)$_3$ (**34**). H atoms omitted for clarity (except for H(1)). Selected bond lengths (Å) and angles (°): Cu(1)-C(1) 1.969(2), Cu(1)-P(1) 2.1907(6), N(1)-C(1)-N(2) 108.92(19), C(1)-Cu(1)-P(1) 174.05(8).

Complex **34** is a two co-ordinate phosphine copper alkyl complex in an approximately trans-linear geometry (C-Cu-P = 174.05(8)°). No other two co-ordinate copper complex of P(*p*-Tol)$_3$ has been structurally characterised, but the Cu-P bond length of **34** (2.1907(6) Å) is identical to that of (Mes)$_3$PCuBr (2.193(2) Å).[13] The 6-MesDAC·H ligand resembles the 6-MesDAC·R ligands of complexes **28** and **32**, with an sp^3 hybridised C2 carbon centre (N-C-N = 108.92(19)°). In contrast to the approximately planar heterocyclic rings of 6-MesDAC·R in **28** and **32**, the smaller steric bulk of the migrated hydride allows the ring to pucker and adopt a pseudo-boat conformation. This conformation is preserved in solution, as evidenced by the observation of an NOE interaction between the migrated hydride and axial backbone methyl, in the same manner as observed for complex **33**.

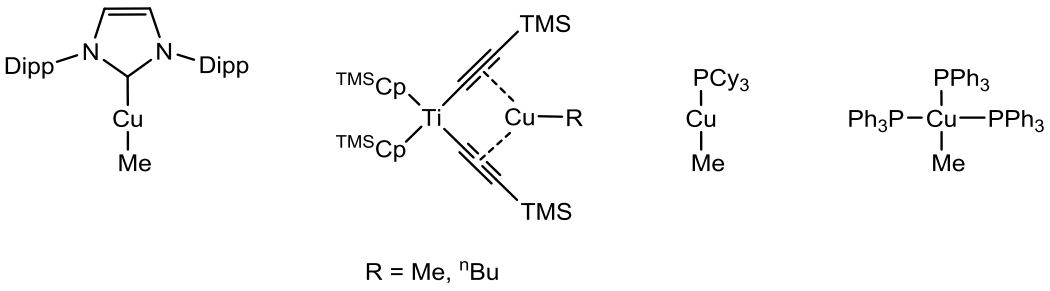

Figure 5.3: Structurally characterised examples of copper alkyl complexes. (IPr)CuMe (far left),[14] (^{TMS}Cp)$_2$Ti(C≡CTMS)$_2$CuR (R = Me,[15] ^{n}Bu)[16] (centre left), (PCy$_3$)CuMe (centre right),[17] (PPh$_3$)$_3$CuMe (far right).[18]

Structurally characterised copper alkyl complexes are rare, in part due to the explosive nature of [Cu(R)]$_n$ precursors; the known examples are shown in Figure 5.3. The Cu-C bond length of **34** (1.969(2) Å) is significantly longer than those of the structurally characterised two co-ordinate copper alkyl complexes (IPr)CuMe (1.913(6) Å)[14] and (PCy$_3$)CuMe (1.9164(15) Å).[17] This is perhaps due to the steric repulsion between the bulky 6-MesDAC·H and P(*p*-Tol)$_3$ ligands, and indeed, other sterically encumbered copper alkyl complexes have similar Cu-C bond lengths ((^{TMS}Cp)$_2$Ti(C≡CTMS)$_2$CuMe = 1.966(2) Å;[15] (^{TMS}Cp)$_2$Ti(C≡CTMS)$_2$Cu^{n}Bu = 1.991(6) Å;[16] (PPh$_3$)$_3$CuMe = 2.043(12) Å).[18]

5.4 DFT Studies

DFT calculations were conducted in collaboration with Macgregor and co-workers at Heriot-Watt University to further investigate this chemistry. A small model system was used in which all alkyl and aryl substituents are replaced by methyl groups (for example, 6-MesDAC becomes 6-MeDAC; O^{t}Bu becomes OMe).

Figure 5.4 shows two possible pathways for the reaction between (6-MeDAC)CuOMe and Me$_3$SiH. Pathway I (black data, Figure 5.4) shows a σ-bond metathesis reaction resulting in the formation of (6-MeDAC)CuH and Me$_3$SiOMe, in a process calculated to be exergonic by 4.2 kcal mol^{-1}. The activation barrier for this reaction was calculated to be 15.5 kcal mol^{-1}, which is in agreement with the observed room temperature reactivity of **11** and Et$_3$SiH. Pathway II (red data, Figure 5.4) shows a σ-bond metathesis reaction with the opposite regiochemistry, resulting in the formation of (6-MeDAC)CuSiMe$_3$ and MeOH. The products were

found to be 13.9 kcal mol^{-1} less stable than the starting materials, and no stable conformation of the transition state could be calculated. These calculations corroborate the experimental evidence that reactivity of (6-MesDAC)CuO^{t}Bu with Et_3SiH results in the formation of Et_3SiO^tBu, alongside (6-MesDAC)CuH.

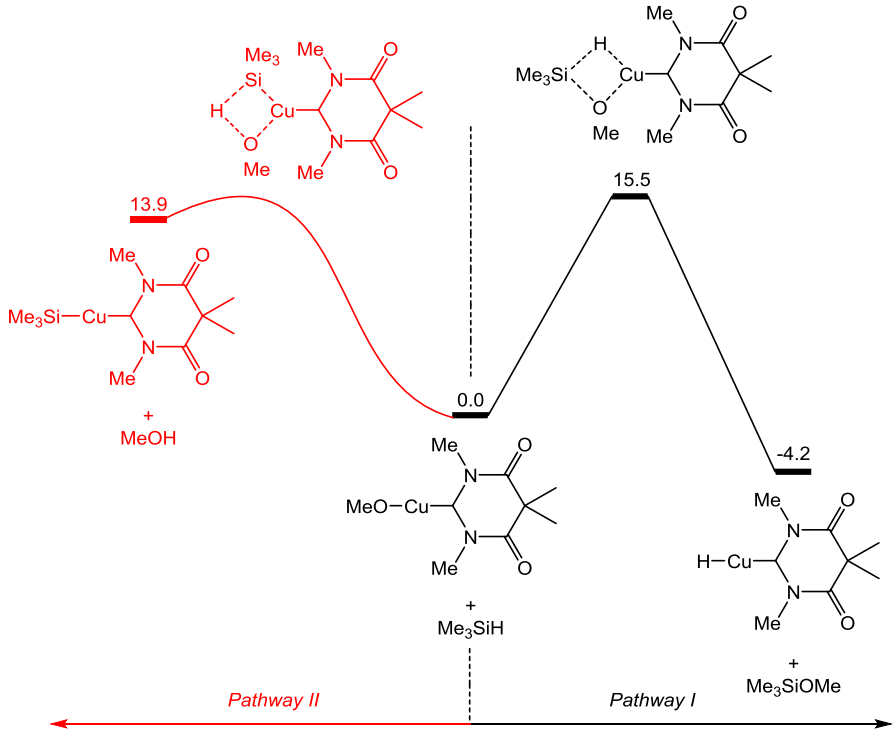

Figure 5.4: Calculated product and transition state energies for the reaction of (6-MeDAC)CuOMe with Me_3SiH. All energies are quoted in kcal mol^{-1}.

5.4.1 Migratory Insertion Processes of (6-MeDAC)CuH

Direct migratory insertion of mononuclear (6-MeDAC)CuH was investigated, and the resultant [(6-MeDAC·H)Cu] fragment was found to be less stable than the copper hydride complex by 0.8 kcal mol^{-1} (Figure 5.5). Furthermore, the activation barrier to this process was calculated to be 38.7 kcal mol^{-1}, and therefore incompatible with the facile migratory insertion observed experimentally.

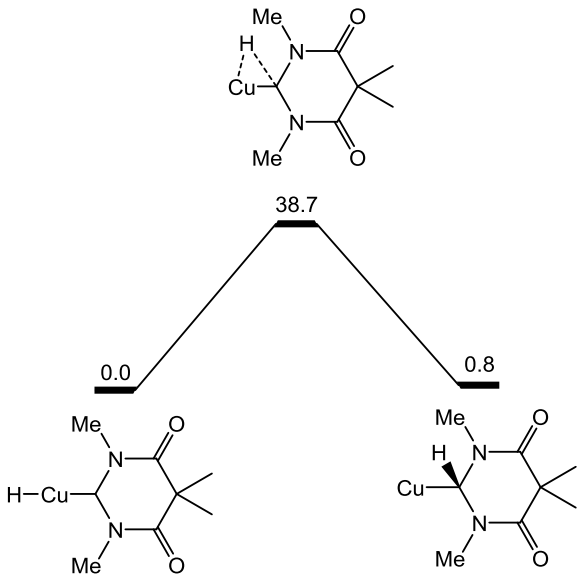

Figure 5.5: Figure showing the direct migratory insertion of hydride to form [(6-MeDAC·H)Cu]. All energies are quoted in kcal mol^{-1}.

The involvement of a range of Lewis bases was found to stabilise both the transition state and product of hydride migratory insertion. Co-ordination of the Lewis basic amide carbonyl of (6-MeDAC)CuOMe to (6-MeDAC)CuH was found to be energetically neutral (black data, Figure 5.6). However, the subsequent Lewis base assisted hydride migratory insertion from this three co-ordinate complex was calculated to have a much smaller activation barrier (16.7 kcal mol^{-1}) than direct migration from two co-ordinate (6-MeDAC)CuH (38.7 kcal mol^{-1}). The formation of MeOCu(μ-6-MeDAC)Cu(6-MeDAC·H) through this pathway was calculated to be exergonic by 10.4 kcal mol^{-1} (black data, Figure 5.6).

Co-ordination of the Lewis basic alkoxide in place of the Lewis basic amide carbonyl resulted in a similar trend, but with an overall greater stabilising effect (red data, Figure 5.6). Initial formation of (6-MeDAC)Cu(μ-OMe)Cu(H)(6-MeDAC) resulted in a stabilisation of 7.9 kcal mol^{-1} and migratory insertion from this three co-ordinate intermediate was calculated to have an activation barrier of just 6.7 kcal mol^{-1} (red data, Figure 5.6). The product of this reaction, (6-MeDAC)Cu(μ-OMe)Cu(6-MeDAC·H), is the model system analogue of **33**, and the small activation barrier and strong thermodynamic driving force (27.4 kcal mol^{-1}) for its formation is in agreement with the experimental observations.

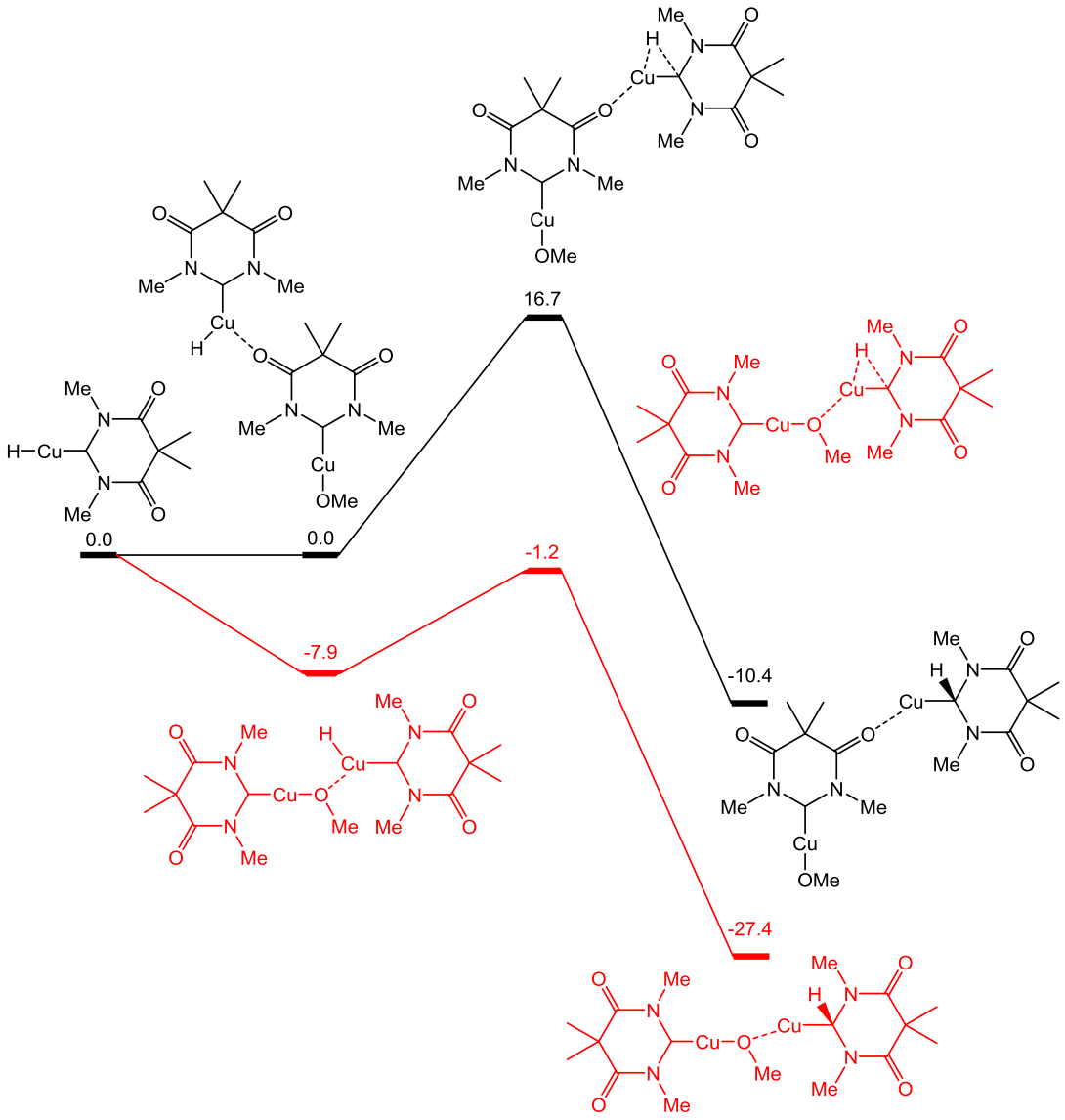

Figure 5.6: Calculated transition states and energies for Lewis base assisted hydride migratory insertion reactions of (6-MeDAC)CuH. Black data: μ-(6-MeDAC) assisted hydride migratory insertion. Red data: copper alkoxide assisted hydride migratory insertion. All energies are quoted in kcal mol^{-1}.

A further mechanism was investigated, in which two molecules of (6-MeDAC)CuH interact to form the copper hydride dimer $[(6\text{-MeDAC})CuH]_2$ (black data, Figure 5.7). The formation of this dimer was calculated to be significantly more exergonic (-30.9 kcal mol^{-1}) than the formation of the alkoxide bridged species (6-MeDAC)Cu(μ-OMe)Cu(H)(6-MeDAC) (-7.9 kcal mol^{-1}, red data, Figures 5.6 and 5.7). However, hydride assisted migratory insertion was calculated to be endergonic

(0.9 kcal mol^{-1}, black data, Figure 5.7), with a significantly larger activation barrier (19.6 kcal mol^{-1}) than for alkoxide assisted migratory insertion (6.7 kcal mol^{-1}).

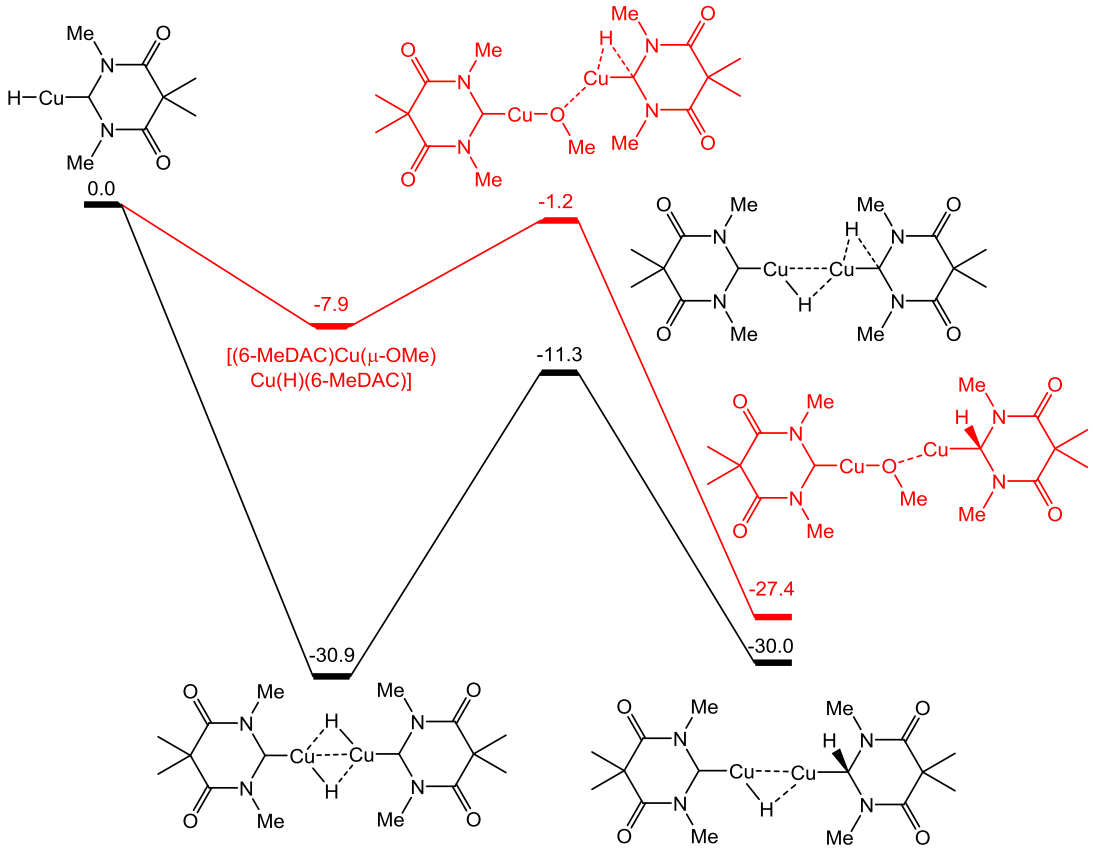

Figure 5.7: Calculated transition states and energies for Lewis base assisted hydride migratory insertion reactions of (6-MeDAC)CuH. Black data: copper hydride assisted hydride migratory insertion. Red data: copper alkoxide assisted hydride migratory insertion. All energies are quoted in kcal mol^{-1}.

Experimentally, addition of P(*p*-Tol)$_3$ resulted in different reactivity with the formation of complex **34**. One possibility for the formation of **34** is phosphine displacing the alkoxide bridge from complex **33**, liberating (6-MesDAC)CuO^{t}Bu and forming complex **34**. However, it is also possible for phosphine to assist migratory insertion itself. This process was modelled using the small model system (Figure 5.8) and initial co-ordination of PMe$_3$ to (6-MeDAC)CuH was found to be exergonic (-6.7 kcal mol^{-1}). Phosphine assisted hydride migratory insertion occurs with an activation barrier of 6.5 kcal mol^{-1}, in a process that is exergonic by 21.0 kcal mol^{-1} (Figure 5.8). With a similar activation barrier to alkoxide assisted hydride migratory

insertion (6.7 kcal mol^{-1}, red data, Figure 5.6), these two processes may be competitive.

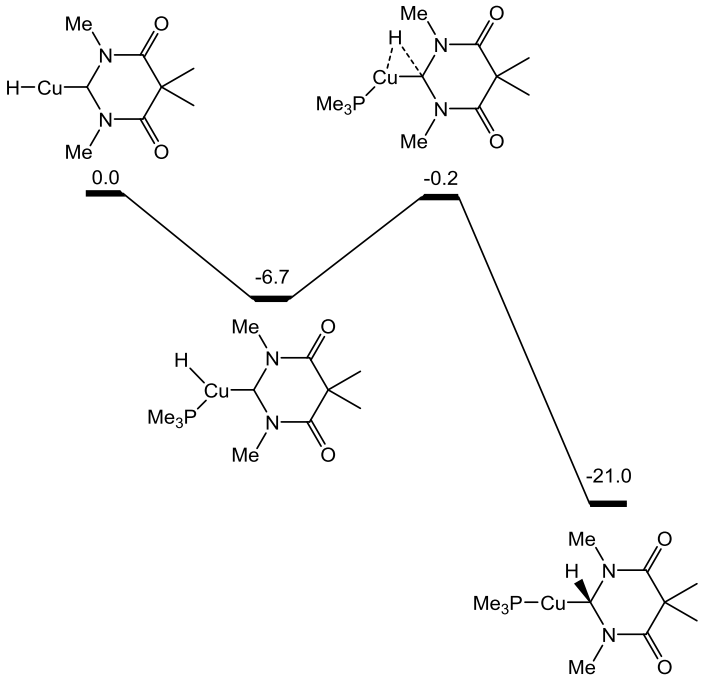

Figure 5.8: Calculated transition states and energies for a phosphine assisted hydride migratory insertion reaction of (6-MeDAC)CuH. All energies are quoted in kcal mol^{-1}.

Whether assisted by pre-co-ordination of phosphine (Figure 5.8) or copper alkoxide (Figure 5.6), hydride migratory insertion of (6-MeDAC)CuH occurs with an activation barrier (6.5 or 6.7 kcal mol^{-1}) that is less than half as large as the activation barrier to its formation through σ-bond metathesis between (6-MeDAC)CuOMe and Me_3SiH (15.5 kcal mol^{-1}, Figure 5.4). Whilst the calculated energies of the full system may differ from the energies calculated for this small model system, these results support the experimental findings and help to explain the underlying chemistry.

5.5 Reactivity of (6-Mes)CuO^{t}Bu (20) with Et_3SiH

Addition of one equivalent of Et_3SiH to (6-Mes)CuO^{t}Bu (**20**) in benzene at room temperature resulted in the immediate formation of a bright yellow solution. This colour faded over the course of several hours, alongside the precipitation of metallic copper (characterised by PXRD, see Appendix for details). ^{1}H NMR spectroscopy revealed a very slow reaction, with the consumption of **20** only being complete after four days, or after twenty five hours in the presence of three and a half equivalents of Et_3SiH. At the end of the reaction, ^{1}H NMR spectroscopy revealed the formation of Et_3SiO^tBu in a 2 : 1 ratio with each of two types of 6-Mes ligand, demonstrating that a simple $[(6\text{-Mes})CuH]_n$ complex was not the final product of the reaction. One copper-bound, C_s symmetric 6-Mes ligand was identified by its low field carbenic $^{13}C\{^1H\}$ resonance (204.2 ppm) and triplet and pentet backbone ^{1}H NMR resonances. The other, desymmetrised, 6-Mes ligand was identified as 6-Mes·H, with a complicated multiplet in the ^{1}H NMR spectrum (3.07 ppm) assigned to the α-amino methylene protons. This resonance showed an NOE interaction to a 1H integral, singlet resonance at 4.10 ppm, which in turn showed a $^1J_{CH}$ interaction to a $^{13}C\{^1H\}$ NMR resonance at 81.0 ppm. These resonances closely resemble the NMR signatures of the C2 methine regions of 6-MesDAC·H in complexes **33** and **34** (^{1}H = 5.59 and 5.96 ppm respectively; $^{13}C\{^1H\}$ = 67.7 and 68.7 ppm respectively). Isolation of the product (76 % yield) and X-ray diffraction analysis confirmed its assignment as (6-Mes·H)Cu(6-Mes) (**35**). Scheme 5.4 shows a proposed reaction scheme for the formation of complex **35**. The proposed stoichiometry of the product distribution is supported by the isolated yields with respect to copper (**35** = 38 %; Cu metal = 43 %) and ^{1}H NMR spectroscopy revealing that complex **35** was the only 6-Mes containing product of the reaction. The observation of a small singlet in the ^{1}H NMR spectrum at 4.47 ppm confirmed the evolution of hydrogen gas in the reaction, allowing for a mass-balanced reaction scheme to be proposed (Scheme 5.4).

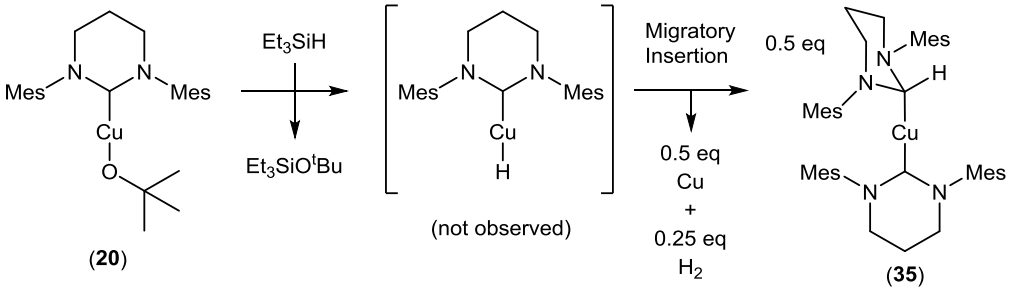

Scheme 5.4: Reactivity of **20** with Et_3SiH, resulting in the formation of complex **35**.

The observation of migratory insertion onto a non-chelating diaminocarbene is unprecedented,[i] and raises questions about the generality of hydride migration as a decay process in reductive catalysis.

5.5.1 Molecular Structure of (6-Mes·H)Cu(6-Mes) (35)

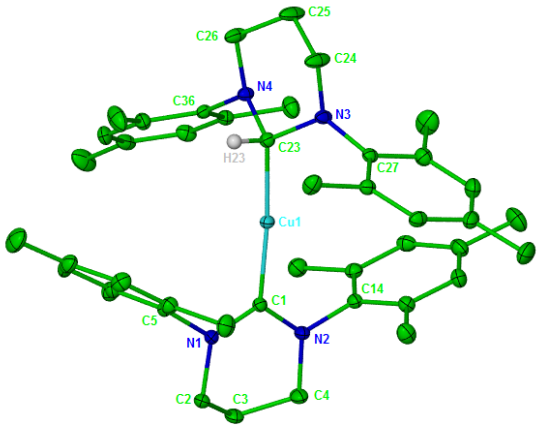

Figure 5.8: Displacement ellipsoid plot (30 % probability) of (6-Mes·H)Cu(6-Mes) (**35**). H atoms omitted for clarity (except for H(23)). Selected bond lengths (Å) and angles (°): Cu(1)-C(1) 1.929(2), Cu(1)-C(23) 1.953(2), N(1)-C(1)-N(2) 117.08(17), N(3)-C(23)-N(4) 106.39(16), C(1)-Cu(1)-C(23) 173.04(9).

Complex **35** is a two co-ordinate NHC copper alkyl complex in an approximately trans-linear (173.04(9)°) geometry, with 6-Mes·H adopting a chair conformer in the solid state, in contrast to the boat conformer of 6-MesDAC·H in **34**. The presence of both 6-Mes and 6-Mes·H ligands in the same complex allows for a direct comparison of their structural parameters. The NCN angle of 6-Mes·H (106.39(16)°) is consistent with that of an sp^3 alkyl ligand and significantly more

[i] The literature precedent for migratory insertion processes was discussed in Section 4.11.

acute than the NCN angle of the sp^2 hybridised 6-Mes (117.08(17)°). The Cu-C_{NHC} bond length (1.929(2) Å) is identical to that of the similarly sterically crowded homoleptic complex $[(6\text{-Mes})_2Cu][BF_4]$ (**7**, 1.9266(19) Å), but significantly shorter than the Cu-$C_{6\text{-Mes}\cdot H}$ bond (1.953(2) Å). This Cu-$C_{6\text{-Mes}\cdot H}$ bond is also shorter than the Cu-$C_{6\text{-MesDAC}\cdot H}$ bond of complex **34** (1.969(2) Å).

5.6 Synthesis of (6-Mes)Cu(C(Ph)=C(Me)H) (36)

Attempts to observe a copper hydride intermediate by NMR were unsuccessful due to the slow reactivity of complex **20** with Et_3SiH. Monitoring the reaction by ^1H NMR spectroscopy at room temperature (with either one equivalent or an excess of Et_3SiH) only revealed a sluggish decay of complex **20**, accompanied by the formation of complex **35**, Et_3SiO^tBu, hydrogen gas, and the deposition of metallic copper (Scheme 5.4). Conducting the reaction at lower temperature only served to further slow the reactivity.

Trapping experiments were conducted to try to intercept the intermediate copper hydride species. Reaction of **20** with Et_3SiH in the presence of PhC≡CMe resulted in the quantitative formation of (6-Mes)Cu(C(Ph)=C(Me)H) (**36**, Scheme 5.5).

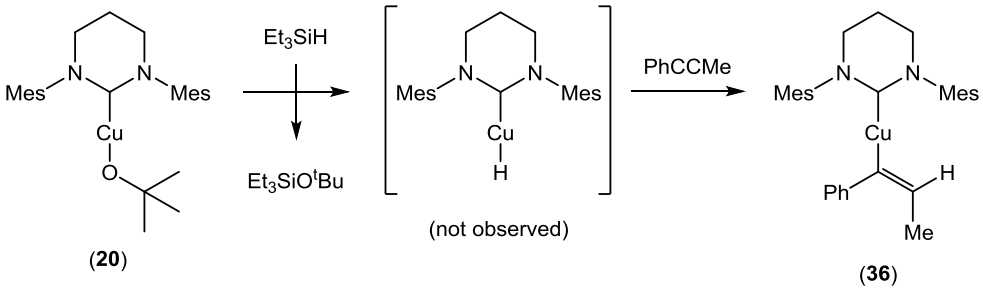

(**20**) (**36**)

Scheme 5.5: Reactivity of **20** with Et_3SiH in the presence of PhC≡CMe.

Addition of one equivalent of Et_3SiH to a benzene solution of **20** and PhC≡CMe resulted in the immediate formation of an orange solution. Complete consumption of **20** was achieved after four days (or twenty five hours in the presence of three equivalents of Et_3SiH) and (6-Mes)Cu(C(Ph)=C(Me)H) (**36**) was isolated as an off-white powder in 58 % yield.

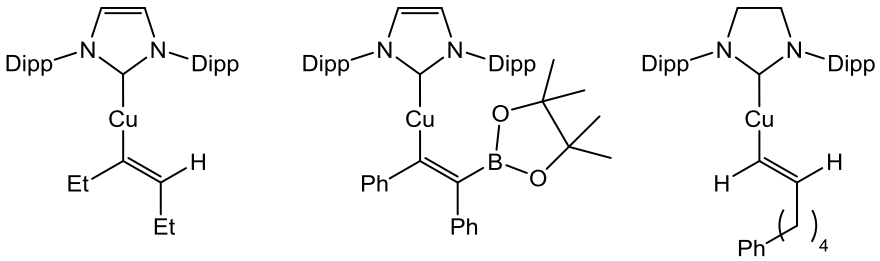

Figure 5.9: Structurally characterised examples of copper alkenyl complexes. (IPr)Cu(C(Et)=C(Et)H) (left),[9] (IPr)Cu(C(Ph)=C(Ph)BPin) (centre),[19] (SIPr)Cu(C(H)=C($(CH_2)_4$Ph)H) (right).[20]

Complex **36** displayed ^{1}H NMR resonances for a single, C_s symmetrical 6-Mes environment, with characteristic triplet and pentet backbone resonances. The carbenic carbon was found to resonate at 205.2 ppm by $^{13}C\{^1H\}$ NMR spectroscopy. The alkenyl $^{13}C\{^1H\}$ NMR resonances were located at 171.2 ppm and 128.4 ppm (cf: (IPr)Cu(C(Et)=C(Et)H) = 171.4 ppm and 136.4 ppm, Figure 5.9),[9] with the latter displaying a clear $^1J_{CH}$ interaction to a 1H integral, quartet ^{1}H NMR resonance at 5.61 ppm (cf: (IPr)Cu(C(Et)=C(Et)H) = 5.51 ppm;[9] (SIPr)Cu(C(H)=C($(CH_2)_4$Ph)H) = 5.83 ppm, Figure 5.9).[20] This signal corresponds to the inserted copper hydride, and ^{1}H-^{1}H COSY NMR spectroscopy showed correlation to a 3H integral, doublet ($^3J_{HH}$ = 6.4 Hz) resonance at 1.82 ppm, corresponding to the vicinal methyl protons. The NMR data support the syn, Markovnikov regioselectivity of copper hydride insertion shown in Scheme 5.5, and this was confirmed by X-ray diffraction studies.

5.6.1 Molecular Structure of (6-Mes)Cu(C(Ph)=C(Me)H) (36)

Single crystals of **36** were grown by layering a saturated benzene solution with hexane.

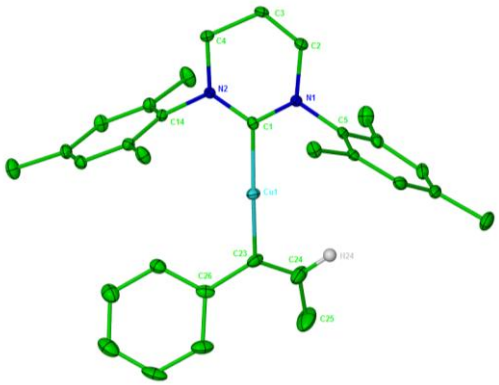

Figure 5.10: Displacement ellipsoid plot (30 % probability) of (6-Mes)Cu(C(Ph)=C(Me)H) (**36**). Selected bond lengths (Å) and angles (°): Cu(1)-C(1) 1.916(2), Cu(1)-C(23) 1.919(2), C(23)-C(24) 1.331(4), N(1)-C(1)-N(2) 117.23(19), C(1)-Cu(1)-C(23) 172.92(10), Cu(1)-C(23)-C(24) 119.4(2).

Complex **36** consists of one 6-Mes and one 1-phenylprop-1-enyl ligand, coordinated to copper in an approximately trans-linear geometry (C-Cu-C = 172.92(10)°). The Cu-C_{NHC} bond length of **36** (1.916(2) Å) is significantly longer than the Cu-C_{NHC} bond length of (IPr)Cu(C(Et)=C(Et)H) (1.897(3) Å, Figure 5.9), but similar in length to that of the more sterically crowded (IPr)Cu(C(Ph)=C(Ph)BPin) (1.910(3) Å, Figure 5.9). The metrics of the copper alkenyl moiety (Cu-$C_{alkenyl}$ = 1.919(2) Å, C=C = 1.331(4) Å) show no significant difference to those of the other structurally characterised copper alkenyl complexes ((IPr)Cu(C(Et)=C(Et)H): Cu-$C_{alkenyl}$ = 1.902(4) Å, C=C = 1.317(7) Å;[9] (IPr)Cu(C(Ph)=C(Ph)BPin): Cu-$C_{alkenyl}$ = 1.924(4) Å, C=C = 1.356(5) Å;[19] (SIPr)Cu(C(H)=C((CH$_2$)$_4$Ph)H): Cu-$C_{alkenyl}$ = 1.9108(18) Å, C=C = 1.341(3) Å, Figure 5.9).[20]

5.7 Catalytic Hydrocarboxylation of Internal Alkynes

Having successfully demonstrated that 6-Mes is able to support a copper hydride species which is competent in the reduction of alkynes, the potential for further derivatisation was investigated. Tsuji and co-workers employed a range of five-membered NHCs to support the copper catalysed hydrocarboxylation of internal alkynes.[4] They proposed a catalytic cycle (Scheme 5.6) and experimentally verified the interconversion of each of the intermediates. Reaction of $(Cl_2IPr)CuF$ with $(EtO)_3SiH$ at room temperature generated a copper hydride complex with concomitant elimination of $(EtO)_3SiF$ within minutes. Insertion of 1-phenyl-3,3-dimethylbut-1-yne afforded a copper alkenyl species within hours at room temperature. The rate determining step was found to be the insertion of CO_2 to this alkenyl complex, requiring overnight heating at 343 K. Regeneration of the hydride and elimination of the product was effected within minutes at room temperature by reaction of the copper carboxylate complex with $(EtO)_3SiH$.[4]

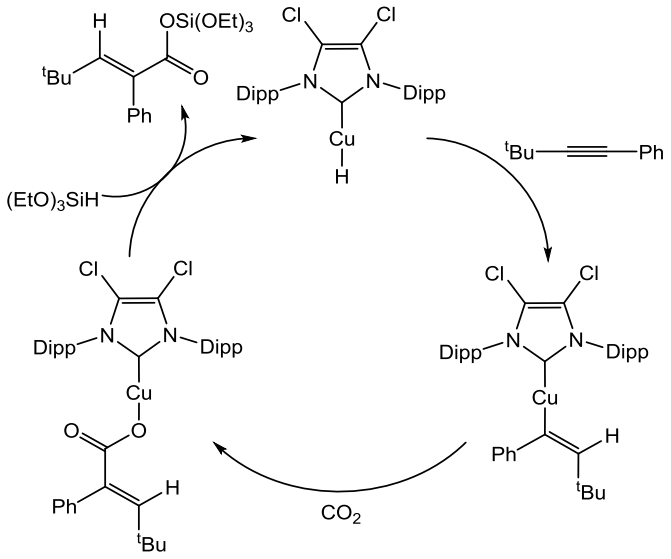

Scheme 5.6: Proposed catalytic cycle for the hydrocarboxylation of internal alkynes, catalysed by $(Cl_2IPr)CuH$.[4]

5.7.1 Synthesis of $[(6\text{-Mes})_2Cu][Cu(OC(O)C(Ph)=C(Me)H)_2]$ (37)

To assess whether 6-Mes is a suitable ligand for supporting catalytic hydrocarboxylation, the reaction of **36** with CO_2 was investigated. Exposure of a benzene solution of **36** to one atmosphere of ^{13}C-enriched CO_2 at room temperature

resulted in an immediate colour change to give a yellow solution. $^{13}C\{^{1}H\}$ NMR spectroscopy revealed the complete consumption of **36** within minutes and the appearance of an intense $^{13}C\{^{1}H\}$ NMR signal at 173.6 ppm confirmed the insertion of CO_2, and formation of a copper carboxylate species (cf: $(Cl_2IPr)Cu(OC(O)C(Ph)=C(^{t}Bu)H)$ = 174.0 ppm). However, the product formed was not the heteroleptic (6-Mes)Cu(OC(O)C(Ph)=C(Me)H), but the ionic homoleptic complex $[(6\text{-Mes})_2Cu][Cu(OC(O)C(Ph)=C(Me)H)_2]$ (**37**, Scheme 5.7), which was isolated in 48 % yield and characterised by X-ray diffraction studies (Figure 5.11).

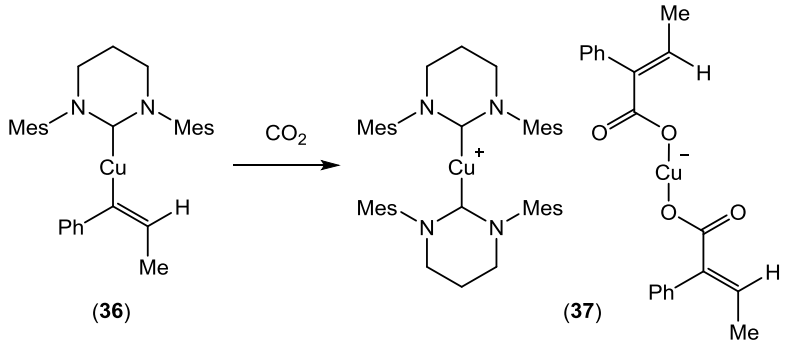

Scheme 5.7: Reactivity of CO_2 with (6-Mes)Cu(C(Ph)=C(Me)H) (**36**), leading to the ionic homoleptic species $[(6\text{-Mes})_2Cu][Cu(OC(O)C(Ph)=C(Me)H)_2]$ (**37**).

The propensity of 6-Mes to form homoleptic complexes of the form $[(6\text{-Mes})_2Cu][CuX_2]$ was seen before in the formation of $[(6\text{-Mes})_2Cu][CuI_2]$ (**24**, Section 3.9) from reaction of 6-Mes with CuI, as well as from the cross coupling of $(6\text{-Mes})CuC_6F_5$ (**22**) with 3,5-bis(trifluoromethyl)iodobenzene.

5.7.2 Molecular Structure of $[(6\text{-Mes})_2Cu][Cu(OC(O)C(Ph)=C(Me)H)_2]$ (37)

Single crystals of **37** were grown from layering a saturated benzene solution with hexane and the structure determined by X-ray diffraction studies.

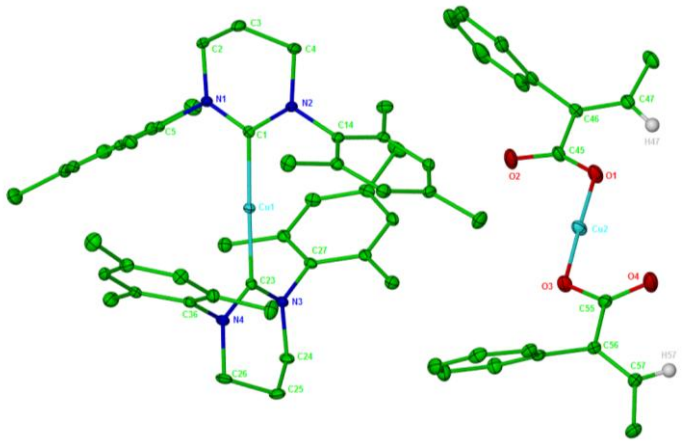

Figure 5.11: Displacement ellipsoid plot (30 % probability) of $[(6\text{-Mes})_2Cu][Cu(OC(O)C(Ph)=C(Me)H)_2]$ (**37**). H atoms omitted for clarity. Selected bond lengths (Å) and angles (°): Cu(1)-C(1) 1.932(2), Cu(1)-C(23) 1.934(2), Cu(2)-O(1) 1.8331(17), Cu(2)-O(3) 1.8468(16), C(45)-O(1) 1.265(3), C(45)-O(2) 1.232(12), C(46)-C(47) 1.334(3), C(55)-O(3) 1.274(3), C(55)-O(4) 1.233(3), C(56)-C(57) 1.334(3), C(1)-Cu(1)-C(23) 177.22(8), N(1)-C(1)-N(2) 117.26(17), N(3)-C(23)-N(4) 117.26(18), O(1)-Cu(2)-O(3) 178.04(8), O(1)-C(45)-O(2) 123.1(6), C(45)-C(46)-C(47) 120.3(2), O(3)-C(55)-O(4) 123.9(2), C(55)-C(56)-C(57) 117.7(2).

Complex **37** comprises two homoleptic, ionic species. The approximately trans-linear (177.22(8)°) cationic $[(6\text{-Mes})_2Cu]^+$ complex has been characterised previously ($[(6\text{-Mes})_2Cu][BF_4]$ (**7**, Section 2.6) and $[(6\text{-Mes})_2Cu][CuI_2]$ (**24**, Section 3.9)) and displays identical Cu-C bond lengths (1.932(2) Å and 1.934(2) Å) to both **7** and **24**. The anionic $[Cu(OC(O)C(Ph)=C(Me)H)_2]^-$ consists of two κ^1 co-ordinated α,β-unsaturated carboxylate ligands in a trans-linear geometry (178.04(8)°), with one Cu-O bond being significantly longer (Cu(2)-O(3) = 1.8468(16) Å) than the other (Cu(2)-O(1) = 1.8331(17) Å). This asymmetry in Cu-O bonding perhaps reflects the different geometries adopted by each ligand, whereby the alkenyl proton of each is proximal to either the copper bound (O1) or terminal

(O4) oxygen atom of the carboxylate. Both ligands are approximately co-planar (dihedral angle between C=C planes = 17.9°), allowing for extensive delocalisation of their π systems, which is perhaps reflected in the relatively long Cu-O bonds of **37** (1.8468(16) Å and 1.8331(17) Å) compared to those of $[Cu(OC(O)Me)_2]^-$ (1.821(8) Å, Figure 5.12).[21]

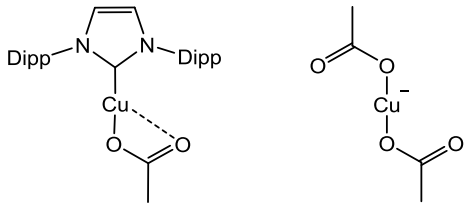

Figure 5.12: Examples of copper(I) carboxylate complexes. (IPr)Cu(OC(O)Me) (left),[14] $[(Phen)_2Cu][Cu(OC(O)Me)_2]\cdot[(Phen)_2Cu][H(OC(O)Me)_2]$ (cuprate anion depicted, right).[21]

5.8 (6-Mes)CuO^{t}Bu (20) as a Precatalyst for Reductive Processes

Given the homoleptic nature of **37**, it is perhaps unsurprising that no reactivity was observed with Et_3SiH, even after 65 hours at 343 K. Attempts to form complex **37** without the prior isolation of **36** were also unsuccessful. Addition of Et_3SiH to a benzene solution of **20** and PhC≡CMe under an atmosphere of CO_2 resulted in no formation of complex **37**. The major organometallic product of the reaction was identified as a copper formate species (1H integral singlet = 8.56 ppm; cf: (P(*o*-(CH_2NMe_2)-$C_6H_4)_3$)Cu(OC(O)H) = 8.42 ppm),[22] suggesting that $[(6\text{-Mes})CuH]_n$ reacts preferentially with CO_2 over PhC≡CMe. Although these results rule out the potential for catalytic hydrocarboxylation supported by 6-Mes, they raise interesting questions about the differences in reactivity between 6-Mes and the five-membered NHCs studied by Tsuji and co-workers.[4] In the case of the five-membered NHC copper hydride species, reduction of alkyne occurred preferentially over reduction of CO_2, with the subsequent reaction of CO_2 with the copper alkenyl complex being the rate determining step in catalysis, and requiring the use of elevated temperatures (Scheme 5.6). In the case of $[(6\text{-Mes})CuH]_n$, copper hydride formation is very slow and CO_2 reactivity is facile. The enhanced reactivity of this RENHC copper hydride system towards CO_2 over five-membered NHC copper hydride systems warrants further study.

5.8.1 Catalytic Semi-Reduction of PhC≡CMe

Addition of ^{t}BuOH (ten equivalents) to complex **36** in C_6D_6 at room temperature resulted in the quantitative formation of complex **20** after one hour, with protonolysis of (Z)-1-phenylprop-1-ene (characteristic ^{1}H NMR resonances at: 6.41 (1 H, d q, $^{3}J_{HH}$ = 11.6 Hz, $^{4}J_{HH}$ = 1.8 Hz, PhC(H)=C(H)Me), 5.64 (1 H, d q, $^{3}J_{HH}$ = 11.6 and 7.2 Hz, PhC(H)=C(H)Me), 1.70 (3 H, d d, $^{3}J_{HH}$ = 7.2 Hz, $^{4}J_{HH}$ = 1.8 Hz, PhC(H)=C(H)Me) ppm)[23] (Scheme 5.8).

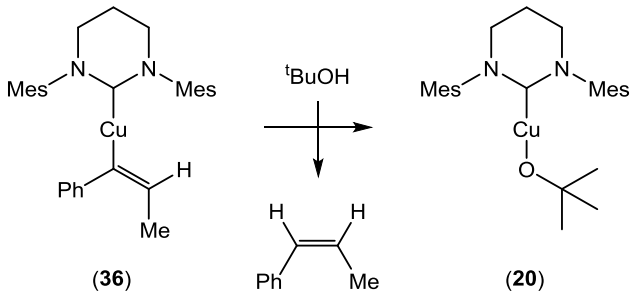

Scheme 5.8: Protonolysis of **36** with ^{t}BuOH to regenerate complex **20**.

This protonolysis constitutes the final step in a catalytic cycle for the *cis*-selective semi-reduction of PhC≡CMe to Ph(H)C=C(H)Me. Indeed, under catalytic conditions (Scheme 5.9), **20** was a competent precatalyst for semi-reduction at 5 mol % loading. However, the very slow turnover of this system (twenty turnovers after thirteen days at room temperature) compares poorly to the activity of the five-membered NHC precatalyst (IPr)CuO^{t}Bu (2 mol % loading, 298 K, 4 hours: 98 % conversion to (Z)-PhC(H)=C(H)Me).[8] Raising the temperature to 333 K did accelerate catalysis to now reach completion within 17 hours, although only at the expense of selectivity, with a 96 : 4 ratio of (Z)- and (E)-alkene isomers produced. Further attempts at optimisation were beyond the scope of this investigation.

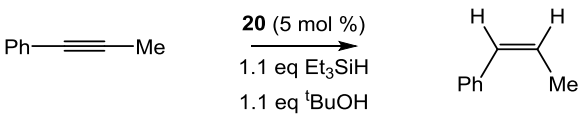

Scheme 5.9: Reaction scheme for the catalytic semi-reduction of PhC≡CMe.

5.8.2 Catalytic Hydrosilylation of Cyclohexanone

20 was also found to be a successful precatalyst for the hydrosilylation of cyclohexanone at 298 K (Scheme 5.10). With a 5 mol % catalyst loading, Et_3SiOCy was formed quantitatively within 160 minutes. Optimisation studies were not conducted, but this initial result demonstrates high activity, comparable to established five-membered NHC systems ((SIMes)CuCl or $[(IPr)_2Cu][BF_4]$, 3 mol % loading, 298 K = 98 % conversion to Et_3SiOCy within 30 minutes).[7,24]

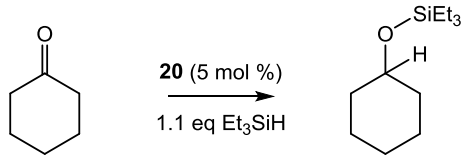

Scheme 5.10: Reaction scheme for the catalytic hydrosilylation of cyclohexanone.

5.8.3 Discussion

The catalytic turnover frequency for hydrosilylation of cyclohexanone (7.5 hr^{-1}) is two orders of magnitude greater than that for the semi-reduction of PhC≡CMe (0.06 hr^{-1}) under identical conditions (5 mol % **20**, 298 K). This dramatic rate enhancement raises interesting questions about the mechanisms of these reactions.

Scheme 5.11 shows a proposed catalytic cycle for the semi-reduction of PhC≡CMe which is supported by experimental evidence. Reaction of **20** with Et_3SiH in the presence, or absence, of PhC≡CMe results in the formation of Et_3SiO^tBu and either complex **36** or **35**, respectively, at identical rates (complete conversion after four days at room temperature in the presence of one equivalent of Et_3SiH). This is consistent with the rate determining formation of a copper hydride species, followed by either alkyne insertion (**36**) or migratory insertion (**35**). The formation of **20** by stoichiometric reaction of **36** and ^tBuOH supports protonolysis being the final step in the catalytic cycle.

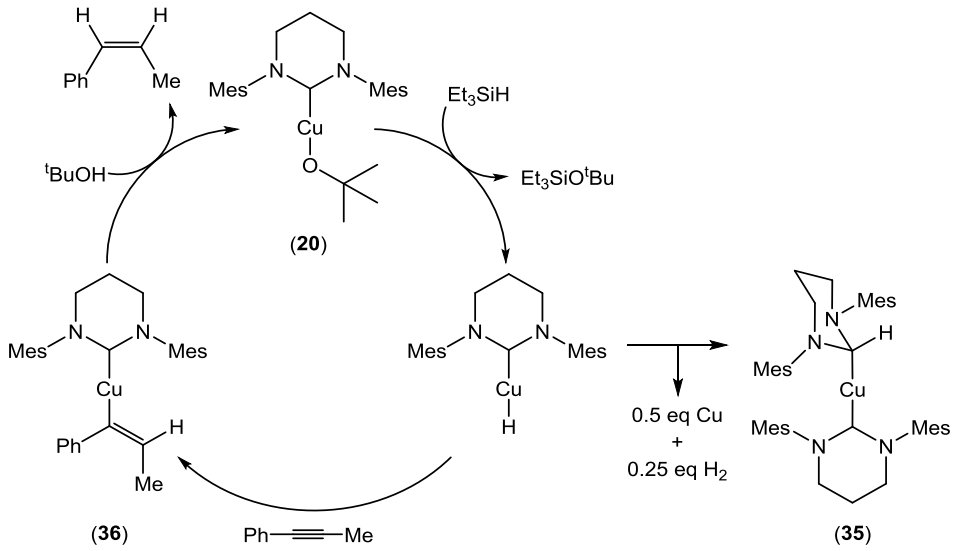

Scheme 5.11: Proposed catalytic cycle for the semi-reduction of PhCCMe.

Proposed mechanisms of copper hydride catalysed hydrosilylation were discussed in Section 1.8.1. One such mechanism (Scheme 1.9) involves formation of a copper hydride and subsequent insertion of a ketone to the C-H bond, in a similar manner to that shown in Scheme 5.11 for alkyne reduction. With copper hydride formation being the rate determining step in the catalytic semi-reduction of PhC≡CMe, the rate enhancement for hydrosilylation can only be explained by this hydride insertion mechanism if cyclohexanone assists copper hydride formation. A second mechanism in which copper acts as a Lewis acid catalyst (Scheme 1.10, bottom) could also explain this rate enhancement. Addition of cyclohexanone to **20** in the absence of Et_3SiH resulted in broadening of the ^1H NMR spectrum, consistent with co-ordination of the ketone to copper. This observation could support the proposal of Lewis acid catalysed reduction, with the Lewis acid being either complex **20** or a less sterically encumbered hydride complex. However, co-ordination of ketone to **20** could also serve to accelerate the formation of a copper hydride complex through reaction with silane and further investigation is required to determine the role of copper in catalytic reduction processes.

5.9 DFT Studies

To better understand the chemistry of copper hydride formation and migratory insertion with 6-Mes, Macgregor and co-workers have conducted preliminary DFT calculations using a small model system with methyl substituents replacing all alkyl

and aryl groups. Figure 5.13 shows the two possible σ-bond metathesis reactions between (6-Me)CuOMe and Me_3SiH.

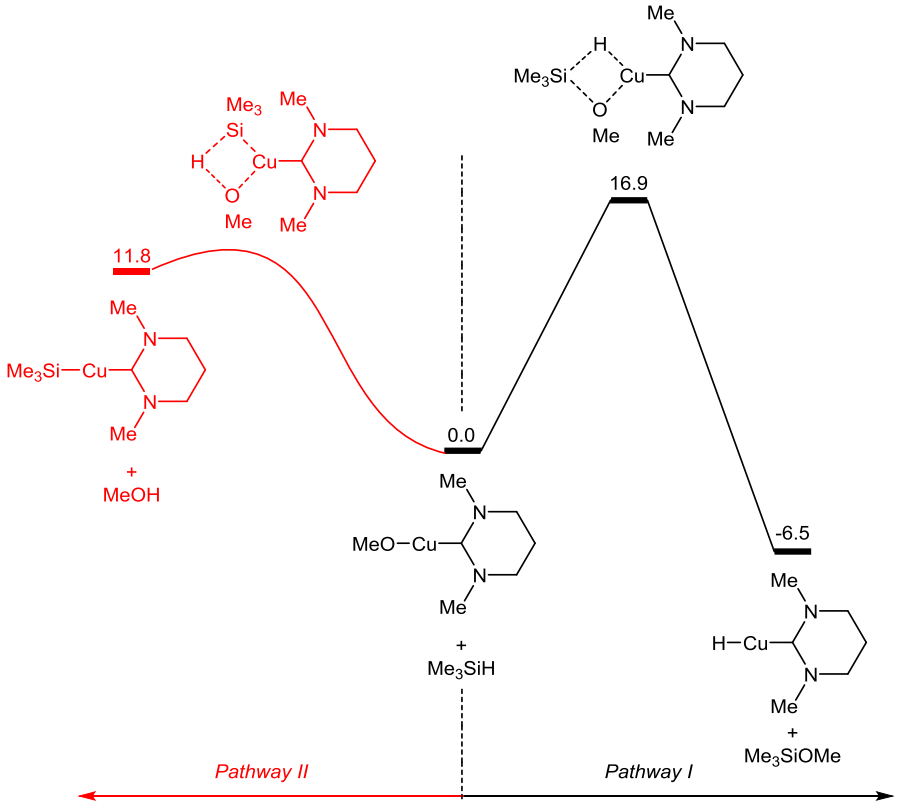

Figure 5.13: Calculated transition states and energies for the reaction of (6-Me)CuOMe with Me_3SiH. All energies are quoted in kcal mol^{-1}.

Formation of a copper silyl complex (red data, Figure 5.13) is calculated to be endergonic (11.8 kcal mol^{-1}) and no stable transition state could be found. Pathway I (Figure 5.13, black data), resulting in the formation of (6-Me)CuH and Me_3SiOMe, is calculated to be more thermodynamically favourable (-6.5 kcal mol^{-1}) than the formation of the diamidocarbene complex (6-MeDAC)CuH (-4.2 kcal mol^{-1}, Figure 5.4). The activation barrier to (6-Me)CuH formation was calculated at 16.9 kcal mol^{-1} which, although slightly larger than that calculated for the formation of (6-MeDAC)CuH (15.5 kcal mol^{-1}, Figure 5.4), does not account for the slow reaction kinetics observed. Expansion of the model system to include the true steric bulk of the system could reveal a further destabilisation of the transition state. However, given that Et_3SiH reacts rapidly with the isosteric 6-MesDAC complex **11**, steric arguments seem unlikely to be the sole cause of the slow reactivity between **20** and

Et_3SiH. Furthermore, the possibility of a rate enhancement in the presence of cyclohexanone invites further investigation.

5.9.1 Migratory Insertion Processes of (6-Me)CuH

Figure 5.14 shows that direct hydride migratory insertion of (6-Me)CuH (black data) is not a feasible reaction pathway due to a prohibitively high activation barrier (56.1 kcal mol^{-1}) and the formation of [(6-Me·H)Cu] being endergonic by 21.9 kcal mol^{-1}. Comparison to the analogous data for (6-MeDAC)CuH (red data, Figure 5.14) reveals that the diamidocarbene stabilises the transition state to migratory insertion by 17.4 kcal mol^{-1} (activation barrier of 38.7 kcal mol^{-1}) and the product of migratory insertion by 21.1 kcal mol^{-1}. This direct comparison is free of all external influences, such as Lewis bases or different steric environments, and reveals the sensitivity of migratory insertion to the electrophilicity of an NHC.

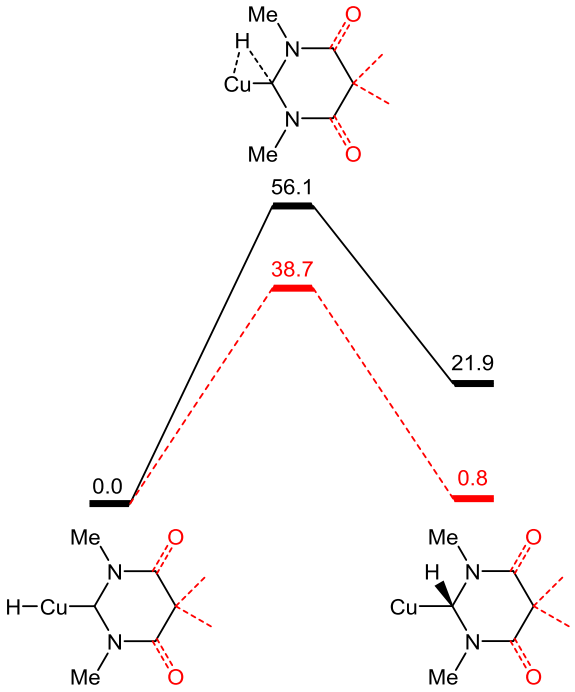

Figure 5.14: Figure showing the direct migratory insertion of hydride to form [(6-Me·H)Cu] (black data). The analogous energies for the direct migratory insertion reaction of (6-MeDAC)CuH (Figure 5.5) are shown for comparison (red data). All energies are quoted in kcal mol^{-1}.

Co-ordination of (6-Me)CuOMe to (6-Me)CuH, resulting in a dinuclear complex bridged by one hydride and one alkoxide ligand, was found to be exergonic by 2.6

kcal mol^{-1} (red data, Figure 5.15). Subsequent alkoxide assisted hydride migratory insertion proceeds with an activation barrier of 23.2 kcal mol^{-1}, but results in a product which is 3.7 kcal mol^{-1} less stable than the starting materials. Alternatively, dimerisation of (6-Me)CuH to form [(6-Me)CuH]$_2$ results in a stabilisation of 15.5 kcal mol^{-1}, and migratory insertion from this intermediate occurs with an activation barrier of 22.6 kcal mol^{-1} (black data, Figure 5.15). The product of this hydride assisted hydride migratory insertion, (6-Me)Cu(μ-H)Cu(6-Me·H), is thermodynamically more stable than the starting materials, albeit by only 1.4 kcal mol^{-1}.

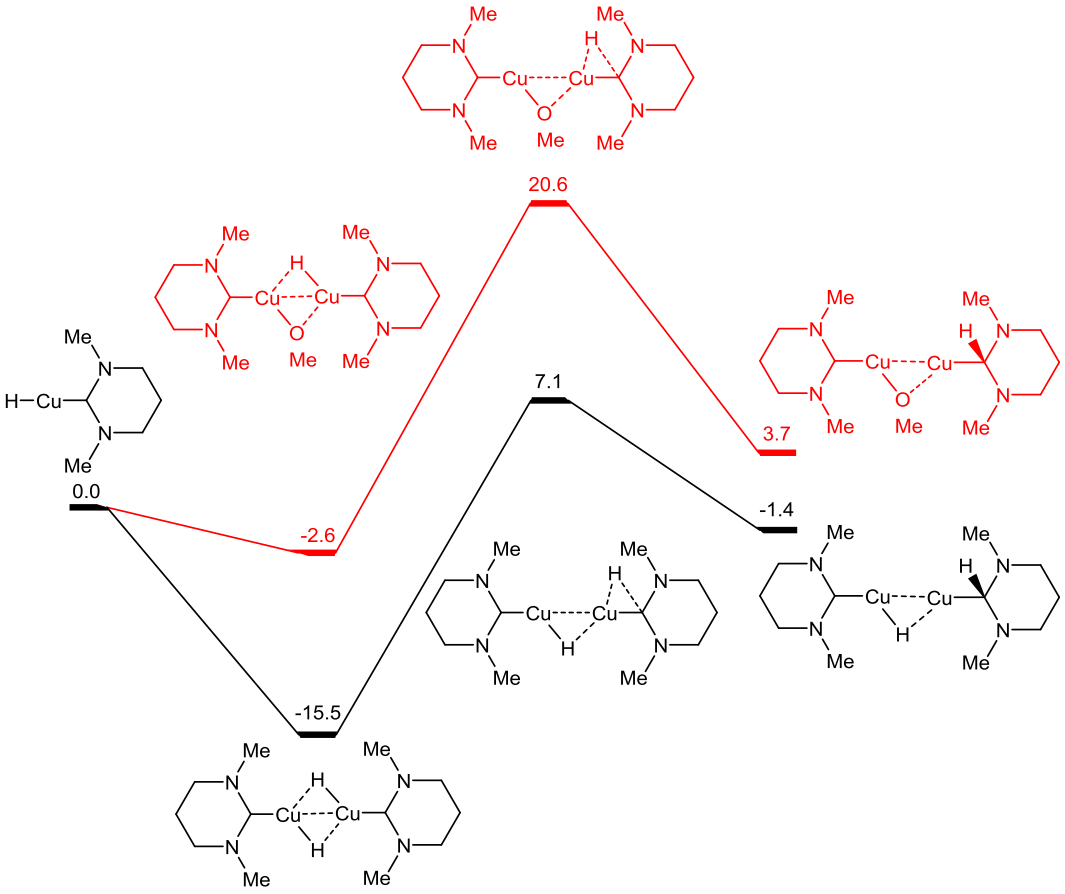

Figure 5.15: Calculated energies for the Lewis base assisted hydride migratory insertion reactions of (6-Me)CuH. All energies are quoted in kcal mol^{-1}.

Figure 5.15 shows that migratory insertion is most likely to occur via a hydride assisted mechanism, with (6-Me)CuH itself acting as the Lewis base (activation barrier of 22.6 kcal mol^{-1}). The product of this reaction, (6-Me)Cu(μ-H)Cu(6-Me·H), does not represent the experimentally observed products of (6-Mes)CuH

migratory insertion (**35**, dihydrogen and copper metal, Scheme 5.4). However it seems feasible that this species could decompose to (6-Me·H)Cu(6-Me), dihydrogen and copper metal, and whilst calculations for this process were not performed, this could reveal a greater thermodynamic driving force than the exergonicity of 1.4 kcal mol^{-1} shown in Figure 5.15.

5.10 Comparison of Hydride Migratory Insertion Processes of Diamido- and Diaminocarbenes

The formation of a copper hydride species from the reaction of a copper alkoxide species with a hydrosilane is calculated to be thermodynamically favourable for both ring expanded diamido- and diaminocarbenes (6-MeDAC = -4.2 kcal mol^{-1}; 6-Me = -6.5 kcal mol^{-1}) as well as kinetically accessible at room temperature (6-MeDAC = 15.5 kcal mol^{-1}; 6-Me = 16.9 kcal mol^{-1}). The slightly higher activation barrier for (6-Me)CuH formation goes some way towards explaining the slower rate of reaction observed between Et_3SiH and complex **20**, than complex **11**. Expansion of the model system to include the full alkyl and aryl substituents may shed further light on this, but a question remains over whether (6-Mes)CuH formation was accelerated during the catalytic hydrosilylation of cyclohexanone (Scheme 5.10).

The involvement of a range of Lewis bases assist hydride migratory insertion, lowering the inaccessible activation barriers of direct migratory insertion (6-MeDAC = 38.7 kcal mol^{-1}; 6-Me = 56.1 kcal mol^{-1}) and allowing for facile room temperature reactivity. The nature of the Lewis base which affords the lowest energy pathway is different for 6-MeDAC and 6-Me, explaining why the nature of the products of migratory insertion for 6-MesDAC and 6-Mes were found to be different experimentally. An alkoxide assisted mechanism for (6-MeDAC)CuH was found to be lowest in energy, and corroborates the observation of the alkoxide bridged product **33**. In contrast, a hydride assisted mechanism provided the lowest energy pathway for (6-Me)CuH. The calculations also support the experimental evidence that 6-Mes is a suitable ligand for supporting reductive chemistry, and that 6-MesDAC is not, explained by lower susceptibility of 6-Mes to hydride migratory insertion (activation energy for (6-Me)CuH = 22.6 kcal mol^{-1}; (6-MeDAC)CuH = 6.7 kcal mol^{-1}).

The isosteric nature of both the experimental (6-MesDAC/6-Mes) and computational (6-MeDAC/6-Me) comparisons support the proposal that the differences in reactivity are electronic in origin. Three contributory factors may be highlighted as determining the susceptibility to hydride migratory insertion. Firstly, the greater electrophilicity of diamidocarbenes compared to diaminocarbenes resulted in the stabilisation of both the transition state and product of migratory insertion. This is most clearly shown in the case of direct migratory insertion (Figures 5.5 and 5.14), in the absence of other influences. Secondly, in the case of Lewis base assisted mechanisms where the complexes are themselves the Lewis bases, the effect of the NHC on the relative Lewis basicity of the copper alkoxide or hydride is a potential explanation for the differing reactivity of the diamino- and diamidocarbene systems. Finally, the Lewis base assisted mechanisms implicate dinuclear intermediates in these transformations. In the case of 6-MeDAC, the lowest energy pathway for migratory insertion occurred via the alkoxide bridged intermediate (6-MeDAC)Cu(μ-OMe)Cu(H)(6-MeDAC) (Figure 5.6) with a wide Cu-O-Cu angle (87.2°) and long Cu-Cu distance (2.628 Å). The analogous structure calculated for 6-Me ((6-Me)Cu(μ-OMe)(μ-H)Cu(6-Me) (Figure 5.15)) contains both hydride and alkoxide bridging ligands, with a significantly narrower Cu-O-Cu angle (72.6°) and shorter Cu-Cu distance (2.476 Å). The cause of this different reactivity is likely to be electronic in nature, due to the very similar steric demands of 6-MeDAC and 6-Me. The potential role of copper-copper bonding (both Cu-Cu distances are significantly smaller than twice the covalent radius of copper (1.32(4) Å))[25] in determining the reactivity of dinuclear NHC copper hydride species merits further investigation.

Immediately prior to submission of this Thesis, Sadighi and co-workers reported the synthesis of $[(6\text{-Dipp})CuH]_2$ by reaction of (6-Dipp)CuO^tBu with pinacolborane (Scheme 5.12).[26] $[(6\text{-Dipp})CuH]_2$ is stable at room temperature, with no evidence of migratory insertion observed. Furthermore, addition of the Lewis basic BnNC did not result in migratory insertion, but instead in 1,1-addition of the copper hydride to the isonitrile (Scheme 5.12). This reactivity dramatically contrasts that of the 6-Mes supported systems described in this Chapter. 6-Dipp is a significantly more bulky ligand than 6-Mes ($\%V_{bur}$ for 6-Dipp = 50.8 %; for 6-Mes = 42.2 %),[27] and we propose that this increased steric demand inhibits migratory insertion for [(6-

Dipp)CuH]$_2$ by increasing the energy of the transition state. Calculations to support or refute this proposal are in progress.

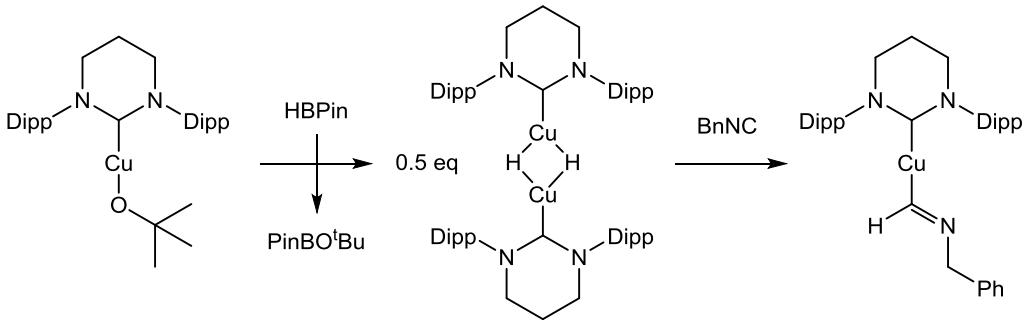

Scheme 5.12: Formation of the room temperature stable [(6-Dipp)CuH]$_2$ and its reaction with BnNC.[26]

5.11 Conclusion

This Chapter has presented the attempted syntheses of (6-MesDAC)CuH and (6-Mes)CuH. Reaction of the copper alkoxide complexes (6-MesDAC)CuO^{t}Bu (**11**) or (6-Mes)CuO^{t}Bu (**20**) with Et_3SiH resulted in the initial formation of copper hydride complexes, alongside Et_3SiO^tBu. The rate of reaction for these two systems differs substantially; the reaction of complex **20** with Et_3SiH (one equivalent) only reaches completion after four days at room temperature, in contrast to the facile reactivity of **11**. Neither copper hydride complex was isolable, with both undergoing facile hydride migratory insertion processes, resulting in the formation of (6-MesDAC·H)Cu(μ-O^{t}Bu)Cu(6-MesDAC) (**33**) and (6-Mes·H)Cu(6-Mes) (**35**), respectively. The formation of such different products is corroborated by DFT calculations which show that a different Lewis base assists the migratory insertion in each case. The calculations also show that the barrier to migratory insertion in the case of (6-Me)CuH is much greater than that of (6-MeDAC)CuH. The longer lifetime of (6-Mes)CuH allowed it to insert into a C≡C bond preferentially over migratory insertion, giving this system catalytic applications for the semi-reduction of alkynes, as well as the hydrosilylation of ketones. The extremely facile migratory insertion of (6-MesDAC)CuH resulted in a very short lifetime for this species, and no onward reductive chemistry was possible.

5.12 References for Chapter Five

(1) Collins, L. R.; Riddlestone, I. M.; Mahon, M. F.; Whittlesey, M. K. *Chem. Eur. J.* **2015**, *21*, 14075–14084.

(2) Lazreg, F.; Nahra, F.; Cazin, C. S. J. *Coord. Chem. Rev.* **2015**, *293-294*, 48–79.

(3) Cox, N.; Dang, H.; Whittaker, A. M.; Lalic, G. *Tetrahedron* **2014**, *70*, 4219–4231.

(4) Fujihara, T.; Xu, T.; Semba, K.; Terao, J.; Tsuji, Y. *Angew. Chem. Int. Ed.* **2011**, *50*, 523–527.

(5) Díez-González, S.; Stevens, E. D.; Scott, N. M.; Petersen, J. L.; Nolan, S. P. *Chem. Eur. J.* **2008**, *14*, 158–168.

(6) Deutsch, C.; Krause, N. *Chem. Rev.* **2008**, *108*, 2916–2927.

(7) Díez-González, S.; Escudero-Adán, E. C.; Benet-Buchholz, J.; Stevens, E. D.; Slawin, A. M. Z.; Nolan, S. P. *Dalton Trans.* **2010**, *39*, 7595–7606.

(8) Whittaker, A. M.; Lalic, G. *Org. Lett.* **2013**, *15*, 1112–1115.

(9) Mankad, N. P.; Laitar, D. S.; Sadighi, J. P. *Organometallics* **2004**, *23*, 3369–3371.

(10) Goeden, G. V.; Caulton, K. G. *J. Am. Chem. Soc.* **1981**, *103*, 7354–7355.

(11) Lemmen, T. H.; Folting, K.; Huffman, J. C.; Caulton, K. G. *J. Am. Chem. Soc.* **1985**, *107*, 7774–7775.

(12) Goeden, G. V.; Huffman, J. C.; Caulton, K. G. *Inorg. Chem.* **1986**, *25*, 2484–2485.

(13) Alyea, E. C.; Ferguson, G.; Malito, J.; Ruhl, B. *Inorg. Chem.* **1985**, *24*, 3719–3720.

(14) Mankad, N. P.; Gray, T. G.; Laitar, D. S.; Sadighi, J. P. *Organometallics* **2004**, *23*, 1191–1193.

(15) Janssen, M. D.; Köhler, K.; Herres, M.; Dedieu, A.; Smeets, W. J. J.; Spek, A. L.; Grove, D. M.; Lang, H.; van Koten, G. *J. Am. Chem. Soc.* **1996**, *118*, 4817–4829.

(16) Stein, T.; Lang, H. *J. Organomet. Chem.* **2002**, *664*, 142–149.

(17) Schaper, F.; Foley, S. R.; Jordan, R. F. *J. Am. Chem. Soc.* **2004**, *126*, 2114–2124.

(18) Coan, P. S.; Folting, K.; Huffman, J. C.; Caulton, K. G. *Organometallics*

1989, *8*, 2724–2728.

(19) Zhang, L.; Cheng, J.; Carry, B.; Hou, Z. *J. Am. Chem. Soc.* **2012**, *134*, 14314–14317.

(20) Suess, A. M.; Uehling, M. R.; Kaminsky, W.; Lalic, G. *J. Am. Chem. Soc.* **2015**, *137*, 7747–53.

(21) Darensbourg, D. J.; Longridge, E. M.; Atnip, E. V.; Reibenspies, J. H. *Inorg. Chem.* **1992**, *31*, 3951–3955.

(22) Lang, H.; Shen, Y.; Rüffer, T.; Walfort, B. *Inorg. Chim. Acta.* **2008**, *361*, 95–102.

(23) Belger, C.; Neisius, N. M.; Plietker, B. *Chem. Eur. J.* **2010**, *16*, 12214–12220.

(24) Díez-González, S.; Scott, N. M.; Nolan, S. P. *Organometallics* **2006**, *25*, 2355–2358.

(25) Cordero, B.; Gómez, V.; Platero-Prats, A. E.; Revés, M.; Echeverría, J.; Cremades, E.; Barragán, F.; Alvarez, S. *Dalton Trans.* **2008**, 2832–2838.

(26) Jordan, A. J.; Wyss, C. M.; Bacsa, J.; Sadighi, J. P. *Organometallics* **2016**, *35*, 613–616.

(27) Dunsford, J. J.; Cavell, K. J.; Kariuki, B. M. *Organometallics* **2012**, *31*, 4118–4121.

CHAPTER SIX

CHAPTER SIX: Synthesis and Stabilisation of Copper Hydrides

6.1 Introduction

Chapter Five discussed the σ-bond metathesis reactions of (6-MesDAC)CuO^{t}Bu (**11**) and (6-Mes)CuO^{t}Bu (**20**) with Et_3SiH. Copper hydride complexes were formed by this method but could not be directly observed due to their susceptibility to migratory insertion. This Chapter will discuss different approaches to the attempted synthesis of copper hydride complexes, issues associated with their isolation, and factors affecting their stabilisation.

6.2 Literature Precedent for Copper Hydride Syntheses

In copper catalysed reductive processes, silanes are often employed as the hydride source. The wide range of commercially available silanes allows for easy screening of a range of steric and electronic properties to suit the system being studied. Other hydride sources may not be so easy to incorporate in homogeneous catalysis, but can offer synthetic access to discrete copper hydride complexes for further study.

In 1971, the first copper hydride complex, $[(PPh_3)CuH]_6$, was isolated by reaction of $[(PPh_3)CuCl]_4$ with $NaHB(OMe)_3$.[1,2] In the 1980s, Caulton and co-workers synthesised a range of $[(PR_3)CuH]_n$ complexes either by reduction of the respective chloride complexes with $LiHBEt_3$ (R = Ph, *p*-Tol, O^{i}Pr),[3] or by hydrogenolysis (1-100 atm) of $[CuO^tBu]_4$ in the presence of phosphine ($P(NMe_2)_3$,[4] $Ph_2P(CH_2)_3PPh_2$,[4] $MeC(CH_2PPh_2)_3$).[5] These complexes were found to consist of cluster-like structures, whose lowest nuclearity system was characterised as a dimer in the solid state (Figure 6.1).[5]

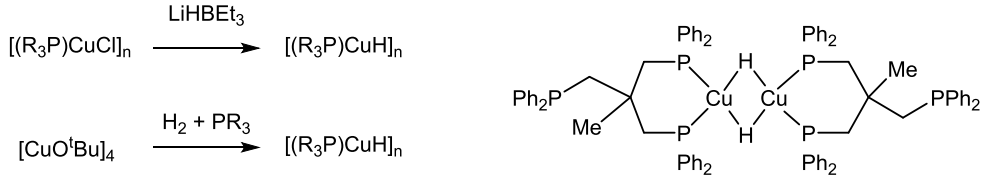

Figure 6.1: Examples of phosphine copper hydride syntheses (left) and the lowest nuclearity phosphine copper hydride (right).[5]

The only example of an $[(NHC)CuH]_n$ complex being synthesised using a source of hydride other than silane was reported by Bertrand and co-workers in 2011. Reaction of the bulky cyclic alkyl amino carbene copper alkoxide precursor with $LiHBEt_3$ resulted in the formation of the room temperature stable $[(CAAC)CuH]_2$ (Scheme 6.1).[6] This complex, alongside the less stable $[(IPr)CuH]_2$,[7] remains the lowest nuclearity copper hydride complex in the literature, as a dinuclear complex comprising three co-ordinate copper centres. Neither mononuclear or two co-ordinate copper hydride complexes have yet been structurally characterised.

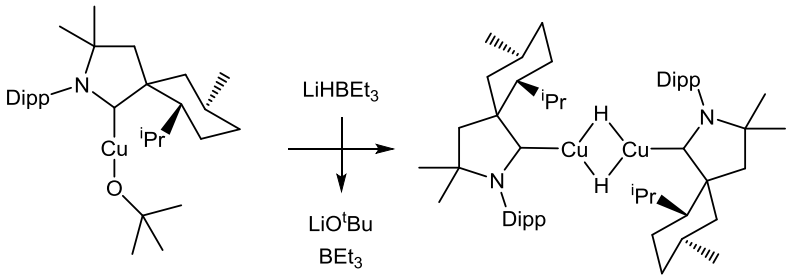

Scheme 6.1: Reaction of $(CAAC)CuO^tBu$ with $LiHBEt_3$, resulting in the formation of the dimeric $[(CAAC)CuH]_2$.

This Chapter will discuss a range of synthetic approaches employed for the attempted synthesis of copper hydride complexes supported by the RENHC 6-Mes. Analogous reactions were conducted with 6-MesDAC complexes but these yielded intractable mixtures in all cases. This outcome may be a result of incomplete salt metathesis (Chapter 3), facile migratory insertion (Chapter 5) or reduction of the functionalised backbone of 6-MesDAC.

6.3 Synthesis and Characterisation of $[(6\text{-Mes})CuH]_2$ (38)

Alkali metal hydrides such as NaH were found to be inert towards $(6\text{-Mes})CuO^tBu$ (**20**) in THF, even after prolonged heating at 333 K. In contrast, reaction of **20** with $LiAlH_4$ in THF at room temperature resulted in the immediate formation of a bright yellow solution. Over the course of minutes, this solution turned colourless and precipitated copper metal. Analysis of the solution by ^1H NMR spectroscopy revealed the formation of hydrogen gas (4.55 ppm) and (6-Mes·H)Cu(6-Mes) (**35**), alongside other unidentified products. The formation of **35** revealed that a copper hydride complex had been formed. Indeed, repeating this reaction at 178 K

indefinitely stabilised the bright yellow solution, allowing the characterisation of [(6-Mes)CuH]$_2$ (**38**, Scheme 6.2).

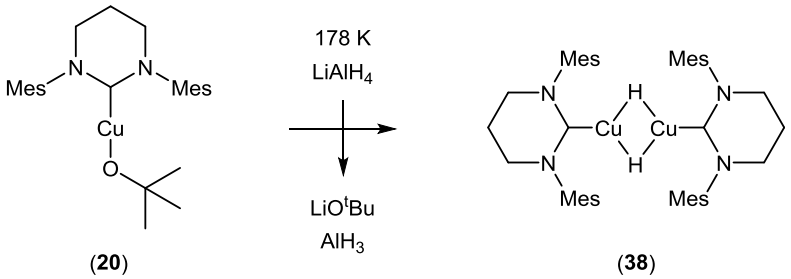

Scheme 6.2: Reaction scheme for the reaction of (6-Mes)CuO^{t}Bu (**20**) with $LiAlH_4$, resulting in the formation of [(6-Mes)CuH]$_2$ (**38**).

Low temperature ^{1}H NMR spectroscopy revealed the complete consumption of **20** within seconds and formation of LiO^{t}Bu and [(6-Mes)CuH]$_2$ (**38**), which was characterised by ^{1}H and ^{13}C{^{1}H} NMR spectroscopy at 209 K. The presence of a high frequency signal (211.5 ppm) in the ^{13}C{^{1}H} NMR spectrum was consistent with a carbenic carbon, indicating that migratory insertion had not taken place. The ^{1}H NMR spectrum showed resonances for a single C_s symmetric 6-Mes environment, alongside a 1H integral singlet at 0.96 ppm. This signal displayed a clear $^2J_{CH}$ correlation to the carbenic carbon in the HMBC spectrum, confirming the connectivity of 6-Mes and hydride to the same copper centre. The proton coupled ^{13}C NMR spectrum revealed the presence of this coupling through an increase in the line width of the carbenic resonance (measured as the full width at half peak height) from 6.1 Hz to 16.7 Hz. Furthermore, NOE interactions were found between the hydride resonance and the ortho mesityl methyl protons of 6-Mes. DOSY measurements gave a value of r_H (6.2 Å) consistent with a dimeric structure, which was also corroborated by DFT calculations showing that dimerisation of (6-Me)CuH is exergonic (15.5 kcal mol^{-1}, Figure 5.15).

6.3.1 Migratory Insertion of [(6-Mes)CuH]$_2$ (38)

Although THF solutions of **38** were stable at 209 K for hours, warming to 255 K led to broadening of the resonances for **38** and their eventual transformation to resonances attributable to **35**, alongside other unidentified, minor products. The observation of migratory insertion of copper hydride to 6-Mes at 255 K is consistent with the calculated activation barrier for this process in the model 6-Me system (22.6 kcal mol^{-1}, Figure 5.15).

The facile migratory insertion of **38** contrasts with the room temperature stability of [(CAAC)CuH]$_2$, which was attributed to kinetic stabilisation by the bulky menthyl substituents.[6] The importance of steric factors was shown by the replacement of the menthyl substituent with a cyclohexyl group preventing the isolation of any hydride complex.

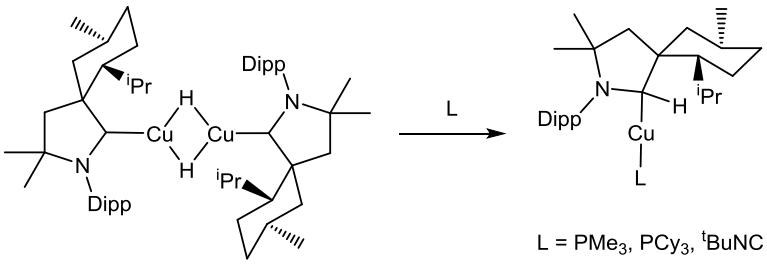

Scheme 6.3: Reaction scheme for the Lewis base assisted migratory insertion of [(CAAC)CuH]$_2$.[6]

Whilst [(CAAC)CuH]$_2$ is stable in isolation, the addition of Lewis bases (PMe_3, PCy_3 or ^{t}BuNC) results in migratory insertion (Scheme 6.3). In the case of **38**, migratory insertion requires no additional Lewis base, with the bridging hydrides assisting the migratory insertion. Whether this different reactivity reflects a difference in the electrophilicity of CAACs and RENHCs, or indeed a difference in the Lewis basicity of their copper hydrides, warrants further investigation.

6.3.2 Attempts to Isolate [(6-Mes)CuH]$_2$ (38)

Although complex **38** could be reproducibly synthesised in THF solution at cryogenic temperatures, all attempts to isolate it by low temperature evaporation, precipitation, filtration or crystallisation were unsuccessful. On several occasions, crystalline material was isolated, but characterised as (6-Mes)AlH_3 by comparison to literature data (Scheme 6.4).[8] This alane was consistently formed in all experiments, and whilst migratory insertion to produce **35** could be suppressed by working at low temperatures, the formation of (6-Mes)AlH_3 could not be prevented. Reacting **20** with $LiAlH_4$ in THF at 178 K in the presence of a further equivalent of 6-Mes, to trap AlH_3, successfully resulted in the formation of a 1 : 1 mixture of **38** and (6-Mes)AlH_3. However, this mixture could not be separated and attempts at crystallisation resulted only in crystals of (6-Mes)AlH_3 (determined by unit cell parameter analysis of a representative sample).[8]

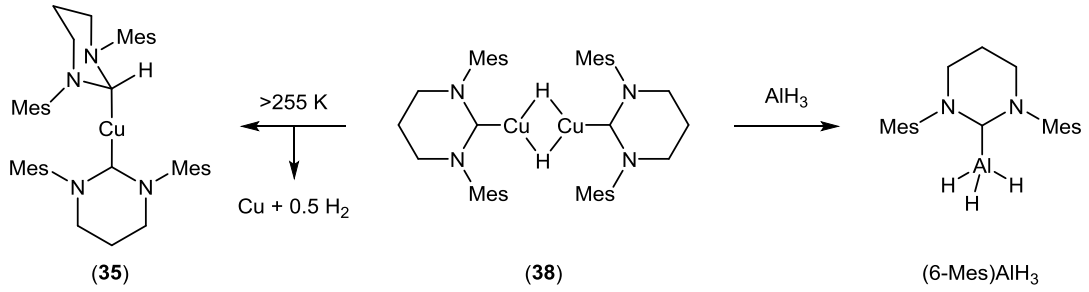

Scheme 6.4: Decomposition pathways of **38**. The formation of other species alongside (6-Mes)AlH_3 (presumed to be copper metal and hydrogen gas) could not be identified due to their formation also as by-products of the formation of **35**.

6.4 Synthesis of (6-Mes)CuHBEt$_3$ (39)

To circumvent the formation of AlH_3, a different hydride source was sought. Reacting complex **20** with $LiHBEt_3$ in THF at 178 K resulted in a salt metathesis reaction that yielded a yellow solution of (6-Mes)CuHBEt$_3$ (**39**, Scheme 6.5).[i] This reactivity directly contrasts with that of the CAAC system shown in Scheme 6.1, in which reaction of the analogous alkoxide precursor with $LiHBEt_3$ resulted in the formation of a copper hydride complex with release of BEt_3.

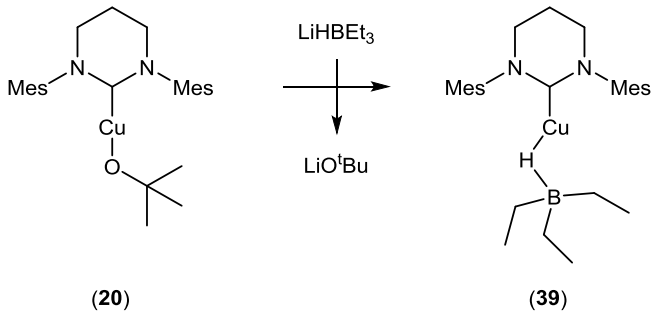

(**20**) (**39**)

Scheme 6.5: Synthesis of (6-Mes)CuHBEt$_3$ (**39**).

The literature contains an abundance of examples of the use of $MHBEt_3$ reagents in organic and organometallic synthesis. However, the study of these complexes in their own right is less common. Several ligated group I metal complexes are known (for example, $[(Mes)Na_2(HBEt_3)_2]_2$ and $(tmta)K(HBEt_3)_2$),[11,12] as are complexes of the lanthanide metals supported by cyclopentadienyl,[13–15] or tris-pyrazolylborate type ligands.[16,17] A range of transition metal polyhydride and nitroso complexes have also been shown to co-ordinate $LiHBEt_3$ ($(dmpe)_2TaH_3(\mu\text{-}H)_2Li(HBEt_3)$),[18] $(dippe)Pt/Rh(\mu\text{-}H))_2Li(HBEt_3)$[19] and $[(dmpe)_2Mo(H)(\mu\text{-}NO)(\mu\text{-}Li)(HBEt_3)]_2$).[20] Four $[HBEt_3]^-$ complexes are known from Groups II ($(2,6\text{-}p\text{-}Tol\text{-}C_6H_3)Ca(HBEt_3)(THF)(dme)$[12] and $(TMS_3Cp)Ca(HBEt_3)(THF)_2$,[21] Figure 6.2)[12,21] and III ($(Nacnac)Sc(HNDipp)(HBEt_3)$[22] and $((TMS)_2NC(N^iPr)_2)Y(HBEt_3)_2(THF)$,[23] Figure 6.2). The examples from the literature outlined above contain 'hard' metals,

[i] Several other complexes were formed alongside **39** (including **40** and **41**, Section 6.6) as a result of impurities in the THF solutions of $LiHBEt_3$ used. Use of a different batch of $LiHBEt_3$, with different proportions of impurities, resulted in a different ratio of impurities formed. Newly bought stock solutions of $LiHBEt_3$ were analysed by ^1H and ^{11}B NMR spectroscopy and found to contain >80% of $LiHBEt_3$, alongside a range of impurities.[9] More consistent results may be obtained by synthesising $LiHBEt_3$ by reaction of LiH and BEt_3 in THF, with 50% excess of LiH as a stabiliser to prevent BEt_3 dissociation.[10] This approach was not pursued since complex **39** could be isolated as crystalline material from the resultant mixtures of products.

whose chemistry is largely dominated by electrostatic interactions. In contrast, copper is a much 'softer' metal and consequently, the bonding in complex **39** has significant covalent character.

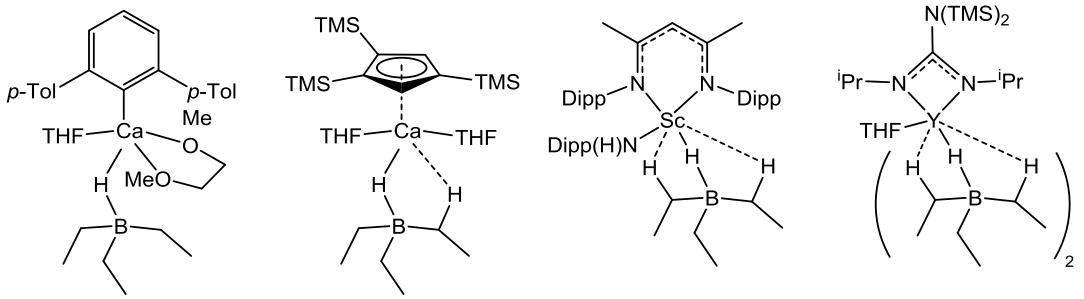

Figure 6.2: $[HBEt_3]^-$ complexes of the group II and III metals: (2,6-*p*-Tol-C_6H_3)Ca($HBEt_3$)(THF)(dme) (far left),[12] (TMS_3Cp)Ca($HBEt_3$)$(THF)_2$ (centre left),[21] (Nacnac)Sc(HNDipp)($HBEt_3$) (centre right),[22] ($(TMS)_2NC(N^iPr)_2$)Y($HBEt_3$)$_2$(THF)) (far right).[23]

6.4.1 Characterisation of (6-Mes)CuHBEt$_3$ (39)

Complex **39** was purified and isolated in 42 % yield by repeated crystallisation from THF/hexane at 238 K and characterised by multinuclear NMR spectroscopy at 209 K. The ^1H NMR spectrum revealed a single C_s symmetric 6-Mes environment in a 1 : 3 ratio with broad multiplets (0.16 and -0.21 ppm) attributed to the ethyl substituents on boron. A broad (peak width measured at half peak height = 25 Hz; $^1H\{^{11}B\}$ = 13 Hz) 1H integral singlet was located at -2.60 ppm for the bridging hydride, significantly upfield of the hydride resonance of complex **38** (0.96 ppm). The $^{11}B\{^1H\}$ spectrum showed a single broad resonance (-8.2 ppm) at a similar frequency to those reported for (2,6-*p*-Tol-C_6H_3)Ca($HBEt_3$)(THF)(dme) (-15.6 ppm),[12] (Nacnac)Sc(HNDipp)($HBEt_3$) (-8.7 ppm)[22] and ($(TMS)_2NC(N^iPr)_2$)Y($HBEt_3$)$_2$(THF) (-9.3 ppm).[23] The $^{13}C\{^1H\}$ NMR spectrum revealed a resonance at 201.9 ppm for the carbenic carbon of 6-Mes, which resolved into a doublet ($^2J_{HC}$ = 11.6 Hz) in the proton coupled ^{13}C NMR spectrum due to coupling to the bridging hydride. This observation of scalar coupling between the carbenic carbon and the bridging hydride of **39** suggests the involvement of the s-orbital of copper in covalent bonding to both carbene and hydride, implying that the Cu-H-B interaction is not purely electrostatic.

The proton coupled ^{13}C NMR spectrum also revealed different $^{1}J_{CH}$ coupling constants for the methylene and methyl resonances of the boron ethyl substituents. Whilst the methyl C-H coupling constant of 122.0 Hz is common for an sp^3 hybridised C-H bond, the methylene coupling constant (114.1 Hz) was significantly lower, suggesting a weaker methylene C-H bond, which is consistent with a fluxional agostic interaction with copper.[i] Attempts to record ^{13}C spectra at lower temperatures to investigate this fluxional behaviour were unsuccessful, and only broad resonances were observed at higher temperatures.

6.4.2 Molecular Structure of (6-Mes)CuHBEt$_3$ (39)

Crystals of **39** that were suitable for X-ray diffraction studies were grown by vapour diffusion of hexane into a saturated THF solution of the complex at 238 K.

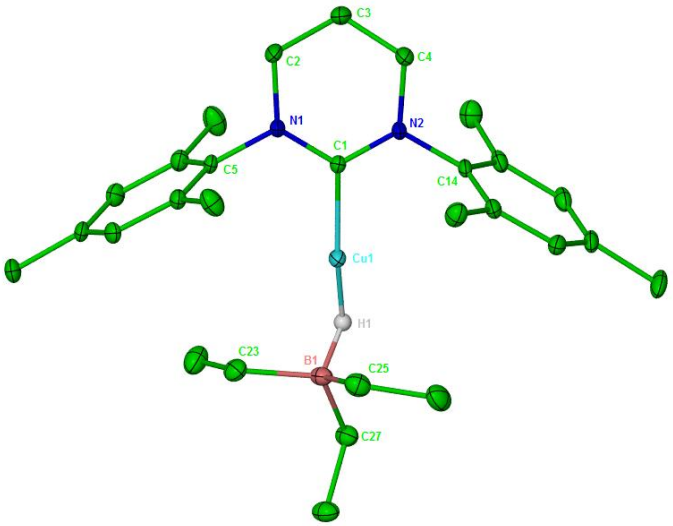

Figure 6.3: Displacement ellipsoid plot (30 % probability) of (6-Mes)CuHBEt$_3$ (**39**). H atoms omitted for clarity (except for H(1)). Selected bond lengths (Å) and angles (°): Cu(1)-C(1) 1.908(3), Cu(1)-H(1) 1.56(3), B(1)-H(1) 1.22(3), N(1)-C(1)-N(2) 117.6(3), C(1)-Cu(1)-B(1) 167.14(13), C(1)-Cu(1)-H(1) 162.4(13), Cu(1)-H(1)-B(1) 110.3(15).

Figure 6.3 confirms the monomeric nature of complex **39** with one 6-Mes ligand (Cu-C = 1.908(3) Å) and one co-ordinated $[HBEt_3]^-$ moiety. The $[HBEt_3]^-$ ligand is

[i] Green and Brookhart compiled experimental data and found that static agostic interactions display $^{1}J_{CH}$ values of 70-100 Hz. Fluxionality has the effect of averaging the agostic and non agostic interaction, resulting in $^{1}J_{CH}$ values of 110-130 Hz.[24]

co-ordinated through a terminal, bridging hydride. The Cu-H bond length (1.55(5) Å) is the shortest reported for all $[HBEt_3]^-$ complexes, and comparable to the shortest Cu-H bonds of $[(CAAC)CuH]_2$ (ranging from 1.52(6) Å to 1.73(5) Å).[6] Whilst one ethyl group is pointing away from copper, the other two are oriented in such a way that there could be an agostic interaction in the solid state. One hydrogen of each of these methylene groups is indeed oriented towards copper with C-H··Cu angles of 103.5° and 99.2° and Cu-H distances of 2.205 Å and 2.541 Å respectively. The latter distance is too long to represent an agostic interaction, whereas the former (2.205 Å) is at the long end of the spectrum of agostic bonding.[25] Before proposing whether or not this represents a solid state agostic interaction, it seems pertinent to review the agostic bonding in other $[HBEt_3]^-$ complexes.

6.4.3 Agostic bonding in $HBEt_3$ complexes

The various co-ordination modes adopted by the structurally characterised $[HBEt_3]^-$ complexes of Group II, III and Ln metals are shown in Figure 6.4. Table 6.1 presents these complexes alongside their co-ordination mode and the metrics of their agostic interactions.

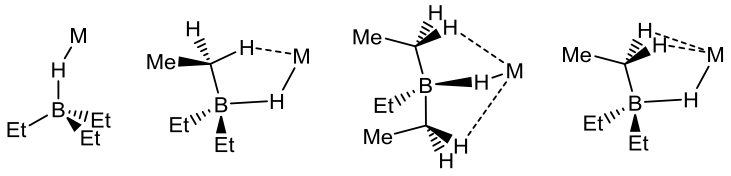

Figure 6.4: Structurally characterised co-ordination modes in $MHBEt_3$ complexes (M = Group II, III and Ln): (μ-H)BEt_3 (far left),[12] (μ-H)(κ^1*H*-μEt)BEt_2 (centre left),[21] (μ-H)(κ^1*H*-μEt)$_2$BEt (centre right),[15,22,23] (μ-H)(κ^2*H*-μEt)BEt_2 (far right).[15,17]

The length of a C-H··M agostic bond (M-$H_{agostic}$) depends on the strength of that interaction, as well as the radius of the metal involved. For this reason, the respective metals' ionic radii (r_M) are also included in Table 6.1,[26] alongside the difference between M-$H_{agostic}$ and the ionic radius (M-$H_{agostic}$ - r_M) which here represents an approximate quantification of agostic bond strength. Ionic radii have been chosen owing to the predominantly electrostatic nature of the complexes being compared. However, a degree of covalency may be involved, and it should be noted that ionic and covalent radii can differ by a factor of two.[27]

Complex and co-ordination mode	M-$H_{agostic}$ (Å)	r_M[26] (Å)	M-$H_{agostic}$ - r_M (Å)
(6-Mes)CuHBEt$_3$ (**39**)	2.205	0.46	1.75
(μ-H)BEt$_3$	2.541		2.08
(2,6-*p*-Tol-C_6H_3)Ca(HBEt$_3$)(THF)(dme)[12]	2.439	1.00	1.44
(μ-H)BEt$_3$ or (μ-H)B(κ^1*H*-μEt)BEt$_2$[i]			
(TMS$_3$Cp)Ca(HBEt$_3$)(THF)$_2$[21]	2.412	1.00	1.41
(μ-H)B(κ^1*H*-μEt)BEt$_2$			
(Nacnac)Sc(HNDipp)(HBEt$_3$)[22]	2.166	0.75	1.42
(μ-H)B(κ^1*H*-μEt)$_2$BEt	2.187		1.44
((TMS)$_2$NC(N^{i}Pr)$_2$)Y(HBEt$_3$)$_2$(THF)[23]	2.242	1.08	1.16
(μ-H)B(κ^1*H*-μEt)$_2$BEt	2.276		1.20
(μ-H)B(κ^1*H*-μEt)$_2$BEt	2.302		1.22
	2.499		1.42
(Cp*)$_2$La(HBEt$_3$)[15]	2.559	1.36	1.20
(μ-H)B(κ^1*H*-μEt)$_2$BEt	2.676		1.32
(Cp*)$_2$La(HBEt$_3$)(THF)[15]	2.589	1.36	1.23
(μ-H)B(κ^2*H*-μEt)BEt$_2$	2.665		1.31
(Tp^{tBu,Me})Tm(HBEt$_3$)(THF)[17]	2.546	1.09	1.46
(μ-H)B(κ^2*H*-μEt)BEt$_2$	2.706		1.62

Table 6.1: Data for agostic interactions in MHBEt$_3$ complexes (M = Group II, III and Ln) in comparison to data for complex **39**.

The values of M-$H_{agostic}$ - r_M range from 1.16 Å to 1.62 Å and show no correlation with co-ordination mode. The respective values for **39** (1.75 Å and 2.08 Å) are significantly greater than any of the assigned agostic interactions and support the assignment of **39** as adopting a (μ-H)BEt$_3$ co-ordination mode without any agostic interactions in the solid state. While this interpretation of bonding does not consider covalent interactions, these will be discussed in a QTAIM analysis in Section 6.5.

[i] (2,6-*p*-Tol-C_6H_3)Ca(HBEt$_3$)(THF)(dme) was assigned by the authors as having a (μ-H)BEt$_3$ bonding mode.[12] However, given the similarity of its metrics with those of (TMS$_3$Cp)Ca(HBEt$_3$)(THF)$_2$,[21] it seems reasonable to treat it as adopting a (μ-H)B(κ^1*H*-μEt)BEt$_2$ bonding mode.

6.5 DFT Investigation of (6-Mes)CuHBEt$_3$ (39)

DFT calculations were performed in collaboration with Macgregor and co-workers to gain insight into the geometric and electronic structure of (6-Mes)CuHBEt$_3$ (**39**). Molecular optimisation in the gas phase with a broad range of Gaussian functionals failed to accurately reproduce the experimentally determined structure. Subjecting the structure to periodic boundary conditions to mimic the solid state structure in a repeating unit cell produced data that aligned more closely with the experimental bond metrics. Figure 6.5 shows the calculated structure which best matches the experimental data (Cu-C_{NHC}: calc = 1.898 Å; expt = 1.908(3) Å, Cu-H: calc = 1.588 Å, expt = 1.56(3) Å). The calculated M-$H_{agostic}$ distance (2.349 Å) is even greater than the experimentally determined value (2.205 Å), further supporting the conclusion that complex **39** adopts a (μ-H)BEt$_3$ co-ordination mode.

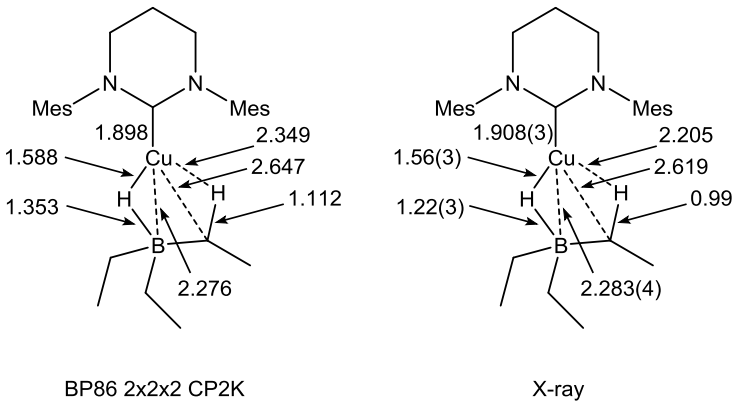

Figure 6.5: Optimised geometry (left) (CP2K calculation using a BP86 functional in a 2x2x2 super cell) and experimentally determined X-ray diffraction data (right) for (6-Mes)CuHBEt$_3$ (**39**).

To investigate both the possibility of a covalent agostic interaction and the nature of Cu-H-B bonding, DFT calculations were performed using a quantum theory of atoms in molecules (QTAIM) analysis.[28–30] An electron density distribution map was calculated and a charge density topology plot (Figure 6.6) produced. The contour lines represent regions of equal electron density (ρ). Through differentiation of the electron density map, the stationary points are identified as positions where $\nabla\rho = 0$. Local maxima coincide with the position of atoms. The other stationary points relevant to this discussion are those saddle points (represented as green dots) where electron density increases in the direction of the

adjacent atoms and decreases in all other directions. These stationary points are termed bond critical points and their presence denotes a covalent bonding interaction between two atoms.[i]

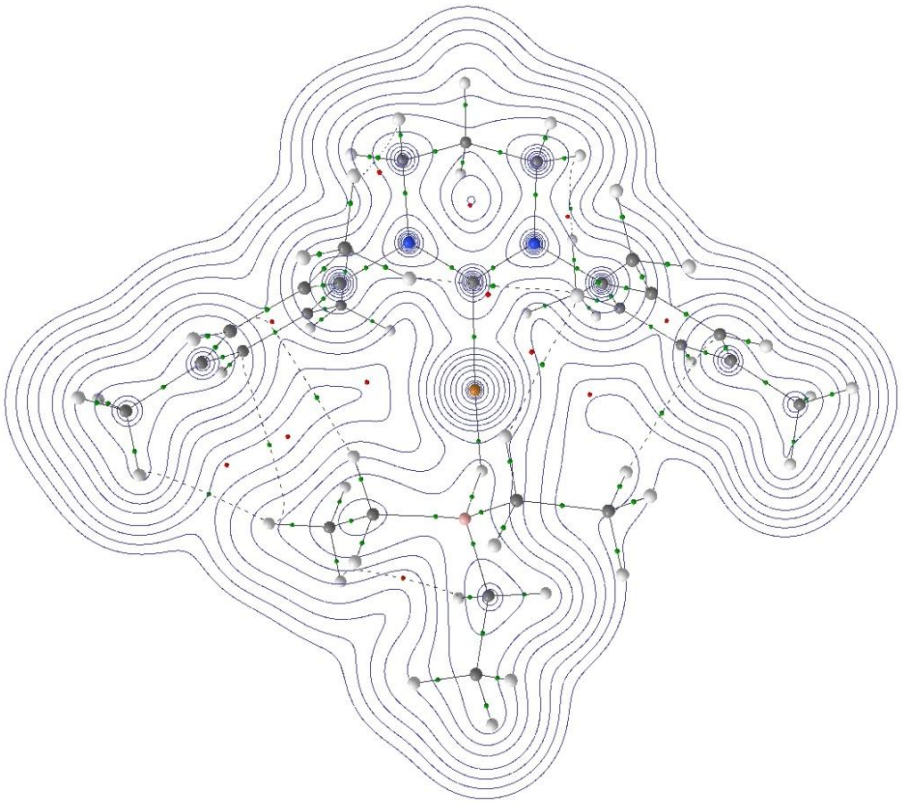

Figure 6.6: Calculated charge density topology plot for (6-Mes)CuHBEt$_3$ (**39**).

Figure 6.6 supports the hypothesis that **39** adopts a (μ-H)BEt$_3$ co-ordination mode. The calculated electron density map shows that copper is bonded to the carbenic carbon and the bridging hydride, with no bond critical point located between copper and the methylene protons. Five long range interactions (dashed lines) between the ethyl protons and the mesityl groups of 6-Mes appear to provide additional stabilisation to the complex.

[i] Ring critical points (red dots) are stationary points located at positions where electron density increases in two dimensions, and decreases in a third. They denote the electronic centre of a cyclic series of bonds (for example an aromatic ring).

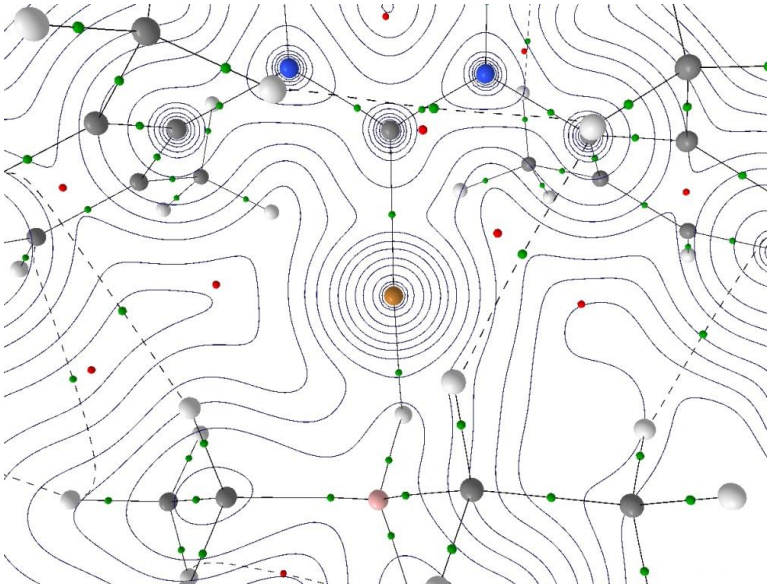

Figure 6.7: Calculated charge density topology plot for (6-Mes)CuHBEt$_3$ (**39**).

Closer inspection of the electron density map in the vicinity of copper (Figure 6.7) reveals that the two bonding interactions with copper are approximately linear. A very small curvature of the B-H and Cu-H bond pathways reflects the electron deficiency in the three-centre two-electron bond. The electron density at the bond critical point is a measure of bond strength,[28] and the calculations reveal $\rho_{(B\text{-}H)}$ (0.105) to be greater than $\rho_{(Cu\text{-}H)}$ (0.092), signifying a greater degree of covalent bonding for B-H than Cu-H. The assignment of **39** as either a complex in which $[HBEt_3]^-$ is donating electron density to copper, or in which BEt_3 is withdrawing electron density from a copper hydride is discussed below (Section 6.9).

6.6 Decomposition of (6-Mes)CuHBEt$_3$ (39)

Complex **39** was found to be stable both in the solid state and in THF solution for several days at temperatures below 243 K. Warming a THF solution of a crystalline sample of **39** inside an NMR spectrometer to 267 K revealed the onset of H-B cleavage through the formation of a broad resonance at 73 ppm in the $^{11}B\{^1H\}$ NMR spectrum assigned to BEt_3. In addition, the migratory insertion product (6-Mes·H)Cu(6-Mes) (**35**), copper metal and hydrogen gas (Scheme 6.7) were apparent, confirming the occurrence of migratory insertion from a copper hydride complex. Leaving a sample of **39** at room temperature for 21 hours led to the formation of only 5 % of **35** due to the occurrence of a second decomposition pathway, involving the 'disproportionation' of $[HBEt_3]^-$ to $[H_2BEt_2]^-$ and $[BEt_4]^-$.

Several $LiHBR_3$ salts have been shown to undergo this reaction, with trace amounts of BR_3 implicated in catalysing the disproportionation process.[9,31,32] Garcia and co-workers investigated the stoichiometric reaction of BEt_3 with $LiHBEt_3$, which resulted in the formation of $LiBEt_4$ and $(HBEt_2)_2$ (Scheme 6.6).[10] Reaction of $(HBEt_2)_2$ with further $LiHBEt_3$ would yield LiH_2BEt_2 and BEt_3. Scheme 6.6 shows how this series of reactions results in the overall disproportionation of $LiHBEt_3$, catalysed by BEt_3, which may be formed as a result of trace dissociation or hydrolysis.

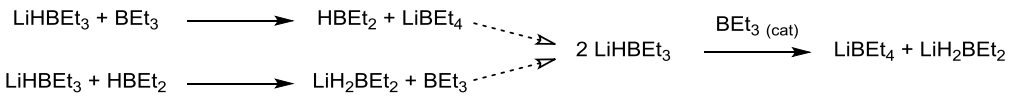

Scheme 6.6: Stoichiometric reactivity of $LiHBEt_3$ and BEt_3, resulting in the BEt_3 catalysed disproportionation of $LiHBEt_3$.

In the case of complex **39**, B-H cleavage results in the formation of BEt_3, which could then induce the disproportionation as described above. It is uncertain whether the mechanism takes place on copper, but the final products were identified as (6-Mes)Cu(H_2BEt_2) (**40**) and [(6-Mes)$_2$Cu][BEt_4] (**41**) (Scheme 6.7). Other boron containing species which may accompany the formation of **40** and **41** from **39** could not be identified.

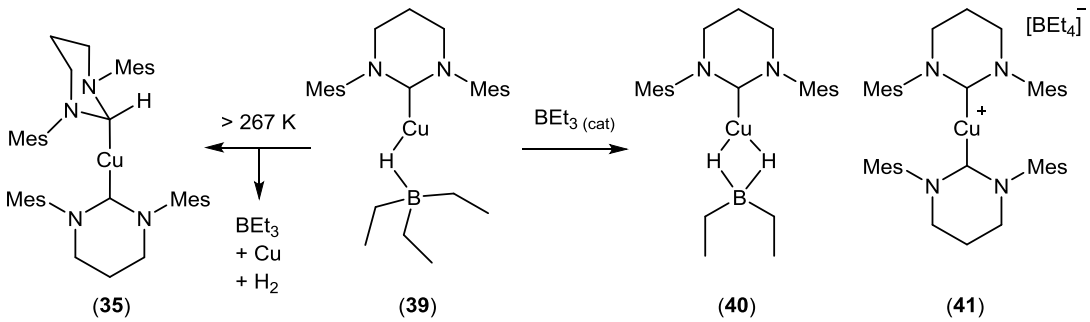

Scheme 6.7: Decomposition of (6-Mes)CuHBEt$_3$ (**39**) to (6-Mes·H)Cu(6-Mes) (**35**), (6-Mes)Cu(H_2BEt_2) (**40**) and [(6-Mes)$_2$Cu][BEt_4] (**41**).

6.6.1 Characterisation of (6-Mes)Cu(H_2BEt_2) (40) and [(6-Mes)$_2$Cu][BEt_4] (41)

(6-Mes)Cu(H_2BEt_2) (**40**) could not be isolated from the decomposition reactions of **39** and its selective synthesis was not pursued. However, co-crystals of **39** and **40** (3 : 2 occupancy) were isolated and X-ray crystallography revealed that the $[H_2BEt_2]^-$ moiety adopts a κ^2-H,H co-ordination mode ($[H_2BEt_2]^-$: $^1H\{^{11}B\}$ NMR = 0.80, 0.11 and -0.40 ppm; $^{11}B\{^1H\}$ NMR = -8.9 ppm), similar to the co-ordination environments reported for yttrium and zirconium complexes of $[H_2(9\text{-BBN})]^-$.[33,34] The bonding metrics of **40** will not be discussed further due to the mixed occupancy of the crystals.

Adding a THF solution of $LiHBEt_3$ to **20** at room temperature and layering the resultant mixture with hexane yielded crystals of [(6-Mes)$_2$Cu][BEt_4] (**41**) in 22 % yield. In this reaction, complex **41** may be formed both by a direct reaction of **20** with the $LiBEt_4$ impurity in the $LiHBEt_3$ stock solution, as well as by the decomposition of **39**. The ^1H NMR spectrum of **41** in THF-d_8 showed resonances indicative of a C_s symmetric 6-Mes environment in a 1 : 4 ratio with broad ethyl signals which resolved to mutually coupled triplet and quartet resonances ($^3J_{HH}$ = 7.8 Hz) upon boron decoupling. A sharp singlet in the $^{11}B\{^1H\}$ NMR spectrum at -16.5 ppm is consistent with a tetrahedrally symmetrical boron centre. The appearance of a carbenic resonance at 199.5 ppm in the $^{13}C\{^1H\}$ NMR spectrum is in agreement with $[(6\text{-Mes})_2Cu]^+$ species containing other anions (**7** = 199.3 ppm; **24** = 199.4 ppm; **37** = 202.3 ppm). The molecular structure of **41** is shown in Figure 6.8 with metrics matching those in **7**, **24** and **37**.

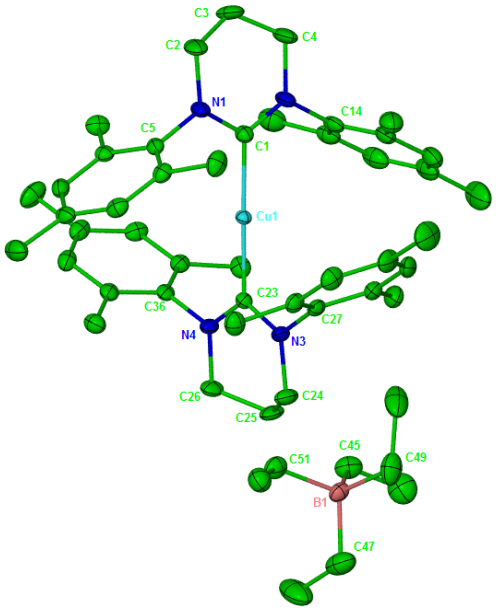

Figure 6.8: Displacement ellipsoid plot (30 % probability) of $[(6\text{-Mes})_2Cu][BEt_4]$ (**41**). H atoms omitted for clarity. Selected bond lengths (Å) and angles (°): Cu(1)-C(1) 1.930(4), Cu(1)-C(23) 1.938(4), N(1)-C(1)-N(2) 117.7(4), N(3)-C(23)-N(4) 117.8(4), C(1)-Cu(1)-C(23) 179.1(2).

6.7 Synthesis of (6-Mes)CuHB$(C_6F_5)_3$ (42)

Reaction of **20** with Et_3SiH in C_6D_6 in the presence of one equivalent of the strong Lewis acid $B(C_6F_5)_3$ resulted in the formation of (6-Mes)CuHB$(C_6F_5)_3$ (**42**, Scheme 6.8). Perfluorinated aryl boranes have been shown to weaken the Si-H bond of hydrosilanes.[35] In accordance with this, the presence of $B(C_6F_5)_3$ accelerated the reaction of **20** with Et_3SiH, which consequently occurred within seconds at room temperature instead of days.

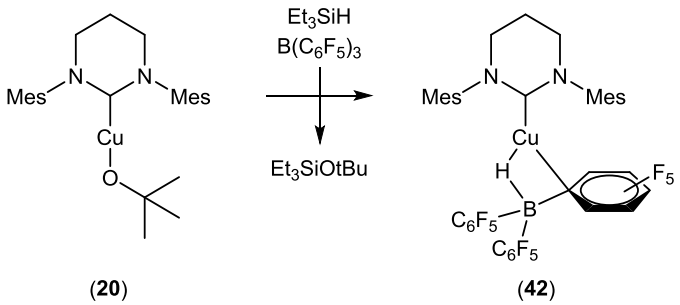

Scheme 6.8: Reaction of **20** with Et_3SiH in the presence of $B(C_6F_5)_3$, resulting in the formation of (6-Mes)CuHB$(C_6F_5)_3$ (**42**).

Several other species were apparent in multinuclear NMR spectra alongside **42**, formed from the reaction shown in Scheme 6.7. In contrast to results from Aldridge and co-workers on the reaction of (7-Dipp)AuH with $B(C_6F_5)_3$,[36] no B-C_6F_5 cleavage to afford (6-Mes)CuC_6F_5 (**22**) was detected. The major side product of the reaction was identified as $[(6\text{-Mes})_2Cu][B(C_6F_5)_4]$ by comparison of ^1H, ^{11}B and ^{19}F NMR data with an in-situ generated sample (^{11}B = -15.8 ppm; ^{19}F = -131.6, -162.7, -166.7 ppm), formed from the reaction of $[(6\text{-Mes})_2Cu][BF_4]$ (**7**) and $NaB(C_6F_5)_4$.

Despite extensive effort, **42** could not be isolated in weighable quantities due to the very similar solubilities of **42**, $[(6\text{-Mes})_2Cu][B(C_6F_5)_4]$, Et_3SiO^tBu and other unidentified contaminants. Of the methods employed (washing with hexane, pentane or ether; reprecipitation from benzene/hexane or THF/hexane; crystallisation from benzene/hexane solutions or evaporation of benzene or toluene at either room temperature or 243 K), the best results obtained were through extraction of **42** into 1 : 5 (v : v) mixtures of benzene/hexane. The yield of this extraction was very low, and only milligrams of pure material could be isolated and no yield could be recorded. However, layering benzene solutions of **42** with hexane did afford crystals suitable for X-ray diffraction studies (Section 6.7.2) and NMR spectroscopic analysis (Section 6.7.1).

Complex **42** was also formed upon addition of $B(C_6F_5)_3$ to in-situ generated $[(6\text{-Mes})CuH]_2$ (**38**) at 190 K. Numerous unidentified side products were also formed, presumably due to the aluminium containing species present in the reaction mixture. Alternative syntheses were not pursued due to time constraints, but future work should explore the possibility of salt metathesis of **20** with $NaHB(C_6F_5)_3$,[37] in an analogous manner to the synthesis of **39**, or the use of silanes other than Et_3SiH.

6.7.1 Characterisation of (6-Mes)CuHB$(C_6F_5)_3$ (42)

$[HB(C_6F_5)_3]^-$ salts are commonly reported in the context of frustrated Lewis pair activation of dihydrogen (for example, a mixture of $^tBu_3P$ and $B(C_6F_5)_3$ heterolytically cleaves H_2 at room temperature to give $[^tBu_3PH][HB(C_6F_5)_3]$)[38] as well as in hydride abstraction reactions (for example, in the boron-boron coupling reaction to yield $[B_4H_2(\mu\text{-hpp})_4][HB(C_6F_5)_3]_2$).[39] Many cationic organometallic

complexes are known with a $[HB(C_6F_5)_3]^-$ counterion but very few have been shown to exhibit metal co-ordination (Figure 6.9).[40–43]

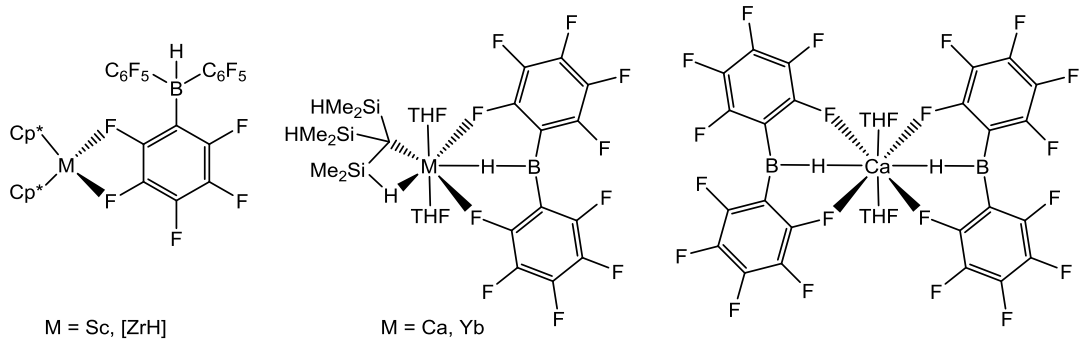

Figure 6.9: Structurally characterised examples of organometallic complexes displaying $[HB(C_6F_5)_3]^-$ co-ordination: $(Cp^*)_2Sc(HB(C_6F_5)_3)$[41] and $(Cp^*)_2Zr(H)(HB(C_6F_5)_3)$[42] (left), $(C(SiMe_2H)_3)Ca/Yb(THF)_2(HB(C_6F_5)_3)$ (centre),[43] $Ca(THF)_2(HB(C_6F_5)_3)_2$ (right).[43]

Isolated, crystalline samples of **42** were analysed by multinuclear NMR spectroscopy and found to be stable for days at room temperature. Hydride migratory insertion was completely suppressed, with no evidence of either H-B cleavage or formation of **35** observed. ^1H NMR spectroscopy revealed that **42** comprises a single, C_s symmetric 6-Mes ligand. The bridging hydride could not be located by ^1H or $^1H\{^{11}B\}$ NMR spectroscopy or ^{11}B-^1H correlation experiments, although the appearance of a doublet signal in the ^{11}B NMR spectrum (-28.1 ppm, $^1J_{BH}$ = 60 Hz) confirmed the B-H interaction. The ion separated species $[^tBu_3PH][HB(C_6F_5)_3]$, with no bridging hydride interaction, displays a similar ^{11}B chemical shift (-25.5 ppm) to **42**, but has a much higher $^1J_{BH}$ coupling constant (100 Hz).[38] The lower $^1J_{BH}$ coupling constant in **42** reveals a significant degree of B-H bond weakening upon co-ordination of $[HB(C_6F_5)_3]^-$ to copper. The $[HB(C_6F_5)_3]^-$ complexes of the more electropositive group II and III metals (Figure 6.9) exhibit B-H coupling constants intermediate of **42** and $[^tBu_3PH][HB(C_6F_5)_3]$, consistent with these complexes having less covalent M··H-B bonding character than **42** ($(Cp^*)_2Sc(HB(C_6F_5)_3)$ = -25.3 ppm (broad),[41] $(C(SiMe_2H)_3)Ca(THF)_2(HB(C_6F_5)_3)$ = -21.3 ppm ($^1J_{BH}$ = 76.2 Hz),[43] $(C(SiMe_2H)_3)Yb(THF)_2(HB(C_6F_5)_3)$ = -20.8 ppm ($^1J_{BH}$ = 72.8 Hz),[43] $Ca(THF)_2(HB(C_6F_5)_3)_2$ = -26.4 ppm ($^1J_{BH}$ = 90.8 Hz)).[43] ^{19}F NMR spectroscopy revealed three multiplets (-129.3 ppm (*o*-C_6F_5), -158.4 ppm (*p*-

C_6F_5) and -163.8 ppm (m-C_6F_5)) in a 2 : 1 : 2 ratio, showing that the aryl groups are equivalent in solution at room temperature. Furthermore, the value of $\Delta\delta(m,p\text{-F})$[i] (5.4 Hz) is consistent with strong metal co-ordination of $[HB(C_6F_5)_3]^-$ in complex **42**.[44]

6.7.2 Molecular Structure of (6-Mes)CuHB(C_6F_5)$_3$ (42)

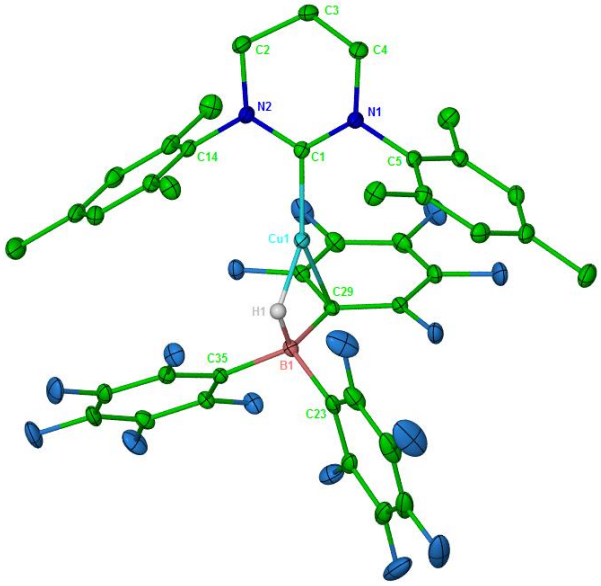

Figure 6.10: Displacement ellipsoid plot (30 % probability) of (6-Mes)CuHB(C_6F_5)$_3$ (**42**). H atoms omitted for clarity (except for H(1)). Selected bond lengths (Å) and angles (°): Cu(1)-C(1) 1.8991(18), Cu(1)-C(29) 2.2183(17), Cu(1)-H(1) 1.58(2), B(1)-H(1) 1.16(2), B(1)-C(29) 1.657(3), B(1)-C(23) 1.624(3), B(1)-C(35) 1.628(3), N(1)-C(1)-N(2) 118.47(16), C(1)-Cu(1)-B(1) 173.80(8), C(1)-Cu(1)-H(1) 146.5(8), C(1)-Cu(1)-C(29) 141.18(7), Cu(1)-H(1)-B(1) 110.2(10), Cu(1)-C(29)-B(1) 69.89(9).

Single crystal X-ray diffractometry revealed that complex **42** is three co-ordinate in the solid state (Figure 6.10) with copper bonded to 6-Mes as well as to $[HB(C_6F_5)_3]^-$ in a co-ordination mode (μ-H, μ-i-C_6F_5) not previously observed for $[HB(C_6F_5)_3]^-$. Complex **42** shows no difference in its Cu-$C_{6\text{-Mes}}$ and Cu-H bond lengths (1.8991(18) Å and 1.58(2) Å, respectively) to complex **39** (1.908(3) Å and 1.56(3) Å, respectively).

[i] The chemical shift difference between the m-C_6F_5 and p-C_6F_5 fluorines ($\Delta\delta(m,p\text{-F})$) of C_6F_5 substituted borates has been shown to be a sensitive measure of boron's co-ordination environment.[44]

In all other structurally characterised complexes of $[HB(C_6F_5)_3]^-$, metal co-ordination takes place through the *o*-C_6F_5 or *m*-C_6F_5 fluorines (Figure 6.9).[41–43] These complexes all contain very electropositive metal centres (Ca^{2+}, Sc^{3+}, Zr^{4+} and Yb^{2+}) and the unique co-ordination mode in complex **42** may be due to the relatively electron rich copper centre favouring an orbital (*i*-C_6F_5) interaction over electrostatic attractions to fluorine. Close inspection of the molecular structure reveals that the plane of the bridging C_6F_5 ring is almost perpendicular to the B-H bond (H-B-C_{ipso} = 94.01°) with the $\sigma_{B\text{-}H}$ bond approximately coplanar with the π_{aryl} system. This represents a significant distortion from tetrahedral geometry about boron and suggests a degree of electronic delocalisation between the $\sigma_{B\text{-}H}$ bond and the π_{aryl} system of the bridging C_6F_5. This copper co-ordinated aryl group has a significantly longer B-C_{ipso} bond length (1.657(3) Å) than the two non co-ordinated aryl groups (B-C_{ipso} = 1.624(3) Å and 1.628(3) Å), consistent with back donation from copper to the delocalised H-B-C_6F_5 π-system.

6.8 DFT Investigation of (6-Mes)CuHB(C_6F_5)$_3$ (42)

DFT calculations were performed in collaboration with Macgregor and co-workers to gain insight into the structure of (6-Mes)CuHB(C_6F_5)$_3$ (**42**). Molecular optimisation in the gas phase was found to agree well with the experimental data, with the best match achieved with a PBE/D3 Gaussian function. The calculated and experimental structures are shown in Figure 6.11 for comparison.

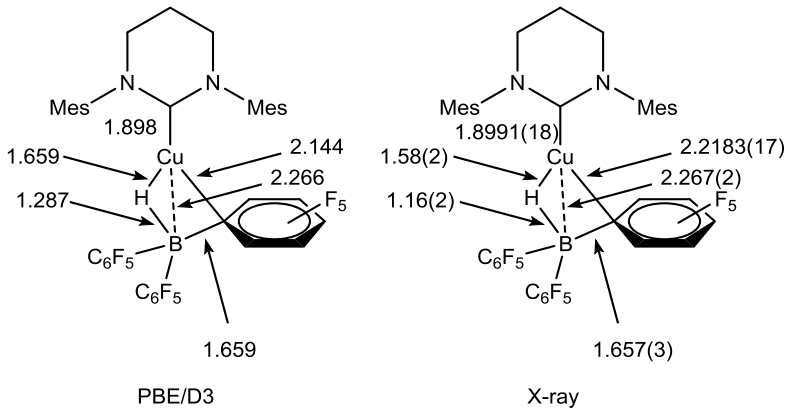

Figure 6.11: Optimised geometry (left) (PBE/D3 functional) and experimentally determined X-ray diffraction data (right) for (6-Mes)CuHB(C_6F_5)$_3$ (**42**).

The optimised molecular structure of **42** shows good agreement in the Cu-$C_{6\text{-Mes}}$, B-C_{ipso} and Cu-B distances. However, both the Cu-H and B-H bond lengths were over estimated computationally (calc: Cu-H = 1.659 Å; B-H = 1.287 Å, expt: Cu-H = 1.58(2) Å; B-H = 1.16(2) Å), while the Cu-C_{ipso} distance was calculated (2.144 Å) to be much shorter than the experimentally measured value (2.2183(17) Å).

An electron density distribution map of **42** was calculated by a QTAIM analysis and Figure 6.12 shows a charge density topology plot in the plane of the Cu-H-B-C_{ipso} core.

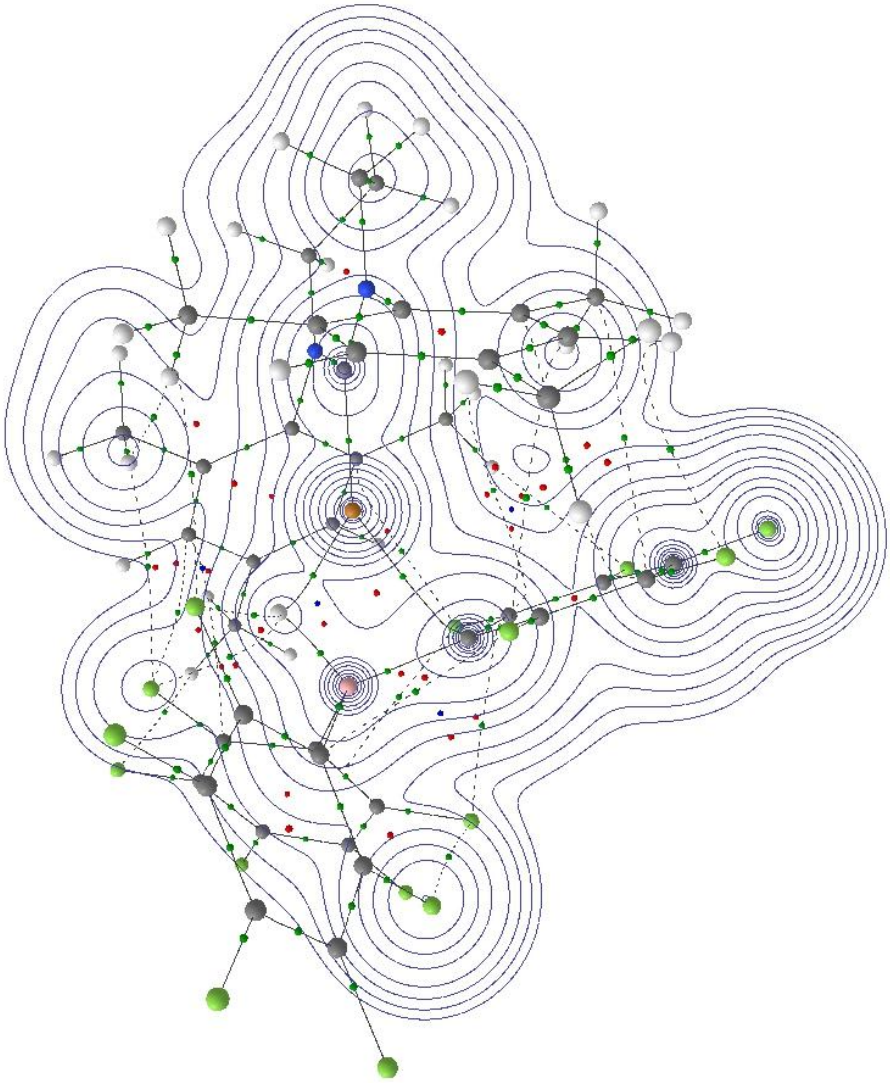

Figure 6.12: Calculated charge density topology plot for (6-Mes)CuHB(C_6F_5)$_3$ (**42**).

Three bond pathways connect copper to the carbenic carbon of 6-Mes, the bridging hydride and the ipso carbon of one pentafluorophenyl ring. In addition, multiple

long range interactions (dashed lines) between the fluorine atoms and the mesityl rings appear to provide additional stabilisation to complex **42**.

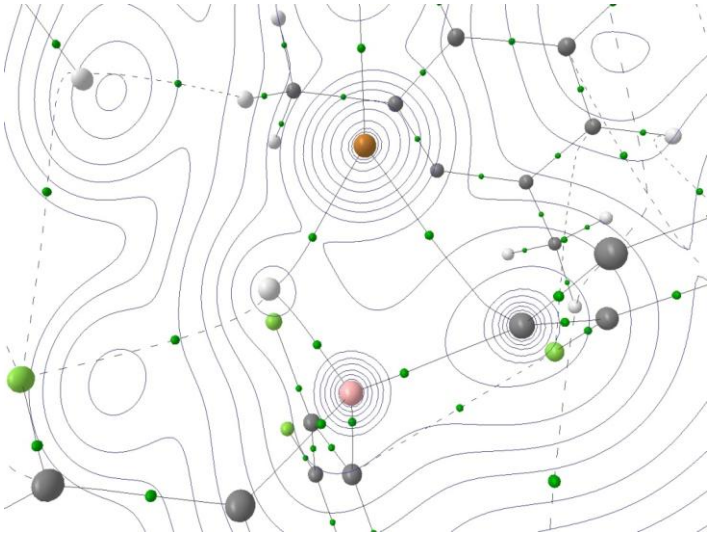

Figure 6.13: Calculated charge density topology plot for (6-Mes)CuHB(C_6F_5)$_3$ (**42**).

Figure 6.13 shows the bonding situation about copper in more detail and reveals that the Cu-H, B-H and Cu-C_{ipso} bond paths exhibit significant curvature towards their mutual centre, representing a situation of electron deficiency and delocalisation in their bonding. This delocalisation is reflected in the high ellipticity[i] of the Cu-H and Cu-C_{ipso} bond critical points (ε = 0.330 and 1.016, respectively). However, the B-H and B-C_{ispo} bonds show a high degree of σ-bond character (ε = 0.014 and 0.039, respectively), inconsistent with the proposal in Section 6.7.2 that the $\sigma_{B\text{-}H}$ bond is to some degree engaged in delocalised bonding with the π_{aryl} system.

In complex **42**, a higher degree of electron density resides between the hydride and boron than between the hydride and copper ($\rho_{(Cu\text{-}H)}$ = 0.083; $\rho_{(B\text{-}H)}$ = 0.135; 1 : 1.62 ratio). In the case of complex **39**, the electron density is more evenly distributed across the two bond paths ($\rho_{(Cu\text{-}H)}$ = 0.092; $\rho_{(Cu\text{-}H)}$ = 0.105; 1 : 1.14 ratio). These results are consistent with the higher Lewis acidity of B(C_6F_5)$_3$ withdrawing more electron density from a bridging hydride than the less Lewis acidic BEt_3.

[i] The ellipticity of a bond critical point (ε) denotes how cylindrical the electron density along the bond path is. Since the bond critical point represents a point in space where electron density decreases in two dimensions, if these two gradients are equal then the bond is cylindrical (for example in σ or δ bonding). If one dimension exhibits a slower rate of decay of the electron density, this denotes ellipticity of the electron density (for example in π bonding). Ellipticity is defined as $\varepsilon = \lambda_1/\lambda_2 - 1$, where λ_2 is the smaller gradient of electron density decay and λ_1 the larger of the two.

6.9 Factors Affecting the Stability of NHC Copper Hydride Complexes

N-heterocyclic carbenes offer a diverse platform for the study of copper hydride complexes and several factors have already been identified as contributing to their stability.

Firstly, steric bulk has been shown to be vital in their kinetic stabilisation. For example, Bertrand's $[(CAAC)CuH]_2$ complex (Scheme 6.1) proved isolable only when a bulky menthyl substituted CAAC was employed, and not when the less bulky cyclohexyl substituted CAAC was used.[6] Very recently, Sadighi has shown that by replacing the five-membered NHC IPr with the more bulky RENHC 6-Dipp, the thermal stability of their respective copper hydride complexes could be enhanced, with $[(6\text{-Dipp})CuH]_2$ being stable at room temperature (Scheme 5.12).[45]

Secondly, this Thesis has shown that the electrophilicity of NHCs is crucial in determining the stability of copper hydride complexes, and their susceptibility to migratory insertion. The highly electrophilic 6-MesDAC undergoes migratory insertion at very low temperatures, and is unsuitable as a supporting ligand for reductive processes. The less electrophilic 6-Mes does support a dinuclear copper hydride complex (**38**), although this is still susceptible to migratory insertion at just 255 K. Whilst electrophilicity is a very important factor in determining the susceptibility of an NHC to migratory insertion, the isolation of $[(6\text{-Dipp})CuH]_2$ reveals that steric bulk must also provide protection against migratory insertion, given that the electrophilicity of 6-Dipp is very similar to that of 6-Mes.

Thirdly, Lewis bases have been shown to promote migratory insertion. Addition of phosphine or isonitrile to the otherwise stable, menthyl substituted $[(CAAC)CuH]_2$ resulted in migratory insertion (Scheme 6.3).[6] In Chapter Five, it was shown that an intramolecular Lewis base assisted mechanism was responsible for the copper hydride migratory insertion reactions of 6-Mes and 6-MesDAC.

Chapter Six has demonstrated a fourth factor, regarding the stabilisation of copper hydride complexes. The introduction of a Lewis acid greatly stabilised 6-Mes copper hydride complexes with respect to migratory insertion, with the stronger Lewis acid $B(C_6F_5)_3$ affording more stabilisation than BEt_3.

The use of Lewis acids to stabilise sensitive metal hydride complexes has been referred to in the literature (for example, the relative stabilisation of calcium hydroborates over calcium hydrides),[12] and even demonstrated synthetically (for example, addition of BEt_3 to $[(Cp^*)_2LaH]_n$ results in the formation of $(Cp^*)_2LaHBEt_3$ with a higher decomposition temperature).[15] However, whilst the propensity for Lewis bases to accelerate migratory insertion is known,[6] it has never before been observed that Lewis acids may inhibit this reaction.

As well as representing a rare study into the effect of Lewis acids on the stability of copper hydride complexes, complexes **39** and **42** are themselves fascinating in their own right as the first mononuclear complexes to contain a copper-hydride bond. The issue of whether to refer to them as Lewis acid stabilised copper hydrides or as copper complexes of hydroborate anions is largely one of semantics. QTAIM analysis supports a three-centre two-electron bonding description of the Cu-H-B system, with covalent Cu-H and B-H interactions each showing a degree of electron deficiency. The bond critical point electron density is greater for the B-H bond than the Cu-H bond in both complexes, and greatest for **42** with the more Lewis acidic $B(C_6F_5)_3$. Synthetically, contrasting approaches have been taken towards the synthesis of **39** and **42**. Complex **39** was formed by the intact delivery of $[HBEt_3]^-$ by salt metathesis of complex **20**, whereas **42** is the product of σ-bond metathesis of **20** with silane (or reaction of **20** with $LiAlH_4$) and subsequent trapping by $B(C_6F_5)_3$.

These results should prompt further research into the stabilisation of copper hydrides with Lewis acids. The synthesis of a range of analogues of **39** and **42** with different NHCs and different Lewis acids, coupled with further DFT calculations, would bring further insight into the nature of the bonding in these complexes. The reactivity of these complexes is also as yet unknown and warrants investigation.

6.10 Conclusion

This Chapter has shown that reaction of (6-Mes)CuO^{t}Bu (**20**) with $LiAlH_4$ at low temperatures generates a dimeric copper hydride complex (**38**). Complex **38** underwent migratory insertion of Cu-H onto 6-Mes at 255 K, resulting in the formation of (6-Mes·H)Cu(6-Mes) (**35**). Reaction of **20** with $LiHBEt_3$ led to the formation of (6-Mes)CuHBEt$_3$ (**39**), which displayed greater stability towards migratory insertion than **38**, but underwent H-B cleavage and subsequent decomposition to mixtures of **35**, **39**, **40** and **41**. The strong Lewis acid $B(C_6F_5)_3$ stabilised the copper hydride still further, forming the room temperature stable (6-Mes)CuHB$(C_6F_5)_3$ (**42**). Complexes **39** and **42** are the first mononuclear complexes to contain a Cu-H bond, with **39** being the only structurally characterised two co-ordinate copper hydride. Both complexes were investigated computationally, with QTAIM analysis giving insight into the nature of their bonding. The discovery of Lewis acid stabilisation of copper hydrides is an exciting area for future research.

6.11 References for Chapter Six

(1) Churchill, M. R.; Bezman, S. A.; Osborn, J. A.; Wormald, J. *J. Am. Chem. Soc.* **1971**, *93*, 2063–2065.

(2) Churchill, M. R.; Bezman, S. A.; Osborn, J. A.; Wormald, J. *Inorg. Chem.* **1972**, *11*, 1818–1825.

(3) Goeden, G. V.; Caulton, K. G. *J. Am. Chem. Soc.* **1981**, *103*, 7354–7355.

(4) Lemmen, T. H.; Folting, K.; Huffman, J. C.; Caulton, K. G. *J. Am. Chem. Soc.* **1985**, *107*, 7774–7775.

(5) Goeden, G. V.; Huffman, J. C.; Caulton, K. G. *Inorg. Chem.* **1986**, *25*, 2484–2485.

(6) Frey, G. D.; Donnadieu, B.; Soleilhavoup, M.; Bertrand, G. *Chem. Asian J.* **2011**, *6*, 402–405.

(7) Mankad, N. P.; Laitar, D. S.; Sadighi, J. P. *Organometallics* **2004**, *23*, 3369–3371.

(8) Abdalla, J. A. B.; Riddlestone, I. M.; Tirfoin, R.; Phillips, N.; Bates, J. I.; Aldridge, S. *Chem. Commun.* **2013**, *49*, 5547–5549.

(9) Smith, G.; Cole-Hamilton, D. J.; Thornton-Pett, M.; Hursthouse, M. B. *J. Chem. Soc., Dalton Trans.* **1983**, 2501–2507.

(10) Crestani, M. G.; Muñoz-Hernández, M.; Arévalo, A.; Acosta-Ramírez, A.; García, J. J. *J. Am. Chem. Soc.* **2005**, *127*, 18066–18073.

(11) Köster, R.; Schüßler, W.; Boese, R.; Bläser, D. *Chem. Ber.* **1991**, *124*, 2259–2262.

(12) Krieck, S.; Görls, H.; Westerhausen, M. *Inorg. Chem. Commun.* **2010**, *13*, 1466–1469.

(13) Baudry, D.; Dormond, A.; Lachot, B.; Visseaux, M.; Zucchi, G. *J. Organomet. Chem.* **1997**, *547*, 157–165.

(14) Visseaux, M.; Baudry, D.; Dormond, A.; Qian, C. *J. Organomet. Chem.* **1999**, *574*, 213–218.

(15) Evans, W. J.; Perotti, J. M.; Ziller, J. W. *Inorg. Chem.* **2005**, *44*, 5820–5825.

(16) Zhang, X. W.; Maunder, G. H.; Giessmann, S.; MacDonald, R.; Ferguson, M. J.; Bond, A. H.; Rogers, R. D.; Sella, A.; Takats, J. *Dalton Trans.* **2011**, *40*, 195–210.

(17) Cheng, J.; Takats, J.; Ferguson, M. J.; McDonald, R. *J. Am. Chem. Soc.* **2008**, *130*, 1544–1545.

(18) Dawson, D. M.; Meetsma, A.; Roedelof, J. B.; Teuben, J. H. *Inorg. Chim. Acta.* **1997**, *259*, 237–239.

(19) Swartz, B. D.; Ateşin, T. A.; Grochowski, M. R.; Oster, S. S.; Brennessel, W. W.; Jones, W. D. *Inorg. Chim. Acta.* **2010**, *363*, 517–522.

(20) Liang, F.; Schmalle, H. W.; Berke, H. *J. Organomet. Chem.* **2006**, *691*, 5655–5663.

(21) Harvey, M. J.; Hanusa, T. P.; Pink, M. *Chem. Commun.* **2000**, 489–490.

(22) Basuli, F.; Tomaszewski, J.; Huffman, J. C.; Mindiola, D. J. *Organometallics* **2003**, *22*, 4705–4714.

(23) Lyubov, D. M.; Fukin, G. K.; Trifonov, A. A. *Inorg. Chem.* **2007**, *46*, 11450–11456.

(24) Brookhart, M.; Green, M. L. H. *J. Organomet. Chem.* **1983**, *250*, 395–408.

(25) Brookhart, M.; Green, M. L. H.; Parkin, G. *Proc. Natl. Acad. Sci. USA* **2007**, *104*, 6908–6914.

(26) Shannon, R. D. *Acta Crystallogr., Sect. A* **1976**, *32*, 751–767.

(27) Cordero, B.; Gómez, V.; Platero-Prats, A. E.; Revés, M.; Echeverría, J.; Cremades, E.; Barragán, F.; Alvarez, S. *Dalton Trans.* **2008**, 2832–2838.

(28) Bader, R. F. W. *Chem. Rev.* **1991**, *91*, 893–928.

(29) Tognetti, V.; Joubert, L.; Raucoules, R.; De Bruin, T.; Adamo, C. *J. Phys. Chem. A.* **2012**, *116*, 5472–5479.

(30) Popelier, P. L. .; Logothetis, G. *J. Organomet. Chem.* **1998**, *555*, 101–111.

(31) Brown, H. C.; Schlesinger, H. I.; Sheft, I.; Ritter, D. M. *J. Am. Chem. Soc.* **1953**, *75*, 192–195.

(32) Brown, H. C.; Mead, E. J.; Shoaf, C. J. *J. Am. Chem. Soc.* **1956**, *78*, 3616–3620.

(33) Evans, W. J.; Lorenz, S. E.; Ziller, J. W. *Chem. Commun.* **2007**, 4662–4664.

(34) Chen, X.; Liu, S.; Plečnik, C. E.; Liu, F.-C.; Fraenkel, G.; Shore, S. G. *Organometallics* **2003**, *22*, 275–283.

(35) Houghton, A. Y.; Hurmalainen, J.; Mansikkamäki, A.; Piers, W. E.; Tuononen, H. M. *Nat. Chem.* **2014**, *6*, 983–988.

(36) Phillips, N.; Dodson, T.; Tirfoin, R.; Bates, J. I.; Aldridge, S. *Chem. Eur. J.* **2014**, *20*, 16721–16731.

(37) Lawrence, E. J.; Oganesyan, V. S.; Hughes, D. L.; Ashley, A. E.; Wildgoose, G. G. *J. Am. Chem. Soc.* **2014**, *136*, 6031–6036.

(38) Welch, G. C.; Stephan, D. W. *J. Am. Chem. Soc.* **2007**, *129*, 1880–1881.

(39) Litters, S.; Kaifer, E.; Enders, M.; Himmel, H.-J. *Nat. Chem.* **2013**, *5*, 1029–1034.

(40) Chen, Y.-X.; Marks, T. J. *Organometallics* **1997**, *16*, 3649–3657.

(41) Berkefeld, A.; Piers, W. E.; Parvez, M.; Castro, L.; Maron, L.; Eisenstein, O. *J. Am. Chem. Soc.* **2012**, *134*, 10843–10851.

(42) Yang, X.; Stern, C. L.; Marks, T. J. *Angew. Chem. Int. Ed.* **1992**, *31*, 1375–1377.

(43) Yan, K.; Upton, B. M.; Ellern, A.; Sadow, A. D. *J. Am. Chem. Soc.* **2009**, *131*, 15110–15111.

(44) Horton, A. D.; de With, J. *Organometallics* **1997**, *16*, 5424–5436.

(45) Jordan, A. J.; Wyss, C. M.; Bacsa, J.; Sadighi, J. P. *Organometallics* **2016**, *35*, 613–616.

CHAPTER SEVEN

CHAPTER SEVEN: Experimental Procedures and Characterising Data

Some of the work in this Chapter has been published in:[1–5]

Copper Diamidocarbene Complexes: Characterization of Monomeric to Tetrameric Species: Collins, L. R.; Lowe, J. P.; Mahon, M. F.; Poulten, R. C.; Whittlesey, M. K. *Inorg. Chem.* **2014**, *53*, 2699 − 2707

Use of Ring-Expanded Diamino- and Diamidocarbene Ligands in Copper Catalyzed Azide−Alkyne "Click" Reactions: Collins, L. R.; Rookes, T. M.; Mahon, M. F.; Riddlestone, I. M.; Whittlesey, M. K. *Organometallics* **2014**, *33*, 5882 − 5887

Unexpected Migratory Insertion Reactions of $M(alkyl)_2$ (M=Zn, Cd) and Diamidocarbenes: Collins, L. R.; Hierlmeier, G.; Mahon, M. F.; Riddlestone, I. M.; Whittlesey, M. K. *Chem. Eur. J.* **2015**, *21*, 3215 – 3218

A Comparison of the Stability and Reactivity of Diamido- and Diaminocarbene Copper Alkoxide and Hydride Complexes: Collins, L. R.; Riddlestone, I. M.; Mahon, M. F.; Whittlesey, M. K. *Chem. Eur. J.* **2015**, *21*, 14075 – 14084

Lactide Polymerisation by Ring-expanded NHC Complexes of Zinc: Collins, L. R.; Moffat, L. A.; Mahon, M. F.; Jones, M. D.; Whittlesey, M. K. *Polyhedron* **2016**, *103*, 121 – 125

7.1 General Methods and Instrumentation

All manipulations were carried out using standard Schlenk line or glovebox techniques under an atmosphere of argon unless stated otherwise. Solvents were purified using an MBraun solvent system (dichloromethane, diethyl ether, hexane, toluene) or refluxed over sodium under a dinitrogen atmosphere and collected by distillation (benzene, tetrahydrofuran) and subsequently degassed and stored over activated 4 Å molecular sieves or over a potassium mirror (benzene, hexane, toluene). Deuterated solvents were vacuum transferred from potassium (C_6D_6, C_7D_8, THF-d_8) or calcium hydride (CD_2Cl_2). ^{1}H, ^{7}Li, ^{11}B, ^{13}C, ^{19}F, ^{31}P and ^{113}Cd NMR spectra were recorded on Bruker Avance 400 and 500 MHz NMR spectrometers at 298 K unless stated otherwise. ^{1}H and ^{13}C NMR spectra are referenced internally to residual protio-solvent (^{1}H) or solvent (^{13}C) resonances (C_6D_6 = 7.16 and 128.0 ppm; CD_2Cl_2 = 5.32 and 54.0 ppm; THF-d_8 = 3.58 and 67.2 ppm; C_7D_8 = 2.08 and 20.4 ppm).[6] ^{7}Li, ^{11}B, ^{19}F, ^{31}P and ^{113}Cd NMR spectra are referenced externally to $\delta = 0.00$ (^{7}Li = 9.7 M LiCl in D_2O; ^{11}B = 15 % $BF_3{\cdot}OEt_2$ in $CDCl_3$; $^{19}F = CFCl_3$; $^{31}P = H_3PO_4$; $^{113}Cd = CdMe_2$). Assignments were confirmed as

necessary with the use of selective decoupling and two dimensional correlation experiments. Chemical shifts (δ) are quoted in ppm and coupling constants (J) in Hz. IR spectra were recorded on a Nicolet Nexus FTIR spectrometer as KBr discs. The data are quoted in wavenumbers (cm^{-1}) between the range of 4000-400 cm^{-1}. Elemental analyses were carried out by the Elemental Analysis Service at the London Metropolitan University and by Elemental Microanalysis Ltd.

7.1.1 Catalytic Procedure for CuAAC

All catalyses were conducted in air, with no purification of reagents. Into a 2 mL sample vial was weighed 0.01 mmol (2.0 mol %) or 0.0025 mmol (0.5 mol %) of copper complex. H_2O (0.50 mL) was added if the reaction was to be conducted on water. Alkyne (0.51 mmol) and then azide (0.50 mmol) were added by microsyringe, and the vial was sealed and secured to an agitator set to 2000 rpm. After the appropriate reaction time (45 or 180 min), the contents of the vial were extracted with $CDCl_3$ (3 × 0.35 mL) and NMR spectra were recorded. Conversions represent the ratio of triazole to unreacted azide, as an average of three separate experiments.

7.1.2 Catalytic Procedure for ROP of *rac*-Lactide

For polymerisations, the monomer:Zn/RE-NHC:BnOH ratio employed was 100:1:1 at room temperature; in all cases 0.72 g of rac-lactide were used. After the appropriate reaction time, the vessel was opened to air to quench the reaction, the resulting solid then dissolved in CH_2Cl_2 and all solvents then removed in vacuo. ^1H NMR spectroscopy ($CDCl_3$) and GPC (THF) were used to determine tacticity and molecular weights (Mn and Mw) of the polymers produced; Pm (the probability of isotactic linkages) were determined by analysis of the methine region of the homonuclear decoupled ^1H NMR spectra. GPC were recorded on a Polymer Labs 50 instrument and referenced to polystyrene standards.

7.2 Literature Procedures and Starting Materials

$[CuO^tBu]_4$,[7] $[CuMes]_n$,[8] $[CuOSiPh_3]_4$,[9] 6-MesDAC,[10] 6-Mes,[11] 7-Mes,[11] and [7-*o*-Tol·H][BF_4][12] were synthesised according to published procedures. 6-MesDAC·HCl was prepared according to the modified literature procedure described in Section

7.2.1.[10,13] All other reagents were purchased from Sigma Aldrich or Alfa Aesar, degassed, stored over activated 4 Å molecular sieves and used without further purification.

7.2.1 Synthesis and Characterising Data for 6-MesDAC·HCl

To a stirring suspension of dimesitylformamidine (2.226 g, 7.939 mmol) in a mixture of CH_2Cl_2 : hexane (1 : 2, v : v) (30 mL), was added triethylamine (1.65 mL, 11.87 mmol) at 273 K. Dimethylmalonyldichloride (1.05 mL, 7.94 mmol) was added dropwise and the solution stirred for 45 minutes at 273 K before being filtered through Celite. The Celite was washed with CH_2Cl_2:hexane (1:2, v:v) (3 x 20 mL) before volatiles were removed under reduced pressure from the combined solution, affording a white powder which was dried in vacuo. Yield = 3.259 g (99 %). ^{1}H NMR (C_6D_6, 500 MHz): δ 6.81 (1 H, s, NCH(Cl)N), 6.71 (4 H, s, *m*-ArH), 2.15 (12 H, s, *p*-ArCH_3), 2.08 (6 H, s, *o*-ArCH_3), 1.81 (6 H, s, C$(CH_3)_2$) ppm. ^{13}C{^{1}H} NMR (C_6D_6, 126 MHz): δ 171.0 (s,CO), 138.9 (s, *p*-Ar), 136.9 (s, *i*-Ar), 133.6 (s, *o*-Ar), 130.7 (s, *m*-Ar), 92.2 (s, NCN), 49.1 (s, $\underline{C}(CH_3)_2$), 24.2 (s, C$(\underline{C}H_3)_2$), 21.2 (s, *p*-Ar$\underline{C}H_3$), 19.7 (s, *o*-Ar$\underline{C}H_3$) ppm. Further NMR and IR characterisation was in agreement with published data.[13]

7.3 Experimental Details and Characterising Data for Chapter Two

7.3.1 Synthesis and Characterising Data for [(6-MesDAC)(CuCl)]$_2$ (1)[1]

To a mixture of 6-MesDAC (0.248 g, 0.659 mmol) and CuCl (0.060 g, 0.606 mmol) was added THF (15 mL). The solution was stirred at room temperature for 30 minutes. Volatiles were removed under reduced pressure and the red oily solid was dissolved in toluene (10 mL). Hexane (30 mL) was added to the vigorously stirring toluene solution, precipitating a red powder which was isolated by filtration. Yield = 0.217 g (69 %). Single crystals suitable for X-ray diffraction studies were grown from a toluene solution layered with hexane. ^{1}H NMR (C_6D_6, 500 MHz): δ 6.81 (8 H, s, *m*-ArH), 2.22 (12 H, s, *p*-ArCH_3), 2.05 (24 H, s, *o*-ArCH_3), 1.34 (12 H, s, C(CH_3)$_2$) ppm. ^{13}C{^{1}H} NMR (C_6D_6, 126 MHz): δ 212.7 (s, NCN), 172.3 (s, CO), 139.2 (s, *p*-Ar), 136.4 (s, *i*-Ar), 135.1 (s, *o*-Ar), 130.4 (s, *m*-Ar), 51.5 (s, $\underline{C}(CH_3)_2$), 24.7 (s, C($\underline{C}H_3$)$_2$), 21.7 (s, *p*-Ar$\underline{C}H_3$), 18.4 (s, *o*-Ar$\underline{C}H_3$) ppm. IR (KBr disc): ν_{CO} = 1740, 1717 cm^{-1}. Elemental analysis (%) for $C_{48}H_{56}Cl_2Cu_2N_4O_4$ (951.0) – calc: C 60.62, H 5.94, N 5.89; expt: C 60.73, H 5.90, N 5.79.

7.3.2 Synthesis and Characterising Data for (6-MesDAC)$_2$(CuCl)$_3$ (2)[1]

To a mixture of 6-MesDAC (0.193 g, 0.512 mmol) and CuCl (0.082 g, 0.823 mmol) was added THF (15 mL). The solution was stirred at room temperature for 22 hours. Volatiles were removed under reduced pressure and the orange oily solid was dissolved in toluene (10 mL). Hexane (30 mL) was added to the vigorously stirring toluene solution, precipitating an orange powder which was isolated by filtration. Yield = 0.226 g (84 %). Single crystals suitable for X-ray diffraction studies were grown from a toluene solution, layered with hexane. ^{1}H NMR (C_6D_6, 500 MHz): δ 6.77 (8 H, s, *m*-ArH), 2.15 (12 H, s, *p*-ArCH_3), 2.11 (24 H, s, *o*-ArCH_3), 1.38 (12 H, s, C(CH_3)$_2$) ppm. ^{13}C{^{1}H} NMR (C_6D_6, 126 MHz): δ 214.9 (s, NCN), 172.2 (s, CO), 139.9 (s, *p*-Ar), 136.4 (s, *i*-Ar), 135.2 (s, *o*-Ar), 130.6 (s, *m*-Ar), 51.6 (s, $\underline{C}(CH_3)_2$), 24.7 (s, C($\underline{C}H_3$)$_2$), 21.6 (s, *p*-Ar$\underline{C}H_3$), 18.5 (s, *o*-Ar$\underline{C}H_3$) ppm. IR (KBr disc): ν_{CO} = 1740, 1717 cm^{-1}. Elemental analysis (%) for

$C_{48}H_{56}Cl_3Cu_3N_4O_4$ (1050.0) – calc: C 54.91, H 5.38, N 5.34; expt: C 55.02, H 5.49, N 5.23.

7.3.3 Synthesis and Characterising Data for [(6-MesDAC)(CuCl)]$_2$·[(6-MesDAC)(CuCl)] (1·3)[1]

To a crystalline sample of [(6-MesDAC)CuCl]$_2$ (**1**) (0.050g, 0.053 mmol) was added Et_2O (10 mL). The solution was stirred at room temperature for 10 minutes before being filtered. The orange solution was slowly evaporated at 238 K, yielding orange crystals of the title compound. Yield = 0.036 g (68 %). Single crystals suitable for X-ray diffraction studies were grown from slow evaporation of an Et_2O solution at 238 K. ^{1}H NMR (C_6D_6, 500 MHz): δ 6.81 (12 H, s, *m*-ArH), 2.22 (18 H, s, *p*-ArCH_3), 2.06 (36 H, s, *o*-ArCH_3), 1.35 (18 H, s, C$(CH_3)_2$) ppm. ^{13}C{^{1}H} NMR (C_6D_6, 126 MHz): δ 212.9 (s, NCN), 172.3 (s, CO), 139.3 (s, *p*-Ar), 136.4 (s, *i*-Ar), 135.2 (s, *o*-Ar), 130.4 (s, *m*-Ar), 51.5 (s, $\underline{C}(CH_3)_2$), 24.7 (s, C($\underline{C}H_3)_2$), 21.7 (s, *p*-Ar$\underline{C}H_3$), 18.4 (s, *o*-Ar$\underline{C}H_3$) ppm. IR (KBr disc): ν_{CO} = 1739, 1716 cm^{-1}. Elemental analysis (%) for $C_{72}H_{84}Cl_3Cu_3N_6O_6$ (1426.5) – calc: C 60.62, H 5.94, N 5.89; expt: C 60.50, H 6.03, N 5.64.

7.3.4 Synthesis and Characterising Data for (6-MesDAC)$_2$(CuCl)$_4$ (4)[1]

To a mixture of 6-MesDAC (0.081 g, 0.215 mmol) and CuCl (0.435 g, 4.391 mmol) was added THF (25 mL), to give an orange solution with a large amount of pale precipitate. This was stirred at room temperature for 43 hours before being filtered. The precipitate was washed with THF (2 x 20 mL) and the THF portions combined by filtration. Volatiles were removed under reduced pressure and the resultant orange powder was dissolved in toluene (10 mL). Hexane (30 mL) was added to the vigorously stirring toluene solution, precipitating an orange powder which was isolated by filtration. Single crystals suitable for X-ray diffraction studies were grown from a toluene solution of this powder, layered with hexanes. Orange crystals of (6-MesDAC)$_2$(CuCl)$_3$ (**2**) were identified by unit cell analysis of a representative sample. Yield = 0.031 g (27 %). Brown crystals of (6-MesDAC)$_2$(CuCl)$_4$ (**4**) were identified by unit cell analysis of a representative sample. Yield = 0.004 g (3 %). Due the title compound's instability in solution,

NMR characterisation could not be obtained. IR (KBr disc): ν_{CO} = 1743, 1719 cm^{-1}. Elemental analysis (%) for $C_{48}H_{56}Cl_4Cu_4N_4O_4$ (1149.0) – calc: C 50.18, H 4.91, N 4.88; expt: C 49.96, H 4.83, N 4.92.

7.3.5 Synthesis and Characterising Data for [(6-MesDAC)$_2$Cu][PF$_6$] (5)[2]

To a mixture of 6-MesDAC (0.360 g, 0.955 mmol) and $[Cu(MeCN)_4][PF_6]$ (0.169 g, 0.453 mmol) was added CH_2Cl_2 (15 mL). The solution was stirred at room temperature for 45 minutes. Volatiles were removed under reduced pressure and the yellow powder was dried in vacuo. The product was washed with toluene (10 mL) and THF (10 mL) and the resultant pale green powder dried in vacuo before being dissolved in CH_2Cl_2 (10 mL). Hexane (30 mL) was added to precipitate a green powder which was isolated by filtration and dried in vacuo. Yield = 0.238 g (55 %). Single crystals suitable for X-ray diffraction studies were grown from a CH_2Cl_2 solution layered with hexane. ^{1}H NMR (CD_2Cl_2, 500 MHz): δ 7.10 (8 H, s, *m*-ArH), 2.43 (12 H, s, *p*-ArCH_3), 1.71 (24 H, s, *o*-ArCH_3), 1.61 (12 H, s, C$(CH_3)_2$) ppm. ^{13}C{^{1}H} NMR (CD_2Cl_2, 126 MHz): δ 213.0 (s, NCN), 171.0 (s, CO), 142.0 (s, *p*-Ar), 135.3 (s, *o*-Ar), 134.7 (s, *i*-Ar), 131.0 (s, *m*-Ar), 52.5 (s, $\underline{C}(CH_3)_2$), 25.0 (s, C($\underline{C}H_3)_2$), 21.5 (s, *p*-Ar$\underline{C}H_3$), 18.8 (s, *o*-Ar$\underline{C}H_3$) ppm. ^{31}P{^{1}H} NMR (CD_2Cl_2, 202 MHz): δ -143.5 (sept, $^1J_{PF}$ = 710 Hz, $[PF_6]^-$) ppm. IR (KBr disc): ν_{CO} = 1768, 1738 cm^{-1}. Elemental analysis (%) for $C_{48}H_{56}CuF_6N_4O_4P$ (961.5) – calc: C 59.96, H 5.87, N 5.83; expt: C 59.73, H 5.98, N 5.76.

7.3.6 Synthesis and Characterising Data for [(6-MesDAC)$_2$Cu][BF$_4$] (6)[2]

To a mixture of 6-MesDAC (0.303 g, 0.805 mmol) and $[Cu(MeCN)_4][BF_4]$ (0.121 g, 0.384 mmol) was added DCM (15 mL). The solution was stirred at room temperature for 45 minutes. Volatiles were removed under reduced pressure and the yellow powder was dried in vacuo. The product was washed with THF (2 x 10 mL) and the resultant pale green powder dried in vacuo before being dissolved in DCM (10 mL). Pentane (30 mL) was added to precipitate a green powder which was isolated by filtration and dried in vacuo. Yield = 0.127 g (37 %). ^{1}H NMR (CD_2Cl_2, 500 MHz): δ 7.10 (8 H, s, *m*-ArH), 2.43 (12 H, s, *p*-ArCH_3), 1.71 (24 H,

s, *o*-ArCH$_3$), 1.61 (12 H, s, C(CH$_3$)$_2$) ppm. ^{13}C{^{1}H} NMR (CD_2Cl_2, 126 MHz): δ 213.0 (s, NCN), 171.0 (s, CO), 142.0 (s, *p*-Ar), 135.3 (s, o-Ar), 134.7 (s, *i*-Ar), 131.0 (s, *m*-Ar), 52.5 (s, C(CH$_3$)$_2$), 25.0 (s, C(CH$_3$)$_2$), 21.5 (s, *p*-ArCH$_3$), 18.8 (s, *o*-ArCH$_3$) ppm. IR (KBr disc): ν_{CO} = 1768, 1738 cm^{-1}. Elemental analysis (%) for $C_{48}H_{56}BCuF_4N_4O_4$ (903.4) – calc: C 63.82, H 6.25, N 6.20; expt: C 63.90, H 6.19, N 6.16.

7.3.7 Synthesis and Characterising Data for [(6-Mes)$_2$Cu][BF$_4$] (7)[2]

To a mixture of 6-Mes (0.180 g, 0.562 mmol) and [Cu(MeCN)$_4$][BF$_4$] (0.059 g, 0.187 mmol) was added benzene (15 mL) and the solution was stirred at room temperature for 30 minutes. A colourless precipitate was formed, isolated by filtration and washed with benzene (3 x 10 mL) and hexane (2 x 10 mL) and dried in vacuo. Single crystals suitable for X-ray diffraction studies were grown from a CH_2Cl_2 solution layered with hexane. Yield = 0.117 g (79 %). ^{1}H NMR (CD_2Cl_2, 500 MHz): δ 6.94 (8 H, s, *m*-ArH), 3.06 (8 H, t, $^3J_{HH}$ = 5.8 Hz, NCH$_2$), 2.35 (12 H, s, *p*-ArCH$_3$), 2.04 (4 H, m, NCH$_2$CH$_2$), 1.75 (24 H, s, *o*-ArCH$_3$) ppm. ^{13}C{^{1}H} NMR (CD_2Cl_2, 126 MHz): δ 199.3 (s, NCN), 141.9 (s, *i*-Ar), 138.6 (s, *p*-Ar), 135.3 (s, *o*-Ar), 130.2 (s, *m*-Ar), 44.6 (s, NCH$_2$), 21.2 (s, *p*-ArCH$_3$), 20.7 (s, NCH$_2$CH$_2$), 18.1 (s, *o*-ArCH$_3$) ppm. Elemental analysis (%) for $C_{44}H_{56}BCuF_4N_4$ (791.3) – calc: C 66.79, H 7.13, N 7.08; expt: C 66.65, H 6.99, N 7.17.

7.3.8 Synthesis and Characterising Data for [(7-Mes)$_2$Cu][BF$_4$] (8)[2]

To a mixture of 7-Mes (0.300 g, 0.897 mmol) and [Cu(MeCN)$_4$][BF$_4$] (0.137 g, 0.436 mmol) was added THF (10 mL). The solution was stirred at 323 K for 14 hours, during which time a colourless precipitate was formed. The THF solution was concentrated and the precipitate isolated by filtration and washed with hexane (3 x 10 mL) and dried in vacuo. Single crystals suitable for X-ray diffraction studies were grown from a CH_2Cl_2 solution layered with hexane. Yield = 0.079 g (25 %). ^{1}H NMR (CD_2Cl_2, 500 MHz): δ 6.93 (8 H, s, *m*-ArH), 3.55 (8 H, m, NCH$_2$), 2.36 (12 H, s, *p*-ArCH$_3$), 2.00 (8 H, m, NCH$_2$CH$_2$), 1.82 (24 H, s, *o*-ArCH$_3$) ppm. ^{13}C{^{1}H} NMR (CD_2Cl_2, 126 MHz): δ 208.6 (s, NCN), 144.1 (s, *i*-Ar), 138.3 (s, *p*-

Ar), 135.0 (s, *o*-Ar), 130.4 (s, *m*-Ar), 53.6 (s, NCH_2), 25.5 (s, $NCH_2\underline{C}H_2$), 21.2 (s, *p*-Ar$\underline{C}H_3$), 19.0 (s, *o*-Ar$\underline{C}H_3$) ppm. Elemental analysis (%) for $C_{46}H_{60}BCuF_4N_4$ (819.4) – calc: C 67.43, H 7.38, N 6.84; expt: C 67.32, H 7.42, N 6.77.

7.3.9 Synthesis and Characterising Data for $[(7\text{-}o\text{-Tol})_2Cu][BF_4]$ (9)[2]

To a sample of [7-*o*-Tol·H][BF_4] (0.906 g, 2.473 mmol) was added a THF solution (20 mL) of KHMDS (0.538 g, 2.697 mmol). The suspension was stirred for 30 minutes, yielding a bright green solution and white precipitate. This mixture was transferred, without filtration, by cannula to [$Cu(MeCN)_4$][BF_4] (0.390 g, 1.240 mmol) and the suspension was stirred for a further 16 hours. The resultant white powder was isolated by filtration and washed with THF (2 x 10 mL). From this powder, the product was extracted into CH_2Cl_2 (3 x 15 mL) and filtered. The volatiles were removed under reduced pressure and the product dried in vacuo. Single crystals suitable for X-ray diffraction studies were grown from a solution of CH_2Cl_2 layered with hexane. Yield = 0.418 g (48 %). ^{1}H NMR (CD_2Cl_2, 400 MHz, 298 K): δ 7.47-6.37 (16 H, br, ArH), 3.99-3.31 (8 H, br, NCH_2), 2.40-1.76 (20 H, br, $NCH_2C\underline{H_2}$ and *o*-ArCH_3) ppm. ^{1}H NMR (CD_2Cl_2, 400 MHz, 224 K): δ 7.44-6.31 (16 H, m, ArH), 3.91-3.30 (8 H, m, NCH_2), 2.37-1.69 (20 H, m, $NCH_2C\underline{H_2}$ and o-ArCH_3) ppm. $^{13}C\{^1H\}$ NMR (CD_2Cl_2, 100 MHz, 224 K): δ 207.2 (s, NCN), 206.6 (s, NCN), 147.4, 147.3, 147.1, 147.0, 146.8, 146.6 (all quaternary Ar), 135.0, 134.8, 134.5, 134.4, 134.3 (s, all quaternary Ar), 131.4, 131.3, 131.1 (all ArH), 128.8, 128.3, 128.2, 128.1, 128.0, 127.7, 127.6, 127.1, 127.0 (s, all ArH), 53.0, 52.8, 52.7, 52.5 (s, all NCH_2), 25.1, 25.0, 24.7 (s, all $NCH_2C\underline{H_2}$), 18.9, 18.5, 18.4, 18.3, 18.1, 18.0 (s, all Ar$\underline{C}H_3$) ppm. Elemental analysis (%) for $C_{38}H_{44}BCuF_4N_4$ (707.2) – calc: C 64.54, H 6.27, N 7.92; expt: C 64.32, H 6.25, N 7.92.

7.4 Experimental Details and Characterising Data for Chapter Three

7.4.1 NMR Scale Reaction for the Synthesis of (6-MesDAC)Cu(μ-Cl)(μ-O^{t}Bu)Li(THF)$_2$ (10)[1]

To a THF solution of [(6-MesDAC)$_2$CuCl]$_2$ (**1**) (0.018 g, 0.019 mmol) was added LiO^{t}Bu (0.003 g, 0.038 mmol) and the resultant purple solution transferred to an NMR tube. After 40 minutes at room temperature, volatiles were removed. The green/red solid was thoroughly dried in vacuo before being redissolved in THF-d$_8$ to give a dark red solution. ^{1}H NMR (THF-d$_8$, 500 MHz, 298 K): δ 6.91 (4 H, s, *m*-ArH), 3.62 (8 H, t, $^3J_{HH}$ = 6.6 Hz, OCH$_2$), 2.27 (6 H, s, *p*-ArCH$_3$), 2.26 (12 H, s, *o*-ArCH$_3$), 1.77 (8 H, m, OCH$_2$C<u>H$_2$</u>), 1.67 (6 H, s, C(CH$_3$)$_2$), 0.66 (8 H (chemical exchange with LiO^{t}Bu was confirmed by EXSY NMR experiments), br, OC(CH$_3$)$_3$) ppm. ^{1}H NMR (THF-d$_8$, 400 MHz, 200 K): δ 6.95 (4 H, s, *m*-ArH), 3.62 (8 H, m, OCH$_2$), 2.35 (6 H, s, ArCH$_3$), 2.28 (6 H, s, ArCH$_3$), 2.20 (6 H, s, ArCH$_3$), 1.77 (8 H, m, OCH$_2$C<u>H$_2$</u>), 1.71 (3 H, s, C(CH$_3$)$_2$), 1.66 (3 H, s, C(CH$_3$)$_2$), 0.64 (9 H, s, OC(CH$_3$)$_3$) ppm. ^{7}Li NMR (THF-d$_8$, 194 MHz, 298 K): δ -0.74 (s) ppm.

7.4.2 Synthesis and Characterising Data for (6-MesDAC)CuO^{t}Bu (11)[4]

6-MesDAC (0.060 g, 0.160 mmol) and [CuO^{t}Bu]$_4$ (0.022 g, 0.040 mmol) were stirred in benzene (5 mL) for 5 minutes before the volatiles were removed and the dark orange solid dried in vacuo. The solid was vigorously washed with hexane (3 x 10 mL) and filtered to leave a bright orange powder, which was dried in vacuo. Yield = 0.061g (72 %). An alternative (and preferred) synthetic procedure (performed entirely inside a glovebox unless otherwise stated) involved the addition of ^{t}BuOH (0.074 g, 1.00 mmol) to a non-stirred solution of (6-MesDAC)CuMes (**12**) (0.260 g, 0.465 mmol) in benzene (5 mL) in a rigorously flame dried ampoule fitted with a J. Young's resealable valve. After 3 hours, bright orange crystals of the product begin to precipitate from solution. After a total of 24 hours, the solution was decanted and the crystals washed with hexane (4 x 5 mL). The ampoule was sealed, removed from the glovebox, thoroughly cycled onto a Schlenk line, opened to vacuum and the crystals dried in vacuo before being taken back into the glovebox. Single crystals suitable for X-ray diffraction were grown from THF/hexane. Yield =

0.155 g (65 %). ^{1}H NMR (C_6D_6, 500 MHz): δ 6.72 (4 H, s, *m*-ArH), 2.05 (12 H, s, *o*-ArCH_3), 2.03 (6 H, s, *p*-ArCH_3), 1.35 (6 H, s, C$(CH_3)_2$), 1.11 (9 H, s, OC$(CH_3)_3$) ppm. ^{1}H NMR (THF-d_8, 500 MHz, 200 K): δ 7.06 (4 H, s, *m*-ArH), 2.31 (6 H, s, *p*-ArCH_3), 2.23 (12 H, s, *o*-ArCH_3), 1.73 (6 H, s, C$(CH_3)_2$), 0.49 (9 H, s, OC$(CH_3)_3$) ppm. ^{13}C{^{1}H} NMR (THF-d_8, 126 MHz, 200 K):* δ 213.5 (s, NCN), 172.1 (s, CO), 139.8 (s, *p*-Ar), 136.8 (s, *i*-Ar), 135.4 (s, *o*-Ar), 130.5 (s, *m*-Ar), 52.7 (s, $\underline{C}(CH_3)_2$), 36.3 (s, OC($\underline{C}H_3)_3$), 24.0 (s, C($\underline{C}H_3)_2$), 21.0 (s, *p*-Ar$\underline{C}H_3$), 18.5 (s, *o*-Ar$\underline{C}H_3$). * O$\underline{C}(CH_3)_3$ not observed, but found at 69.2 ppm (C_6D_6, 500 MHz, 298 K) in HMBC experiments. IR (KBr disc): ν_{CO} = 1741, 1720 cm^{-1}. Elemental analysis (%) for $C_{28}H_{37}CuN_2O_3$ (513.2) – calc: C 65.54, H 7.27, N 5.46; expt: C 65.42, H 7.38, N 5.54.

7.4.3 Synthesis and Characterising Data for (6-MesDAC)CuMes (12)[4]

This procedure was conducted entirely inside a glovebox unless otherwise stated. A pale yellow benzene (15 mL) solution of 6-MesDAC (0.405 g, 1.08 mmol) was added to a pale green benzene (5 mL) solution of $[CuMes]_n$ (0.196 g, 1.07 mmol) in a rigorously flame dried ampoule. A red solution was formed immediately, and stirred for 20 minutes. The ampoule was sealed and cycled (at least five times) onto a Schlenk line, before opening it to vacuum. Volatiles were removed and the resultant orange powder dried in vacuo. The ampoule was sealed under vacuum (without backfilling with argon) and opened inside the glovebox. Single crystals suitable for X-ray diffraction studies were grown from a benzene solution layered with hexane. Yield = 0.522 g (87 %). ^{1}H NMR (C_6D_6, 500 MHz): δ 6.82 (2 H, s, *m*-CuArH), 6.71 (4 H, s, *m*-NArH), 2.23 (3 H, s, *p*-CuArCH_3), 2.08 (12 H, s, *o*-NArCH_3), 2.04 (6 H, s, *p*-NArCH_3), 1.98 (6 H, s, *o*-CuArCH_3), 1.37 (6 H, s, C$(CH_3)_2$) ppm. ^{13}C{^{1}H} NMR (C_6D_6, 126 MHz): δ 217.1 (s, NCN), 172.2 (s, CO), 161.1 (s, *i*-CuAr), 147.6 (s, *o*-CuAr), 140.2 (s, *p*-NAr), 135.9 (s, *i*-NAr), 135.1 (s, *o*-NAr), 134.1 (s, *p*-CuAr), 130.8 (s, *m*-NAr), 125.0 (s, *m*-CuAr), 51.8 (s, $\underline{C}(CH_3)_2$), 28.6 (s, *o*-CuAr$\underline{C}H_3$), 24.7 (s, C($\underline{C}H_3)_2$), 21.8 (s, *p*-CuAr$\underline{C}H_3$), 21.3 (s, *p*-NAr$\underline{C}H_3$), 18.7 (s, *o*-NAr$\underline{C}H_3$) ppm. IR (KBr disc): ν_{CO} = 1734, 1718 cm^{-1}. Elemental analysis (%) for $C_{33}H_{39}CuN_2O_2$ (559.2) – calc: C 70.88, H 7.03, N 5.01; expt: C 70.32, H 6.99, N 5.18.

7.4.4 Synthesis and Characterising Data for "Ring Exploded Carbene Complex" (13)[4]

A benzene solution (30 mL) of 6-MesDAC (0.159 g, 0.423 mmol) and $[CuO^tBu]_4$ (0.057 g, 0.105 mmol) was stirred at room temperature for 140 minutes before the volatiles were removed under reduced pressure. The resultant orange powder was dissolved in toluene (5 mL) and hexane (25 mL) added with vigorous stirring to precipitate an orange powder. This was isolated by filtration and further washed with hexane (10 mL). Crystals of the title compound were grown from toluene/hexane. Yield = 0.008 g (17 %). ^{1}H NMR (THF-d_8, 500 MHz, 298 K): δ 7.00-6.55 (16 H, m, *m*-ArH), 2.50-0.50 (96 H, m, CH_3). ^{1}H NMR (THF-d_8, 500 MHz, 223 K): δ 7.10-6.45 (16 H, m, *m*-ArH), 2.55-0.17 (96 H, m, CH_3) ppm. $^{13}C\{^1H\}$ NMR (THF-d_8, 126 MHz, 298 K): δ 172.9 (s, CO), 140.7, 139.4, 137.4, 136.4, 136.2, 135.9, 135.6, 135.3, 134.8, 125.0, 130.8, 130.5, 129.6, 129.0, 51.2, 21.5, 21.4, 21.3, 21.2, 19.1, 18.8, 18.4 ppm. IR (KBr disc): $\nu_{C\equiv N}$ = 2139; ν_{CO} = 1735, 1713 cm^{-1}. Elemental analysis (%) for $C_{96}H_{112}Cu_4N_8O_{10}$ (1792.2) – calc: C 64.36, H 6.30, N 6.25; expt: C 64.12, H 6.37, N 6.13.

7.4.5 Synthesis and Characterising Data for (6-MesDAC)Cu(OC(O)CMe$_2$C(O)N(H)Mes)(CNMes) (14)[4]

The dropwise addition of H_2O (0.040 mL, 2.222 mmol) to a THF (10 mL) solution of (6-MesDAC)CuO^tBu (**11**) (0.251 g, 0.489 mmol) afforded a dark red solution, which rapidly faded to pale orange. After stirring for 15 minutes, the volatiles were removed under reduced pressure and the oily orange product dried in vacuo. Extraction into benzene (3 x 5 mL) yielded a red/orange suspension. The orange solid was isolated (Yield = 0.007 g, 40 %) by filtration, dried in vacuo and characterised by PXRD as Cu_2O. The red filtrate was reduced to dryness and the residue reprecipitated from toluene and hexane, filtered and washed with hexane (2 x 5 mL) to afford a red powder. Yield = 0.110 g (54 %). Single crystals suitable for X-ray diffraction studies were grown from a concentrated toluene solution layered with hexane. ^{1}H NMR (C_6D_6, 500 MHz): δ 10.66 (1 H, s, NH), 6.82 (2 H, s, HN-*m*-Ar<u>H</u>), 6.78 (4 H, s, DAC-*m*-ArH), 6.29 (2 H, s, CuCN-*m*-ArH), 2.32 (6 H, s, HN-*o*-ArC<u>H$_3$</u>), 2.26 (12 H, s, DAC-*o*-ArCH$_3$), 2.18 (3 H, s, HN-*p*-ArC<u>H$_3$</u>), 1.97 (6 H, s, DAC-*p*-ArCH$_3$), 1.90 (6 H, br, $O_2CC(CH_3)_2$), 1.89 (6 H, s, CuCN-*o*-ArCH$_3$),

1.82 (3 H, s, CuCN-*p*-ArCH$_3$), 1.50 (6 H, s, DAC-C(CH$_3$)$_2$). ^{13}C{^{1}H} NMR (C_6D_6, 126 MHz): δ 218.3 (s, NCN), 180.6 (s, O$_2$CC(CH$_3$)$_2$C(O)N(H)Mes or O$_2$CC(CH$_3$)$_2$C(O)N(H)Mes), 174.1 (s, O$_2$CC(CH$_3$)$_2$C(O)N(H)Mes or O$_2$CC(CH$_3$)$_2$C(O)N(H)Mes), 172.2 (s, DAC-CO), 150.3 (s, CuCNAr), 139.9-139.8 (overlapping, DAC-*p*-Ar and CuCN-*p*-Ar), 136.3 (s, DAC-*i*-Ar), 135.5-135.3 (overlapping, DAC-*o*-Ar and CuCN-*o*-Ar and HN-*o*-Ar), 135.1 (s, HN-*p*-Ar), 134.9 (s, HN-*i*-Ar), 130.5 (s, DAC-*m*-Ar), 129.2 (s, HN-*m*-Ar), 128.9 (s, CuCN-*m*-Ar), 123.9 (s, CuCN-*i*-Ar), 51.6 (s, DAC-C(CH$_3$)$_2$), 51.2 (s, O$_2$CC(CH$_3$)$_2$), 27.1 (s, O$_2$CC(CH$_3$)$_2$), 24.8 (s, DAC-C(CH$_3$)$_2$), 21.4-21.3 (overlapping, DAC-*p*-ArCH$_3$ and CuCN-*p*-ArCH$_3$ and HN-*p*-ArCH$_3$), 19.4 (s, HN-*o*-ArCH$_3$), 18.5 (overlapping, DAC-*o*-ArCH$_3$ and CuCN-*o*-ArCH$_3$). IR (KBr disc): $\nu_{C\equiv N}$ = 2154; $\nu_{DAC\text{-}CO}$ = 1741, 1720; $\nu_{HN\text{-}CO}$ = 1684; ν_{CuOCO} = 1631, 1608 cm^{-1}. Elemental analysis (%) for $C_{48}H_{57}CuN_4O_5$ (833.6) – calc: C 69.17, H 6.89, N 6.72; expt: C 69.48, H 6.97, N 6.71.

7.4.6 Synthesis and Characterising Data for (18-crown-6)K(OC(O)CMe$_2$C(O)N(H)Mes) (15)[4]

To a stirring mixture of (6-MesDAC)CuO^{t}Bu (**11**) (0.134 g, 0.260 mmol) and KOH (0.048 g, 0. 856 mmol) was added THF (10 mL), giving a dark red solution with a dark coloured precipitate. The reaction was monitored by aliquots until all (6-MesDAC)CuO^{t}Bu was consumed. After 9 hours, the precipitate was isolated by filtration and washed with THF (2 x 5 mL). Volatiles were removed from the combined THF washings and the red product characterised as ^{t}BuOCuCNMes by NMR. To a THF (5 mL) suspension of the precipitate was added a THF (5 mL) solution of 18-crown-6 (0.177 g, 0.670 mmol), causing the immediate solvation of the precipitate to form a red solution which fades to pale yellow within seconds, then appearing green over the course of 30 minutes due to a fine black precipitate. This solution was filtered to separate insoluble material before removal of volatiles, yielding a yellow microcrystalline material. This was reprecipitated from THF/hexane (2 x 6 mL, 1 : 5, v : v) and stirred overnight with hexane (10 mL) to remove excess 18-crown-6, yielding a white powder which was dried in vacuo. Single crystals suitable for X-ray diffraction studies were grown from a concentrated solution in THF layered with hexane. Yield = 0.041 g (29 %). ^{1}H NMR (C_6D_6,

500 MHz): δ 12.39 (1 H, s, NH), 6.88 (2 H, s, *m*-ArH), 3.17 (24 H, s, OCH_2), 2.50 (6 H, s, *o*-$ArCH_3$), 2.20 (3 H, s, *p*-$ArCH_3$), 2.13 (6 H, s, $C(CH_3)_2$) ppm. $^{13}C\{^1H\}$ NMR (C6D6, 126 MHz): δ 181.5 (s, one of $O_2\underline{C}C(CH_3)_2\underline{C}(O)N(H)Mes$), 175.9 (s, one of $O_2\underline{C}C(CH_3)_2\underline{C}(O)N(H)Mes$), 135.8 (s, *i*-Ar), 135.3 (s, *o*-Ar), 134.5 (s, *p*-Ar), 129.2 (s, *m*-Ar), 70.5 (s, OCH_2), 51.5 (s, $\underline{C}(CH_3)_2$), 27.7 (s, $C(\underline{C}H_3)_2$), 21.4 (s, *p*-$Ar\underline{C}H_3$), 19.6 (s, *o*-$Ar\underline{C}H_3$) ppm. IR (KBr disc): $\nu_{HN\text{-}CO}$ = 1665; ν_{OCO} = 1580 cm^{-1}. Elemental analysis (%) for $C_{26}H_{42}KNO_9$ (551.7) – calc: C 56.60, H 7.67, N 2.54; expt: C 56.80, H 7.36, N 2.47.

Characterising data for MesNCCuO^{t}Bu: ^1H NMR (C_6D_6, 500 MHz): δ 6.42 (2 H, s, *m*-ArH), 2.32 (6 H, s, *o*-$ArCH_3$), 2.21 (9 H, s, O^{t}Bu), 1.91 (3 H, s, *p*-$ArCH_3$) ppm. $^{13}C\{^1H\}$ NMR (C_6D_6, 126 MHz):* δ 137.1 (s, *p*-Ar), 134.6 (s, *o*-Ar), 128.8 (s, *m*-Ar), 127.2 (s, *i*-Ar), 70.4 (s, $O\underline{C}(CH_3)_3$), 34.4 (s, $OC(\underline{C}H_3)_3$), 21.1 (s, *p*-$Ar\underline{C}H_3$), 19.2 (s, *o*-$Ar\underline{C}H_3$) ppm. * Mes$N\underline{C}$ not observed.

7.4.7 Synthesis and Characterising Data for (6-MesDAC)CuOSiPh$_3$ (16)

To a mixture of (6-MesDAC)CuO^{t}Bu (**11**) (0.455 g, 0.886 mmol) and Ph_3SiOH (0.273 g, 0.989 mmol) was added benzene (20 mL). The orange solution was stirred at room temperature for 1 hour, with a yellow precipitate forming immediately. Volatiles were removed under reduced pressure and the resultant yellow powder reprecipitated from addition of hexane to a concentrated toluene solution. The product was washed with hexane (20 mL), filtered and dried in vacuo. Single crystals suitable for X-ray diffraction studies were grown from a toluene solution layered with hexane. Yield = 0.543 g (86 %). ^1H NMR (C_6D_6, 500 MHz): δ 7.63 (6 H, m, *o*-SiArH), 7.19 (9 H, overlapping, *m*-SiArH and *p*-SiArH), 6.68 (4 H, s, *m*-NArH), 2.05 (6 H, s, *p*-$NArCH_3$), 1.93 (12 H, s, *o*-$NArCH_3$), 1.30 (6 H, s, $C(CH_3)_2$) ppm. $^{13}C\{^1H\}$ NMR (C_6D_6, 126 MHz): δ 202.5 (s, NCN), 164.8 (s, CO), 140.8 (s, *i*-SiAr), 138.4 (s, *p*-NAr), 135.2 (s, *i*-NAr), 133.6 (s, *o*-NAr), 134.8 (s, *o*-SiAr), 130.4 (s, *m*-NAr), 128.6 (s, *p*-SiAr), 127.8 (s, *m*-SiAr), 63.8 (s, $O\underline{C}(CH_3)_3$), 41.0 (s, $OC(\underline{C}H_3)_3$), 38.3 (s, *p*-$NAr\underline{C}H_3$), 35.8 (s, *o*-$NAr\underline{C}H_3$) ppm. IR (KBr disc): ν_{CO} = 1759, 1729 cm^{-1}. Elemental analysis (%) for $C_{42}H_{43}CuN_2O_3Si$ (715.5) – calc: C 70.51, H 6.06, N 3.92; expt: C 70.45, H 6.19, N 4.00.

7.4.8 Synthesis and Characterising Data for [(6-MesDAC)CuN$_3$]$_2$ (17)

To a solution of (6-MesDAC)CuOSiPh$_3$ (**16**) (0.117 g, 0.163 mmol) in benzene (10 mL) was added TMSN$_3$ (0.025 mL, 0.186 mmol). The orange solution was stirred at room temperature for 5 hours. Volatiles were removed under reduced pressure and the resultant red powder dried in vacuo. Layering a toluene solution of this powder with hexane resulted in red crystals of the title compound. Single crystals suitable for X-ray diffraction studies were grown from a solution of toluene layered with hexane. Yield = 0.018 g (26 %). ^{1}H NMR (C$_6$D$_6$, 500 MHz): δ 6.90 (8 H, s, *m*-ArH), 2.26 (12 H, s, *p*-ArCH$_3$), 2.09 (24 H, s, *o*-ArCH$_3$), 1.38 (12 H, s, C(CH$_3$)$_2$) ppm. ^{13}C{^{1}H} NMR (C$_6$D$_6$, 126 MHz): δ 209.7 (s, NCN), 172.5 (s, CO), 139.1 (s, *p*-Ar), 136.6 (s, *i*-Ar), 135.1 (s, *o*-Ar), 130.5 (s, *m*-Ar), 51.4 (s, C(CH$_3$)$_2$), 24.8 (s, C(CH$_3$)$_2$), 21.8 (s, *p*-ArCH$_3$), 18.2 (s, *o*-ArCH$_3$) ppm. IR (KBr disc): ν_{NNN} = 2059; ν_{CO} = 1740, 1717 cm^{-1}. Elemental analysis (%) for C$_{48}$H$_{56}$Cu$_2$N$_{10}$O$_4$ (964.1) – calc: C 59.80, H 5.85, N 14.53; expt: C 59.94, H 5.91, N 14.34.

7.4.9 Synthesis and Characterising Data for (6-MesDAC)CuC$_6$F$_5$ (18)

To a dark red benzene (10 mL) solution of (6-MesDAC)CuMes (**12**) (0.498 g, 0.89 mmol) was added C$_6$F$_5$H (0.150 mL, 1.35 mmol) in a rigorously flame dried ampoule. This solution was heated at 333 K, and monitored by ^{1}H NMR analysis of aliquots. After 21 hours, volatiles were removed and the resultant dull orange powder dried in vacuo. The product was washed with a mixture of benzene/hexane (20 mL, 1 : 4, v : v), then with hexane (3 x 10 mL) and dried in vacuo to give a bright orange powder. Yield = 0.285 g (53 %). Single crystals suitable for X-ray diffraction studies were grown by slow evaporation of a benzene/hexane solution (1 : 4, v : v). ^{1}H NMR (C$_6$D$_6$, 500 MHz): δ 6.78 (4 H, s, *m*-ArH), 2.06 (12 H, s, *o*-ArCH$_3$), 2.05 (6 H, s, *p*-ArCH$_3$), 1.34 (6 H, s, C(CH$_3$)$_2$) ppm. ^{13}C{^{1}H} NMR (C$_6$D$_6$, 126 MHz):* δ 217.2 (s, NCN), 171.7 (s, CO), 140.8 (s, *p*-Ar), 135.7 (s, *i*-Ar), 134.6 (s, *o*-Ar), 130.8 (s, *m*-Ar), 52.1 (s, C(CH$_3$)$_2$), 24.7 (s, C(CH$_3$)$_2$), 21.4 (s, *p*-ArCH$_3$), 18.6 (s, *o*-ArCH$_3$) ppm. * C$_6$F$_5$ not observed. ^{19}F NMR (C$_6$D$_6$, 470 MHz): δ -112.5 (2 F, m, *o*-C$_6$F$_5$), -159.4 (1 F, t, $^3J_{FF}$ = 20.0 Hz, *p*-C$_6$F$_5$), -163.0 (2 F, m, *m*-C$_6$F$_5$) ppm. IR (KBr disc): ν_{CO} = 1763, 1732 cm^{-1}. Elemental analysis (%)

for $C_{30}H_{28}CuF_5N_2O_2$ (607.1) – calc: C 59.35, H 4.65, N 4.61; expt: C 59.98, H 4.57, N 4.70.

7.4.10 Synthesis and Characterising Data for (6-Mes)CuMes (19)[4]

A benzene (15mL) solution of 6-Mes (0.454 g, 1.42 mmol) was added to $[CuMes]_n$ (0.261 g, 1.43 mmol). A white precipitate formed, suspended in a yellow solution which was stirred at room temperature for 90 minutes. Volatiles were removed under reduced pressure and the white powder dried in vacuo. Single crystals suitable for X-ray diffraction studies were grown from a solution of benzene layered with hexane. Yield = 0.674 g (95 %). ^{1}H NMR (C_6D_6, 500 MHz): δ 6.87 (2 H, s, *m*-CuArH), 6.76 (4 H, s, *m*-NArH), 2.52 (4 H, t, $^3J_{HH}$ = 5.9 Hz, NCH_2), 2.28 (3 H, s, *p*-CuArCH_3), 2.20 (12 H, s, *o*-NArCH_3), 2.12 (6 H, s, *p*-NArCH_3), 2.00 (6 H, s, *o*-CuArCH_3), 1.38 (2 H, p, $^3J_{HH}$ = 5.9 Hz, $NCH_2C\underline{H}_2$) ppm. $^{13}C\{^1H\}$ NMR (C_6D_6, 126 MHz): δ 205.1 (s, NCN), 164.1 (s, *i*-CuAr), 147.8 (s, *o*-CuAr), 143.1 (s, *i*-NAr), 138.2 (s, *p*-NAr), 135.5 (s, *o*-NAr), 132.7 (s, *p*-CuAr), 130.4 (s, *m*-NAr), 124.7 (s, *m*-CuAr), 44.5 (s, NCH_2), 28.4 (s, *o*-CuAr$\underline{C}H_3$), 22.0 (s, *p*-CuAr$\underline{C}H_3$), 21.4 (s, $NCH_2\underline{C}H_2$), 21.3 (s, *p*-NAr$\underline{C}H_3$), 18.5 (s, *o*-NAr$\underline{C}H_3$) ppm. Elemental analysis (%) for $C_{31}H_{39}CuN_2$ (503.2) – calc: C 73.99, H 7.81, N 5.57; expt: C 74.14, H 7.77, N 5.22.

7.4.11 Synthesis and Characterising Data for (6-Mes)CuO^{t}Bu (20)[4]

A THF (15 mL) solution of 6-Mes (0.321 g, 1.00 mmol) and $[CuO^tBu]_4$ (0.137 g, 0.251 mmol) was stirred at room temperature for 2 hours and then concentrated under vacuum. Addition of hexane (30 mL) under vigorous stirring gave a brown powder, which was isolated by filtration, washed with hexane (2 x 10 mL) and dried in vacuo. Yield = 0.404 g (88 %). An alternative (and preferred) procedure (conducted entirely inside a glovebox unless otherwise stated) employed the addition of ^{t}BuOH (0.216 g, 2.92 mmol) to a stirred solution of (6-Mes)CuMes (**19**) (0.575 g, 1.14 mmol) in benzene (15 mL) in a rigorously flame dried ampoule fitted with a J. Young's resealable valve. After 26 hours, the ampoule was removed from the glovebox, thoroughly cycled onto a Schlenk line and the volatiles removed under vacuum to give a colourless powder. Yield = 0.470 g (90 %). Single crystals suitable for X-ray diffraction studies were formed from sufficiently concentrated

reaction mixtures of **19** and ^{t}BuOH in benzene. ^{1}H NMR (C_6D_6, 500 MHz): δ 6.74 (4 H, s, *m*-ArH), 2.48 (4 H, t, $^{3}J_{HH}$ = 5.8 Hz, NCH_2), 2.15 (12 H, s, *o*-$ArCH_3$), 2.09 (6 H, s, *p*-$ArCH_3$), 1.32 (2 H, p, $^{3}J_{HH}$ = 5.8 Hz, $NCH_2\underline{C}H_2$), 1.20 (9 H, s, $OC(CH_3)_3$). $^{13}C\{^{1}H\}$ NMR (C_6D_6, 126 MHz): δ 203.5 (s, NCN), 143.3 (s, *i*-Ar), 138.1 (s, *p*-Ar), 135.0 (s, *o*-Ar), 130.4 (s, *m*-Ar), 68.7 (s, $O\underline{C}(CH_3)_3$), 44.1 (s, $N\underline{C}H_2$), 36.8 (s, $OC(\underline{C}H_3)_3$), 21.4 (s, *p*-$Ar\underline{C}H_3$), 21.2 (s, $NCH_2\underline{C}H_2$), 18.4 (s, *o*-$Ar\underline{C}H_3$). Elemental analysis (%) for $C_{26}H_{37}CuN_2O$ (457.1) – calc: C 68.31, H 8.16, N 6.13; expt: C 68.13, H 7.87, N 6.23.

7.4.12 Synthesis and Characterising Data for (6-Mes)$CuOSiPh_3$ (21)

To a mixture of 6-Mes (0.343 g, 1.07 mmol) and $[CuOSiPh_3]_4$ (0.361 g, 0.266 mmol) was added toluene (15 mL). A white precipitate formed immediately, suspended in a clear solution which was stirred at room temperature for 90 minutes before being filtered. The precipitate was then washed with hexane (10 mL) and dried in vacuo. The resultant white powder was reprecipitated by addition of hexane to a concentrated CH_2Cl_2 solution, filtered and dried in vacuo. Single crystals suitable for X-ray diffraction studies were grown from a solution of CH_2Cl_2 layered with hexane. Yield = 0.485 g (69 %). ^{1}H NMR (CD_2Cl_2, 500 MHz): δ 7.28-7.17 (15 H, overlapping, SiArH), 6.87 (4 H, s, *m*-NArH), 3.29 (4 H, t, $^{3}J_{HH}$ = 5.9 Hz, NCH_2), 2.26 (2 H, m, $NCH_2C\underline{H_2}$), 2.22 (12 H, s, *o*-$NArCH_3$), 2.21 (6 H, s, *p*-$NArCH_3$) ppm. $^{13}C\{^{1}H\}$ NMR (CD_2Cl_2, 126 MHz): δ 202.0 (s, NCN), 143.1 (s, NAr), 142.8 (s, SiAr), 138.3 (s, NAr), 135.4 (s, SiAr), 135.2 (s, NAr), 130.3 (s, NAr), 128.4 (s, SiAr), 127.5 (s, SiAr), 44.9 (s, NCH_2), 21.5 (s, $NCH_2\underline{C}H_2$), 21.4 (s, *p*-$NAr\underline{C}H_3$), 18.3 (s, *o*-$NAr\underline{C}H_3$) ppm. Elemental analysis (%) for $C_{40}H_{43}CuN_2OSi$ (659.4) – calc: C 72.86, H 6.57, N 4.25; expt: C 72.81, H 6.66, N 4.39.

7.4.13 Synthesis and Characterising Data for (6-Mes)CuC_6F_5 (22)

This reaction was conducted entirely inside the glovebox, unless otherwise stated. HC_6F_5 (0.066 mL, 0.594 mmol) was added to a stirring benzene (10 mL) solution of (6-Mes)CuMes (**19**) (0.150 g, 0.298 mmol). The reaction was stirred, with the precipitation of a pale powder after 30 minutes. The reaction was monitored by ^{1}H NMR analysis of a reaction conducted in parallel in C_6D_6. After 2.5 hours, the

starting material was almost completely consumed. After 25 hours, volatiles were removed and the off-white powder dried in vacuo. Yield = 0.119 g (73 %). Single crystals formed overnight from the monitored reaction in C_6D_6. ^{1}H NMR (C_6D_6, 500 MHz): δ 6.79 (4 H, s, *m*-ArH), 2.51 (4 H, t, $^3J_{HH}$ = 5.8 Hz, NCH_2), 2.18 (12 H, s, *o*-$ArCH_3$), 2.07 (6 H, s, *p*-$ArCH_3$), 1.34 (2 H, p, $^3J_{HH}$ = 5.8 Hz, $NCH_2C\underline{H}_2$) ppm. $^{13}C\{^1H\}$ NMR (C_6D_6, 126 MHz):* δ 203.1 (s, NCN), 142.4 (s, *i*-Ar), 138.6 (s, *p*-Ar), 135.0 (s, *o*-Ar), 130.4 (s, *m*-Ar), 44.0 (s, NCH_2), 21.3 (s, *p*-$Ar\underline{C}H_3$), 21.0 (s, $NCH_2\underline{C}H_2$), 18.4 (s, *o*-$Ar\underline{C}H_3$) ppm. * C_6F_5 not observed. ^{19}F NMR (C_6D_6, 470 MHz): δ -112.3 (2 F, m, *o*-C_6F_5), -161.3 (1 F, t, $^3J_{FF}$ = 20.0 Hz, *p*-C_6F_5), -163.6 (2 F, m, *m*-C_6F_5) ppm. Elemental analysis (%) for $C_{28}H_{28}CuF_5N_2$ (551.1) – calc: C 61.03, H 5.12, N 5.08; expt: C 60.93, H 5.10, N 5.02.

7.4.14 Synthesis and Characterising Data for [(6-MesDAC)CuI]$_2$ (23)

To a mixture of 6-MesDAC (0.148 g, 0.393 mmol) and CuI (0.059 g, 0.312 mmol) was added THF (10 mL). The red solution was stirred at room temperature for 2 hours. Volatiles were removed under reduced pressure and the pink residue was dissolved in toluene (20 mL). Hexane (20 mL) was added to the vigorously stirring toluene solution, precipitating a red powder which was isolated by filtration and further washed with hexane (20 mL). Yield = 0.159 g (90 %). Single crystals suitable for X-ray diffraction studies were grown from a solution of toluene layered with hexane, but were only of sufficient quality to confirm connectivity. ^{1}H NMR (C_6D_6, 500 MHz, 298 K): δ 6.82 (8 H, s, *m*-ArH), 2.26 (12 H, s, *p*-$ArCH_3$), 2.16 (24 H, s, *o*-$ArCH_3$), 1.37 (12 H, s, $C(CH_3)_2$) ppm. $^{13}C\{^1H\}$ NMR (C_6D_6, 126 MHz, 298 K):* δ 172.1 (s, CO), 139.1 (s, *i*-Ar), 135.9 (s, *p*-Ar), 135.3 (s, *o*-Ar), 130.5 (s, *m*-Ar), 51.4 (s, $\underline{C}(CH_3)_2$), 24.8 (s, $C(\underline{C}H_3)_2$), 21.8 (s, *p*-$Ar\underline{C}H_3$), 19.2 (s, *o*-$Ar\underline{C}H_3$) ppm. * NCN not observed due to poor solubility. Characterised at high temperature to strengthen signal. ^{1}H NMR (C_6D_6, 500 MHz, 338 K): δ 6.83 (8 H, s, *m*-ArH), 2.28 (12 H, s, *p*-$ArCH_3$), 2.15 (24 H, s, *o*-$ArCH_3$), 1.41 (12 H, s, $C(CH_3)_2$) ppm. $^{13}C\{^1H\}$ NMR (C_6D_6, 126 MHz, 338 K): δ 219.3 (s, NCN), 171.8 (s, CO), 138.6 (s, *i*-Ar), 135.7 (s, *p*-Ar), 135.0 (s, *o*-Ar), 130.1 (s, *m*-Ar), 51.0 (s, $\underline{C}(CH_3)_2$), 24.6 (s, $C(\underline{C}H_3)_2$), 21.3 (s, *p*-$Ar\underline{C}H_3$), 18.7 (s, *o*-$Ar\underline{C}H_3$) ppm. IR (KBr

disc): ν_{CO} = 1740, 1719 cm^{-1}. Elemental analysis (%) for $C_{48}H_{56}Cu_2I_2N_4O_4$ (1133.9) – calc: C 50.84, H 4.98, N 4.94; expt: C 51.44, H 5.05, N 4.66.

7.4.15 Synthesis and Characterising Data for $[(6\text{-Mes})_2Cu][CuI_2]$ (24)

To a mixture of 6-Mes (0.220 g, 0.686 mmol) and CuI (0.130 g, 0.683 mmol) was added THF (10 mL). A white powder was immediately formed, suspended in a colourless solution which was stirred for 15 minutes before addition of hexane (10 mL) and filtration. The white powder was washed with hexane (10 mL) and dried in vacuo. Extraction into CH_2Cl_2 (10 mL), concentration and precipitation of the product with hexane yielded a white powder which was dried in vacuo. Yield = 0.245 g (70 %). Single crystals suitable for X-ray diffraction studies were grown from a CH_2Cl_2 solution layered with hexane. ^{1}H NMR (CD_2Cl_2, 500 MHz): δ 6.94 (8 H, s, *m*-ArH), 3.07 (8 H, t, $^3J_{HH}$ = 5.9 Hz, NCH_2), 2.35 (12 H, s, *p*-$ArCH_3$), 2.05 (4 H, m, $NCH_2C\underline{H}_2$), 1.76 (24 H, s, *o*-$ArCH_3$) ppm. $^{13}C\{^1H\}$ NMR (CD_2Cl_2, 126 MHz): δ 199.4 (s, NCN), 142.1 (s, *i*-Ar), 138.8 (s, *p*-Ar), 135.4 (s, *o*-Ar), 130.3 (s, *m*-Ar), 44.8 (s, NCH_2), 21.4 (s, *p*-$Ar\underline{C}H_3$), 21.0 (s, $NCH_2\underline{C}H_2$), 18.4 (s. *o*-$Ar\underline{C}H_3$) ppm. Elemental analysis (%) for $C_{44}H_{56}Cu_2I_2N_4$ (1021.9) – calc: C 51.72, H 5.52, N 5.48; expt: C 51.92, H 5.52, N 5.45.

7.5 Experimental Details and Characterising Data for Chapter Four

7.5.1 Synthesis and Characterising Data for (6-Mes)$ZnMe_2$ (25)[5]

To a stirring benzene (10 mL) solution of 6-Mes (0.252 g, 0.786 mmol) was added a 2.0 M toluene solution of $ZnMe_2$ (0.400 mL, 0.800 mmol). After stirring for 20 minutes, the volatiles were removed under reduced pressure and the product extracted into toluene. This solution was reduced to dryness and the residue washed with hexane, resulting in a white powder which was dried in vacuo. Yield = 0.145 g (44 %). Single crystals suitable for X-ray diffraction studies were grown from a toluene solution layered with hexane. ^{1}H NMR (C_6D_6, 500 MHz): δ 6.75 (4 H, s, *m*-ArH), 2.57 (4 H, t, $^3J_{HH}$ = 5.9 Hz, NCH_2), 2.29 (12 H, s, *o*-$ArCH_3$), 2.00 (6 H, s, *p*-$ArCH_3$), 1.44 (2 H, m, $NCH_2C\underline{H}_2$), -0.67 (6 H, s, $ZnCH_3$) ppm. $^{13}C\{^1H\}$ NMR (C_6D_6, 126 MHz): δ 214.7 (s, NCN), 140.9 (s, *i*-Ar), 138.1 (s, *p*-Ar), 135.5 (s, *o*-

Ar), 129.8 (s, *m*-Ar), 43.7 (s, NCH_2), 21.0 (s, *p*-Ar$\underline{C}H_3$), 20.8 (s, $NCH_2\underline{C}H_2$), 18.1 (s, *o*-Ar$\underline{C}H_3$), -8.8 (s, $ZnCH_3$) ppm. Elemental analysis (%) for $C_{24}H_{34}N_2Zn$ (415.9) – calc: C 69.31, H 8.24, N 6.74; expt: C 69.16, H 8.23, N 6.80.

7.5.2 Synthesis and Characterising Data for (7-Mes)$ZnMe_2$ (26)[5]

To a stirring benzene (10 mL) solution of 7-Mes (0.310 g, 0.927 mmol) was added a 1.0 M hexane solution of $ZnMe_2$ (1.300 mL, 1.300 mmol). After 30 minutes, the volatiles were removed under reduced pressure and the white powder dried in vacuo. The product was reprecipitated from benzene/hexane and dried in vacuo. Yield = 0.230 g (58 %). Single crystals suitable for X-ray diffraction studies were grown from a toluene solution layered with hexane. ^{1}H NMR (C_6D_6, 500 MHz): δ 6.76 (4 H, s, *m*-ArH), 3.11 (4 H, m, NCH_2), 2.36 (12 H, s, *o*-ArCH_3), 2.00 (6 H, s, *p*-ArCH_3), 1.59 (4 H, m, $NCH_2C\underline{H}_2$), -0.75 (6 H, s, $ZnCH_3$) ppm. $^{13}C\{^1H\}$ NMR (C_6D_6, 126 MHz): δ 225.8 (s, NCN), 143.2 (s, *i*-Ar), 137.8 (s, *p*-Ar), 135.1 (s, *o*-Ar), 129.9 (s, *m*-Ar), 52.4 (s, NCH_2), 25.9 (s, $NCH_2\underline{C}H_2$), 20.9 (s, *p*-Ar$\underline{C}H_3$), 18.8 (s, *o*-Ar$\underline{C}H_3$), -8.6 (s, $ZnCH_3$) ppm. Elemental analysis (%) for $C_{25}H_{36}N_2Zn$ (430.0) – calc: C 69.84, H 8.44, N 6.52; expt: C 70.35, H 8.47, N 6.70.

7.5.3 NMR Scale Reaction for the Synthesis of (6-MesDAC)$ZnEt_2$ (27)[3]

To an NMR tube fitted with a J. Young's cap was added 6-MesDAC (0.010 g, 0.027 mmol) and THF-d_8 (0.5 mL). This suspension was cooled to 178 K in a slurry of frozen acetone. A 1.0 M solution of $ZnEt_2$ in heptane (27 μL, 0.027 mmol) was added slowly by microsyringe. Upon mixing, a blood red solution was formed. NMR characterisation was obtained by transferring the tube to a pre-cooled NMR spectrometer. Decomposition to a white precipitate was evident at temperatures above 210 K. In a separate experiment, removal of the volatiles under reduced pressure, keeping the solution at temperatures below 200 K, afforded a red solid. The product immediately decomposed to a white solid when warmed to room temperature. ^{1}H NMR (THF-d_8, 400 MHz, 181 K): δ 7.05 (4 H, s, *m*-ArH), 2.31 (6 H, s, *p*-ArCH_3), 2.24 (12 H, s, *o*-ArCH_3), 1.77 (6 H, s, $C(CH_3)_2$), 0.70 (6 H, t, $^3J_{HH}$ = 5.8 Hz, $ZnCH_2C\underline{H}_3$), -0.48 (4 H, q, $^3J_{HH}$ = 5.8 Hz, $ZnC\underline{H}_2CH_3$) ppm. $^{13}C\{^1H\}$ NMR (THF-d_8, 100 MHz, 181 K): δ 236.9 (s, NCN), 171.1 (s, CO), 140.1 (s, *p*-Ar), 136.0 (s, *o*-Ar), 134.6 (s, *i*-Ar), 130.1 (s, *m*-Ar), 53.3 (s, $\underline{C}(CH_3)_2$), 24.0 (s,

$C(\underline{C}H_3)_2$), 20.8 (s, *p*-Ar$\underline{C}H_3$), 18.4 (s, *o*-Ar$\underline{C}H_3$), 14.3 (s, $ZnCH_2\underline{C}H_3$), 4.9 (s, $Zn\underline{C}H_2CH_3$) ppm.

7.5.4 Synthesis and Characterising Data for $[(6\text{-MesDAC}\cdot Et)ZnEt]_n$ (28)[3]

To a suspension of 6-MesDAC (0.409 g, 1.087 mmol) in hexane (5 mL) was added a 1.0 M solution of $ZnEt_2$ in heptane (110 μL, 1.100 mmol). A red solution was formed, before immediately precipitating a very thick white solid. This precipitate was isolated by filtration, washed with hexane (2 x 10 mL) and dried in vacuo. Single crystals suitable for X-ray diffraction studies were grown from CH_2Cl_2/hexane. Yield = 0.496 g (91 %). ^{1}H NMR (CD_2Cl_2, 500 MHz): δ 7.03 (2 H, s, *m*-ArH), 6.98 (2 H, s, *m*-ArH), 2.37 (6 H, s, $ArCH_3$), 2.30 (6 H, s, $ArCH_3$), 2.27 (2 H, q, $^3J_{HH}$ = 5.8 Hz, NC($C\underline{H}_2CH_3$)N), 2.22 (6 H, s, $ArCH_3$), 1.73 (3 H, s, $C(CH_3)_2$), 1.51 (3 H, s, $C(CH_3)_2$), 0.84 (3 H, t, $^3J_{HH}$ = 5.8 Hz, $ZnCH_2C\underline{H}_3$), 0.73 (3 H, t, $^3J_{HH}$ = 5.8 Hz, NC($CH_2C\underline{H}_3$)N), 0.00 (2 H, q, $^3J_{HH}$ = 5.8 Hz, $ZnC\underline{H}_2CH_3$) ppm. $^{13}C\{^1H\}$ NMR (CD_2Cl_2, 126 MHz): δ 171.3 (s, CO), 139.0 (s, Ar), 138.6 (s, Ar), 138.0 (s, Ar), 132.9 (s, Ar), 131.4 (s, *m*-Ar), 131.1 (s, *m*-Ar), 88.0 (s, N$\underline{C}(CH_2CH_2)$N), 46.7 (s, $\underline{C}(CH_3)_2$), 33.1 (s, NC($\underline{C}H_2CH_3$)N), 28.0 (s, $C(\underline{C}H_3)_2$), 23.2 (s, $C(\underline{C}H_3)_2$), 21.1 (s, $Ar\underline{C}H_3$), 19.6 (s, $Ar\underline{C}H_3$), 19.5 (s ,$Ar\underline{C}H_3$), 14.8 (s, NC($CH_2\underline{C}H_3$)N), 10.6 (s, $ZnCH_2\underline{C}H_3$), 5.2 (s, $Zn\underline{C}H_2CH_3$) ppm. IR (KBr disc): ν_{CO} = 1651; ν_{COZn} = 1576 cm^{-1}. Elemental analysis (%) for $C_{28}H_{38}N_2O_2Zn$ (500.0) – calc: C 67.26, H 7.66, N 5.60; expt: C 67.09, H 7.51, N 5.61.

7.5.5 NMR Scale Reaction for the Synthesis of (6-MesDAC)$ZnMe_2$ (29)[3]

To an NMR tube fitted with a J. Young's cap was added 6-MesDAC (0.026 g, 0.055 mmol) and THF-d_8 (0.5 mL). This suspension was cooled to 178 K in a slurry of frozen acetone. A 2.0 M solution of $ZnMe_2$ in toluene (26 μL, 0.052 mmol) was added slowly by microsyringe. Upon mixing, a yellow solution was formed. NMR characterisation was obtained by transferring the tube to a pre-cooled NMR spectrometer. Decomposition to a white precipitate was evident at temperatures above 245 K. ^{1}H NMR (THF-d_8, 500 MHz, 204 K): δ 7.02 (4 H, s, *m*-ArH), 2.29 (6 H, s, *p*-$ArCH_3$), 2.24 (12 H, s, *o*-$ArCH_3$), 1.77 (6 H, s, $C(CH_3)_2$), -1.40 (6 H, s,

$ZnCH_3$) ppm. $^{13}C\{^1H\}$ NMR (THF-d_8, 126 MHz, 204 K): δ 237.6 (s, NCN), 171.2 (s, CO), 140.2 (s, *p*-Ar), 136.0 (s, *o*-Ar), 134.4 (s, *i*-Ar), 130.1 (s, *m*-Ar), 53.2 (s, $\underline{C}(CH_3)_2$), 24.1 (s, $C(\underline{C}H_3)_2$), 21.0 (s, *p*-Ar$\underline{C}H_3$), 18.4 (s, *o*-Ar$\underline{C}H_3$), -9.1 (s, $ZnCH_3$) ppm.

7.5.6 Synthesis and Characterising Data for [(6-MesDAC·Me)ZnMe]$_n$ (30)[3]

To a solution of 6-MesDAC (0.198 g, 0.526 mmol) in THF (10 mL) was added a 2.0 M solution of $ZnMe_2$ in toluene (275 μL, 0.550 mmol). A yellow solution was formed, before precipitating a white solid over the course of 5 seconds. This suspension was stirred for 15 minutes, hexane (15 mL) added and the solid isolated by filtration. The precipitate was further washed with THF (5 mL) and hexane (2 x 10 mL) and dried in vacuo. Yield = 0.176 g (71 %). The insolubility and instability of the product, along with the formation of insoluble by-products, precluded full spectroscopic or structural characterisation. NMR analysis of a saturated (2.2 mg in 0.5 mL of CD_2Cl_2 at 313 K) solution showed this sample to be ~60 % pure, with numerous other resonances which could not be assigned. Washing the sample vigorously with DCM (3 x 10 mL) and isolating the remaining powder (Yield = 0.020 g, 8%) by filtration afforded a sample of ~92 % purity. ^1H NMR (CD_2Cl_2, 500 MHz, 313 K): δ 7.02 (2 H, s, *m*-ArH), 7.01 (2 H, s, *m*-ArH), 2.35 (6 H, s, $ArCH_3$), 2.31 (6 H, s, $ArCH_3$), 2.22 (6 H, s, $ArCH_3$), 1.72 (3 H, s, $C(CH_3)_2$), 1.64 (3 H, s, $NC(CH_3)N$), 1.53 (3 H, s, $C(CH_3)_2$), -0.87 (3 H, s, $ZnCH_3$) ppm. Attempts to acquire $^{13}C\{^1H\}$ NMR spectra at 313 K failed due to decomposition over the period of acquisition. IR (KBr disc): ν_{CO} = 1654; ν_{COZn} = 1575 cm^{-1}.

7.5.7 NMR Scale Reaction for the Synthesis of (6-MesDAC)$CdMe_2$ (31)[3]

To an NMR tube fitted with a J. Young's cap was added 6-MesDAC (0.009 g, 0.025 mmol) and THF-d_8 (0.5 mL). A 2.0 M solution of $CdMe_2$ in hexane (12.5 μL, 0.025 mmol) was added by microsyringe and the tube quickly placed in a slurry of frozen acetone (178 K). Upon mixing, a yellow solution was formed. NMR characterisation was obtained by transferring the tube to a pre-cooled NMR spectrometer. Decomposition to a white precipitate was evident at temperatures

above 255 K. ^{1}H NMR (THF-d_8, 500 MHz, 235 K): δ 7.01 (4 H, s, *m*-ArH), 2.30 (6 H, s, *p*-ArCH_3), 2.21 (12 H, s, *o*-ArCH_3), 1.75 (6 H, s, C$(CH_3)_2$), -1.12 (6 H, s (75%) with satellites (25%): $^{2}J_{HCd}$ = 24.7 Hz, CdCH_3) ppm. ^{13}C{^{1}H} NMR (THF-d_8, 126 MHz, 235 K): δ 252.9 (s, NCN), 171.4 (s, CO), 140.1 (s, *p*-Ar), 136.4 (s, *i*-Ar), 135.9 (s, *o*-Ar), 130.4 (s, *m*-Ar), 53.1 (s, $\underline{C}(CH_3)_2$), 24.7 (s, C($\underline{C}H_3)_2$), 21.4 (s, *p*-Ar$\underline{C}H_3$), 18.7 (s, *o*-Ar$\underline{C}H_3$), -7.9 (s (75%) with two pairs of satellites (25%): $^{1}J_{111CdC}$ = 294 Hz; $^{1}J_{113CdC}$ = 309 Hz, CdCH_3) ppm. ^{113}Cd{^{1}H} NMR (THF-d_8, 111 MHz, 235 K): δ -263.5 (s, Cd) ppm.

7.5.8 Synthesis and Characterising Data for [(6-MesDAC·Me)CdMe]$_n$ (32)[3]

To a solution of 6-MesDAC (0.043 g, 0.115 mmol) in THF (5 mL) was added a 2.0 M solution of $CdMe_2$ in hexane (60 μL, 0.120 mmol). A yellow solution was immediately formed, before precipitating a white solid over the course of 2 minutes. The reaction was stirred for 45 minutes. Hexane (5 mL) was added to the THF suspension and the product isolated by filtration before being further washed with hexane (2 x 5 mL) and dried in vacuo. Single crystals suitable for X-ray diffraction studies were grown from CH_2Cl_2/hexane. Yield = 0.036 g (60 %). ^{1}H NMR (CD_2Cl_2, 500 MHz): δ 7.02 (2 H, s, *m*-ArH), 7.00 (2 H, s, *m*-ArH), 2.30 (12 H, s, *o*-ArCH_3), 2.21 (6 H, s, *p*-ArCH_3), 1.72 (3 H, s, NC(CH_3)N), 1.70 (3 H, s, C$(CH_3)_2$), 1.50 (3 H, s, C$(CH_3)_2$), -0.69 (3 H, s (75%) with satellites (25%): $^{2}J_{HCd}$ = 29.9 Hz, CdCH_3) ppm. ^{13}C{^{1}H} NMR (CD_2Cl_2, 126 MHz): δ 171.7 (s, CO), 139.1 (s, *i*-Ar), 138.7 (s, o-Ar), 137.3 (s, *p*-Ar), 133.9 (s, *o*-Ar), 131.3 (s, *m*-Ar), 131.2 (s, *m*-Ar), 89.5 (s, N$\underline{C}(CH_3)$N), 46.7 (s, $\underline{C}(CH_3)_2$), 28.4 (s, NC($\underline{C}H_3$)N), 28.2 (s, C($\underline{C}H_3)_2$), 23.4 (s, C($\underline{C}H_3)_2$), 21.2 (s, *p*-Ar$\underline{C}H_3$), 19.4 (s, *o*-Ar$\underline{C}H_3$), 19.3 (s, *o*-Ar$\underline{C}H_3$), -7.7 (s, CdCH_3) ppm. ^{113}Cd{^{1}H} NMR (CD_2Cl_2, 111 MHz, 298 K): δ -243.7 (s, Cd) ppm. IR (KBr disc): ν_{CO} = 1655; ν_{COCd} = 1591 cm^{-1}. Elemental analysis (%) for $C_{26}H_{34}CdN_2O_2$ (519.0) – calc ($C_{26}H_{34}CdN_2O_2 \cdot 0.3(CH_2Cl_2)$ as confirmed by ^{1}H NMR): C 58.02, H 6.41, N 5.15; expt: C 57.54, H 6.36, N 4.90.

7.6 Experimental Details and Characterising Data for Chapter Five

7.6.1 NMR Scale Reaction for the Synthesis of (6-MesDAC·H)Cu(μ-O^{t}Bu)Cu(6-MesDAC) (33)[4]

This synthetic procedure was conducted entirely inside a glovebox unless otherwise stated. Et_3SiH (1.1 μL, 0.007 mmol) was added to a C_6D_6 (0.4 mL) solution of (6-MesDAC)CuO^{t}Bu (**11**) (0.008 g, 0.016 mmol) resulting in the immediate formation of an orange solution of Et_3SiO^tBu and the title compound. All attempts at workup resulted in decomposition. ^{1}H NMR (C_6D_6, 500 MHz): δ 6.76 (2 H, s, (DAC·H)-*m*-Ar), 6.72 (6 H, overlapping, (DAC·H)-*m*-Ar and (DAC)-*m*-Ar), 5.59 (1 H, s, NCHN), 2.49 (6 H, s, (DAC·H)-$ArCH_3$), 2.31 (6 H, s, (DAC·H)-$ArCH_3$), 2.18 (9 H, overlapping, (DAC·H)-$ArCH_3$ and (DAC·H)-$C(CH_3)_2$), 2.10 (6 H, s, (DAC)-*p*-$ArCH_3$), 1.96 (3 H, s, (DAC·H)-$C(CH_3)_2$), 1.88 (12 H, s, (DAC)-*o*-$ArCH_3$), 1.28 (6 H, s, (DAC)-$C(CH_3)_2$), 0.33 (9 H, s, $OC(CH_3)_3$) ppm. $^{13}C\{^1H\}$ NMR (C_6D_6, 126 MHz): δ 215.2 (s, (DAC)-NCN), 173.3 (s, (DAC·H)-CO), 171.4 (s, (DAC)-CO), 143.6 (s, (DAC·H)-*i*-Ar), 140.8 (s, (DAC)-*p*-Ar), 136.0 (s, (DAC·H)-*o*-Ar), 135.8 (s, (DAC)-*i*-Ar), 135.7 (s, (DAC·H)-*o*-Ar), 135.2 (s, (DAC·H)-*p*-Ar), 134.6 (s, (DAC)-*o*-Ar), 130.8 (s, (DAC)-*m*-Ar), 129.7 (s, (DAC·H)-*m*-Ar), 129.2 (s, (DAC·H)-*m*-Ar), 72.5 (s, O$\underline{C}(CH_3)_3$), 67.7 (s, (DAC·H)-NC(H)N), 51.8 (s, (DAC)-$\underline{C}(CH_3)_2$), 49.2 (s, (DAC·H)-$\underline{C}(CH_3)_2$), 35.0 (s, OC($\underline{C}H_3)_3$), 24.8 (s, (DAC)-C($\underline{C}H_3)_2$), 23.8 (s, (DAC·H)-C($\underline{C}H_3)_2$), 21.5 (overlapping, (DAC·H)-*p*-Ar$\underline{C}H_3$ and (DAC)-*p*-Ar$\underline{C}H_3$), 21.0 (s, (DAC·H)-C($\underline{C}H_3)_2$), 20.5 (s, (DAC·H)-*o*-Ar$\underline{C}H_3$), 18.4 (s, (DAC)-*o*-Ar$\underline{C}H_3$) ppm. IR (KBr disc): $\nu_{DAC\text{-}CO}$ = 1733, 1698; $\nu_{DAC\cdot H\text{-}CO}$ = 1669, 1635 cm^{-1}.

7.6.2 Synthesis and Characterising Data for (6-MesDAC·H)Cu(P(*p*-Tol)$_3$) (34)[4]

This reaction was conducted entirely inside a glovebox unless otherwise stated. A benzene (2 mL) solution of Et_3SiH (0.030 g, 0.258 mmol) was added dropwise to a stirring suspension of (6-MesDAC)CuO^{t}Bu (**11**) (0.127 g, 0.247 mmol) and P(*p*-Tol)$_3$ (0.077 g, 0.253 mmol) in benzene (5 mL) in a J. Young's ampoule. A red suspension was formed immediately, which became a homogeneous red solution after 30 minutes. After 1 hour, the ampoule was removed from the glovebox,

rigorously cycled onto a Schlenk line and the volatiles removed. The resultant pale red powder was dried under vacuum, taken back into the glovebox, redissolved in benzene (5 mL) and filtered. Addition of hexane (15 mL) to the filtrate produced the title compound as a microcrystalline red solid, which was isolated by decantation, washed with hexane (3 x 10 mL) and dried in vacuo. Yield = 0.112 g (61 %). Single crystals suitable for X-ray diffraction were grown from benzene/hexane. ^{1}H NMR (C_6D_6, 500 MHz): δ 6.83 (6 H, m, *m*-PArH), 6.73 (6 H, m, *o*-PArH), 6.66 (2 H, s, *m*-NArH), 6.57 (2 H, s, *m*-NArH), 5.96 (1 H, s, NCHN), 2.45 (6 H, s, $NArCH_3$), 2.38 (6 H, s, $NArCH_3$), 2.19 (3 H, s, $C(CH_3)_2$), 1.99 (9 H, s, *p*-$PArCH_3$), 1.98 (6 H, s, $NArCH_3$), 1.89 (3 H, s, $C(CH_3)_2$) ppm. $^{13}C\{^{1}H\}$ NMR (C_6D_6, 126 MHz): δ 172.9 (s, CO), 143.1 (s, NAr), 141.5 (s, *p*-PAr), 136.0 (s, NAr), 135.9 (s, NAr), 135.7 (s, NAr), 134.3 (d, $^{2}J_{CP}$ = 15 Hz, *o*-PAr), 130.0 (overlapping, *m*-PAr and NAr), 129.8 (s, NAr), 127.3 (d, $^{1}J_{CP}$ = 44 Hz, *i*-PAr), 68.7 (d, $^{2}J_{CP}$ = 62 Hz, NCHN), 49.1 (s, $\underline{C}(CH_3)_2$), 23.2 (s, $C(\underline{C}H_3)_2$), 21.5 (s, $PAr\underline{C}H_3$), 21.4 (s, $NAr\underline{C}H_3$), 21.1 (s, $C(\underline{C}H_3)_2$), 20.1 (s, $NAr\underline{C}H_3$), 19.7 (s, $NAr\underline{C}H_3$) ppm. $^{31}P\{^{1}H\}$ NMR (C_6D_6, 202 MHz): δ 3.17 (s) ppm. IR (KBr disc): ν_{CO} = 1662, 1632cm^{-1}. Elemental analysis (%) for $C_{45}H_{50}CuN_2O_2P$ (745.4) – calc: C 72.51, H 6.76, N 3.76; expt: C 72.88, H 6.76, N 3.74.

7.6.3 Synthesis and Characterising Data for (6-Mes·H)Cu(6-Mes) (35)[4]

Et_3SiH (0.150 mL, 0.940 mmol) was added to a stirring suspension of (6-Mes)CuO^tBu (**20**) (0.134 g, 0.293 mmol) in benzene (15 mL) resulting in an immediate colour change from colourless to bright yellow. After 30 min, a black precipitate started to form. The reaction was shown by ^{1}H NMR spectroscopy to be complete after 25 hours. The suspension was filtered, and product further extracted from the black precipitate with benzene (2 x 5 mL). The black solid was dried in vacuo and identified as copper metal by PXRD (Yield = 0.008 g, 86 %). The pale yellow benzene solutions were combined, concentrated and hexane added to yield the title compound as an off-white precipitate. This was isolated by filtration and dried in vacuo. Yield = 0.074 g (76 %). Slow evaporation of concentrated benzene solutions led to the formation of single crystals suitable for X-ray diffraction. ^{1}H NMR (C_6D_6, 500 MHz): δ 6.94 (2 H, s, (6-Mes)-*m*-ArH), 6.87 (4 H, s, (6-Mes·H)-

m-ArH), 6.79 (2 H, s, (6-Mes)-*m*-ArH), 4.10 (1 H, s, NCHN), 3.07 (4 H, m, (6-Mes·H)-NCH_2), 2.37 (6 H, s, (6-Mes)-$ArCH_3$), 2.34-2.11 (23 H, overlapping, (6-Mes·H)-$ArCH_3$ and (6-Mes)-$ArCH_3$ and (6-Mes)-NCH_2 and (6-Mes)-$ArCH_3$ and (6-Mes·H)-$NCH_2C\underline{H}_2$), 2.07-1.48 (12 H, br, (6-Mes·H)-$ArCH_3$), 1.44 (1 H, m, (6-Mes·H)-$NCH_2C\underline{H}_2$), 1.13 (2 H, m, (6-Mes)-$NCH_2C\underline{H}_2$) ppm. $^{13}C\{^1H\}$ NMR (C_6D_6, 126 MHz): δ 204.2 (s, NCN), 152.8 (s, (6-Mes)-*i*-Ar), 142.8 (br, (6-Mes·H)-*i*-Ar), 138.8 (s, (6-Mes)-*o*-Ar), 138.3 (s, (6-Mes)-*o*-Ar), 137.6 (br, (6-Mes·H)-Ar), 135.5 (br, (6-Mes·H)-Ar), 131.8 (s, (6-Mes)-*p*-Ar), 130.3 (s, (6-Mes·H)-*m*-Ar), 129.8 (s, (6-Mes)-*m*-Ar), 129.3 (s, (6-Mes)-*m*-Ar), 81.0 (s, NCHN), 53.6 (s, (6-Mes·H)-NCH_2), 44.0 (s, (6-Mes)-NCH_2), 31.0 (s, (6-Mes·H) $NCH_2\underline{C}H_2$), 22.0 (s, (6-Mes)-$Ar\underline{C}H_3$), 21.6 (overlapping, (6-Mes)-$Ar\underline{C}H_3$ and (6-Mes·H)-$Ar\underline{C}H_3$), 21.2 (s, (6-Mes)-$Ar\underline{C}H_3$), 21.0 (s, (6-Mes)-$NCH_2\underline{C}H_2$), 18.6-18.2 (br, (6-Mes·H)-$Ar\underline{C}H_3$) ppm. Elemental analysis (%) for $C_{44}H_{57}CuN_4$ (705.5) – calc: C 74.91, H 8.14, N 7.94; expt: C 74.71, H 8.04, N 8.02.

7.6.4 Synthesis and Characterising Data for (6-Mes)Cu(C(Ph)=C(Me)H) (36)[4]

This procedure was conducted entirely inside a glovebox unless otherwise stated. PhC≡CMe (0.300 mL, 2.395 mmol), followed by Et_3SiH (0.350 mL, 2.193 mmol), were added to a stirring suspension of (6-Mes)CuO^tBu (**20**) (0.335 g, 0.733 mmol) in benzene (10 mL), resulting in an immediate colour change from colourless to orange. The reaction was followed by NMR analysis of aliquots. After 25 hours, the reaction mixture was reduced to dryness and the resultant beige/off-white powder dried in vacuo. This was washed twice with benzene/hexane (1 : 5, v : v), and then once with hexane. The precipitate was dried in vacuo to give a beige/off-white product. Yield = 0.212 g (58 %). Single crystals suitable for X-ray diffraction studies were grown from benzene/hexane. ^1H NMR (C_6D_6, 500 MHz): δ 7.14 (overlapping with C_6D_5H, m, *m*-CArH), 6.97 (1 H, m, *p*-CArH), 6.77 (6 H, overlapping, *o*-CArH and *m*-NArH), 5.61 (1 H, q, $^3J_{HH}$ = 6.4 Hz, C(Ph)=C(Me)$\underline{H}$), 2.49 (4 H, t, $^3J_{HH}$ = 5.9 Hz, NCH_2), 2.17 (6 H, s, *p*-$NArCH_3$), 2.13 (12 H, s, *o*-$NArCH_3$), 1.82 (3 H, d, $^3J_{HH}$ = 6.4 Hz, C(Ph)=C($\underline{Me}$)H), 1.33 (2 H, p, $^3J_{HH}$ = 5.9 Hz, $NCH_2C\underline{H}_2$) ppm. $^{13}C\{^1H\}$ NMR (C_6D_6, 126 MHz): δ 205.2 (s, NCN), 171.2 (s, $\underline{C}$(Ph)=C(Me)H), 154.3 (s, *i*-CAr), 142.9 (s, *i*-NAr), 137.9 (s, *p*-NAr), 135.1 (s,

o-NAr), 130.3 (s, *m*-NAr), 128.4 (s, C(Ph)=C(Me)H), 128.0 (s, *o*-CAr), 127.5 (s, *m*-CAr), 121.5 (s, *p*-CAr), 43.8 (s, NCH_2), 21.5 (s, *p*-$NArCH_3$), 21.2 (s, NCH_2CH_2), 18.5 (s, *o*-$NArCH_3$), 16.4 (s, C(Ph)=C(Me)H) ppm. Elemental analysis (%) for $C_{31}H_{37}CuN_2$ (501.2) – calc: C 74.29, H 7.44, N 5.59; expt: C 74.34, H 7.44, N 5.54.

7.6.5 Synthesis and Characterising Data for $[(6\text{-}Mes)_2Cu][Cu(OC(O)C(Ph)=C(Me)H)_2]$ (37)[4]

A benzene (10 mL) solution of (6-Mes)Cu(C(Ph)=C(Me)H) (**36**) (0.110 g, 0.219 mmol) was freeze-pump-thaw degassed and placed under an atmosphere of $^{13}CO_2$, resulting in an immediate colour change from beige to yellow. After stirring for 30 minutes, the volatiles were removed and the remaining yellow oil dried under vacuum. Reprecipitation from benzene/hexane yielded **37** as a white powder, which was isolated by decantation and dried in vacuo. Yield = 0.058 g (49 %). Single crystals suitable for X-ray diffraction studies were grown from benzene/ hexane. ^{1}H NMR (C_6D_6, 500 MHz): δ 7.19 (4 H, m, *o*-CArH), 7.09 (6 H, overlapping, *m*-CArH and C(Ph)C(Me)H), 6.99 (2 H, m, *p*-CArH), 6.72 (8 H, s, *m*-NArH), 2.50 (8 H, t, $^3J_{HH}$ = 5.7 Hz, NCH_2), 2.21 (24 H, s, *o*-$NArCH_3$), 2.05 (12 H, s, *p*-$NArCH_3$), 1.39 (6 H, d, $^3J_{HH}$ = 7.2 Hz, C(Ph)C(Me)H), 1.33 (4 H, m, NCH_2CH_2) ppm. $^{13}C\{^1H\}$ NMR (C_6D_6, 126 MHz): δ 202.3 (s, NCN), 173.6 (s, $CuO^{13}CO$), 143.1 (s, *i*-NAr), 140.8 (d, $^1J_{CC}$ = 69 Hz, $CuO^{13}C(O)C$), 140.2 (s, *i*-CAr), 138.0 (s, *p*-NAr), 135.3 (s, *o*-NAr), 133.4 (s, C(Ph)C(Me)H), 131.1 (s, *o*-CAr), 130.4 (s, *m*-NAr), 127.5 (s, *m*-CAr), 126.1 (s, *p*-CAr), 44.2 (s, NCH_2), 21.5 (s, *p*-$NArCH_3$), 21.1 (s, NCH_2CH_2), 18.5 (s, *o*-$NArCH_3$), 15.4 (s, C(Ph)C(Me)H) ppm. IR (KBr disc): ν_{CuOCO} = 1649, 1593 cm^{-1}. Elemental analysis (%) for $C_{64}H_{74}Cu_2N_4O_4$ (1090.4) – calc: C 70.50, H 6.84, N 5.14; expt: C 70.98, H 6.92, N 5.17.

7.7 Experimental Details and Characterising Data for Chapter Six

7.7.1 NMR Scale Reaction for the Synthesis of [(6-Mes)CuH]$_2$ (38)

To a THF-d_8 suspension of $LiAlH_4$ (0.002 g, 0.039 mmol) was added a THF-d_8 suspension of (6-Mes)CuO^tBu (**20**) (0.014 g, 0.031 mmol), all cooled in a liquid nitrogen/acetone slurry (178 K). A bright yellow solution was immediately formed. Maintaining the temperature at 178 K, the sample was transferred to a pre-cooled NMR spectrometer where data were recorded at 209 K. At this temperature, **38** was stable for hours. Warming to 255 K resulted in the slow decomposition to (6-Mes·H)Cu(6-Mes) (**35**) and (6-Mes)AlH_3 alongside precipitation of metallic copper and the evolution of hydrogen gas. ^{1}H NMR (THF-d_8, 500 MHz, 209 K): δ 6.65 (8 H, s, *m*-ArH), 3.13 (8 H, m, NCH_2), 2.29 (12 H, s, *p*-ArCH_3), 2.19 (28 H, overlapping, *o*-ArCH_3 and $NCH_2C\underline{H}_2$), 0.96 (2 H, s, CuH) ppm. $^{13}C\{^1H\}$ NMR (THF-d_8, 126 MHz, 209 K): δ 211.5 (s, NCN), 143.5 (s, *i*-Ar), 135.7 (s, *o*-Ar), 135.3 (s, *p*-Ar), 129.1 (s, *m*-Ar), 44.1 (s, NCH_2), 22.4 (s, $NCH_2\underline{C}H_2$), 21.5 (s, *p*-Ar$\underline{C}H_3$), 18.3 (s, *o*-Ar$\underline{C}H_3$) ppm.

7.7.2 Synthesis and Characterising Data for (6-Mes)CuHBEt$_3$ (39)

All reagents, solvents and glassware were pre-cooled to 238 K in the freezer compartment of a glove-box. A '1.0 M' solution of $LiHBEt_3$ (assessed by ^{11}B NMR to contain ~80 % $LiHBEt_3$) in THF (0.140 mL, 0.112 mmol) was transferred by syringe to a vial containing a THF suspension of (6-Mes)CuO^tBu (**20**) (0.050 g, 0.109 mmol). A yellow solution was formed immediately and filtered through a glass microfiber plug to a clean vial after five minutes. Layering with hexane yielded colourless crystals overnight which were isolated by decantation, washed with hexane (2 x 2 mL) and dried under reduced pressure. NMR analysis revealed these crystals to consist of 85 % of **39** and 15 % of [(6-Mes)$_2$Cu][BEt_4] (**40**). Redissolution in THF and recrystallisation by vapour diffusion of hexane at 238 K afforded crystals of **39**. Yield = 0.022 g (42 %). ^{1}H NMR (THF-d_8, 500 MHz, 209 K): δ 6.95 (4 H, s, *m*-ArH), 3.40 (4 H, m, NCH_2), 2.34-2.29 (14 H, overlapping, $NCH_2C\underline{H}_2$ and *o*-ArCH_3), 2.25 (6 H, s, *p*-ArCH_3), 0.14 (9 H, t, $^3J_{HH}$ = 7.4 Hz, $BCH_2C\underline{H}_3$), -0.19 (6 H, m, $BC\underline{H}_2CH_3$), -2.60 (1 H, s, CuHB) ppm. $^{13}C\{^1H\}$ NMR (THF-d_8, 126 MHz, 209 K): δ 201.9 (s, NCN), 143.6 (s, *i*-Ar), 138.6 (s, *p*-Ar),

135.8 (s, *o*-Ar), 130.5 (s, *m*-Ar), 44.8 (s, NCH_2), 21.8 (s, $NCH_2\underline{C}H_2$), 21.3 (s, *p*-$Ar\underline{C}H_3$), 18.4 (s, *o*-$Ar\underline{C}H_3$), 12.5 (s, $BCH_2\underline{C}H_3$), 10.9 (broad, $B\underline{C}H_2CH_3$) ppm. ^{13}C NMR (THF-d_8, 126 MHz, 209 K): δ 201.9 (d, $^2J_{CH}$ = 11.6 Hz, NCN), 143.6 (s, *i*-Ar), 138.6 (d, $^2J_{CH}$ = 5.8 Hz, *p*-Ar), 135.8 (d, $^2J_{CH}$ = 5.3 Hz, *o*-Ar), 130.5 (d, $^1J_{CH}$ = 155.9 Hz, *m*-Ar), 44.8 (t, $^1J_{CH}$ = 142.3 Hz, NCH_2), 22.8-19.8 (m, overlapping $NCH_2\underline{C}H_2$ and *p*-$Ar\underline{C}H_3$), 18.4 (q, $^1J_{CH}$ = 126.6 Hz, *o*-$Ar\underline{C}H_3$), 12.5 (q, $^1J_{CH}$ = 122.0 Hz, $BCH_2\underline{C}H_3$), 10.9 (t (broad), $^1J_{CH}$ = 114.1 Hz, $B\underline{C}H_2CH_3$) ppm. $^{11}B\{^1H\}$ NMR (THF-d_8, 160 MHz, 209 K): δ -8.2 (broad, $HBEt_3$) ppm. Thermal sensitivity of the complex precluded the recording of elemental analysis.

7.7.3 NMR Scale Reaction for the Synthesis of (6-Mes)Cu(H_2BEt_2) (40)

A crystalline sample of (6-Mes)$CuHBEt_3$ (**39**) (0.020 g, 0.041 mmol) was dissolved in THF-d_8 and left at room temperature for five days. Evaporation of the volatiles and redissolution in THF-d_8 resulted in a sample consisting of (6-Mes)Cu(H_2BEt_2) (**40**), alongside (6-Mes·H)Cu(6-Mes) (**35**) and [(6-Mes)$_2$Cu][BEt_4] (**41**). Selected NMR data could be assigned to **40** by comparison to clean samples of **35** and **41**. ^1H NMR (THF-d_8, 500 MHz): δ 6.89 (br, *m*-ArH), 6.73 (br, *m*-ArH), 3.37 (br, NCH_2), 2.35 (br, $NCH_2C\underline{H}_2$), 2.30 (br, $ArCH_3$), 2.22 (br, $ArCH_3$), 2.16 (br, $ArCH_3$), 0.80 (br, $BCH_2C\underline{H}_3$), 0.11 (br, $BC\underline{H}_2CH_3$), -0.40 (br, CuH_2B) ppm. $^{11}B\{^1H\}$ NMR (THF-d_8, 160 MHz): δ -8.9 (br, H_2BEt_2) ppm.

7.7.4 Synthesis and Characterising Data for [(6-Mes)$_2$Cu][BEt_4] (41)

A '1.0 M' solution of $LiHBEt_3$ (assessed by ^{11}B NMR to contain ~80 % $LiHBEt_3$) in THF (0.325 mL, 0.260 mmol) was added to a stirring suspension of (6-Mes)CuO^tBu (**20**) (0.114 g, 0.249 mmol) in THF (5 mL). The yellow solution initially formed turned black within 30 minutes. All starting material was confirmed to have reacted by aliquot analysis after 27 hours. The reaction was filtered to remove copper (5.2 mg isolated, 33 % yield) and volatiles were removed under reduced pressure, leaving a brown oil which was dried in vacuo. Vigorous stirring with benzene yielded a brown solution which was isolated by filtration. The remaining black precipitate was further washed with benzene and extracted into THF, yielding a beige solution. Removal of volatiles resulted in an off-white powder which was dried in vacuo.

Yield = 0.023 g (22 %). Single crystals suitable for X-ray diffraction studies were grown by vapour diffusion of hexane to a saturated THF solution. ^{1}H NMR (THF-d_8, 500 MHz): δ 7.00 (8 H, s, *m*-ArH), 3.13 (8 H, t, $^{3}J_{HH}$ = 5.7 Hz, NCH_2), 2.35 (12 H, s, *p*-$ArCH_3$), 2.07 (4 H, m, $NCH_2C\underline{H}_2$), 1.81 (24 H, s, *o*-$ArCH_3$), 0.63 (12 H, m ($^{1}H\{^{11}B\}$ NMR: t, $^{3}J_{HH}$ = 7.8 Hz), $BCH_2C\underline{H}_3$), -0.14 (8 H, m ($^{1}H\{^{11}B\}$ NMR: q, $^{3}J_{HH}$ = 7.8 Hz), $BC\underline{H}_2CH_3$) ppm. $^{13}C\{^{1}H\}$ NMR (THF-d_8, 126 MHz): δ 199.5 (s, NCN), 142.6 (s, *i*-Ar), 138.7 (s, *p*-Ar), 135.8 (s, *o*-Ar), 130.5 (s, *m*-Ar), 44.8 (s, NCH_2), 21.0 (overlapping, *p*-$Ar\underline{C}H_3$ and $NCH_2\underline{C}H_2$), 18.2 (s, *o*-$Ar\underline{C}H_3$), 17.6 (broad, $B\underline{C}H_2CH_3$), 12.1 (s, $BCH_2\underline{C}H_3$) ppm. $^{11}B\{^{1}H\}$ NMR (THF-d_8, 160 MHz): δ -16.5 (s, $[BEt_4]^-$) ppm. Elemental analysis (%) for $C_{52}H_{76}BCuN_4$ (831.6) – calc ($C_{52}H_{76}BCuN_4 \cdot 0.3(CH_2Cl_2)$ as confirmed by ^{1}H NMR): C 73.30, H 9.01, N 6.54; expt: C 73.35, H 9.04, N 6.52.

7.7.6 NMR Scale Reaction for the Synthesis of (6-Mes)CuHB(C_6F_5)$_3$ (42)

To a C_6D_6 suspension of (6-Mes)CuO^tBu (**20**) (0.010 g, 0.022 mmol) was added a C_6D_6 solution of $B(C_6F_5)_3$ (0.012 g, 0.023 mmol) and Et_3SiH (0.018 mL, 0.113 mmol). Volatiles were removed from the resultant yellow solution after 30 minutes and the product extracted into C_6D_6/hexane (3 mL, 1 : 5, v : v). The solution was evaporated under reduced pressure and the pale yellow microcrystalline product was washed with hexane and dried in vacuo. Crystallisation from C_6D_6/hexane yielded crystals of the title complex suitable for X-ray diffraction studies and NMR analysis. ^{1}H NMR (C_6D_6, 500 MHz):* δ 6.71 (4 H, s, *m*-ArH), 2.27 (4 H, t, $^{3}J_{HH}$ = 5.7 Hz, NCH_2), 2.04 (6 H, s, *p*-$ArCH_3$), 1.92 (12 H, s, *o*-$ArCH_3$), 1.13 (2 H, p, $^{3}J_{HH}$ = 5.7 Hz, $NCH_2C\underline{H}_2$) ppm. * Bridging hydride not observed. $^{13}C\{^{1}H\}$ NMR (C_6D_6, 126 MHz):* δ 201.0 (s, NCN), 141.9 (s, *i*-Ar), 139.4 (s, *p*-Ar), 134.7 (s, *o*-Ar), 130.4 (s, *m*-Ar), 43.6 (s, NCH_2), 21.0 (s, *p*-$Ar\underline{C}H_3$), 20.4 (s, $NCH_2\underline{C}H_2$), 17.6 (s, *o*-$Ar\underline{C}H_3$) ppm. * C_6F_5 not observed. ^{19}F NMR (C_6D_6, 470 MHz): δ -129.3 (2 F, m, *o*-C_6F_5), -158.4 (1 F, m, *p*-C_6F_5), -163.8 (2 F, m, *m*-C_6F_5) ppm. ^{11}B NMR (C_6D_6, 160 MHz): δ -28.1 (d, $^{1}J_{BH}$ = 60.0 Hz, CuHB) ppm.

7.8 References for Chapter Seven

(1) Collins, L. R.; Lowe, J. P.; Mahon, M. F.; Poulten, R. C.; Whittlesey, M. K. *Inorg. Chem.* **2014**, *53*, 2699–2707.

(2) Collins, L. R.; Rookes, T. M.; Mahon, M. F.; Riddlestone, I. M.; Whittlesey, M. K. *Organometallics* **2014**, *33*, 5882–5887.

(3) Collins, L. R.; Hierlmeier, G.; Mahon, M. F.; Riddlestone, I. M.; Whittlesey, M. K. *Chem. Eur. J.* **2015**, *21*, 3215–3218.

(4) Collins, L. R.; Riddlestone, I. M.; Mahon, M. F.; Whittlesey, M. K. *Chem. Eur. J.* **2015**, *21*, 14075–14084.

(5) Collins, L. R.; Moffat, L. A.; Mahon, M. F.; Jones, M. D.; Whittlesey, M. K. *Polyhedron* **2016**, *103*, 121–125.

(6) Fulmer, G. R.; Miller, A. J. M.; Sherden, N. H.; Gottlieb, H. E.; Nudelman, A.; Stoltz, B. M.; Bercaw, J. E.; Goldberg, K. I. *Organometallics* **2010**, *29*, 2176–2179.

(7) Tsuda, T.; Hashimoto, T.; Saegusa, T. *J. Am. Chem. Soc.* **1972**, *94*, 658–659.

(8) Tsuda, T.; Yazawa, T.; Watanabe, K.; Fujii, T.; Saegusa, T. *J. Org. Chem.* **1981**, *46*, 192–194.

(9) McGeary, M. J.; Wedlich, R. C.; Coan, P. S.; Folting, K.; Caulton, K. G. *Polyhedron* **1992**, *11*, 2459–2473.

(10) Hudnall, T. W.; Moerdyk, J. P.; Bielawski, C. W. *Chem. Commun.* **2010**, *46*, 4288–4290.

(11) Iglesias, M.; Beetstra, D. J.; Knight, J. C.; Ooi, L.; Stasch, A.; Coles, S.; Male, L.; Hursthouse, M. B.; Cavell, K. J.; Dervisi, A.; Fallis, I. A. *Organometallics* **2008**, *27*, 3279–3289.

(12) Iglesias, M.; Beetstra, D. J.; Kariuki, B.; Cavell, K. J.; Dervisi, A.; Fallis, I. A. *Eur. J. Inorg. Chem.* **2009**, *2009*, 1913–1919.

(13) César, V.; Lugan, N.; Lavigne, G. *Eur. J. Inorg. Chem.* **2010**, *2010*, 361–365.

APPENDICES

APPENDIX 1

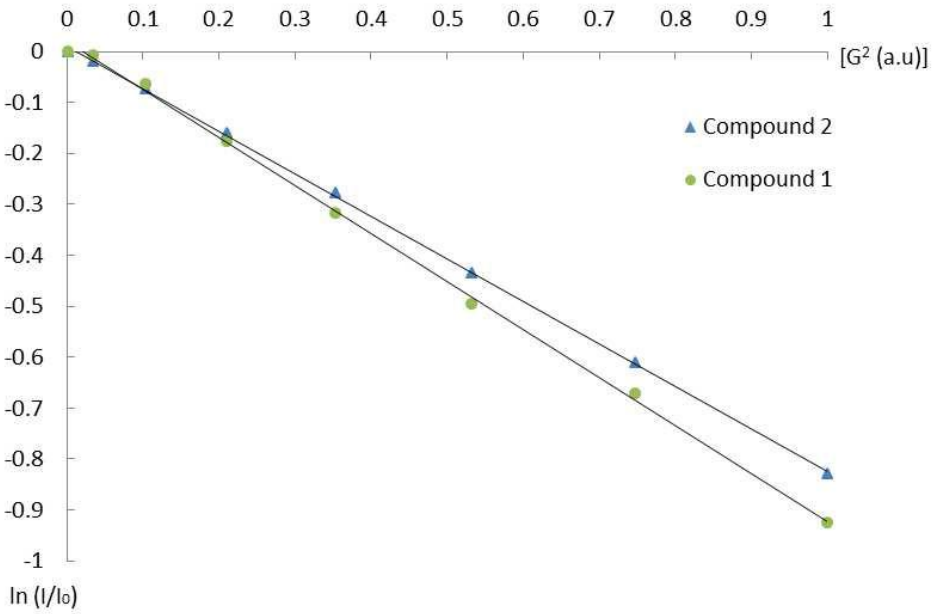

Figure A.1: Graph showing the natural log of relative ^{1}H NMR peak intensity (ln (I/I_o)) as a function of the square of the applied field gradient (G^2) for complexes **1** and **2**.

Hydrodynamic radii were calculated using Bruker's T1/T2 software, with ^{1}H DOSY experiments carried out using a double stimulated echo pulse sequence, with values of Δ = 75 ms and δ = 1.5 ms. The gradient strengths (previously calibrated using a sample of H_2O) were incremented in eight equal steps from 1.74 to 33.14 G cm^{-1}.

APPENDIX 2

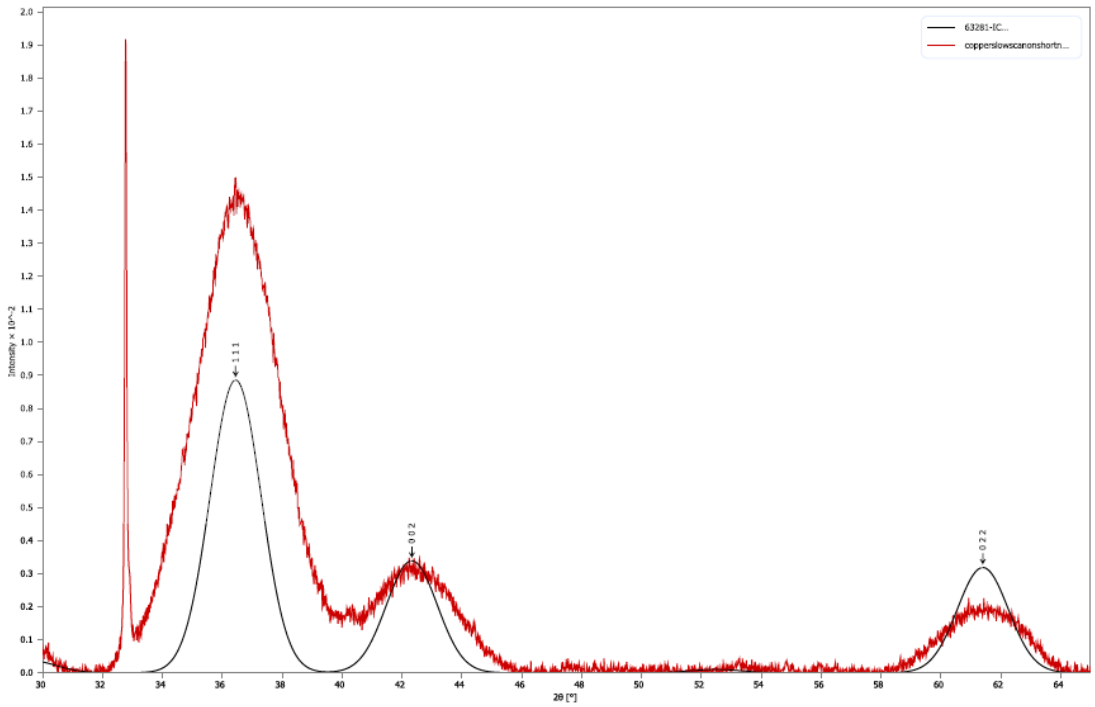

Figure A.2: Observed (red) and calculated (for Cu_2O, black) powder X-ray diffraction patterns (λ = 1.541 Å) of orange residue from the hydrolytic degradation of **11**. The sharp peak at 32.5° is from sample holder. Particle size can be estimated from the Scheerer formula to be about 0.5-1 nm.

APPENDIX 3

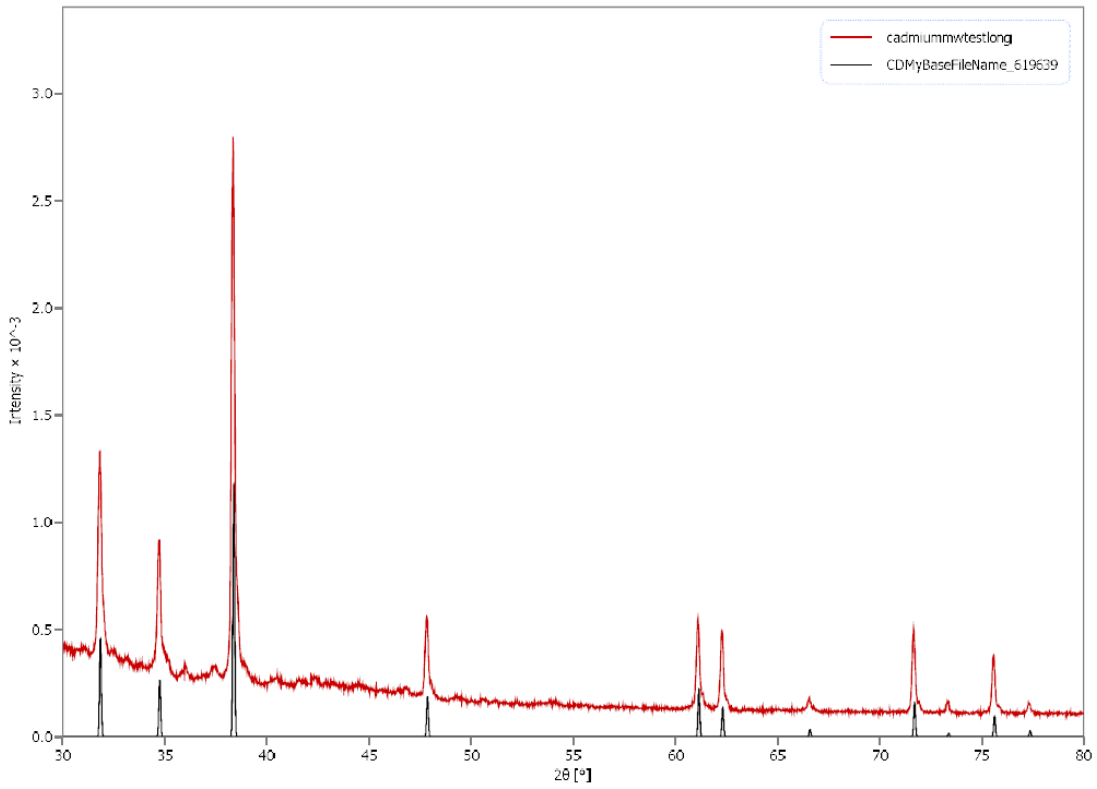

Figure A.3: Powder X-ray diffraction data (CuK$_{\alpha 1}$ radiation 1.5406 Å) collected using a Bruker D8 diffractometer in the angular range 30-80°. Upper trace (red) is the experimental data from the degradation of **32** and lower trace (black) is the pattern calculated for pure cadmium metal (hexagonal, a=2.977 Å, c=5.612 Å).

APPENDIX 4

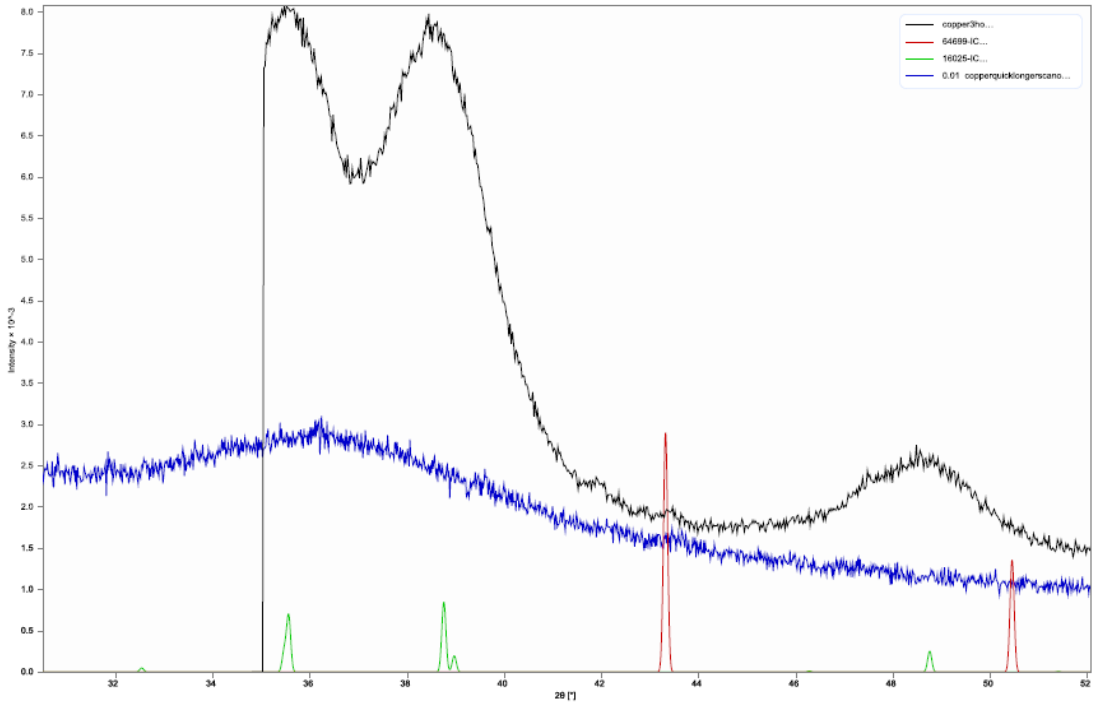

Figure A.4: Powder X-ray diffraction patterns (λ=1.541 Å) for solid material isolated from the reaction of **20** with Et_3SiH. Blue trace is that initially recorded upon removal of the solid from glove box (the broad feature at 36° is from a Mylar® film covering the sample); no clear diffraction peak is visible, but an extremely broad peak corresponding to Cu metal may be discerned at 43.3°. The black trace shows the same sample re-recorded after 4 days in air under the Mylar® film and demonstrates conversion to nano-particulate Cu_2O (green and red traces are those for Cu_2O and Cu metal respectively for comparison). Overall, it appears that the material as produced is probably nanoparticulate copper but with extremely small particle sizes of 1 nm or less, hence the lack of distinct diffraction maxima.